KEK Report 2012-4
October 2012
A/M

Energy Recovery Linac Conceptual Design Report

High Energy Accelerator Research Organization

KEK Reports are available from:

High Energy Accelerator Research Organization (KEK)
1-1 Oho, Tsukuba-shi
Ibaraki-ken, 305-0801
JAPAN

Phone: +81-29-864-5137
Fax: +81-29-864-4604
E-mail: irdpub@mail.kek.jp
Internet: http://www.kek.jp

Energy Recovery Linac
Conceptual Design Report

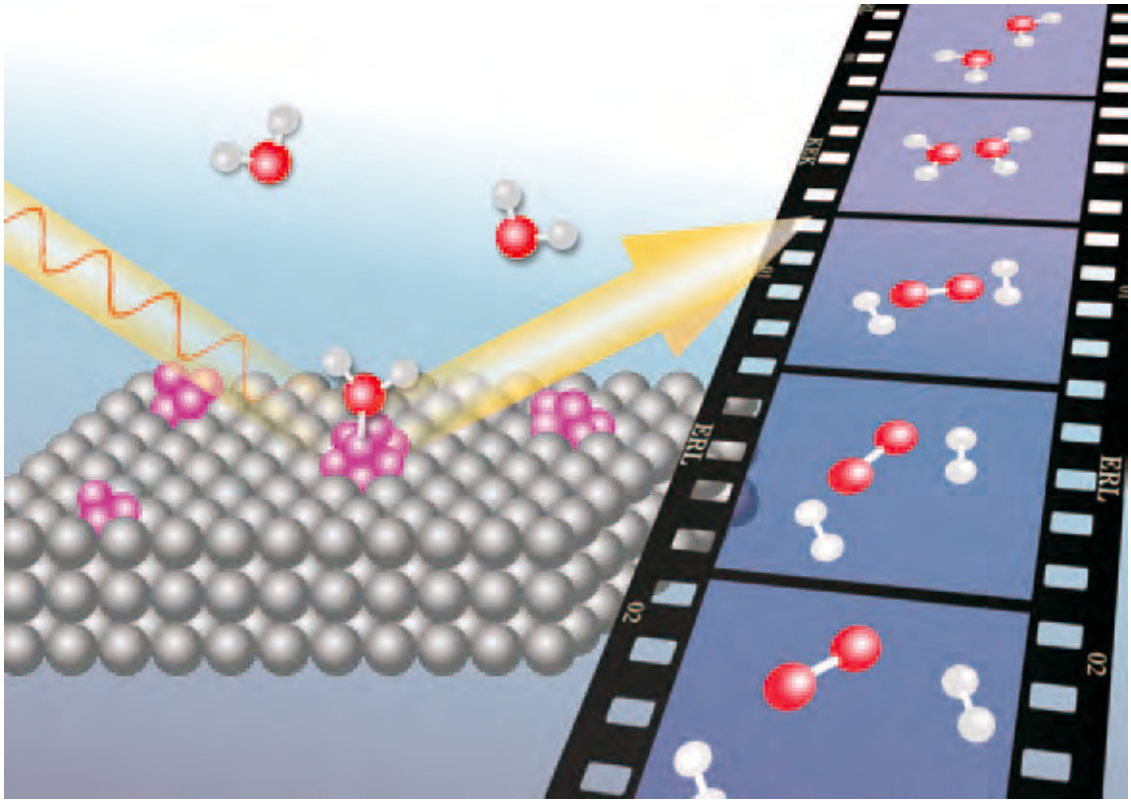

CONTENTS

Layout of the 3GeV ERL and 6~7 GeV XFEL-O in KEK

CONTRIBUTORS

Hitoshi Abe[1], Shin-ichi Adachi[1], Kenta Amemiya[1], Taka-hisa Arima[2], Kiyotaka Asakura[3], Leonard Chavas[1], Nobumasa Funamori[2], Takaaki Furuya[1], Ryoichi Hajima[4], Kentaro Harada[1], Yoshihisa Harada[2], Keiichi Hirano[1], Tohru Honda[1], Sumio Ishihara[5], Kenji Ishii[4], Kaoru Iwano[1], So Iwata[6], Eiji Kako[1], Nobuo Kamiya[7], Hiroshi Kawata[1], Shunji Kishimoto[1], Yoshinori Kitajima[1], Hisao Kobayashi[8], Yukinori Kobayashi[1], Hiroshi Kondoh[9], Tadashi Kondo[11], Shin-ya Koshihara[10], Reiji Kumai[1], Hiroshi Kumigashira[1], Genji Kurisu[11], Shinichiro Michizono[1], Takashi Mizokawa[2], Madoka Mochida[1], Youichi Murakami[1], Hirotaka Nakai[1], Norio Nakamura[1], Hironori Nakao[1], Masaharu Nomura[1], Takashi Obina[1], Eiji Ohtani[5], Shogo Sakanaka[1], Tomoko Sato[12], Norihiro Sei[13], Toshiya Senda[13], Yuya Shinohara[2], Akio Suzuki[5], Hiroki Takahashi[14], Yoshio Takahashi[12], Yukio Takahashi[11], Masaki Takaoka[6], Kimichika Tsuchiya[1], Soichi Wakatsuki[1], Masahiro Yamamoto[1], Yuichi Yamasaki[1], Junko Yano[15], Wataru Yashiro[5].

[1]KEK
[2]The University of Tokyo
[3]Hokkaido University
[4]JAEA
[5]Tohoku University
[6]Kyoto University
[7]Osaka City University
[8]University of Hyogo
[9]Keio University
[10]Tokyo Institute of Technology
[11]Osaka University
[12]Hiroshima University
[13]AIST
[14]Nihon University
[15]LBNL

Chapter 1 Executive Summary

1.1 Introduction

High Energy Accelerator Research Organization (KEK) has prepared a conceptual design report of Energy Recovery Linac (ERL) at the electron beam energy of 3 GeV (Fig. 1-1). ERL is a future X-ray light source designed based on state-of-the-art superconducting linear accelerator technology, which will offer far higher performance than the existing storage ring. The high repetition rate, short pulse, high spatial coherence and high brightness of ERL will enable the filming of ultrafast atomic-scale movies and determination of the structure of heterogeneous systems on the nano-scale. These unique capabilities of ERL will drive forward a distinct paradigm shift in X-ray science from “static and homogeneous” systems to “dynamic and heterogeneous” systems, in other words, from “time- and space-averaged” analysis to “time- and space-resolved” analysis.

This paradigm shift will make it possible to directly witness how heterogeneous functional materials work in real time and space, and will enable predictions to be made in order to design and innovate better functional materials which will eventually solve the grand challenges of society and support life in future. Such functional materials will continue to be used in indispensable technologies such as catalysts, batteries, superconductors, biofuels, random access memories, spintronics devices and photoswitches. On the other hand, life itself is an intrinsically heterogeneous and dynamic system. Structural biology based on the existing storage ring technology has greatly contributed to providing the static atomic coordinates of proteins which are useful information for rational drug design. ERL will further contribute to biological science and biotechnology by shedding light on the heterogeneity and complexity of cellular functions.

In short, ERL will be an unprecedented tool that will bridge the critical gaps in our understanding of material science and technology. More details as to why ERL is needed and how it will help solving problems of society will be presented in the following chapters. ERL is planned to be constructed in late 2010s, and expected to be operational in early 2020s.

In addition, continuous improvement of linear accelerator technology will result in further quantum leaps in X-ray science in the future. One possibility is the realization of a fully coherent X-ray free-electron laser. Although self-amplified spontaneous emission X-ray free-electron lasers (SASE-XFELs) have been constructed around the world, the X-ray beam from SASE-XFEL is essentially not fully coherent in the temporal domain. By configuring a Bragg diamond cavity for lasing in the X-ray region, it is proposed

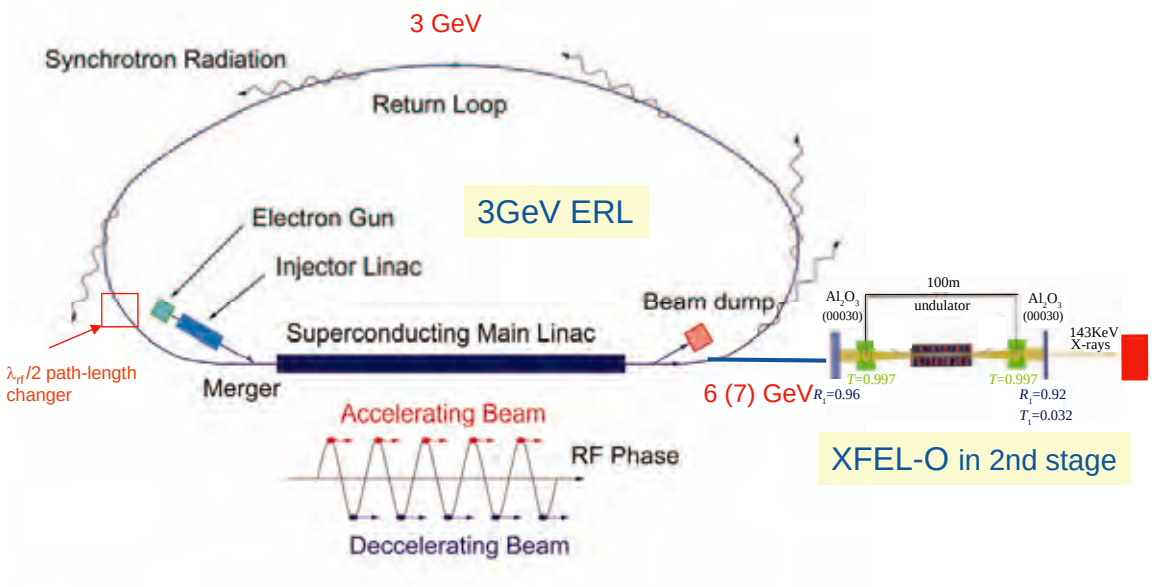

Figure 1-1
Conceptual layout of 3-GeV ERL plan that is integrated with an X-ray free electron-laser oscillator (XFEL-O).

that an X-ray free-electron laser oscillator (XFEL-O) will be feasible by taking full advantage of the unprecedented electron beam quality of ERL. The construction of XFEL-O is planned in the second phase of the ERL project.

1.2 Capabilities

ERL is a next-generation light source that will produce world leading levels of nanobeam, spatial coherence, and short pulse.

The main performance characteristics of ERL in the operational modes are given in Table 1-1.

Table 1-1 Target parameters of the 3-GeV ERL which is integrated with the X-ray free-electron-laser oscillator (XFEL-O).

	Operation modes				
	High-coherence mode	High-flux mode	Ultimate mode	Ultra short-pulse mode	XFEL-O
Beam energy (E)	3 GeV				6-7 GeV
Average beam current (I_0)	10 mA	100 mA	100 mA	Typically, 77 μA (flexible)	20 μA
Charge/bunch (q_b)	7.7 pC	77 pC	77 pC	Typically, 77 pC (flexible)	20 pC
Repetition rate of bunches (f_{rep})	1.3 GHz	1.3 GHz	1.3 GHz	Typically, 1 MHz (flexible)	1 MHz
Normalized beam emittances (ε_{nx}, ε_{ny})	0.1 mm·mrad	1 mm·mrad	0.1 mm·mrad	To be investigated (typically, 1-10 mm·mrad)	0.2 mm·mrad
Beam emittances at full beam energy (ε_x, ε_y)	17 pm·rad	170 pm·rad	17 pm·rad	To be investigated (typically, 0.2-2 nm·rad)	15 pm·rad
Energy spread of beams; in rms (σ_E/E)	2×10^{-4}	2×10^{-4}	2×10^{-4}	To be investigated	5×10^{-5}
Bunch length; in rms (σ_t)	2 ps	2 ps	2 ps	100 fs	1 ps

Chapter 2 Why ERL is Needed

In the early 20th century, X-ray tubes started to serve as indispensable tools for X-ray imaging, pioneered by Wilhelm Conrad Röntgen (the first Nobel Prize Winner in 1901), and for crystal structure analysis, pioneered by Henry and Lawrence Bragg (Nobel Prize Winners in 1915). In the mid-20th century, synchrotron radiation was first observed at General Electric Co. in 1947, since when synchrotron radiation facilities have provided several orders of magnitude more brilliant X-ray beams than X-ray tubes can do. This has led to numerous breakthroughs in X-ray science and a wide range of applications of imaging, atomic structural analysis, and spectroscopy. In the early 21st century, ERL will usher in a new era of scientific inquiry and lead to discoveries not possible with existing facilities. Based on superconducting linear accelerator technology, ERL will deliver breakthroughs in X-ray science by observing not only "static and homogeneous" systems but also "dynamic and heterogeneous" ones. This will lead X-ray science toward the new direction of how heterogeneous functional materials work on a natural time scale and at the nano-scale (Fig. 2-1).

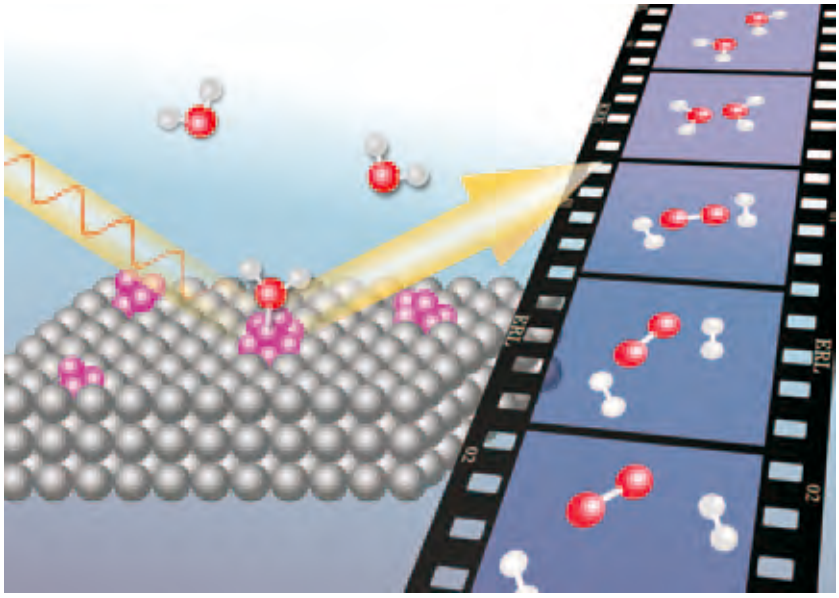

Figure 2-1
Capturing how heterogeneous functional materials work on a natural time scale and at the nano-scale.

Construction of ERL is motivated by the recognition that scientific breakthroughs are essential to solve the important challenges our society is facing, such as depletion of fossil fuels, generation of renewable energy, development of advanced materials, prevention of serious diseases, and attaining healthy lifestyles. Solving these challenges will make society more sustainable. Heading in the same direction, the Japanese government has been promoting social policies that encourage "green and life innovations" as Japan's growth strategy. This direction will require new tools for characterizing the atomic and electronic structures, chemical composition, and magnetic properties of materials under working conditions and at the nano-scale.

The most crucial limitation of existing storage ring technology is the equilibrium nature of electron beam parameters. Because electron bunches circulate in the storage ring many times, the electron beam size, divergence, and bunch length become equilibrated, and eventually the initial beam parameters are broadened. On the other hand, ERL is essentially a linear accelerator; the electron bunch is accelerated, circulated in the ring only once, and then decelerated and dumped. This characteristic is the intrinsic beauty of ERL. The state-of-the-art technology of the linear accelerator enables it to far outperform the existing storage ring and guarantees its future expandability as the basis of next-generation X-ray light sources.

The main features of ERL are short pulse, spatial coherence, and nanobeam. Concerning the short pulse properties, the electron bunch length of ERL is maintained at around 100 femtosecond to 1 picosecond for one turn of the ring then the bunch is dumped without elongating the bunch length. The bunch length of ERL is 2 orders of magnitude shorter than the typical bunch length of a storage ring (~50 picosecond), which enables the observation of ultrafast phenomena of dynamic processes on their natural time scales without damaging samples. The experimental targets will include a wide range of dynamic processes such as catalytic chemical reactions, photosynthetic systems, and phase transitions of functional materials.

The second key feature of synchrotron light from ERL is its high spatial coherence, thanks to the tiny electron beam size and divergence which ERL can attain. Typically, the spatial coherence of synchrotron radiation from the storage ring is essentially very low. Thus, in order to perform structural determination with atomic resolution with such spatially low coherent X-ray beam, spatial coherence in the material (= crystalline order) is mandatory, which limits the applicability of atomic structural determination to only periodic and homogeneous materials. This situation will change dramatically with ERL. The high spatial coherence of ERL will enable recording of the interference of the X-ray beam scattered by even non-periodic and heterogeneous materials, thus eventually allowing structural analysis of heterogeneous materials, in principle, at the spatial resolution of X-ray wavelength (~ 0.1 nm) order. This feature will revolutionize the capability of structural analysis to be widely applied to heterogeneous and functional materials. At the same time, the electron beam emittance of ERL is planned to be as small as 17 pmrad, which is about 60 times smaller than that of the existing storage ring (~ 1 nmrad), and almost equals the diffraction limit of the soft X-ray beam at the wavelength of λ = 0.2 nm. The diffraction-limited X-ray beam can be focused down to a nanometer-size, which is the third key feature of ERL. Spectroscopic measurements such as X-ray photoelectron spectroscopy (XPS), X-ray absorption spectroscopy (XAS), X-ray emission spectroscopy (XES), X-ray magnetic circular dichroism (XMCD), and resonant inelastic X-ray scattering (RIXS) will provide powerful methods for probing the electronic and magnetic properties of heterogeneous materials with nanometer-order spatial resolution.

In comparison with SASE-XFEL, the photon beam characteristics of SASE-XFEL are different from those of ERL, and these two sources are complementary in some respects. SASE-XFEL produces pulses with very high peak power at relatively low repetition rates. ERL produces pulses with relatively low peak power at a very high repetition rate (up to 1.3 GHz). In total, the time-averaged photon flux of these two sources is comparable. Due to the high peak power of SASE-XFEL, the measurement is destructive when the beam is focused down to nanometer size. In this sense, SASE-XFEL will provide completely new opportunities for studying materials in extreme conditions. On the other hand, since the peak power of ERL pulses does not exceed the damage threshold of many samples, ERL enables the provision of high-quality beams in terms of spatial coherence, nanobeam, and short pulses to numerous beamlines and users.

Photon Factory (PF) started user operations in 1982, and has provided valuable resources for X-ray research for more than 3,000 users annually from universities, industries, and government institutions. In order to maintain and even increase the productivity of the user community, it is essential to upgrade the PF to ERL. The ERL facility will be constructed as a replacement for the present PF and PF-AR. The superb beam quality of ERL will open up a new era of X-ray science by extending the capabilities of existing synchrotron X-ray sciences, and will also provide an opportunity for a paradigm shift from “static and homogeneous” systems to “dynamic and heterogeneous” systems to many users.

Chapter 3 Enabling Methodologies

3.1 Diffraction Imaging Using Coherent Beams

3.1.1 Introduction

Microscopy has contributed greatly to our knowledge of structures and functions not only in biology but also in various other fields and is an indispensable tool in nanoscience and nanotechnology today. Recent progress in microscopy techniques has been extraordinary. Surface atomic arrangements can be observed by scanning tunneling microscopy or atomic force microscopy, and the atomic-scale structures of thin films can be evaluated by transmission electron microscopy, while X-ray microscopy has lagged behind with respect to resolution. Very high resolution X-ray imaging has been the subject of considerable research over the past few decades. However, the spatial resolution of X-ray microscopy with a lens is limited by the manufacturing quality of the X-ray optics. More recently, lensless X-ray imaging has emerged as a powerful approach that is able to circumvent this limitation; coherent X-ray diffraction imaging (CXDI) was proposed by Sayre [1] in 1980 and demonstrated by Miao et al. [2] in 1999. When a finite specimen is illuminated by coherent X-rays, the weakly scattered X-ray photons form a continuous diffraction pattern in the far field. This continuous pattern can be sampled at a spacing finer than the Nyquist frequency. Phase retrieval calculation [3] is performed to reconstruct a two-dimensional (2D) or three-dimensional (3D) image. The original geometry of CXDI, in which the sample is illuminated with an X-ray plane wave, is limited to an isolated object. Two experimental approaches have been proposed to overcome this serious limitation. One is keyhole CXDI [4], in which a finite expanding beam can be used to define a finite region for the wavefield leaving the object. The other approach is ptychographic CXDI [5], in which a probe is scanned across the sample and the diffraction pattern is observed at each beam position. CXDI is performed in a forward geometry, which originates from the desire to extend the ideas of crystallography to nonperiodic samples. On the other hand, one of the most productive applications of CXDI has been in the study of nanocrystals, which is Bragg CXDI [6] in a reflection geometry. Bragg CXDI provides high-resolution 3D images of strain within a nanocrystal.

3.1.2 Scientific goals and challenges

A scientific goal of CXDI is the nondestructive and elemental characterization of nano-meso-microscale structures buried within large and/or thick specimens. This multiscale information is particularly important for understanding the element/property relationships linking nano-scale structures to macroscopic functional properties, such as the optical properties of arrayed nanoparticles [7], the mechanical properties of bulk nanostructured materials [8], and neural networks connected with synapses [9]. To achieve this goal, further improvement of the spatial resolution of CXDI remains a challenge. The spatial resolution of CXDI is limited, in principle, by only the X-ray wavelength and the largest scattering angle that can be recorded. The theoretically achievable resolution is half of the X-ray wavelength, which should result in atomic resolution. However, it is difficult to achieve atomic resolution since the diffraction intensity rapidly decays in accordance with a power law. In addition, the dose of X-ray radiation to the object is increased by many orders of magnitude, thus making radiation damage a practical limitation of the achievable spatial resolution. A preliminary analysis of the radiation dose required for CXDI and the dose tolerance of frozen-hydrated life-science samples suggested that 3D tomography at a resolution of about 10 nm may be possible. In materials science, where samples are less sensitive to radiation damage, it is expected that CXDI can achieve a resolution of 1 to 2 nm by using modern X-ray synchrotron sources [10].

3.1.3 Current status and limitations

Following the first demonstration by Miao *et al*. [2], CXDI has been used by a growing number of groups, including for the demonstration of imaging materials and biological specimens. Nishino *et al*. [11] have obtained a very exciting image of a dehydrated chromosome in an experiment at room temperature. The spatial resolution was estimated to be 38 nm for two dimensions and 120 nm for three dimensions. In addition, they noted significant degradation of resolution due to the accumulated radiation dose. Jacobsen *et al*. [12] and Lima *et al*. [13] have reported that artifacts in 2D images due to dehydration, ice crystallization, and radiation damage are greatly reduced by plunge-freezing specimens. These demon-

strations represented an important step towards the high-resolution imaging of cells in their natural, hydrated state.

The use of highly focused incident X-ray beams is also effective for high-resolution imaging since it allows us to collect higher angle diffraction data at a high signal-to-noise ratio. Recently, higher-resolution X-ray diffraction microscopy has been realized using advanced X-ray focusing devices such as refractive lenses and total reflection mirrors. Takahashi *et al*. have developed high-resolution CXDI using the Kirkpatrick-Baez optics installed in SPring-8. The spatial resolution has reached the sub-5-nm scale [14] in two dimensions and the sub-10-nm scale [15] in three dimensions in their measurements of metallic nanoparticles. However, the resolution is still poor compared with the expected dose-limited value. In addition, the X-ray exposure time is rather long, ~1000 s for two dimensions and ~9 h for three dimensions. Therefore, high-brilliant coherent X-ray sources are indispensable for achieving higher-resolution CXDI in a short exposure time.

In CXDI, the stability of the beam, optics, and instrument is also a crucial issue. For example, the performance of ptychographic CXDI is degraded by positioning errors due to the drift between the sample and illumination optics. Therefore, experiments must be performed using a highly stable coherent X-ray beam and in a very stable environment. Recently, Takahashi *et al.* have reported an experimental result of ptychographic CXDI with sub-10-nm resolution in a field of view larger than 5 μm, which was performed in an environment stabilized to less than 0.01ºC on the extremely steady ground of SPring-8 [16]. Further stabilization is necessary to achieve a higher resolution and a larger field of view.

3.1.4 Future prospects with ERL

ERL is expected to provide an extremely high-brightness coherent X-ray beam, which will allow us to easily improve the spatial resolution of CXDI, and will also open up exciting new opportunities such as structural dynamic studies. On the other hand, the X-ray free-electron laser (XFEL) is also a promising X-ray source for CXDI. Recently, the first lasing and operation of angstrom-wavelength free-electron lasers were realized at facilities in the U.S. [17] and Japan [18]. Two exciting results, single-shot imaging [19] and nanocrystallography [20], have been reported. Note that the character of X-rays obtained with ERL and XFEL is markedly different. XFEL provides seven-orders-of-magnitude higher peak brightness than ERL, although the average brightness of both X-ray sources is equivalent. It is expected that the CXDI of single particles using the single-shot “diffract and destroy” approach in XFELs [21] will break the resolution limit due to the radiation and hence can achieve atomic resolution. However, this approach limits the types of samples, i.e., the samples must be reproducible. On the other hand, ERL provides four-orders-of-magnitude higher coherent flux than the third-generation synchrotron radiation. For a generic object, the diffraction intensity decays with a power law $q^{-\alpha}$ ($\alpha \approx 4$). Therefore, by using ERL, the achievable resolution of CXDI will improve by one order of magnitude at the same measurement time as the third-generation synchrotron radiation, which will approach the dose-limited value. Thus, ERL can realize “ultimate nondestructive” CXDI. CXDI with XFEL and CXDI with ERL should be complementary techniques. The most interesting application of CXDI in ERL is the 3D imaging of whole cells. Figure 3-1 shows a schematic of high-resolution 3D ptychographic CXDI for biological samples. Here, first a cell is cryogenically

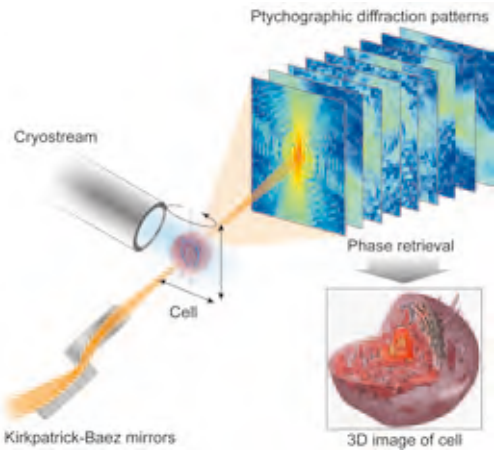

Figure 3-1
Schematic of high-resolution 3D ptychographic CXDI for biological samples.

cooled. A coherent X-ray beam generated from ERL is focused to a 1-μm spot using a Kirkpatrick-Baez mirror. The focused beam is then scanned across the cell and the diffraction pattern is observed at each beam position and at each incident angle. By an iterative phasing method, the shape of the whole cell and the spatial distribution of the organelles can be three-dimensionally visualized at 10 nm resolution, which will provide key insights, for example, about the organization inside cells.

REFERENCES

[1] D. Sayre, *Springer Lecture Notes in Physics* **112**, edited by J. Schlenker, M. Fink, J.P. Goedgebuer, V. Malgrange, J.C. Viénot, and R.H. Wade 229 (1980).
[2] J. Miao, P. Charalambous, J. Kirz and D. Sayre, *Nature* (London) **400**, 342 (1999).
[3] J.R. Fienup, *Appl. Opt*. **21**, 2758 (1982).
[4] B. Abbey *et al*., *Nat. Phys*. **4**, 394 (2008).
[5] J.M. Rodenburg *et al*., *Phys. Rev. Lett.* **98**, 034801 (2007).
[6] M.A. Pfeifer *et al.*, *Nature* (London) **442**, 63 (2006).
[7] H.A. Atwater and A. Polman, *Nature Mater.* **9**, 205 (2010).
[8] "*Bulk Nanostructured Materials*", edited by Michael J. Zehtbauer and Yuntian T. Zhu, (Wiley-VCH, Weinheim, 2009).
[9] J.W. Lichtman and J.R. Sanes, *Nat. Rev. Neurosci.* **9c** 417 (2008).
[10] S. Marchesini *et al*., *Opt. Express* **11**, 2344 (2003).
[11] Y. Nishino *et al*., *Phys. Rev. Lett.* **102**, 018101 (2009).
[12] X. Huang, C. Jacobsen *et al*., *Phys. Rev. Lett.* **103**, 198101 (2009).
[13] E. Lima et al., *Phys. Rev. Lett.* **103**, 198102 (2009).
[14] Y. Takahashi *et al.*, *Phys. Rev. B* **80**, 054103 (2009).
[15] Y. Takahashi *et al*., *Nano Lett.* **10**, 1922 (2010).
[16] Y. Takahashi *et al*., *Phys. Rev. B* **83**, 214109 (2011).
[17] P. Emma *et al*., *Nat. Photonics* **4**, 641 (2010).
[18] T. Ishikawa*t et al*., *Nat. Photonics* **6**, 540 (2012).
[19] M.M. Seibert *et al*., *Nature* (London) **470**, 78 (2011).
[20] H.N. Chapman *et al*., *Nature* (London) **470**, 73 (2011).
[21] R. Neutze *et al.*, *Nature* (London) **406**, 752 (2000).

3.2 Macromolecular Structures from Nanocrystals

3.2.1 Introduction

Macromolecular crystallography (MX) emerged in the early 1970s and is today one of the most powerful techniques for analyzing enzyme mechanisms and macromolecular interactions at the atomic level. To properly understand the three-dimensional conformation of proteins and nucleic acids, and to fully appreciate their mode of regulation at the atomic level is of prime importance to clarify biological reactions and develop a better approach to cell regulation for improving human health. The key role played by third-generation synchrotron sources in solving a large number of crystal structures is now well established, together with novel advances in phasing techniques, data collection and processing, and the associated computer programs that have led the field of structural biology to a more accessible science for many academics and companies.

There are a number of unique applications that demand specific X-ray beam characteristics such as extremely short pulses with durations shorter than that found on most of the third-generation synchrotrons presently under development. These applications are the motivation for MX at ERL. In addition, the scientific capabilities of a novel, sub-picosecond, highly coherent X-ray nanobeam can be greatly enhanced if it is accompanied by an X-ray detector with extremely short read-out time. To motivate the system developed here, we briefly address some of the biological applications envisioned for ERL. Though not a comprehensive set of applications, the experiments described in this section give a flavor of the science program for structural biology which can progress with the construction of ERL. The possibilities of synergistic use of other techniques are considered in order to fully characterize the biological systems studied.

3.2.2 Scientific goals and challenges

Complexes of proteins and/or nucleic acids are the most functional entities within cells. The processes of life fundamentally depend on the interactions of these molecules in the living cells, and are therefore closely related to the atomic and geometrical structures of these complexes. Therefore, the molecular structures of biological complexes are essential for a complete understanding of the processes occurring within the living cell, for a rational design of drugs, and for vaccine design.

The unequal molecular weight distribution in the coordinates available from the Protein Data Bank (PDB) clearly illustrates the challenges faced by structural biologists when dealing with extremely large macromolecular complexes (Fig. 3-2). In order to determine the structure of complexes made of different molecules, it is necessary to overcome several bottlenecks related to the expression and purification of each subunit, formation of stable complexes of biological significance, and then crystallization. A well-known axiom in structural biology is that "the bigger the molecule, the smaller the crystal". In general, if extremely large complexes do form crystals, they tend to assemble in nano-scale crystals, which are difficult to identify, handle, and usually diffract at a poor resolution when exposed to the classical X-ray beam of third-generation synchrotrons. The challenges for structural biologists when attempting to study such extremely large complexes are thus entirely related to the size of these nano-scale crystals, how to identify and present them to the X-ray beam, and how to collect the best data in terms of usable resolution and completeness if not from one single crystal, from a series of crystals which will then be merged.

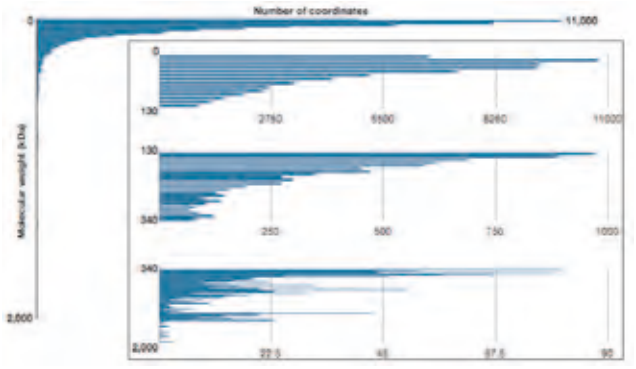

Figure 3-2
Distribution of coordinates in the PDB according to the molecular weight of the molecules.

Described below is a non-exhaustive list of some extremely large macromolecular complexes and applied methodology that would benefit from the implementation of such a nanobeam at ERL, together with a short description of the challenges in attempting to solve such structures.

Chromatin super-structure

The whole genome is enclosed in the DNA sequence and the chromatin that forms compact structures as encountered in chromosomes. While chromosomes within the nucleus adopt preferred conformations, various DNA elements are brought in close contact through defined aggregates, ready for transcription and DNA replication [1]. The overall architecture of eukaryotic genomes remains poorly understood, and so is the precise structure of the chromatin (Fig. 3-3(a)). Chromatin fibers are known to form higher order structures of 30 nm thickness, which could be studied by using such a nanobeam, giving further insights into this highly compact structure of the chromatin at the atomic level.

NEMO signaling complex

Ubiquitination is a reversible posttranslational modification of proteins, which consists of the covalent attachment of ubiquitin. The regulation of the NF-κB canonical pathway is mostly done through the action of kinase complexes, eventually involving the regulatory subunits called NEMO. It has been proposed that NEMO acts as a scaffolding platform for the formation of a large and complicated complex made of several subunits, which will regulate the activation of the NF-κB canonical pathway (Fig. 3-3(b)) [2]. Characterization of how this highly organized complex is structured would deepen our understanding of the NF-κB signaling pathway, and favor the development of new drugs for its control.

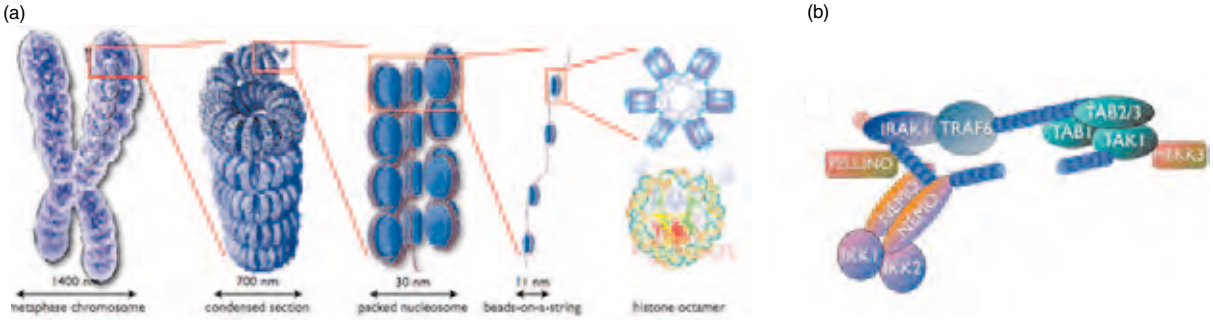

Figure 3-3
Examples of large macromolecular complexes. (a) the chromatin super-structure (adapted from Albert *et al*., 1994). (b) NEMO signaling complex (adapted from [2]).

New imaging and phasing approaches

Novel advances in phasing techniques in the last decade have greatly assisted the structure determination of molecules otherwise "unsolvable" by classical methods. By attempting to solve extremely large macromolecular complex structures, the current state-of-the-art in structure determination techniques may become outdated, and new phasing approaches will need to be developed. Additionally, characterizing the structure of molecules in their natural environment, i.e. in living cells, would greatly help fully unravel their functional mechanism and interacting behavior. New methodologies such as structure determination of non-identical objects, and advanced imaging through the addition of known diffracting "markers" inside the cell matrix are approaches that might enhance further phasing possibilities, and would clearly benefit from ERL.

3.2.3 Current status and limitations

In recent years, a large number of structural genomics projects have actively addressed the purification and crystallization of functional proteins, resulting in an enormous increase in throughput in MX. However, the crystallization of functional complexes remains a problem, as large molecules tend to form nanocrystals, which are difficult to identify, and are often considered as not exploitable and therefore discarded by structural biologists. To date, the smallest crystal that could be used for a complete data collection at a classical third-generation synchrotron beamline was of microscale order, ~3 μm, which was studied at the micro-beam beamline BL32XU in SPring-8 (K. Hirata, personal communication).

Going lower in crystal size requires a more sophisticated setup, as implemented in the Linac Coherent Light Source (LCLS, U.S.) where nano-scale crystals of photosystem I were exploited for structure determination of an extremely large macromolecular complex (1 MDa, 36 proteins, 381 cofactors) [3]. In this work, a singularly high amount of nanocrystals was exposed to a hard X-ray free-electron laser beam, the data sets were merged, and the structure was solved at a final interpretable resolution of 8.5 Å. Although the radiation damage effect depends to some extent on the sensitivity of individual samples to radiation, the use of stronger beams on unfrozen crystals as illustrated at the LCLS clearly showed that the crystals cannot survive multiple exposures to such intense X-rays, leading to a strategy of "on-the-fly shooting" of randomly oriented independent crystals. Although very efficient when crystals are available in large quantities, the ratio of the number of samples successfully shot by the X-ray beam to the number of X-ray pulses used is far from unity, and so the hit rate needs to be improved. An additional problem appears while indexing each picture when the X-ray data are collected from randomly oriented crystals.

MX beamlines as implemented in third-generation synchrotrons are also limited for studies of extremely fast biological reactions, such as very transient complex formations between various proteins, notably because of the low frequency in X-ray delivery, but also due to the slow read-out X-ray detectors. Similarly, highly brilliant X-ray beams are needed to improve the diffracting power of nanocrystals, which are often shadowed by noises resulting from the crystals' surroundings, non-Bragg diffractions, etc. Some of these restrictions can be overcome at the XFEL facilities, although further improvements are still needed.

3.2.4 Future prospects with ERL

The construction of an ERL MX facility would be an unprecedented advantage for the study of extremely large macomolecular complexes. As introduced above, larger molecules tend to adopt smaller crystal forms. The highly coherent and intense X-ray beam with nanometer size resulting from ERL would allow diffraction studies on such small objects. Together with the implementation of extremely fast read-out and highly sensitive X-ray detectors, as well as perfectly synchronized sample changers to optimize the hit rate, it would become possible to conduct structural studies using nanometer-scale biological samples. Efforts should also be made to develop new techniques that would allow the structural characterization of non-crystalline objects present in living cells, which could be implemented by taking advantage of the unique properties of the X-ray beam from ERL. Although X-ray beams from XFEL will remain stronger than those from ERL, the average brightness of the beam at ERL will be higher than all presently implemented third-generation synchrotrons. This is a clear advantage over free-electron laser beams as it will allow data for several images to be collected from single crystals before the samples are completely lost due to radiation damage, which will facilitate the indexing of diffraction pictures. Finally, the significantly higher frequency of ERL X-ray delivery (1.3 GHz) will be particularly valuable for structur-

ally characterizing macromolecular complexes that occur only momentarily and cannot be studied using classical beamlines as implemented in third-generation synchrotrons or free-electron lasers.

REFERENCES

[1] Z. Duan *et al.*, *Nature* **465**, 363 (2010).
[2] J. Gautheron *et al.*, *Cell. Mol. Life Sci*. **67**, 3101 (2010).
[3] H.N. Chapman *et al.*, *Nature* **470**, 73 (2011).

3.3 Capturing Ultrafast Phenomena

3.3.1 Introduction

The speed of modern technology is accelerating. For example, in computing, the speed of the CPU clock and random access memory is now of the order of GHz, or 100 picoseconds in time. The speed increase in computer technology is closely related to the development of advanced materials. Ferroelectric and magnetoresistive materials are critical components in novel fast storage devices, and it is essential to understand which parameters control the fast switching in storage devices. In general, various advanced materials are used as key components in modern devices such as catalytic systems, batteries, random access memory devices, and electronic devices. Proteins are a natural functional material and play a key role in living organisms. Since the working state of advanced and functional materials is intrinsically dynamic, it is important to characterize their atomic and electronic structures, chemical composition, and magnetic properties in the working state.

3.3.2 Scientific goals and challenges

The goal of ultrafast science is to capture fundamental events of chemical, material, and biological processes in real time, and ultimately to understand and develop better functional materials indispensable to modern life. High repetition rate, femtosecond X-ray sources are powerful tools for obtaining element-selective electronic and magnetic information by utilizing core electron excitations and for clarifying structural dynamics with atomic resolution.

A challenge in ultrafast chemistry is to understand the dynamic interplay between electronic structure (energy levels, charge distributions, spin) and molecular structure (bond distances, arrangements, coordination, etc.). Electronic and molecular structures of short-lived intermediate states between reactant and product are particularly important because their subtle changes ultimately determine the reaction pathways. For example, it is well known that catalytic reactions are dynamic and heterogeneous processes. The formation of chemical bonds between the reactant molecules and the catalyst leads to the generation of short-lived intermediate states, which eventually lower the activation energy and thus facilitate the generation of product molecules. Therefore, it is essential to understand the electronic and atomic structures of time- and space-resolved catalytic surfaces in the working state for rational catalyst design (Fig. 3-4).

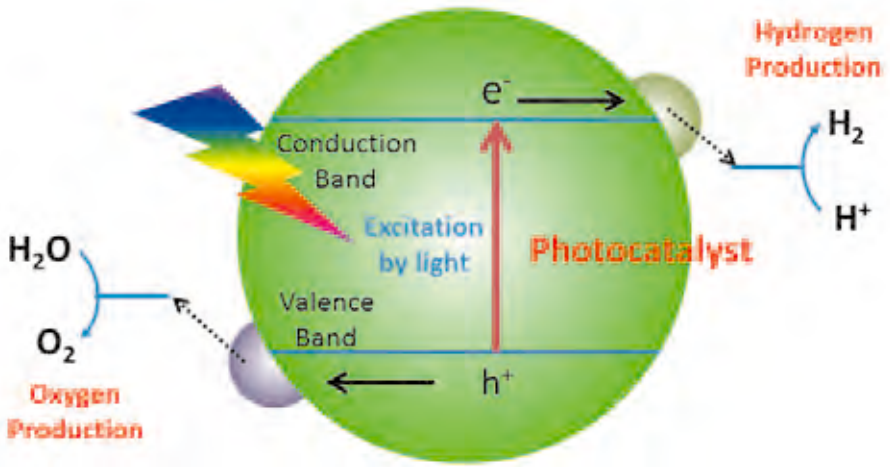

Figure 3-4
Revealing ultrafast dynamics on the photocatalyst surface is a key to realize effective light-energy conversion [1].

Ultrafast condensed matter physics focuses on elementary excitations and their mutual interactions in real time, in order to understand the intrinsically dynamic nature of materials. The energy scale of elementary excitations spans from meV to eV range, which corresponds to the time range of picosecond to femtosecond. For example, the energy scale of phonons is of the order of several meV, which is accessible with sub-picosecond pulse duration. Elementary excitations such as magnon, orbiton, charge transfer, and plasmon have a higher energy scale than phonons, and therefore accessing such excitations requires shorter pulse durations by time-resolved X-ray techniques. In turn, spectroscopic measurement in energy space such as inelastic X-ray scattering is a complementary method for capturing the dynamic nature of elementary excitations in condensed matter.

Ultrafast phenomena in biology are often related to photochemistry and photoresponses. Revealing the mechanism of photosynthetic systems in plants is one of the grand challenges of biological science. It is also relevant to renewable energy by artificial photosynthesis. Although the high-resolution structure of photosystem II (PSII) was recently solved by X-ray crystallography, more studies on ultrafast redox and structural dynamics of the core manganese complex in its working state are still necessary in order to elucidate the key reactions of the PSII, and the oxidation of water molecules to produce dioxygen and protons. Slower dynamics of the order of nanosecond or longer involve unique information on the hierarchal structures in biological systems and soft matter. This time range will also be covered by X-ray photon correlation spectroscopy, as mentioned in Section 3.5.

3.3.3 Current status and limitations

Because current X-ray sources based on storage ring technology have a pulse duration of 50 picoseconds, the capability in the femtosecond time domain is very limited. The bunch slicing technique utilizes the interaction of electron bunches in the storage ring with femtosecond near-IR laser pulses, and eventually produces femtosecond X-ray pulses. However, the total photon flux is three orders of magnitude lower than the flux before slicing which limits the applicability of this technique, and the repetition rate is currently limited to kHz order which is defined by the repetition rate of the laser system.

SASE-XFEL is an attractive X-ray source for ultrafast studies in the femtosecond time domain, since it typically produces X-ray pulses with 10 femtosecond pulse duration with 10^{12} photons per pulse. However, when typical pump-probe type experiments are conducted, the low repetition rate of SASE-XFEL (~100 Hz) mismatches the high repetition rate of optical UV-visible-IR lasers (~MHz). Typically in pump-probe type experiments, a specimen gives only a very weak signal for a single excitation, or sometimes the specimen is easily damaged by the high peak power of the excitation laser. Therefore, the accumulation of weak signals with a high repetition rate is indispensable in such cases to obtain data with an appropriate signal-to-noise ratio. The mismatch of the repetition rate of SASE-XFEL and optical lasers will be a serious problem, given the limited number of beam lines and beam time of SASE-XFEL.

3.3.4 Future prospects with ERL and XFEL-O

The major advantages of the high repetition rate and femtosecond pulsed features of ERL are that element-selective electronic and magnetic information can be obtained by utilizing core electron excitations and that structural dynamics can be accessed with atomic resolution. Weak optical pumps with high-repetition lasers are particularly suitable for pump-probe experiments with ERL. ERL will open up a new era of time-domain science by covering from femtosecond to slower time scales by using a single light source.

High-repetition, ultralow-emittance multi-GeV electron bunches and a low loss optical cavity constructed from high-reflectivity Bragg crystals can create an X-ray FEL Oscillator (XFEL-O), which is planned in the second phase of the ERL project. The X-ray beam from the XFEL-O will be Fourier-transform limited, have tunable wavelength, and the peak power will be small enough that it will not damage samples. The beam will have an average brightness 10^3 – 10^5 times greater than is available with existing or planned sources. The X-ray beams produced by the XFEL-O will be fully Fourier-limited with the energy bandwidth of 1 meV, thus upgrading existing techniques and enabling novel ones such as nonlinear X-ray optics, inelastic scattering, two-photon correlation spectroscopy, and transient grating spectroscopy.

REFERENCES
[1] K. Maeda and K. Domen, *J. Phys. Chem. Lett.* **1,** 2655 (2010).
[2] Y. Umena *et al*., *Nature* **473**, 55 (2011).

3.4 Coherent Nanobeam and Imaging

3.4.1 Introduction

One of the advantages of an ERL source over the conventional third-generation synchrotron sources is that it provides a high-brightness synchrotron X-ray beam with very low emittances in both the horizontal and vertical directions. Because the X-ray beam from the source will be almost diffraction-limited, it will be readily focused to one nanometer by using X-ray focusing devices that will be developed in the near future. Therefore, non-destructive X-ray imaging and tomography with a spatial resolution of one nanometer or less will be achieved. Pump-probe X-ray microscopy with a time resolution of sub-picosecond will also be realized by the ultrashort pulse X-rays from the source. The unprecedented high spatial and temporal resolutions will be useful for a wide range of applications in science and technology such as materials science, environmental science, biology, medicine, archaeology, palaeontology, and industrial technology.

3.4.2 Scientific goals and challenges

Imaging with an X-ray nanobeam will have broad scientific and technological applications. An example of such applications is nano-scale observation of buried structures in electronic devices. To develop new electronic devices, it is necessary to evaluate crystal structures and strain distributions that determine electronic properties. Nano- or subnano-scale spatial resolution X-ray imaging, which will be realized by the X-ray nanobeam, will provide powerful ways to non-destructively investigate buried structures in three-dimensionally integrated devices in the future. Electronic devices involving light-element materials (carbon nanotube, graphene, organic materials, etc.) can also be investigated by high-sensitive X-ray phase imaging techniques. Another example is biological applications: the unprecedented spatial resolution will make it possible to visualize the inner structures of subcellular organelles (nucleolus, mitochondria ribosome, etc.) and biomembranes (cellular membrane, nuclear membrane, mitochondrial membrane, etc.) whose structures and functions in living cells have not yet been fully investigated.

Research on the dynamics of materials is another exciting application of nanobeam imaging, including the investigation of structural transitions through intermediate states that are expected to play important roles in chemical reactions. For example, X-ray microscopy with a sub-picosecond temporal resolution can be used to study the mechanism of photosynthesis in chlorophyll. A full understanding of the mechanism of photosynthesis in plants may lead to the development of high-efficiency artificial photosynthesis. Chemical reactions on the surfaces of catalytic nanoparticles and nanoporouses induced by light illumination are another application of ultra-high-temporal-resolution X-ray microscopy.

Of course, the above examples are not exhaustive; other applications include research on phase transitions under extreme conditions, fuel-cell and solar batteries, optoelectronic and spintronics devices, and so forth. Thus, X-ray nanobeams will be useful for overcoming challenges and attaining various goals in a wide range of scientific and technological fields.

3.4.3 Current status and limitations

An X-ray beam with a size of one nanometer or less requires the development of both the X-ray source and X-ray focusing device. The X-ray source must generate an X-ray beam with high spatial coherence in both the horizontal and vertical directions in order to achieve two-dimensional diffraction-limited X-ray focusing. From the well-known van Cittert-Zernike theorem, the spatial coherence length L is approximately given by

$$L = \frac{1}{2\pi}\frac{\lambda R}{\sigma_s}$$

where λ is the wavelength of X-rays, R is the distance of the observation point from the source, and $2.35\sigma_S$ corresponds to the FWHM of the intensity distribution of the source. Therefore, L is inversely proportional to σ_S for given λ and R. For example, the horizontal and vertical source sizes of a typical undulator beam-

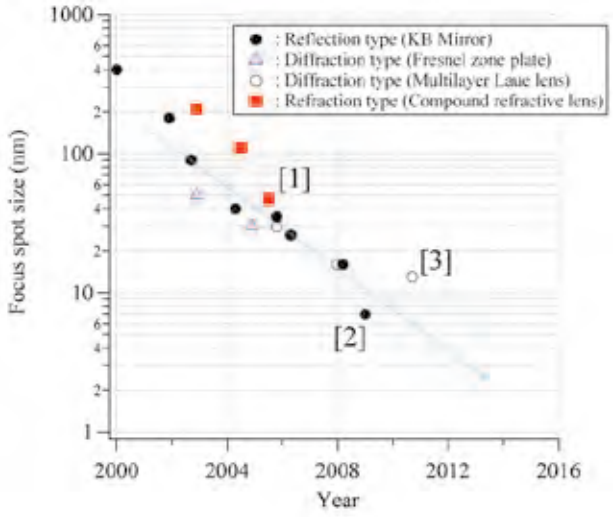

Figure 3-5
Recent progress in X-ray focusing technology.

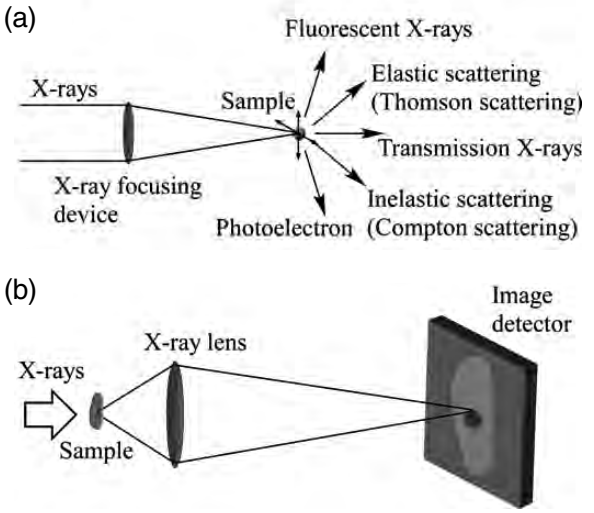

Figure 3-6
Two types of X-ray microscopies: (a) scanning type (scanning X-ray microscopy) and (b) imaging type (X-ray imaging microscopy).

line at SPring-8 are about 300 μm and 7 μm, so the spatial coherence lengths in the horizontal and vertical directions for 8.2 keV are about 2 μm and 100 μm at a position 30 m downstream from the source. Hence, the spatial coherence in the horizontal direction is much lower than that in the vertical direction, preventing us from achieving two-dimensional diffraction-limited focusing. A very small pinhole has been used to overcome this problem, but it reduces the flux of the X-ray beam available by two or three orders of magnitude.

The development of X-ray focusing devices is also essential to obtain an X-ray beam of one nanometer size. Because the interactions of hard X-rays with matter are very small, optical devices for X-rays inevitably require sufficient thickness (typically more than 1 μm), while in the plane perpendicular to the X-ray beam, structures as fine as the desired focal spot are necessary. Such high-aspect ratio structures are generally difficult to fabricate, but much effort has been made for more than half a century. Figure 3-5 shows recent progress in hard-X-ray focusing technology for three types of X-ray focusing devices (reflection, diffraction, and refraction types). It can be seen that the development of X-ray focusing devices is almost linear like Moore's law for ULSI, and now state-of-the-art X-ray focusing devices can produce focusing sizes of around ten nanometers [2, 3]. Thus, it is expected that one nanometer focusing will be achieved by 2020.

3.4.4 Future prospects with ERL

With an ERL source, an X-ray beam with a source size of 7 μm can be achieved in both the horizontal and vertical directions. Hence, an X-ray beam with high spatial coherence in both directions will be readily provided. For example, at an experimental station 30 m downstream from the source, a spatial coherence length of around 100 μm will be possible. This will make it easier to focus the X-ray beam to one nanometer by using X-ray focusing devices that will be developed in the near future. Thus, non-destructive X-ray imaging and tomography with a spatial resolution of one nanometer or less will be achieved.

X-ray microscopy can be classified into two types: scanning type and imaging type (see Fig. 3-6), and both types will reap benefits from an ERL source. In scanning-type X-ray microscopy, a sample is scanned with respect to a focused X-ray beam, and signals such as transmission X-rays (absorption and phase shift), fluorescent X-rays, elastic scattering (Thomson scattering; see 3.1), and photoelectrons are measured. The spatial resolution of this type of X-ray microscopy is determined by the size of the focused X-ray beam, and therefore a spatial resolution of one nanometer will be achieved. For example, the distributions of elements and chemical bondings around them will be mapped with a spatial resolution of nanometer scale by measurements of fluorescent X-rays and EXAFS spectra. Scanning-type X-ray microscopy can be applied only to small samples because of its small field-of-view (FOVs), but imaging-type X-ray microscopy allows us to perform imaging with a large FOV (typically a few hundred micrometers), and thus observe large samples. By combining it with interferometric and holographic techniques, high-sensitivity X-ray imaging should also be possible.

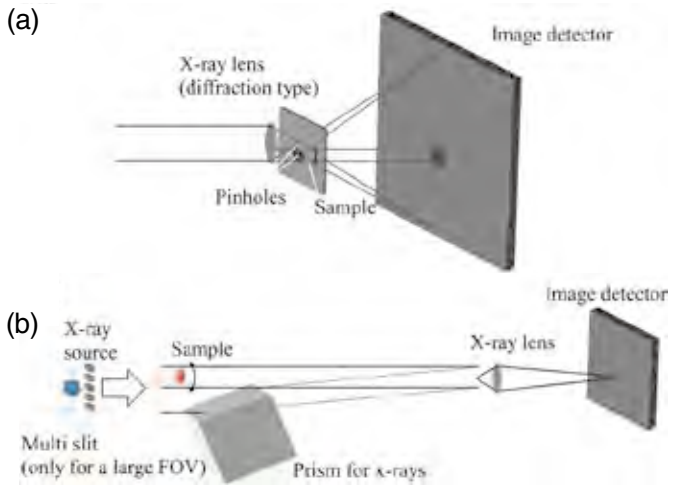

Figure 3-7
Examples of holographic X-ray microscopy that will be realized by ERL.

In addition to performing standard X-ray microscopies as shown in Fig. 3-6 under diffraction-limited conditions, it is also possible to use holographic techniques, as shown by the examples in Fig. 3-7. Figure 3-7 (a) shows an example of Fourier transform holography. With this technique, the phase of X-rays diffracted by a sample is experimentally measured, and the distribution of electron density in real space is uniquely determined. The spatial resolution of this technique is limited by the size of focusing, but if a very small pinhole with a size of less than one nanometer is fabricated and then put at the focusing point, a sub-nanometer spatial resolution should also be possible. Another example is shown in Fig. 3-7 (b) where a Leigh-Upatnieks-type holographic technique [4] is combined with X-ray imaging microscopy. In this case, large FOV X-ray phase imaging with a spatial resolution of one nanometer should be possible.

In addition to high spatial resolution, a high temporal resolution will be attained by sub-picosecond wide ultrashort X-ray pulses from the ERL source. Although the flux of a nano-focus X-ray beam is not enough to achieve real-time measurement with a sub-picosecond time resolution, phenomena that can be repeated by external stimuli can be studied by the so-called pump-probe technique. In pump-probe measurement, a sample is excited (or modified) when it is hit by a pump pulse, and the response to the pump pulse is measured by a probe pulse after an adjustable time delay. Therefore, the time resolution is determined by the widths of the pump and probe pulses. By combining this technique with high-spatial resolution X-ray microscopy, we can study dynamics on the nanometer scale. Thus, the coherent X-ray beam from the ERL source will open up new opportunities for X-ray imaging not available with conventional third-generation synchrotron X-ray sources.

REFERENCES

[1] C.G. Schroer *et al.*, *Proc. 8th Int. Conf. X-ray Microscopy*, IPAP Conf. Series **7**, 94 (2006).
[2] H. Mimura *et al.*, *Nature Physics* **6**, 122 (2010).
[3] T. Koyama *et al.*, *AIP Conf. Proc.* **1365**, 24 (2011).
[4] Y. Suzuki, *Rev. Sci. Instr.* **75**, 1026 (2004).

3.5 X-Ray Photon Correlation Spectroscopy

3.5.1 Introduction

The use of coherence opens up a new opportunity to probe the equilibrium or steady-state dynamics of systems. X-ray Photon Correlation Spectroscopy (XPCS) is a method to observe complex dynamics on the nano-scale [1]. In XPCS, (partially) coherent X-rays are impinged upon a sample, and the dynamics of any fluctuations within the sample are characterized. In the conventional XPCS technique, intensity correlation function, $g^{(2)}(\boldsymbol{q}, t)$, is obtained from the correlation among consecutive speckle scattering images. The time constants of a system are obtained as a function of scattering vector, $\boldsymbol{q}$. Direct information about the dynamic properties of systems can be investigated through the shape of the correlation function. This correlation function is related to the normalized intermediate scattering function (ISF), $f(\boldsymbol{q}, t)$

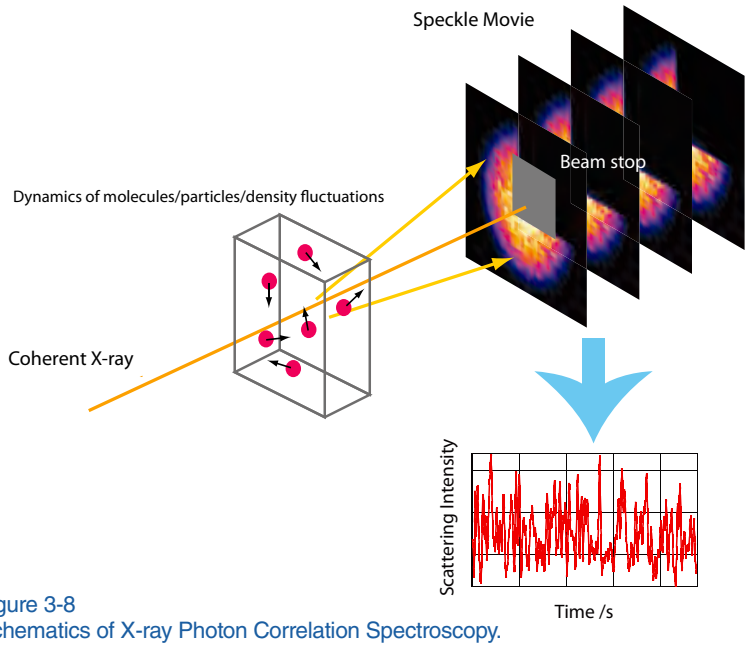

Figure 3-8
Schematics of X-ray Photon Correlation Spectroscopy.

= $S(\boldsymbol{q}, t)/S(\boldsymbol{q}, 0)$, of the system through $g^{(2)}(\boldsymbol{q}, t) = 1 + A\ |f(\boldsymbol{q}, t)|^2$, where A is the optical contrast. The ISF is equivalent to the sample's density-density autocorrelation function; thus, the analysis of XPCS results is crucial for comparing theoretical results with experimental results.

Recently, another class of XPCS technique has attracted much attention: Speckle Visibility Spectroscopy (SVS). This technique analyzes the visibility of each speckle pattern to obtain information equivalent to that which can be obtained with conventional XPCS [2]. If the sample is static on the time scale of exposure time, then the contrast in the speckle pattern will be high. If, on the other hand, the sample evolves on this time scale, the speckle pattern will have a lower contrast, which results in decreased visibility. Thus, by analyzing the visibility of such patterns, each for a different exposure time, the time constant of the system can be measured on time scales down to the minimum exposure time/interval between X-ray pulses.

The correlation of speckle patterns leads to another class of technique. When the sample does not exhibit translational symmetry but shows local symmetry such as icosahedral order, access to such local properties is normally prevented by the intrinsic spatial and temporal averaging in conventional scattering experiments with incoherent X-rays. Recently, X-ray Cross Correlation Analysis (XCCA) has been successfully introduced to investigate a quasi-static hard-sphere glassy system [3]. This analysis reveals the hidden symmetry of a locally ordered structure (Fig. 3-8).

3.5.2 Scientific goals and challenges

The target of XPCS measurement is to reveal the dynamics in the range of nanoseconds to several hours. There are a number of dynamics that can be investigated with XPCS: glassy materials, granular materials, membranes, polymers confined to a narrow space or surfaces, etc. There are several classes of XPCS experiment that will be possible at the ERL facility but are impossible at current facilities. These include:

Hierarchical Dynamics

Soft matter generally shows spatiotemporally hierarchical structures, ranging from nanometers to several millimeters and from nanoseconds to several hours/days or more. This hierarchical structure plays an important role in the appearance of complex and unique properties of soft matter. XPCS will be invaluable for elucidating such hierarchical structures, since it can investigate shorter length scales than can be achieved with optical techniques and longer time scales than can be achieved with neutron inelastic scattering techniques. It can also be used to investigate opaque specimens that cannot be studied with optical techniques. By analyzing the scattering pattern obtained in XPCS measurement, it is possible to investigate the structure of a system in addition to its dynamics; thus, both spatially and temporally hierarchical structures can be elucidated in a single experiment.

Observation of Dynamic Heterogeneity

Dynamic heterogeneity, which is spatiotemporal fluctuations in local dynamic behavior, has recently emerged as a key component underlying the nature of many condensed and disordered materials such as glassy, jammed granular, and soft materials [4]. In conventional XPCS, spatially and temporally averaged information about dynamics is obtained, while the spatiotemporally heterogeneous distribution of different dynamics is to be investigated for a system exhibiting dynamic heterogeneity. In this regard, analysis of the higher-order correlation function of speckle patterns is expected to be highly effective, but it is often hard to perform in a current XPCS with existing light sources. Furthermore, spatially-resolved measurement XPCS combined with, for example, X-ray Near Field Scattering [5] has the potential to visualize the dynamic heterogeneity.

Non-equilibrium dynamics

One of the fascinating things that can be studied with highly coherent X-rays is non-equilibrium dynamics. Dynamics in equilibrium states can be investigated by using conventional XPCS techniques through a second-order intensity correlation function. A higher order correlation function is required as in the case of dynamic heterogeneity to elucidate the non-equilibrium dynamics. The time evolution of dynamics is also important. Regarding the analysis of time-evolved dynamics, the two-time correlation function [6] is a powerful way to elucidate how the time constants and dynamics modes of a system evolve over the course of time. Time-resolved SVS measurement will make it possible to monitor instantaneous dynamics and time-resolved XCCA measurement has the potential to elucidate the time evolution of locally-ordered structures.

High-angle XPCS

Most of the conventional XPCS measurements are limited to the observation of speckle patterns that can be obtained in SAXS geometry. This limitation is defined by the amount of coherent flux. When the scattering angle becomes large, the path difference between the X-rays that are scattered at different positions in a sample increases and will exceed the longitudinal coherent length, which results in the smearing out of speckles. An increase of the coherent length decreases the flux, which results in a lower signal-to-noise ratio of XPCS measurement. In this regard, a high-brightness X-ray source is required to perform XPCS with high Q. A number of targets are within reach if XPCS measurement with high Q is possible: critical fluctuations, order-disorder transitions, and charge or spin dynamics in correlated materials.

As an example of materials showing the properties mentioned above, nanoparticles in suspension are particularly important. There are many daily-life products that consist of nanoparticles in suspension: tires, nanocomposites, and paints. The microscopic mechanism of macroscopic properties such as mechanical, electrical, and viscoelastic properties is a matter of interest. From a static structural analysis such as X-ray scattering and electron microscopy, they are known to form hierarchical structures and to show several stages of dynamics. They possess intrinsic heterogeneity in structure and dynamics and are utilized under conditions far from equilibrium. XPCS studies of non-equilibrium/hierarchical dynamics and dynamic heterogeneity will make it possible to develop, for example, tires with high fuel efficiency and high traction performance, which have a trade-off relationship with each other, based on knowledge of the microscopic viscoelastic mechanism.

3.5.3 Current status and limitations

There are several beamlines at which XPCS is routinely performed: ESRF, APS, and PETRA-III. NSLS-II now plans to construct a new beamline for this technique. Currently, there is no beamline dedicated for XPCS in Japan, although XPCS is available at many SAXS beamlines with an undulator source. XPCS experiments are performed worldwide and many results have been reported. The use of highly intense coherent X-ray pulses at X-ray free-electron laser facilities is now expected to play a vital role in exploring fast dynamics. Combined with the pulse-split-based SVS technique, it is theoretically possible to measure dynamics at time scales of single pulse duration. At LCLS, an X-ray Correlation Spectroscopy beamline is now under construction.

Currently, a major limitation in XPCS experiments is a lack of coherent flux. The signal-to-noise ratio (SNR) of XPCS measurement is linearly proportional to brightness. An XPCS experiment requires (partially) coherent X-rays, and size-defining slits are now utilized to select (partially) coherent X-rays. Owing

to the small coherent fraction in current X-ray sources, most of the incident X-rays should be removed before impinging to samples in order to obtain coherent X-rays; thus, materials with a low scattering power are hardly studied at present. Even with materials with a high scattering power, the SNR is often restricted at a low level, and a long exposure time, sometimes comparable to the time constant of the system, is required.

Another important factor is the development of the detector. Its frame rate restricts the time resolution in conventional XPCS measurement. When the system shows complex dynamics, a two-dimensional detector must be used because ensemble-averaging is necessary; thus, the time resolution is now limited to milliseconds to sub-seconds. A detector suitable for XPCS measurement needs to be developed to improve various kinds of XPCS experiments.

Radiation damage is a main problem to be avoided in XPCS measurement. For the study of dynamics, it is desirable to avoid heating the sample during the measurement because it easily affects the dynamics of the system. Radiation damage can induce, for example, aggregation of particles and cross-linking of polymers. Some XPCS measurements have already suffered from radiation damage. Improved quantum detection efficiency of a novel detector with an appropriate X-ray shutter and sophisticated techniques such as SVS will reduce the effect of heating and radiation damage.

3.5.4 Future prospects with ERL

The SNR of the XPCS technique is linearly proportional to the brightness of the source. Thus, ERL experiments yield greatly improved data for various kinds of XPCS measurement in terms of SNR. Improved SNR makes it possible to analyze higher order correlation functions and instantaneous dynamics with less temporal averaging. The increase of coherent flux makes it easier to perform XPCS with a large scattering angle and short time scale.

One of the fascinating features of ERL in terms of XPCS measurement is its high repetition rate. Although XFEL produces highly coherent X-rays with a short pulse length, the application of XPCS with pulse X-rays from XFEL is restricted to either very fast dynamics (ps - ns) or slow dynamics (> sub-seconds) owing to its slow repetition rate. With a sophisticated detector and X-rays with a high repetition rate from ERL, it will be possible to measure dynamics longer than a nanosecond without any blank in the time domain, thus enabling hierarchical dynamics over a wide temporal scale to be studied. In this regard, development of the XPCS detector is highly required.

Currently, XPCS with ERL is expected to be the best way to investigate hierarchical dynamics, dynamic heterogeneity, and non-equilibrium dynamics. The use of X-rays enables us to investigate the dynamics at nanometer scales, which are superior to other techniques. XPCS studies of dynamics with ERL will cover most of the spatiotemporal scales that are of significance in materials science today.

REFERENCES

[1] M. Sutton, *Cr. Phys.* **9**, 657 (2008).
[2] R. Bandyopadhyay *et al*., *Rev. Sci. Instrum*. **76**, 093110 (2005).
[3] P. Wochner *et al*., *Proc. Nat. Acad. Sci*. **106**, 11511 (2009).
[4] L. Berthier, *Physics* **4**, 42 (2011).
[5] R. Cerbino and A. Vailati, *Curr. Opin. Colloid Inter. Sci*. **14**, 416 (2009).
[6] M. Sutton *et al*., *Optics Express* **11**, 2268 (2003).

Chapter 4 Science Cases

4.1 Natural Photosynthesis

4.1.1 Oxygen evolving manganese complex in photosystem II – Structural approach

4.1.1.1 Introduction

When we consider the sustainability of life on our planet, solar light is the most fundamental energy source to keep the temperature of the atmosphere constant and to enable plants and algae to perform their natural photosynthesis. Many components on the thylakoid membrane are involved in photosynthesis, such as photosystem II (PSII), cytochrome b_6f complex, PSI, NDAP reductase, and ATP synthase, generating NADPH and ATP by using the energy of solar light. Furthermore, RuBP carboxylase and many enzymes in the Calvin cycle generate hydrocarbons from carbon dioxide using the synthesized NADPH and ATP.

PSII performs light-induced electron transfer and water-splitting reactions, which lead to the formation of molecular oxygen. PSII from thermophilic cyanobacteria consists of 17 membrane-spanning subunits, three hydrophilic peripheral subunits, and many cofactors with a total molecular weight of 350 kDa for a monomer. X-ray crystal structures of PSII have been reported at 3.8–2.9 Å resolution for PSII isolated from *Thermosynechococcus elongatus* or *T. vulcanus*, which provide an arrangement of protein subunits and most of the cofactors involved in electron transfer reactions. However, the detailed structure of the Mn_4Ca cluster, which is the catalytic center of light-induced oxygen evolution, has not yet been resolved. The resolution and diffraction quality of PSII crystals have been significantly improved, and the crystal structure of PSII from *T. vulcanus* was successfully solved at a resolution of 1.9 Å [1] as shown in Fig. 4-1.

Electron density distributions for each of the five metal ions in the Mn_4Ca cluster are clearly separated, allowing us to locate the individual metal ions and all of the ligands to the metal cluster unambiguously (Fig. 4-2). Five oxygen atoms forming oxo-bridges between the metal ions are identified, and four water molecules are found to be associated with the metal cluster, some of which may serve as substrates in the oxygen-evolving reaction. The most significant structural feature of the Mn_4CaO_5 cluster is its distorted chair form. The large distortion from a symmetric cubane is principally caused by the existence of Ca and O5, the fifth oxo-bridge connecting three Mn ions and one Ca ion. The distances between the four metal ions and O5 are remarkably longer than those between the other oxygen and metal ions. This suggests that the bonds between O5 and each of the Mn and Ca ions are very weak, implying that O5 is apparently different from the other four oxygen atoms in oxo-bridges and may therefore have a higher reactivity. It also suggests that O5 has a lower negative charge compared with a valence of –2 expected for normal oxygen atoms in oxo-bridges, which in turn suggests that O5 may exist as a hydroxide ion in the S_1-state of the Kok cycle [2], the state whose structure has been resolved.

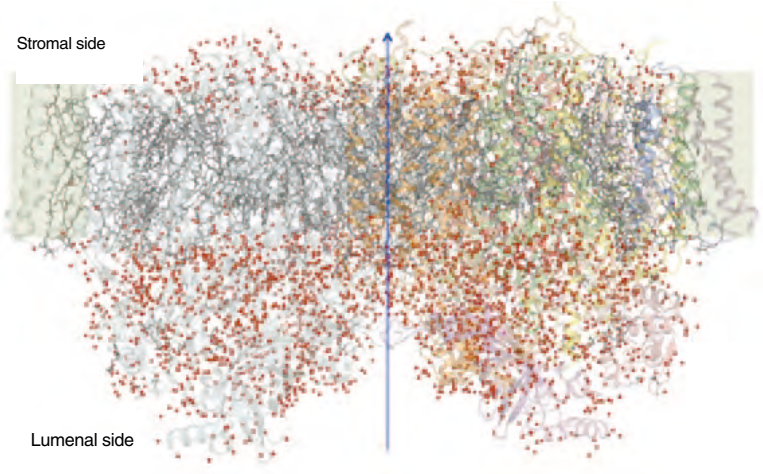

Figure 4-1
Overall structure of photosystem II dimer in a crystallographic asymmetric unit. Blue arrow indicates a non-crystallographic two-hold axis relating two monomers. 2795 water molecules were found and depicted by red spheres.

4.1.1.2 Scientific goals and challenges

In order to elucidate the mechanism of PSII oxygen evolution, it is crucial to identify the two substrate-water molecules participating in the formation of the O-O bond. Based on the above identified structural features of the Mn_4CaO_5 cluster, O5 may form part of the reaction site. Among the four water molecules bound to the Mn_4CaO_5 cluster, two are located most closely to O5, at distances of around 3 Å. In addition, these two water molecules have a distance of 3.3 Å between each other. Thus, it is most probable that the O-O bond forms within these two water molecules and O5. Based on the crystal structure precisely determined at the resolution of 1.9 Å, we may be able to predict the mechanism of oxygen evolution, although it should also be proven scientifically. Our goal is to realize time-resolved protein crystallography for PSII and to reveal the actual mechanism of water oxidation.

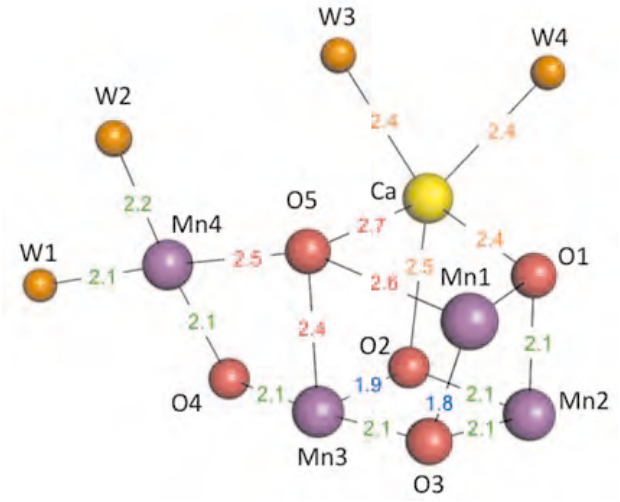

Figure 4-2
Water-splitting Mn_4CaO_5 cluster of photosystem II. Spheres are component atoms, manganese; violet, calcium; yellow, oxo-bridge; red, ligand water; orange. Atomic distances are presented between two corresponding atoms.

4.1.1.3 Current status and limitations

Light-induced water oxidation is catalyzed by the Mn_4CaO_5 cluster, changing its S_i-states (i = 0–4) in the Kok cycle [2] upon extraction of each electron by the PSII reaction center (PSII-RC). When four electrons and four protons are extracted from two molecules of water, one molecule of di-oxygen is formed. In order to elucidate the water oxidation mechanism of PSII, crystallographic analyses for all S_i-states are required. At present, however, we know only the precise structure of the Mn_4CaO_5 cluster in the S_1-state.

4.1.1.4 Future prospects with ERL

In the Kok cycle of the Mn_4CaO_5 cluster mentioned above, the S_1-state is a dark-adaptive stable state. The S_0-state is also a stable one: it is the state reduced after the production of molecular oxygen from two water molecules. In contrast, the S_2- and S_3-states are unstable intermediates, but it is well known that samples in which these intermediates are enriched can be created with pulses of visible-light laser at cryogenic temperature. The remaining S_4-state is actually a transitional state, for which time-resolved X-ray crystallography with the pump-probe technique is expected to provide structural information.

Figure 4-3 is a schematic drawing of the experimental set-up installed in an ERL beamline to prove the proposed reaction mechanism of PSII oxygen evolution. The first pumping pulse of visible-light laser (red arrow in Fig. 4-3) will change the S_1-state of the Mn_4CaO_5 cluster to the S_2-state in a micro-crystal of PSII, pushed out from the micro-crystal stream generator (MCSG, green). To study the structure of the S_2-state, the micro-crystal will be exposed to probe pulses of ERL X-ray laser (black) for several milliseconds to record one diffraction pattern onto a fast-readout X-ray detector. To get a full set of diffraction intensities for crystal structure analysis, many diffraction images will be collected from micro-crystals pushed out in sequence from MCSG in random orientations. When structural information on the S_3- and S_0-states of PSII is required, a second pumping pulse or second and third pulses will be applied to the micro-crystal of the S_2-state prior to the exposure to probe X-ray pulses. If we wish to clarify the process from the S_3-state to S_0-state via the transitional S_4-state, we must collect each set of diffraction images at different times after the generation of the

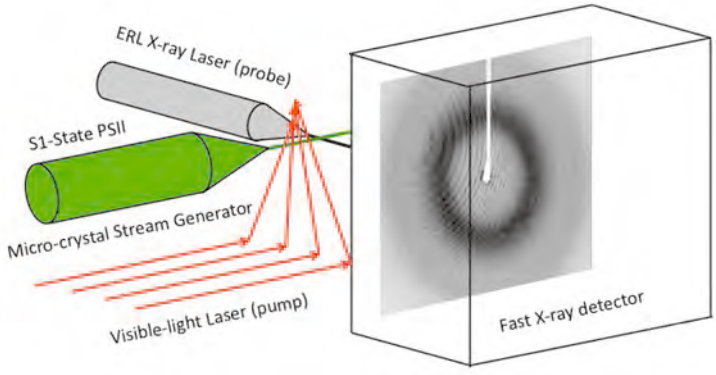

Figure 4-3
Set-up of pump-probe experiment for time-resolved X-ray crystallography of photosystem II.

S_4-state. These experimental proposals are highly challenging, and if the ERL beamline is constructed for time-resolved protein crystallography, clarification of the actual mechanism of water oxidation will provide important information for designing water oxidation catalysts, which are essential for achieving artificial photosynthesis and a sustainable world on our planet.

REFERENCES

[1] Y. Umena, K. Kawakami, J.-R. Shen and N. Kamiya, *Nature* **473**, 55 (2011).
[2] B. Kok, B. Forbush and M. McGloin, *Photochem. Photobiol.* **11**, 457(1970).

4.1.2 Oxygen evolving manganese complex in photosystem II – Spectroscopic approach

4.1.2.1 Introduction

The goal of generating solar fuels by direct conversion of light energy to fuel molecules is inspired by nature's photosynthetic organisms that convert carbon dioxide and water to carbohydrates in a single integrated system. Nature uses remarkably varied systems and mechanisms to perform catalytic reactions with extraordinary efficiency, speed, and complexity. Among the many catalytic reactions, photosynthetic water oxidation in Photosystem II (PSII) is probably one of the most important reactions, as it supports our aerobic life [1]. At the active site of PSII is an oxo-bridged four Mn and one Ca cluster (oxygen evolving complex, OEC), which is responsible for the rearrangement of electrons and atoms in order to carry out the catalytic reaction. Nature performs such reactions under ambient conditions in a sophisticated manner using the protein environment to control the reaction pathway. A detailed understanding of the processes that comprise photosynthesis will therefore have both fundamental and applied importance.

Water oxidation in natural photosynthesis consists of four oxidation steps driven by the successive absorption of four photons by the PSII reaction center. After excitation of the antenna system the light energy is transferred to the primary donor chlorophyll complex P_{680}, located in the reaction center of PSII, and then subsequently to other acceptor pigments. The oxidized P_{680} returns to the ground state by receiving an electron that is extracted from the OEC by the water oxidation reaction. Through this cyclic process, the central Mn_4CaO_5 cluster stores four oxidizing equivalents [2], which are used to extract four protons and four electrons from two water molecules, catalyzing the formation of oxygen, and eventually releasing O_2. The electrons on the acceptors are available for CO_2 reduction, or for the reduction of H^+ to H_2.

Given the role of PSII in maintaining life in the biosphere and the future vision of a renewable energy economy, understanding the water-splitting mechanism of the Mn_4CaO_5 catalyst is considered to be one of science's grand challenges.

4.1.2.2 Scientific goals and challenges

Although the detailed chemistry involved in water oxidation is emerging slowly, there are still competing models of mechanisms, and the data currently available have not provided a definitive answer. The OEC cycles through a series of five intermediate S-states (S_0 to S_4), representing the number of oxidizing equivalents stored on the OEC (Fig. 4-4) [3]. Once four oxidizing equivalents are accumulated in the OEC (S_4-state), a spontaneous reaction occurs that results in the release of O_2 and the formation of the S_0-state. How the OEC accumulates four oxidizing equivalents and stabilizes them for a sufficient period necessary for splitting water remains a central question.

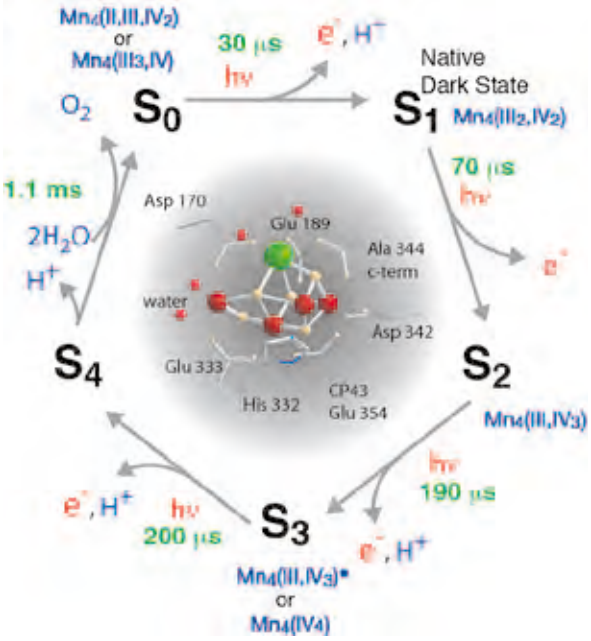

Figure 4-4
The Kok cycle showing the four intermediate S-states, proposed oxidation states and the kinetic parameters. In the center is the structure of the Mn_4CaO_5 cluster [3, 4].

For a complete understanding of this photocatalytic reaction, it is necessary to study (1) how charges, spins, and chemical structure of the catalyst are controlled during the reaction cycle, (2) how the O-O bond is formed and molecular oxygen is released at the last step that goes through the transient S_4 state, (3) what is the role of ligands that give uniqueness to biological catalysts, and (4) what are the chemical dynamics that govern the directionality of the catalytic reaction cycle.

4.1.2.3 Current status and limitations

Among various methods, X-ray-based techniques are a powerful tool for studying catalytic processes because of their element specificity for probing the electronic and geometric structure. Synchrotron-based experiments have provided insights about the PSII: X-ray diffraction studies have revealed the protein scaffold and the overall geometry of the Mn_4CaO_5 cluster [4], and X-ray emission/absorption spectroscopy has provided information about the electronic structure of cryo-trapped intermediate states (S_0 to S_3) [5]. However, there are fundamental limitations in current SR-based X-ray data collection for resolving the above questions such as (a) how to overcome radiation damage and collect data from dilute biological samples within a reasonable time-scale, (b) how to use highly sensitive, yet less probable transitions such as valence-to-core Kβ emission transitions [6] or metal *d-d* transitions as chemical probes, and (c) how to follow the dynamics of the catalytic process of damage-prone samples under ambient conditions.

4.1.2.4 Future prospects with ERL

The femtosecond pulse duration with high brightness of the ERL will enable time-resolved X-ray absorption, emission and RIXS experiments on the OEC in PSII, which will lead to a new level of mechanistic understanding beyond the reach of existing experimental tools.

We expect that ERL will offer several advantages over traditional synchrotrons for resolving the above challenges in PSII, namely: (i) the ability to probe catalytic processes on the time scales and under ambient conditions where bond formation/breaking and charge transfer processes occur, (ii) the capability for tunable two-color X-ray pump, X-ray probe, and multidimensional X-ray spectroscopy techniques for following the flow of valence charges between different atomic sites, and (iii) provision of the requisite average brightness through high emittance with a focused beam for experiments that require photons. To follow the chemistry of biological catalysts, which are often dilute (~ mM concentration of metals in the case of Mn in PSII), it is crucial to have a sufficient number of photons per pulse. The X-ray Free Electron Laser Oscillator (XFEL-O) concept, in which 10^9/pulse flux is expected, is necessary for such experiments.

4.1.2.5 Time-resolved X-ray spectroscopy

Time-resolved X-ray absorption/emission studies are key to understanding the complex chemistry of the catalytic reaction in order to obtain information about the sequential phenomena, particularly during the last step of the catalytic cycle (S_3-S_4-S_0 transition), which includes sequential events of extraction of one electron, release of two protons, release of molecular oxygen, binding of two substrate water molecules to the cluster, and four-electron-reduction of the Mn_4CaO_5 cluster. Valence-to-core X-ray emission spectroscopy (Fig. 4-5) is a sensitive probe for characterizing such events. Unlike other intermediate S-states (S_0 through S_3). The kinetically unstable S_4 state cannot be cryo-trapped by the freeze-quenching method, and therefore requires time-resolved study under ambient conditions [7]. Time-resolved spectroscopy combined with a sample flow system at the ERL will overcome radiation damage [8] to the metal catalytic center under physiological conditions and will enable the same initial state to be prepared for each shot while providing a large number of photons.

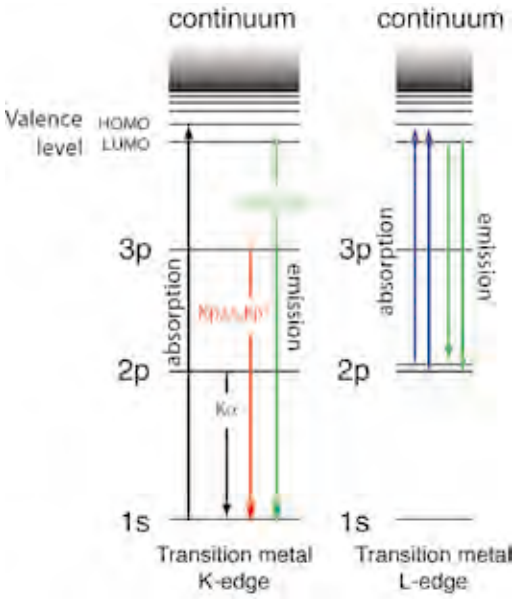

Figure 4-5
Left: The energy level diagrams showing the hard-X-ray Kβ emission lines that probe the charge density and electronic structure of the ligands of Mn. Right: The soft X-ray emission energy level diagram that are sensitive to *d-d* transitions and charge transfer states that are probed by soft X-ray emission and RIXS.

4.1.2.6 Photon-in-Photon-out spectroscopy

Both hard and soft X-ray RIXS spectroscopy provides detailed electronic structural changes at the catalytic sites or light absorbers by simultaneously probing two X-ray photon frequencies, i.e. incoming (absorption) and scattered (emission) photons. In the OEC in PSII, manipulation of the ligand fields of the Mn *d*-electron orbitals in the Mn_4CaO_5 complex modulates the charge-transfer states and the charge density of the metal/ligands, which are critical for catalytic activity. Although such electronic structural changes can be in general studied by UV/VIS spectroscopy, it is difficult to obtain useful UV/VIS spectra on the electronic transitions in the Mn_4CaO_5 complex in PSII due to the strong background of other absorbing groups. Alternatively, such transitions can be attained by soft X-ray emission/RIXS spectroscopies, by monitoring the L- and M-absorption edges (2p-3d or 3p-3d transitions). These valence to core transitions, *d-d* transitions, and charge transfer state transitions are highly sensitive to the chemistry, but are less probable and less intense and therefore more photons are required to collect signals within a reasonable time. The higher brightness and smaller emittance of the ERL X-rays will make such photon-intensive experiments feasible.

4.1.2.7 Two-color spectroscopy

The ERL opens up the possibility of simultaneous measurements with X-rays of two or more different colors. This capability will greatly assist our understanding of interactions between different elements and/or spatially separated units.

REFERENCES

[1] *"Photosystem II: The Light-Driven Water: Plastoquinone Oxidoreductase"*, edited by T. Wydrzynski and K. Satoh, (Springer, Dordrecht, 2005).
[2] J. Yano and V.K. Yachandra, *Inorg. Chem*. **47**, 1711 (2008).
[3] B. Kok et al., *Photochem. Photobiol*. **11**, 457 (1970).
[4] Y. Umena et al., *Nature* **473**, 55 (2011).
[5] J. Messinger et al., *J. Am. Chem. Soc*. **123**, 7804 (2001).
[6] P. Glatzel and U. Bergmann, *Coord. Chem. Rev.* **249**, 65 (2005).
[7] Haumann et al., *Science* **310**, 1019 (2005).
[8] J. Yano et al., *PNAS* **102**, 12047 (2005).

4.1.3 Electron transfer reaction in photosynthesis

4.1.3.1 Introduction

Life on earth depends on photosynthesis, the conversion of light energy from the sun to chemical energy. In oxygenic photosynthesis performed by plants, green algae and cyanobacteria, three integral membrane protein complexes, Photosystem II (PSII), cytochrome b_6f complex (Cyt b_6f) and Photosystem I (PSI), accomplish electron transport and generate the trans-membrane electrochemical gradient used for energy transduction. PSII oxidizes water to molecular oxygen and four protons. The electrons extracted from water are shuttled though a quinone pool and the Cyt b_6f to a soluble copper protein called plastocyanin. Solar energy absorbed by PSI induces the translocation of an electron from plastocyanin to ferredoxin, another electron transfer protein containing an Fe_2S_2 cluster, across the thylakoid membrane (Fig. 4-6). The structures of three membrane protein complexes that catalyze oxygenic photosynthesis in cyanobacteria have been solved at relatively high resolution, and the positions of most of their amino acids and prosthetic groups have been defined [1-3].

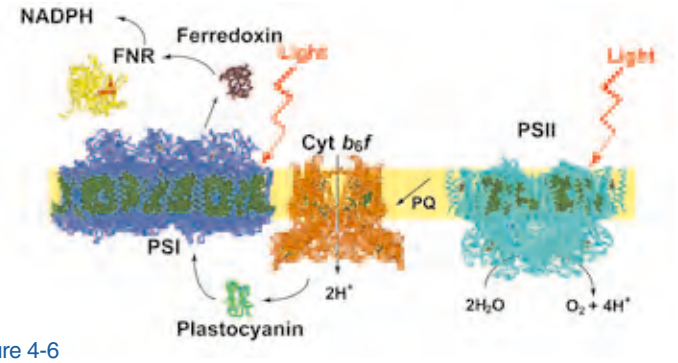

Figure 4-6
The membrane protein complexes responsible for electron transport and protein translocation in oxygenic photosynthesis. The structure of PSI, Cyt b_6f and PSII is colored in purple, orange and cyan, respectively. Lume and stromal side soluble electron transfer proteins are plastocyanin (green), ferredoxin (dark brown) and ferredoxin-$NADP^+$ reductase (FNR, yellow).

4.1.3.2 Scientific goals and challenges

PSI is one of the largest membrane proteins for which a crystal structure has been reported and consists of 11–13 protein subunits, binding approximately 90–100 chlorophyll pigments. The two largest subunits, denoted PsaA and PsaB, form a heterodimer, which binds most of the core

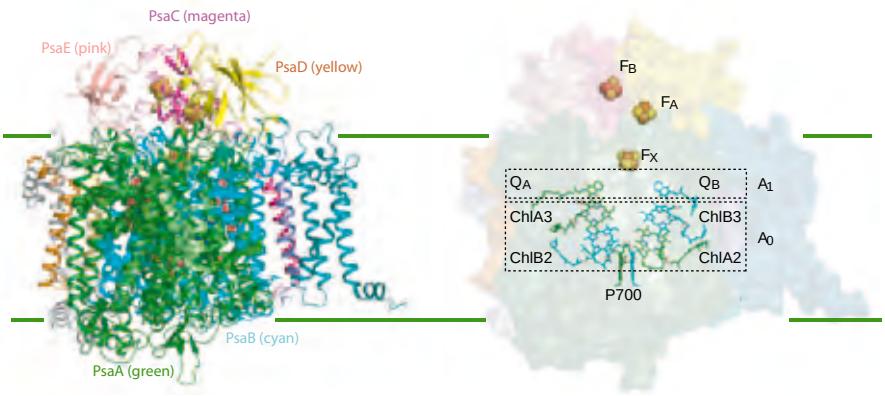

Figure 4-7
Side view of the arrangement of all protein subunits and cofactors of the electron transfer chain. (left) The structures of PsaA, PsaB, PsaC, PsaD and PsaE subunits are labeled in the panel. The other small subunits are not labeled for simplicity. (right) Cofactors of the electron transfer chain are superimposed on the molecular surface of the photosystem I complex colored in each subunit. The two branches of A_0 and A_1 cofactors are arranged in pseudo-C_2 symmetry.

antenna pigments as well as the cofactors of the reaction center, as shown in Fig. 4-7. Primary charge separation is initiated by excitation of the chlorophyll dimer (P700). The intra-molecular electron transfer chain consists of the cofactor A_0 (Chl*a*; ChlA2/ChlB2, ChlA3/ChlB3), A_1 (phylloquinone; Q_A/Q_B) and three Fe_4S_4 clusters (F_X, F_A and F_B). P700 traps the excitation energy collected by the antenna and initiates a series of electron transfer processes giving rise to the formation of a stable charge-separated state. Even using the fast spectroscopy technique, resolving the primary energy and electron transfer kinetics in PSI is very challenging, because in this system the reaction center cannot be isolated from the primary antenna, meaning that time-resolved experiments have to be performed on a system containing ~100 chlorophylls. The last half of the electron transfer pathway of PSI is composed of F_X, F_A and F_B clusters. The PsaC subunit harbors two Fe_4S_4 clusters, F_A and F_B. The binding pocket of ferredoxin is formed by subunits PsaC, PsaD and PsaE. Ferredoxin is photoreduced in the submicrosecond-microsecond time range before it dissociates from PSI. Information concerning the docking site at the atomic level, including the orientation of ferredoxin and the identification of the specific interactions between partners, is still missing. It is also challenging to understand the redox dynamics of dissociable electron transfer complex.

4.1.3.3 Current status and limitations

X-ray structure analysis of PSI at 2.5 Å resolution revealed that pairs of Chl and phylloquinone molecules are bound to subunits PsaA and PsaB, respectively, and located in nearly symmetrical arrangement (Fig. 4-7). The problem of involvement of one or two symmetric branches of cofactors in electron transfer from the exited P700 (P700*) to F_X remains insufficiently understood. The dynamics of the energy and electron transfer processes occurring in PSI upon photo-excitation have been studied with time-resolved techniques, but a general consensus on the interpretation of experimental observations has not been achieved [4].

There are two models describing charge separation in PSI [5, 6]. The first model suggests that upon absorbing light the primary process of charge separation between P700* and the primary acceptor A_0 with the formation of $P700^+A_0^-$ within <10 ps. Then, an electron is transferred to phylloquinone A_1 within 50 ps and then to cluster F_X within < 200 ns. The second model suggests that the primary charge-separated state might be not $P700^+A_0^-$. Both structural models are only discussed based on the spectroscopic analysis upon femtosecond photo-excitation around 700 nm, but are currently very hard to be characterized by X-ray crystallography.

In the inter-molecular electron transfer around PSI, ferredoxins associate reversibly to the photosynthetic reaction center of PSI. Within this reversible electron transfer complex, ferredoxin is photoreduced before it dissociates for later interaction with other ferredoxin dependent enzymes. Although this electron transfer is a key biological process, only a few examples of the structures of dissociable complexes between the electron transfer partner proteins are known to date [7-9]. Information on the docking site at the atomic level, including the orientation of proteins and identification of the specific interactions between partners, is still missing. It is even more difficult to study the dynamics of electron transfer protein in the crystalline state.

4.1.3.4 Future prospects with ERL

In 2011, the femtosecond X-ray structure of PSI was reported [10]. All X-ray diffraction data are collected from a fully hydrated stream of nanocrystals using femtosecond pulses from a hard-X-ray free-electron laser. Although the resolution is not high enough (8.5 Å) to discuss the detailed mechanism of PSI, this analysis shows the potential application to the structural study of fast chemical reaction within a huge membrane protein complex. Pulse X-ray from the ERL light source is considered suitable for studying the initiation event within the reaction centers of PSI, since the time scale of the electron transfer is comparable.

Prof. N. Kamiya's group from Osaka City University reported the 1.9 Å X-ray structure of the PSII reaction center [1], marking a significant breakthrough in membrane protein crystallography. Clearly, the high-resolution structures of metallocenters within PSII are essential for understanding the precise mechanism of water oxidation, and the brilliant X-ray beam of the ERL is also suitable for high-resolution structural analysis of the PSI reaction center. Spectroscopic characterization and high-resolution structural chemistry of metallocenters of PSI will provide fundamental information for a better understanding of the transient electron transfer complex.

REFERENCES

[1] Y. Umena, *et al*., *Nature* **473**, 55 (2011).
[2] G. Kurisu, *et a*l., *Science* **302**, 1009 (2003).
[3] P. Jordan, *et al*., *Nature* **411**, 909 (2001).
[4] K. Brettel and W. Leibl, *Biochem. Biophys. Acta* **1507**, 100 (2001).
[5] "*Photosystem I: The Light-Driven Plastocyanin: Ferredoxin Oxidoreductase*", edited by J.H. Golbeck, (Springer, Dordrecht, S. Savikhin, 155 (2006).
[6] M.G. Muller, *et al.*, *Biophys. J*. **85**, 3899 (2003).
[7] G. Kurisu, *et al*., *Nature Strut. Biol*. **8**, 117 (2001).
[8] S. Dai, *et al*., *Nature* **448**, 92 (2007).
[9] M. Nojiri, *et al*., *Nature* **462**, 117 (2009).
[10] H.N. Chapman, *et al*., *Nature* **470**, 73 (2011).

4.2 Catalysis

4.2.1 Heterogeneous catalysts on a nanoscale order

4.2.1.1 Introduction

Catalysts are used in most important chemical reaction processes to produce more useful substances, keep our living environment clean, convert energy, etc. We cannot imagine society, particularly the sustainable society of the future, without catalysts. Catalysts are used in various processes for producing polymers, fertilizer, medicines, commodities, and sulfur-free gasoline, processes for purifying and cleaning exhaust gases from factories and automobiles, and energy production systems such as fuel cells. Also, life itself is supported by catalytic reactions under very mild conditions. Catalysts and catalyses are becoming increasingly important in view of the growing human population and rapid increase in the consumption of materials and energy as living standards rise. The development of more efficient catalysts will help to minimize the consumption of noble metals and fossil fuels, which are limited resources. A goal of catalysis research is to develop chemical reactions which give high product yield and high selectivity, or few undesirable by-products, with minimum energy consumption. To achieve such reactions, another goal of catalysis research is to understand what is happening in, on, and around catalysts during reactions by means of analysis techniques designed to clarify the unknown aspects of catalysts and catalysis. Such knowledge will accelerate the development of more efficient catalysts and help to optimize the reaction conditions.

Catalysts are divided into two types: homogeneous catalysts such as enzymes and metal organic compounds, and heterogeneous catalysts utilizing solid surfaces. In industry, heterogeneous catalysts are mainly used because of their high efficiency and easy separation from the product, but it is difficult to characterize the surfaces because of their inhomogeneity. In addition, the surface chemical processes are complex with dynamic interactions among inhomogeneous sites through diffusion and energy transfer. Thus, there are drawbacks for understanding and designing new solid catalysts and high-performance surfaces. For example, the structural kinetics and dynamics of the catalyst itself during catalysis

are not clear, and the key factors for controlling catalysis are not known in many cases. Furthermore, there are few in-situ techniques for characterizing the active structures and electronic states of catalyst nanoparticles and surfaces. These issues need to be clarified. Therefore, designing high-efficiency, highly selective catalysts require temporal and spatial analysis techniques in order to gain a clear picture of the surface reactions and to determine the reaction mechanisms.

It is important to study both catalysts themselves and the molecules on them in reactions to understand the mechanisms of catalysis. Both surface gaseous species and catalysts should be carefully observed, focusing on the catalysts rather than reacting molecules.

Catalytic reactions on surfaces are highly complicated processes, requiring careful plans to observe them during actual reactions. One of the most powerful methods to observe catalysts is XAFS in the hard X-ray region. XAFS has long been used to study catalysts at the Photon Factory. According to an article in Shokubai (catalysts) marking the 50th anniversary of the Catalysis Society of Japan, XAFS is one of the most popular tools to study catalysts [1]. This is because XAFS can be applied to non-crystalline materials under various conditions such as elevated temperatures under reaction molecules. Besides XAFS, powder diffraction and photoelectron spectroscopy under ambient conditions are often used to study catalysts and other methods will be used in the near future. Molecules on the surface in reactions have been observed by XPS and NEXAFS techniques in the soft X-ray region. Imaging methods like photoelectron emission microscopy (PEEM) is useful to obtain real space information on catalyst surfaces. IR and other “normal lab methods” are combined with in situ XAFS experiments to observe both molecules and catalysts at the same time.

Real-time observations of catalysts are also required to understand surface reactions. XAFS experiments have usually been carried out to study catalysts so far, and are a promising technique to clarify the unknown issues. XAFS can be applied to non-crystalline materials under various conditions such as elevated temperatures under reaction molecules. A nanometer-size and picosecond-duration X-ray beam is needed to observe catalysts under actual reaction conditions, though at present XAFS experiments are normally performed with a sub-mm or several μm size beam on a time scale of minutes or seconds.

The Energy Recovery Linac is a promising machine with a high brilliance and ultra-short pulse width, which will enable nanometer- and picosecond-scale investigation of surface chemical processes. The X-ray beam from the ERL will provide unprecedented spatial and temporal resolution for various experiments. The high coherence of its X-rays will make the imaging technique more useful. Meanwhile, the flux density of the ERL will not be too high, and so the X-ray beam will not destroy the catalysts. Thus ERL will be an ideal probe for studying catalysts and catalyses.

This section discusses the possible application of the ERL to the surface characterization of catalysts under actual reaction conditions. Achievable results and goals in the field of catalysis research with the ERL are also presented.

4.2.1.2 Scientific goals and challenges

A goal of catalysis research with synchrotron radiation is to observe the structural and electronic variations of catalyst species during catalysis as a microscopic movie, and to observe the reaction sequences of catalysis in real time (μs-s), or in an ultrafast time scale (ps-ns) for an elementary process. However, this is difficult to achieve with the existing millimeter-sized beam, since the catalyst species themselves may take different structures depending on the location even on a single substrate. Even if a high-intensity X-ray beam is focused to less than the cluster size such as nm, it will destroy or modify the catalysts or catalyses. To make matters worse, the reactions of each reactant species on individual catalyst particles do not proceed synchronously, but randomly or statistically.

In order to understand actual heterogeneous catalysts, the following approaches should be considered:

a) to minimize the observed area to ultimately observe a single catalyst cluster/nanoparticle,
b) to understand the catalyst more precisely by using more sophisticated spectroscopic tools, such as resonant X-ray emission spectroscopy (RXES),
c) to observe the variations of microscopic images of the catalyst during reaction,

d) to study the kinetics of catalytic reaction sequences in real time,
e) to study the dynamics of an elementary process with shorter time resolution,
f) to observe using site-specific and state-specific methods,
g) to observe the reaction process simultaneously at the same catalyst position using several independent methods (XAFS, IR, Raman, UV/Vis, product analysis, etc.),
h) to understand catalytic processes hierarchically from atomic to macro level,
i) to achieve mass production (high throughput) and combinatorial measurements.

Based on these key points, the requirements for a new cutting-edge X-ray beam are as follows: ultra-short pulse width to capture the moment of the motions, extremely low divergence and focused beam size to irradiate a particular point of the sample, and sufficient repeating frequency of the beam to make movies of reactions. These conditions have not yet been simultaneously achieved; a sophisticated new X-ray beam is needed that satisfies these requirements concurrently in order to understand the mechanisms of catalysis and to design new functional catalysts with high efficiency and selectivity.

Pulse duration of sub-ps to ps time scale is required to capture the elementary steps of reactions. The elementary steps are fundamental motions of the molecules and catalysts to be observed and understood. A nanometer-scale beam is required to irradiate a specific point of the catalyst or a single nanoparticle of interest. An active point or particle should be selected to observe the mechanisms of catalysts in action. There is a suitable repeating frequency to make a movie of a reaction; movie frames should be captured every ~1 ns with an ultra-short pulse for non-repeatable reactions. In addition, for pump-probe experiments, the delay should be controlled to sub-ps level and almost without jitter.

Moreover, it is necessary to observe the system not only at the atomic level with sub-ps time resolution but also in an expanded region in a single shot with second to millisecond time resolution where the diffusion of reactants and products, reaction sequences, and energy conduction occur. Catalysis is a complex system involving interactions among various sites over a wide time and spatial scale. Projection-type real-time imaging will be effective for this type of analysis such as diffraction imaging and projection-type microscopy. Prototype research was done in the early 1990s by G. Ertl's group by using PEEM with a conventional UV lamp. The detection technique needs to be improved further in addition to the ERL source in order to fully utilize the merits of the ERL. Ultrafast data handling including analyses and large-scale data storage and fast data transfer systems are desired.

Here, the importance of in situ characterization under dynamic conditions should be emphasized. Photocatalysts are a good example for discussing dynamics.

Semiconducting materials as photocatalysts can absorb a photon to create an electron–hole pair. The electron in the conduction band and the hole in the valence band move to the surface to reduce and oxidize the surface species, respectively. The dynamic process in the photocatalyst is not fully understood because of its inhomogeneity. The size of each photocatalyst particle typically ranges from than 20 nm to a few nanometers, and the time scale of phenomena occurring in each particle as listed below is several tens of picoseconds. Vacancies play many roles in photocatalysts including positive and negative effects [2]. Photocatalysts involve many processes such as absorption of photons, creation of electron-hole pairs, diffusion of electron-hole pairs to the surface, adsorption of reactants, electron transfer, and recombination of electrons and holes. The electronic levels of vacancies are located in the middle of the band gap, which reduces the photo-absorption energy (positive). Vacancies provide the adsorption sites (positive), but also serve as the trapping site of electrons and recombination site of electron-hole pairs (negative). Thus, the characterization of vacancies is important, and must be carried out from various perspectives. Dynamic and microscopic approaches on a picosecond or nanometer scale are strongly required.

4.2.1.3 Current status and limitations

At present, XAFS is mainly used to study catalysts by controlling the environment, namely temperature, pressure and reaction molecules. Both transmission and fluorescent XAFS methods are used depending on the concentration of the catalyst species. These techniques are applied to static or rather slow processes like temperature programmed reduction/oxidation. In order to fully understand catalytic reaction sequences, so-called “operando experiments” are carried out, where some other physicochemi-

cal methods such as FT-IR, UV/Vis, MS and GC are also used to observe the variation of catalysts, reaction molecules or reaction products. However, the experimental stations are currently not optimized to carry out such experiments.

Fluorescent XAFS is often used when the concentration of catalytic species is low. However, it is not easy to detect the signal when the concentration of the species is very low or when the substrate or co-existing elements emit more intense fluorescent X-rays since the signal is obscured in the background. Crystal analyzers are used to separate them, but the energy resolution is limited because of the fixed beam size at the Photon Factory.

The redox processes of catalysts, mainly supported catalysts, are being intensively studied by using quick XAFS (QXAFS) or dispersive XAFS (DXAFS). The time resolution is several tens of seconds to several tens of milliseconds in the case of QXAFS and several tens of milliseconds to 100 ps in the case of DXAFS. The reaction scheme, rate constant, and activation energy of each reaction are examined by using time-resolved XAFS results. The time resolution is limited for various reasons, including limited photon flux, limited time-resolution of detection systems, limited time-resolution of environment control, etc.

In general, catalysts are heterogeneous geometrically, electronically and spatially as shown in many TEM images, but the area-averaged results for an area of mm^2 or less are observed limited by the beam size in usual XAFS. The area can be reduced to μm^2 when the micro-beam technique is used, but the available flux is reduced if the brilliance of the synchrotron source is not high enough. At the moment, the micro-beam XAFS technique can observe a single catalyst particle of several hundred nanometers in size [3]. Only integrated information in the beam direction can be obtained and hard X-rays penetrate several mm into samples. In some cases, a well-defined crystal surface is prepared as a model catalyst and is used as the reaction site. Because of limited signal intensity, no kinetic studies have been carried out on such well-defined surfaces by using XAFS until now.

Although the grazing incidence small angle scattering (GISAXS) technique is intensively used to study the variations of cluster size [4], the application of techniques other than XAFS is limited at the Photon Factory. A wide variety and sufficient number of beamline scientists should be assigned to prepare the required research environment for catalysis researchers.

The characterization of catalysts under reaction conditions is possible by using X-rays and photons to understand the kinetics. For example, one can measure the catalysts under several MPa in the presence of gas and liquid [5]. Reactions can be captured in ms order for an unrepeatable process by dispersive XAFS [6] and in ps order for a repeatable process by pump-probe method [7]. The behavior of surface adsorbates can be followed by dispersive NEXAFS [8].

Simultaneous measurement of the catalyst surface is also important because of the multifaceted features of catalytic reactions on surfaces. The hydrodesulfurization (HDS) reactions on Ni_2P catalysts, which are important to remove sulfur from petroleum, are followed by simultaneous measurements of in situ FT-IR, in situ QXAFS and gas phase analysis. Figure 4-8 shows the results of three different methods. In situ FT-IR, QXAFS and gas phase analysis yield the temporal change of adsorbates, the structure of active sites, and the structure of products, respectively. Catalytic activity is not so active at the beginning but it suddenly increases as the intermediate, tetrahydrothiophene (THT), increases. An induction period is necessary to attain the active phase

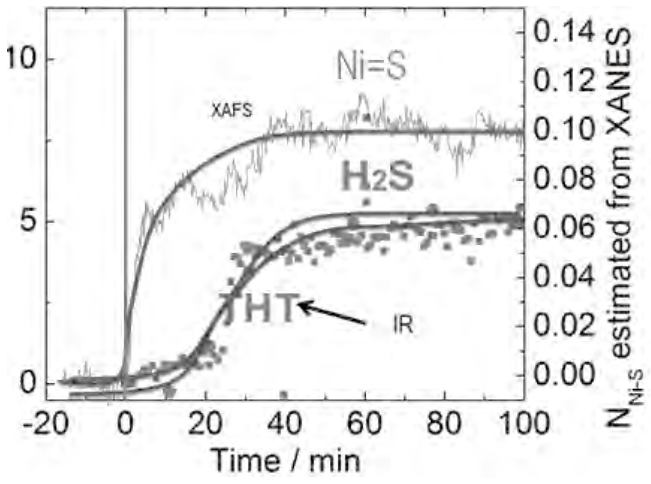

Figure 4-8
Simultaneous measurements of QXAFS, FT-IR and gas phase analysis for Ni_2P under reaction conditions. Time zero means the introduction of thiophene. Thin lines, small squares and large circles indicate the amount of Ni-S bond, THT and H_2S derived from XAFS, FT-IR and gas phase analysis respectively. The bold lines are the best-fit curves of respective data points [9].

of NiPS that is revealed by XAFS measurements. The accumulation of Ni-S bonds is required to become active for hydrogenation of thiophene and then H_2S starts to be produced.

Such simultaneous measurements can provide clear evidence of the structure of the active sites and for determining the reaction mechanism as shown in Fig. 4-9. Thus, this is one of the state-of-the-art experiments to observe the kinetics and to reveal the reaction mechanism in the order of tens of seconds.

However, these efforts are not enough to understand the real dynamics and the elemental steps of the reaction; a time resolution of the order of picoseconds is required. Another point is that this picture is taken from mm-scale observation and is the average of our sample. The actual active sites of the reaction should be observed to take a good picture of each elemental step of the reaction, which requires a spatial resolution of nm scale.

The catalytic process often occurs inhomogeneously in space. Real-time mapping of the catalyst in the reactor has been visualized by CCD camera. The inhomogeneity and its change in the reactor were demonstrated in combination with quick XAFS [10]. The temporal and spatial resolutions are second and sub-mm, respectively. Spatial resolution can be improved by combining with photoelectron emission microscopy (PEEM) [11]. The PEEM spatial resolution is now 1 nm with the development of spherical aberration correction [12]. By selecting the energy of photoelectrons, it is now possible to obtain element-specific PEEM images [13]. Although the spatial resolution of this method is now good, the temporal resolution must be improved to capture a movie of reactions.

The temporal and spatial resolutions of the methods we reviewed here must be improved to the order of picoseconds and nanometers in order to observe the elemental steps of chemical reactions at a certain site on inhomogeneous catalysts. The design of sample cells is very important to study real catalysts under working conditions, since X-ray absorption by the window limits the quality of spectra while diffusion of reaction gases modifies the catalysis. A smaller beam size will make it easier to design cells since thinner windows and smaller amounts of catalysts can be used to yield XAFS spectra with higher S/N ratios.

4.2.1.4 Future prospects with ERL

The importance of standard XAFS techniques is increasing. If dipole radiation could provide higher flux than is available at present at the Photon Factory or PF-AR, it could be used for usual XAFS experiments as a basic research tool and would yield many more results. More sophisticated experiments

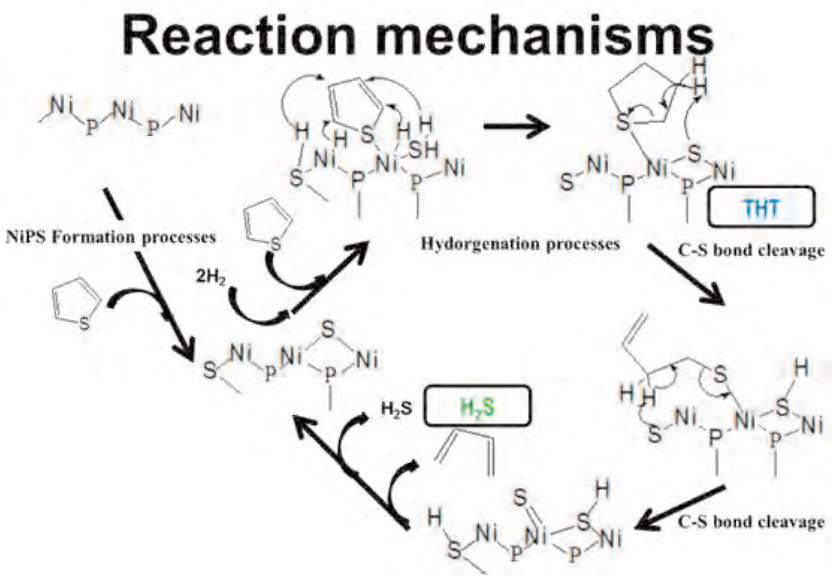

Figure 4-9
Proposed reaction mechanism for HDS reaction on Ni_2P. The reaction starts with the formation of Ni-S bonds in the left part of the figure. Then, the active NiPS gives high activity for thiophene hydrogenation and decomposition.

require synchrotron radiation from insertion devices such as an undulator and multi-pole wiggler (MPW). The ERL will provide ps-order pulses with 10 nm size and 10^7 /pulse/eV. Ultrafast XAFS measurements by the dispersive XAFS method at a MPW station will be performed to determine reaction mechanisms with the pulse features and high repetition rate of the ERL. One target is photocatalysts, which have complex structures with many reaction sites and aspects. In order to utilize an undulator source, secondary processes such as X-ray Raman should be developed or SFG might be used for ultrafast XAFS detection.

How can the temporal and spatial resolutions be improved to clarify the elemental steps of chemical reactions on inhomogeneous catalysts? The short-pulsed X-ray beam from the ERL may achieve sufficient resolutions for such studies. The duration of the beam will be in the range of picoseconds, which is appropriate for capturing the moment of reactions while minimizing radiation damage to the sample. Also, the divergence of the beam is sufficiently small to irradiate a nanometer-size area of interest on a catalyst. The nanometer-sized beam from the ERL source is well suited to the study of local structures of nanoparticle catalysts with higher spatial resolution. XAFS measurements on a single cluster and a single nanoparticle can be carried out since a beam of several tens of nanometers can be obtained at the sample position.

Sample cells having thinner windows will be fabricated and smaller amounts of catalysts will be used for experiments with the nm-sized beam, and will yield XAFS spectra having much higher S/N ratios. An ultrafast X-ray detector such as X-ray streak camera combined with sub-picosecond pulses of the nm-sized beam will make it possible to study reactions with much higher reliability. Although the penetration of X-rays into the sample cannot be controlled since it is a physical property, well-prepared samples and well-designed confocal optics will help to approach such limits. The smaller beam size will improve the energy resolution of crystal spectrometers, thus making it easier to separate the fluorescence from an element of interest from other fluorescence or scatterings. The beam will also make it easier to study resonant X-ray emission spectra in order to obtain more precise interpretation of electron transitions.

Facilities for simultaneous measurements of XAFS and other techniques such as SEM, XRD, IR and gas analysis should be completed. In addition to high-performance synchrotron radiation, good research environments should be created in order to carry out operando experiments at the experimental stations. In other words, it is necessary to introduce the synchrotron beam into good catalysis laboratories instead of taking catalyst samples into experimental hutches. A fixed gas handling system must be installed for safety reasons. Not only simple redox processes but also more complicated actual reaction systems will be studied in operando conditions. More hazardous high-pressure gases may be used at the experimental stations. Thus, the experimental environment, not only the X-ray beam itself, is crucial in order to carry out sophisticated and complicated experiments safely.

Micro-imaging techniques using the small beam size and highly coherent beam can be applied to catalysts. It will be possible to observe migrations of clusters on support surfaces, sintering of working catalysts, or reaction sequences in catalysis in real time by a high-speed 2D detector. Application of the CT technique will enable 3D imaging of heterogeneous catalysts and biocatalysts under working conditions. X-ray anomalous scattering and grazing incidence small angle scattering will be used to study the cluster or nanoparticle growth processes of working catalysts.

The picosecond and nanometer-sized X-ray beams from the ERL will open up a new world of science to study each elemental step of chemical reactions on inhomogeneous catalysts by capturing movies of the reactions. It will be possible to focus on a specific active site of the reaction, and to see exactly how the site serves as a catalyst. The ERL will lead to great advances in studies on catalysts and catalyses. More effective catalysts will then be created based on the new knowledge of the key steps of the reactions. It should be emphasized that beamline scientists specializing in catalytic science will be needed in order to optimize such experimental methods for this important research field. Thus, the ERL is a promising tool for the development of new high-performance catalysts, and the experimental environments should be fabricated to carry out sophisticated experiments at the facility. The splendid ERL machine has a bright future.

REFERENCES

[1] Shokubai, *catalysts* **50**, 224 (2008).
[2] O.-O. Prieto-Hahaney, N. Murakami, R. Abe and B. Ohtani, *Chem. Lett*. **38**, 238 (2009).
[3] M. Tada, N. Ishiguro, T. Uruga, H. Tanida, Y. Terada, S. Nagamatsu, Y. Iwasawa and S. Ohkoshi, *Phys. Chem. Chem. Phys.*, **13**, 14910 (2011).
[4] S.A. Wyrzgol, S. Schäfer, S. Lee, B. Lee, M. Di Vece, X. Li, S. Seifert, R.E. Winans, M. Stutzmann, J.A. Lercher and S. Vajda, *Phys. Chem. Chem. Phys*., **12**, 5585 (2010).
[5] K. Asakura and Y. Iwasawa, *J. Phys.Chem*. **93**, 4213 (1989).;T. Kawai, K.K. Bando, Y.K. Lee, S.T. Oyama, W.J. Chun and K. Asakura, *J. Cat*. **241**, 20 (2006).
[6] A. Suzuki, Y. Inada, A. Yamaguchi, T. Chirara, M. Yuasa, M. Nomura and Y. Iwasawa, *Angewandte Chemie Inter. Ed*. **42**, 4795 (2003).
[7] T. Sato, S. Nozawa, K. Ichiyanagi, A. Tomita, M. Chollet, H. Ichikawa, H. Fujii, S. Adachi and S. Koshihara, *J. Shnchrotron Rad*. **16**, 110 (2009).
[8] I. Nakai, H. Kondoh, T. Shimada, M. Nagasaka, R. Yokota, K. Amemiya, H. Orita and T. Ohta, *J. Phys. Chem. B* **110**, 25578 (2006).
[9] K.K. Bando, T. Wada, T. Miyamoto, K. Miyazaki, S. Takakusagi, Y. Koike, Y. Inada, M. Nomura, A. Yamaguchi, T. Gott, S. Ted Oyama and K. Asakura, *J. Catal.* **286** 165 (2012).
[10] J.D. Grunwaldt, S. Hannemann, C.G. Schroer and A. Baiker, *J. Phys. Chem. B* **110**, 8674 (2006).
[11] J. Stohr, Y. Wu, B.D. Hermsmeier, M.G. Samant, G.R. Harp, S. Koranda, D. Dunham and B.P. Tonner, *Science* **259**, 658 (1993).
[12] T. Schmidt, H. Marchetto, P.L. Lévesque, U. Groh, F. Maier, D. Preikszas, P. Hartel, R. Spehr, G. Lilienkamp, W. Engel, R. Fink, E. Bauer, H. Rose, E. Umbach and H. J. Freund, *Ultramicroscopy* 110 **11**, 1358 (2010).
[13] T. Schmidt, U. Groh, R. Fink, E. Umbach, O. Schaff, W. Engel, B. Richter, H. Kuhlenbeck, R. Schlogl, H.J. Freund, A.M. Bradshaw, D. Preikszas, P. Hartel, R. Spehr, H. Rose, G. Lilienkamp, E. Bauer and G. Benner, *Surf Rev Lett* **9**, 223 (2002).;M. Escher, N. Weber, M. Merkel, B. Kromker, D. Funnemann, S. Schmidt, F. Reinert, F. Forster, S. Hufner, P. Bernhard, D. Ziethen, H.J. Elmers and G. Schonhense, *J. Electron Spectrosc. Relat. Phenom*. **144**, 1179 (2005).; H. Yasufuku, Y. Ohminami, T. Tsutsumi, H. Niimi, N. Matsudaira, K. Asakura, M. Kato, Y. Sakai, Y. Kitajima and Y. Iwasawa, *Jpn.J.Appl. Phys*. **43**, 7682 (2004).

4.2.2 Real-time observation of surface reactions

4.2.2.1 Introduction

Surface reactions are usually a complicated process which involves several different types of elementary steps such as adsorption, diffusion, reaction, and desorption as illustrated in Fig. 4-10. Furthermore, surface adsorbates exhibit various adsorption configurations depending on the surface structure and the adsorption states dynamically change with time. In many cases, the kinetics of surface reactions deviate from the simple collision theory for a homogeneous mixture of adsorbates, and so we need to consider the adsorption states and multiple contributions from the different types of elementary steps which are intertwined with each other. In order to understand surface reactions, to date partial pressures of gaseous species have been monitored during the reaction and kinetic parameters like rate constants and activation energies have been estimated based on simple reaction models. This approach is inadequate to achieve deep insights into reaction mechanisms; it is necessary to directly observe the surface species in real time. Monitoring of surface species with the synchrotron-based electron-detecting technique is promising because it is highly surface sensitive and can provide information on the coverages, structures, and chemical states of surface species. X-ray pulses generated by the ERL will allow us to analyze fast surface reaction kinetics and dynamics, which will be useful for understanding catalytic surface reactions proceeding under practical working conditions.

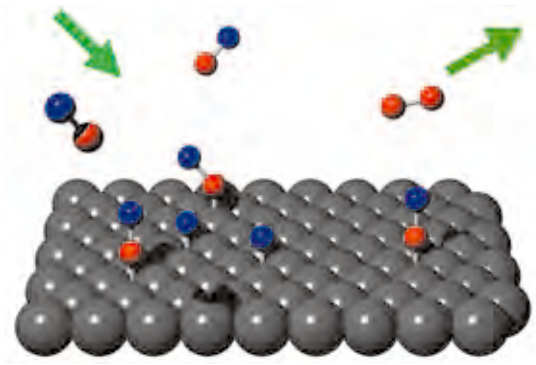

Figure 4-10
Schematics for surface processes.

4.2.2.2 Scientific goals and challenges

We are not focusing on ultrafast photo-induced surface processes but on catalytic surface reactions which proceed by thermal activation. The ultimate goal of the real-time observation of such surface reactions is to understand how molecules arrive, travel and react with others on a surface at the atomic level. The elemental steps of reacting molecules should be revealed to obtain a true understanding of the corresponding catalytic reaction. To achieve this level of understanding, we need to know the time evolution of the whole process from the arrival of molecules to desorption as a product via surface diffusion and reaction. In particular, atomic motions during the course of surface reactions should be traced with a stroboscopic technique.

4.2.2.3 Current status and limitations

Fast XPS and fast NEXAFS have already demonstrated their potential to analyze the kinetics of surface reactions that proceed with a typical timescale of milliseconds. For example, the recently developed dispersive NEXAFS technique can monitor the progress of surface reactions with a time interval of 33 ms, which enables us to analyze even non-repeatable one-way catalytic processes [1]. If we extend this technique to time-resolved monitoring of a repeatable catalytic process by combining a pulsed laser source as a pump and an X-ray pulse from single bunch operation as a probe, the time resolution will be significantly improved to 40 ps with an interval of 620 ns as shown in Fig. 4-11. This time structure is determined by the PF ring operation of the single bunch mode. However, this is not suitable for tracing the catalytic process, because the typical timescale of dynamic atomic motions is of the order of 10–100 femtoseconds, which is much shorter than the X-ray pulse duration (40 ps) and because continuous sampling at an appropriate frequency is necessary to trace the whole reaction process. As for continuous sampling, time-of-flight photoemission experiments have been performed at BESSYII, where the photoelectron signal associated with each electron bunch of a multi-bunch mode could be distinguished on a nanosecond timescale [2]. This measurement was carried out by an electron energy analyzer using a time-to-digital converter with the start signal from the bunch marker provided by the SR storage ring. If a pulsed signal from a pulsed laser source is used as the start signal, we can conduct a pump and probe experiment with continuous snapshot measurement with 2-ns interval. Nevertheless, no pump and probe experiments have been performed so far for catalytic surface reactions driven by thermal activation, because no repeatable catalytic surface process with a precise trigger and an appropriate repetition rate is available at present.

4.2.2.4 Future prospects with ERL

We are interested in how molecules behave during the course of surface reactions. In particular, we are focusing on surface reactions which are driven not by photo-excitation but by thermal activation, because the latter reactions are closely related with practical catalytic reactions. One possible way to give a trigger to the thermal reaction is to use the photo-stimulated-desorption (PSD) of adsorbates, which is followed by quick reoccupation of the empty sites from gas-phase species and several further steps such as diffusion, reaction and desorption as shown in Fig. 4-12, where the typical time constant for each step

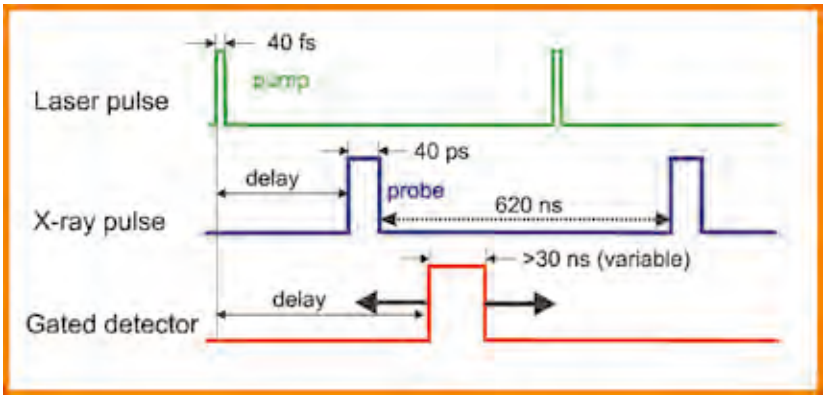

Figure 4-11
Diagram of time-resolved experiment using x-ray pulses delivered from the PF single bunch operation.

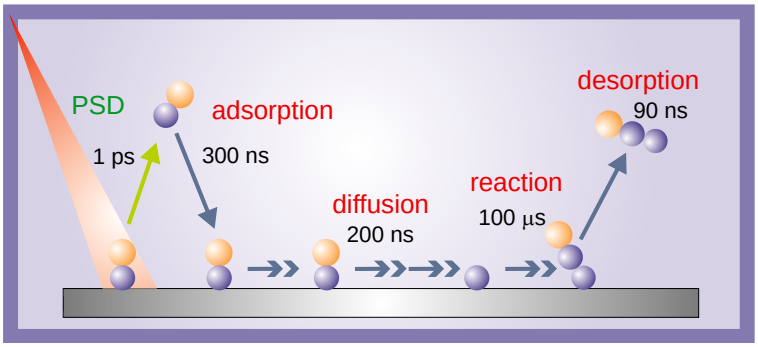

Figure 4-12
Typical timescale for the elementary steps of surface reaction processes.

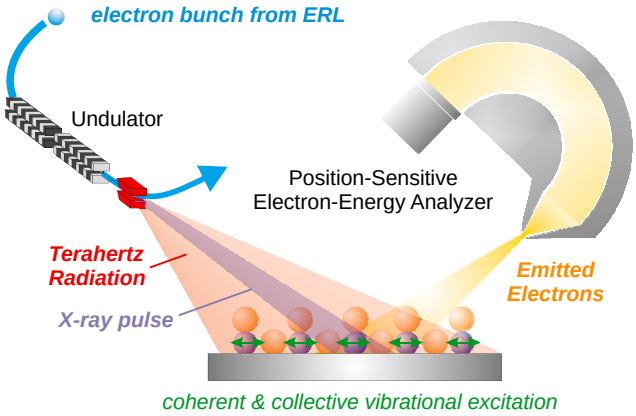

Figure. 4-13
Schematics for a pump and probe experiment using the terahertz radiation and the x-ray pulse from the same electron bunch from ERL.

under ambient pressure conditions is also indicated [3–5]. Even in the case of ambient pressure conditions, the reoccupation timescale is of the order of several hundred nanoseconds. Among the elementary steps, the rate-limiting step is often found to be the reaction step, of which the typical time constant is longer than 100 μs [4]. This means that the required time window for the repetition cycle is as long as approximately 1 ms, that is, 1 kHz. Such a slow repetition rate needs an extremely long data accumulation time, if we record the signal from each electron bunch of the ERL. In this case, considering the X-ray beam from the ERL as a CW source, it is more reasonable to acquire the signal with a high-speed detector which enables spectral readout at every 1 μs. With this technique, we will be able to follow the kinetics of fast catalytic surface reactions which proceed under ambient pressure and high temperature conditions.

Another challenge is direct observation of the atomic motions during thermally activated surface reactions. To initiate such a thermal reaction, we can trigger the reaction by vibrational and/or translational excitation. Recently, Ogasawara and co-workers proposed a direct way to excite a vibrational mode of adsorbates, where broad-band terahertz (THz) radiation from an ultrashort electron bunch of a free-electron laser (FEL) is used for the excitation [6]. Since this electron bunch also emits an ultrashort X-ray pulse as an X-FEL pulse, both THz radiation and an X-ray pulse are generated from the same electron bunch and can be used for pump and probe experiments with high temporal accuracy. This technique can also be applied at the ERL. Figure 4-13 shows a schematic diagram of a pump and probe experiment using the THz radiation and X-ray pulse generated from the same electron bunch from the ERL. Here, lateral vibrational modes of adsorbates are excited collectively in a coherent manner by the THz pulse of electric field. This vibrational excitation helps to overcome the activation barrier which leads to immediate transition to the product. The timescale of a surface reaction induced by the photo-excitation was estimated to be approximately 3 ps [7]. If we can take stroboscopic snapshots after the vibrational excitation by shining X-ray pulses of 100 fs duration on the adsorbates with an appropriate delay time Δt, we may be able to observe directly the atomic motion during the reaction. The remaining issue is to confirm that the sample surface completely recovers to the initial condition within the repetition time of the ERL pulse (0.8 ns). This is quite challenging, although it might be possible to find suitable surface reactions, for example, among reversible surface reactions. The advantage of the ultrashort X-ray pulse from the ERL is that it is not too brilliant to cause significant damage to the reaction system, which is essential from a technical point of view.

REFERENCES

[1] K. Amemiya *et al*., *Appl. Phys. Lett*. **99**, 074104 (2011).
[2] T. Gießel *et al*., *Rev. Sci. Instr*. **74**, 4620 (2003).
[3] Y. R. Shen, *et al*., *Phys. Rev. Lett*. **61**, 2883 (1988).
[4] K. Reuter *et al*., *Phys. Rev. Lett*. **93**, 116105 (2004).
[5] M. Nagasaka, *et al*., *Phys. Rev. Lett*. **100**, 106101 (2008).
[6] H. Ogasawara, *et al*., *http://www.slac.stanford.edu/grp/arb/tn/arbvol5/ARDB432.pdf*
[7] M. Bonn, *et al*., *Science* **285**, 1042 (1999).

4.3 Strongly Correlated Electron Systems

4.3.1 Overview of strongly correlated electron systems

The modern electronics used in computers, communication devices and the like are mainly based on electronic theories of condensed matter physics, and on the one-body approximation in particular. It may be no exaggeration to say that today's electronic devices are designed on the basis of the approximation. However, in recent years many physical phenomena that cannot be accounted for in terms of the one-body approximation have been found, such as high T_C superconductivity, colossal magnetoresistance (CMR), and fractional quantum Hall effect. These phenomena may be understood by considering the strong electron correlation, which is ignored in the one-body approximation. This wide diversity of electronic states in these systems is driven by a small change in external conditions such as doping level, temperature, magnetic field or electric field. In fact, different kinds of order coexist or are close to each other in their phase diagrams. The order parameters in these phases are characterized by multiple degrees of freedom such as charge, spin, and orbitals of electrons, as well as the lattice degrees of freedom. The orderings of these degrees of freedom sometimes appear cooperatively and sometimes compete with each other. CMR, which is a massive decrease of electric resistivity in a magnetic field, of manganese oxides is a typical example. CMR occurs in a temperature region where an antiferromagnetic insulator transforms into a ferromagnetic metal. The phenomena have been roughly understood by the double exchange mechanism based on only the charge and spin degrees of freedom, but some of the phenomena cannot be understood by only this simple mechanism. It is generally considered that the interplay between spin, charge, orbital and lattice degrees of freedom is essential in CMR, and in practice, CMR is often observed in the vicinity of the ordered states of these multiple degrees of freedom. Figure 4-14 shows the role of electronic degrees of freedom in strongly correlated electron systems.

It is very important to study the static and dynamic ordered states of these degrees of freedom in order to understand the electronic and magnetic properties in strongly correlated electron systems. Synchrotron radiation is a very powerful probe to detect these electronic ordered states and the dynamics, and many experimental techniques including resonant elastic and inelastic X-ray scattering have been developed in just the past decade. The spatial and time (or energy) resolution have been improved tremendously: the spatial resolution is as low as tens of nm, while, even though the energy resolution of non-resonant inelastic X-ray scattering is in the order of 0.1 meV, that of resonant inelastic X-ray scattering is tens of meV. The time-resolution in typical repeatable pump and probe experiments is about 100 psec. In the ERL with XFEL-O, these resolutions will be improved dramatically. The estimated reso-

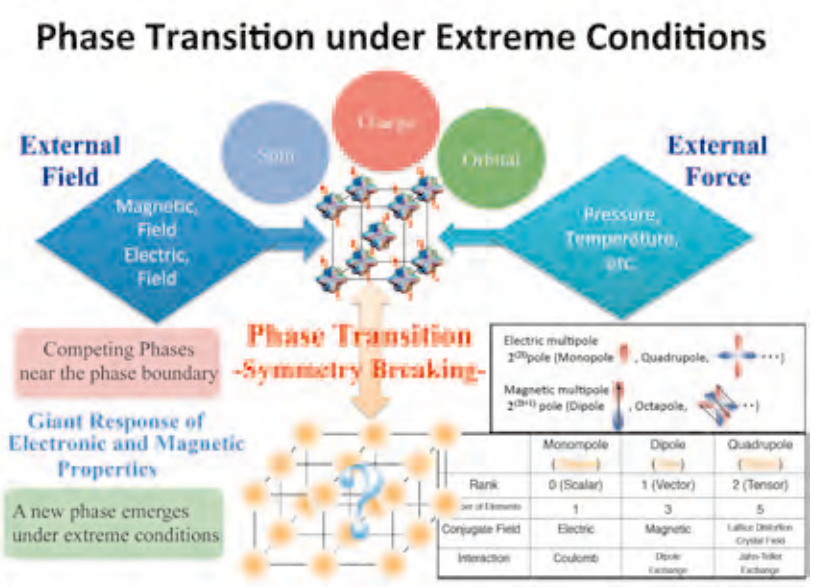

Figure 4-14
The role of electronic degrees of freedom in strongly correlated electron systems. The electronic phases near the phase boundary where competing phases exist can be controlled by applying external fields such as electric and magnetic fields, which may yield great changes in electronic and magnetic properties such as CMR. The ordered states of electronic degrees of freedom can be regarded as multi-pole orderings.

lutions are described in the following sections, as well as the newly developed sciences. By using the ERL light source, we will obtain detailed knowledge about the ordered states of charge, spin, orbital, and lattice degrees of freedoms with very fine spatial and time resolution due to the short pulse property and coherence of the beams. The ERL will also enable a broad range of studies, including organic (molecular) systems, transition metal oxides, rare-earth compounds, and actinoid compounds, in which the electronic correlation is very important, producing rich scientific knowledge as well as valuable applications for materials.

4.3.2 Orderings of electronic degrees of freedom

4.3.2.1 Introduction

Since discovery of high-temperature superconductivity in cuprate oxides in 1987, strongly correlated electron systems have attracted great attention from a number of researchers not only in condensed matter physics but also in other research fields such as elementary particle physics, and device technology. Such novel phenomena and functions in correlated electron systems are mainly attributed to strong competition and correlation between multiple orderings in electronic and lattice degrees of freedom, e.g. spin, charge, orbital and others (see Fig. 4-15) [1–3]. Nowadays, several diffraction techniques are available as tools to identify the long-range orders. In particular, X-rays are a unique probe which can be used to access almost all of the degrees of freedom in solids by tuning its energy, momentum, polarization, and coherence, as shown in Fig. 4-16. X-rays are also used as momentum resolved probes as well as local probes for the electronic degrees of freedom (Fig. 4-17). In this section, we mention the implications of electronic ordering in correlated electron systems, and describes the prospects for X-ray experiments at the ERL.

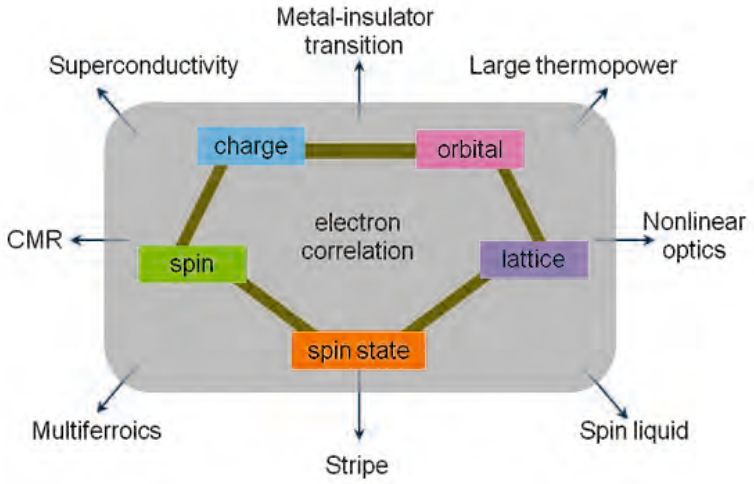

Figure 4-15
Multiple degrees of freedom in correlated electron systems, and novel phenomena and functions.

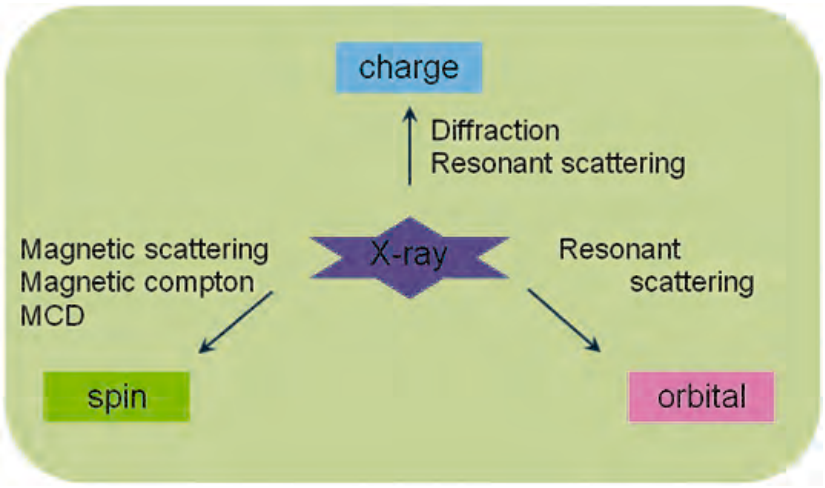

Figure 4-16
X-ray as a probe to detect spin, charge and orbital degrees of freedom.

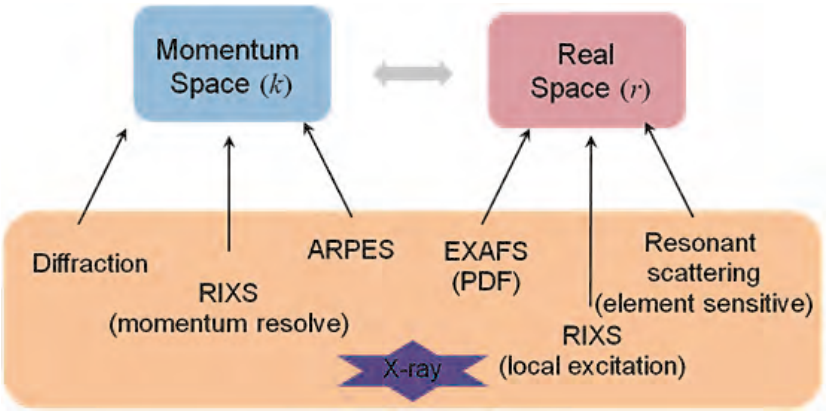

Figure 4-17
X-ray as a momentum resolved probe and a local probe.

4.3.2.2 Scientific goals and challenges

As the temperature of a material is reduced, the thermal motion of electrons and ions diminishes, and some kinds of ordering usually appear to release the entropy. In this manner, the long-range orders of the electronic degrees of freedom are ubiquitously seen in correlated electron systems. Since the early 20th century, X-ray, neutron, and electron diffractions have greatly helped to clarify the long-range orders. The purpose and goals of this research field in modern solid state physics are as follows:

1) Identifying the long-range orders to reveal novel phenomena and functions

It is now widely recognized that when new and exotic phenomena are discovered in a compound, it is essential to identify the long-range ordered phase by changing several parameters and conditions in experimental research on correlated electron systems. A typical example is the study of perovskite manganites. Colossal magneto-resistance was discovered by transport and magnetic measurements. Following the discovery, various diffraction experiments have identified the antiferromagnetic order, charge order, orbital order and others, and the competition and cooperation between them. These outcomes are important for resolving the mechanism of colossal magneto-resistance phenomena, which are believed to be caused by the strong first-order phase transition between the competing electronic and structural phases. Similar examples are also seen in high-temperature superconducting cuprates and multiferroic materials; an antiferromagnetic Neel order and stripe-type charge/spin order are important for resolving the mechanism of superconductivity, and the spiral spin order and its chirality reverse associated with electric polarization flip, which is a candidate microscopic mechanism for multiferroics.

2) Discovery of exotic order or exotic disorder

Conventional long-range orders, such as ferromagnetic, antiferromagnetic, and ferrimagnetic orders in spin systems, often occur and are easily identified by neutron and X-ray diffraction experiments. In contrast, such conventional orders are prevented in some materials because of strong quantum fluctuation, geometrical frustration, and coupling among degrees of freedom. One typical example is the spin liquid state in a frustrated geometrical lattice, where, for some organic materials, no long-range order has been identified down to a few mK, which is much lower than the expected exchange interactions. There are many theories regarding exotic ordered and disordered states for this unusual spin system. Another example is the magnetic octupole order in correlated electron systems. In some f-electron systems, the ordered phase has not been identified for a long time by diffraction experiments, although a large amount of entropy is released at a certain temperature. One plausible candidate is the non-trivial order, the magnetic octupole order in the 4f-orbital where the charge distribution has a cubic symmetry, but the current distribution produces a magnetic octupole at each site. It is difficult to detect such nontrivial orderings and disorders, but doing so would surely shed new light on correlated electron systems.

4.3.2.3 Current status and limitations

As explained above, conventional charge, spin, and orbital orders can be successfully observed by X-ray, neutron and electron diffraction experiments. In the case of X-rays, this is owing to the high brilliance of recent synchrotron X-rays, energy tunability and polarization variation. On the other hand, there is a limitation in the weak amplitude of the ordering. This issue is crucial in correlated electron systems; the

amplitude of the ordering is often reduced by the electron itineracy, geometrical frustration and quantum fluctuation in low dimensional lattices. One example is the charge stripe in high-temperature superconducting cuprates. In a naïve sense, it is believed that doped holes are localized in oxygen sites and a stripe type charge ordered pattern is realized with a certain periodicity. However, in reality, charge modulation in a real space seems to be tiny due to electron itineracy and covalency, and experimental observation of the charge modulation is difficult, even by using a resonant technique.

4.3.2.4 Future prospects with ERL

The high brilliance of the ERL may help to resolve the electronic ordering in correlated systems. The brilliance, which two or three orders higher than that of existing third-generation light sources, might confirm the orderings with weak amplitudes, such as the stripe charge order in cuprates, weak orbital order in titanates, spatially extended charge modulations in organic salts, and small lattice distortion in multiferroic materials. High spatial and temporal coherence will also provide crucial information for ordering, since the nature of short-range orders and characteristics of multi-component domains will be revealed by using speckle and other scattering techniques with X-ray coherence. The short X-ray pulses of pico-second to femto-second order of the ERL will also open up new directions in research of correlated electron systems. In the highly non-equilibrium state created by the laser pulses, this ultrafast X-ray technique might directly detect a hidden ordered state that never occurs in the usual thermal equilibrium state.

REFERENCES

[1] "*Physics of Transition Metal Oxides*", S. Maekawa, T. Tohyama, S.E. Barnes, S. Ishihara, W. Koshibae and G. Khaliullin, (Springer Verlag, Berlin, 2004).
[2] Y. Tokura and N. Nagaosa, *Science* **288**, 261 (2000).
[3] M. Imada, A. Fujimori and Y. Tokura, *Rev. Mod. Phys*. **70**, 1039 (1998).

4.3.3 Dynamics of skyrmion crystal

4.3.3.1 Introduction

In conventional magnets, such as ferromagnets and antiferromagnets, the individual magnetic moments of the magnetic atoms that together comprise the magnetism of the material are all aligned parallel or antiparallel. In some magnets, quantum mechanical interactions between the electrons or the presence of internal electric fields induce more complex spin configurations, such as helical and conical magnets. Recently, a rare arrangement of magnetic moments, the so-called skyrmion crystal, has been observed. A skyrmion can be visualized as a vortex-like arrangement of magnetic moments that, towards the center of the structure, increasingly twist and bend in the downwards direction (Fig. 4-18). The crystal consists not of atoms but exotic swirling magnetic entities. The existence of the magnetic skyrmion crystal state was verified experimentally for the bulk magnets MnSi [1] and FeCoSi [2] and for the thin-film magnet FeGe [3] with a B20-type chiral crystal structure using small angle neutron scattering (SANS) and Lorentz transmission electron microscopy (TEM).

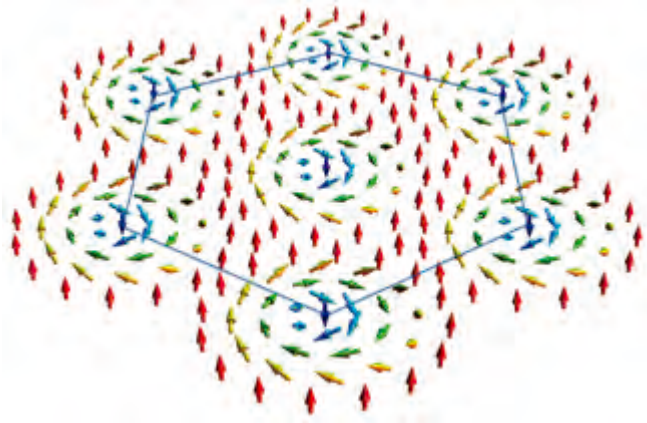

Figure 4-18
Schematic of the spin configuration in skyrmion crystal.

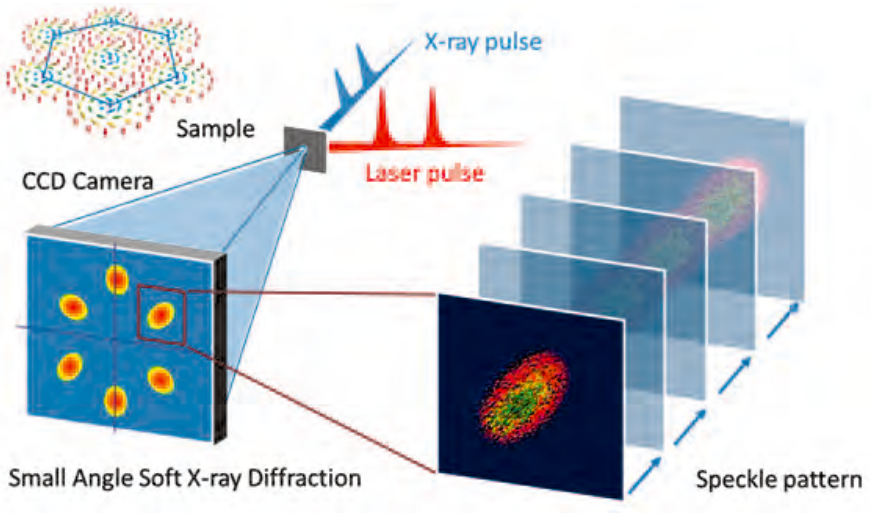

Figure 4-19
Experiment setting for a small angle soft-x-ray diffraction measurement.

For the thin-films of the helimagnet FeGe, the skyrmion crystal exists over a wide temperature range from 50 K to 260 K under a weak magnetic field of 0.1–0.3 T. This compound shows the formation of skyrmion crystal at close to room temperature, in contrast to transition metal silicide materials, MnSi and (Fe,Co)Si, for which the crystal forms at low temperatures below 40 K. These results confirm that skyrmions are very stable and that their manipulation could form the basis for novel magnetic memories or electronic devices.

4.3.3.2 Scientific goals and challenges

The room-temperature stable skyrmion crystal state offers a new route to designing quantum-effect devices based on the controllable skyrmion dynamics. Because the spins have a spiral configuration in a skyrmion crystal, it is thought that large physical interaction occurs in both electricity and magnetism. The advantage over conventional systems is that control is achieved using electric fields, rather than magnetic fields, which are known to be more efficient. The manipulation of individual skyrmions could find application in spintronics, using electron spin to carry information in the same way that electron charge is used in conventional electronics. In addition to the periodic arrangement of many skyrmions, isolated skyrmions were also observed by Lorentz TEM [3] and it was established that they are also stable entities. However, until now, the mechanism responsible for their occurrence was not well understood. Realization of such applications, however, still requires substantial work. In future, we need to understand the dynamics of skyrmions and find ways to manipulate their motion through electromagnetic effect.

4.3.3.3 Current status and limitations

Thus far, skyrmion crystals have been observed only by SANS and Lorentz TEM techniques. However, resonant soft X-ray diffraction measurement would also be a versatile technique for observing skyrmion crystals and their dynamics. In recent years, resonant soft X-ray diffraction has been extensively performed and become a powerful technique for studying electronic and magnetic ordering phenomena. Due to the very large enhancement of the magnetic diffraction signals at the $L_{2,3}$ edges for *3d* ions, skyrmion crystals in transition metal alloys could be observed by this technique. However, one problem in this measurement is that the probed volume is very small, in particular due to the very limited penetration depth of less than several hundred nm at the *3d* transition metal *L* absorption edge. Because of the insufficient soft X-ray flux, it is currently difficult to obtain sufficient soft X-ray diffraction intensities at existing X-ray storage rings.

4.3.3.4 Future prospects with ERL

The X-ray sources of the ERL will deliver coherent hard and soft X-ray beams that are hundreds of times more intense than existing third-generation storage ring X-ray sources. By using the coherence of the X-ray beam, a speckle scattering pattern, which is a diffraction limited structure factor, could reveal some spatial inhomogeneous arrangement of skyrmions and/or scattered isolated skyrmions (Fig. 4-19). Furthermore, these intense X-ray pulse beams will enable novel ways of probing not only speckle scattering but also X-ray photon correlation spectroscopy (XPCS). The XPCS is a novel technique that studies the slow dynamics of various equilibrium and non-equilibrium processes. If the state of a skyrmion crystal changes with time, the speckle pattern will change, thus by studying the time dependence of the scattered intensity at a fixed wave-vector, it will be possible to probe the dynamics of the skyrmion crystal when out of thermodynamic equilibrium. This method is beneficial in shorter length scales than in light scattering and longer time scales than with the neutron spin echo technique. The technique would help clarify skyrmion dynamics and ways of manipulating isolated skyrmions, and may eventually lead to skyrmion-based devices.

REFERENCES

[1] S. Mühlbauer *et al*., *Science* **323**, 915 (2009).
[2] X.Z. Yu, Y. Onose, N. Kanazawa, J.H. Park, J.H. Han, Y. Matsui, N. Nagaosa and Y. Tokura, *Nature* **465**, 901 (2010).
[3] X.Z. Yu, N. Kanazawa, Y. Onose, K. Kimoto, W.Z. Zhang, S. Ishiwata, Y. Matsui and Y. Tokura, *Nature Material.* **10**, 106 (2011).

4.3.4 Electronic structure of transition metal oxide devices

4.3.4.1 Introduction

The voltage-induced nonvolatile resistance switching (RS) phenomena observed in some oxide materials have recently attracted much attention as the basis for next-generation nonvolatile random access memory technology, called resistance random access memory (ReRAM). ReRAM has several advantages such as a simple structure consisting of a metal/oxide/metal sandwich, high-density integration, and high operation speed [1]. However, the mechanism of RS is not yet fully understood, thus hindering the future application potential of ReRAM. One of the main models used to explain the RS phenomena is the “conduction filament” model: conductive filamentary paths are generated by the application of voltage that induces the local reduction of oxides sandwiched between two electrodes. The formation/rupture of conductive (metallic) paths in transition metal oxides occur as a result of local reduction/oxidation in transition metal ions: the oxidation of a segment of the transition metal network induces the high-resistance states (HRS), while the reduction in the oxidized segment induces the low-resistance states (LRS). Thus, partial reduction/oxidation may occur at local areas in the transition metal oxides. Therefore, direct observation of the reduced path formation and the disappearance of the conductive path in ReRAM devices during memory operation is the key to understanding the RS phenomena.

4.3.4.2 Scientific goals and challenges

However, due to the lack of information on the spatial distribution of chemical states in the device structure and the time evolution of the filament rupture/formation, the microscopic origin of the RS phenomena has not been elucidated. Thus, the scientific goals and challenges of this study are direct observation of the spatial distribution and time evolution of chemical states, which are responsible for the changes in the resistance in ReRAM.

4.3.4.3 Current status and limitations

A photoemission electron microscope (PEEM) in combination with wavelength-tunable synchrotron radiation (SR) is a powerful technique for addressing this issue. The PEEM detects the lateral distribution of the photoelectron emission intensity as a function of the photon energy, and so can be used to map the chemical states of constituent elements by X-ray absorption spectroscopy (XAS). In order to investigate the lateral chemical (oxidation/reduction) distributions in CuO-based ReRAM devices [2], PEEM observations of planar-type Pt/CuO/Pt resistance-switching devices fabricated on SiO_2/Si substrates have

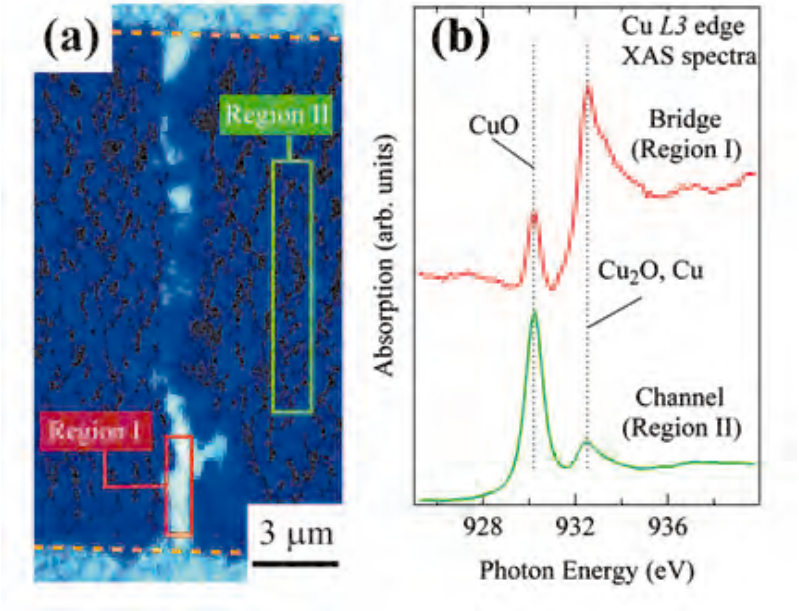

Figure 4-20
(a) Chemical PEEM image of the planar-type Pt/CuO/Pt device after the application of voltage. The PEEM images were recorded at photon energies corresponding to the Cu L_3 absorption edge. (b) XAS spectra recorded in the filament path (Region I) and CuO channel (Region II) near the Cu L_3 absorption edge. These XAS spectra consist of two peaks, which are assigned to the CuO states at 930.3 eV and reduced states (Cu_2O and/or Cu metal) at 932.6 eV.

been performed [3].

Figure 4-20(a) shows the reduced state map of Cu ions at the Pt/CuO/Pt device obtained from XAS-PEEM measurements. The bright regions in the map indicate the abundance of reduced components such as Cu_2O and/or Cu metal in the CuO matrix. It is clearly seen that the reduced regions run vertically from cathode to anode like a chain of islands, suggesting the formation of reduction path due to the application of voltage between the two electrodes. The reduction in chemical states in the filament path is also confirmed by the micro-XAS spectra, as shown in Fig. 4-20(b); a high degree of reduction from CuO to Cu_2O and/or Cu metal is clearly observed in the filament paths (Region I), while the original CuO components are dominant outside of the filament paths (Region II). Since the conductivity is strongly enhanced by the reduction of CuO [2], these results indicate that the reduction path formed in the CuO channel due to application of voltage is responsible for the occurrence of the RS phenomena in Pt/CuO/Pt ReRAM devices.

The present study demonstrates the usefulness of the micro-region XAS measurements using PEEM for studying the chemical distribution in oxide devices and so on. The resistances of LRS and HRS are 1.83 and 41.4 kΩ, respectively [2]. Thus, partial reduction/oxidation may occur at local areas in the ReRAM structure. However, there was no significant difference in the chemical-state distribution between the LRS and HRS within the experimental resolution. These results strongly suggest that the reduction/oxidation area responsible for the RS is considerably smaller than the spatial resolution of the present PEEM measurements (80 nm).

4.3.4.4 Future prospects with ERL

Much higher spatial and time resolution will be achieved with the ERL. Microscopic studies with higher spatial and time resolution will help clarify the chemical reactions in oxide devices, and enable us to observe the change in chemical states during ReRAM operation (Fig. 4-21). We hope that such studies using the ERL will lead to the development of devices having inhomogeneous chemical states in the near future.

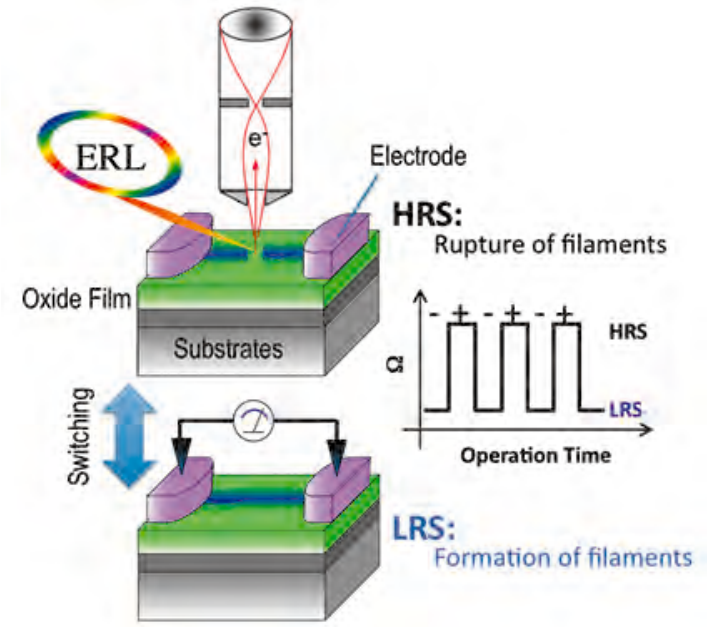

Figure 4-21
Schematic illustration of microscopic measurements using ERL. The high spatial and time resolution will reveal the change in chemical states during operation.

REFERENCES

[1] "International Technology Roadmap for Semiconductors", (ITRS 2009 edition) Online. Available: http://www.itrs.net/
[2] K. Fujiwara *et al.*: *Jpn. J. Appl. Phys.* **47**, 6266 (2008).
[3] R. Yasuhara *et al.*: *Appl. Phys. Lett.* **95**, 012110 (2009).

4.3.5 Electronic structure at the surface and interface of magnetic thin films

4.3.5.1 Introduction

The surface and interface of magnetic thin films play essential roles in the appearance of extraordinary magnetic properties such as perpendicular magnetic anisotropy and giant magnetoresistance effect, which are not observed in bulk materials. To control such fascinating magnetic properties, it is important to clarify the crystalline, magnetic and electronic structures of the surface and interface of magnetic thin films and multilayers. Moreover, lateral inhomogeneity of the thin films is also essential, since most magnetic materials exhibit a domain structure so as to minimize the magnetostatic energy arising from the magnetic poles and domain walls. It should be emphasized that such domain structures, as well as the surface and interface, would affect the magnetization dynamics, which are important in order to develop ultrafast magnetic data writing in magnetic memory devices. Thus, the lateral, depth, and time resolutions need to be achieved in order to investigate and develop magnetic thin film materials.

4.3.5.2 Scientific goals and challenges

Our goal is to clarify the origin of the magnetic properties of thin films from the viewpoint of electronic and crystalline structures. Such information can be used to develop new materials that exhibit much better magnetic properties than those of present available materials. Conventional X-ray techniques can hardly be applied to thin films, however, due to the lack of periodicity in the film normal direction. We need to develop new techniques in order to directly reveal the crystalline, electronic, and magnetic structures of each layer in thin film and multilayer samples.

4.3.5.3 Current status and limitations

X-ray magnetic circular dichroism (XMCD) in absorption is one of the most powerful techniques to determine the spin and orbital magnetic moments element specifically. Although XMCD itself has neither lateral nor depth resolution, a lateral resolution of ~10 nm has been achieved by combining XMCD with photoelectron emission microscopy (PEEM) [1]. On the other hand, a depth-resolved XMCD technique has been developed by using the detection angle dependence of the Auger electrons emitted after X-ray absorption as illustrated in Fig. 4-22(a) [2]. By using the depth-resolved XMCD technique, the magnetic anisotropy energies at the surface, interface, and inner layers can be separately determined, in order to reveal the origin of magnetic anisotropy of a multilayer as shown in Fig. 4-22(b)-(d) [3]. It is still impossible, however, to achieve high lateral and depth resolutions simultaneously, because the depth-resolved technique cannot be combined with PEEM, while lateral resolution cannot be realized in the present depth-resolved XMCD.

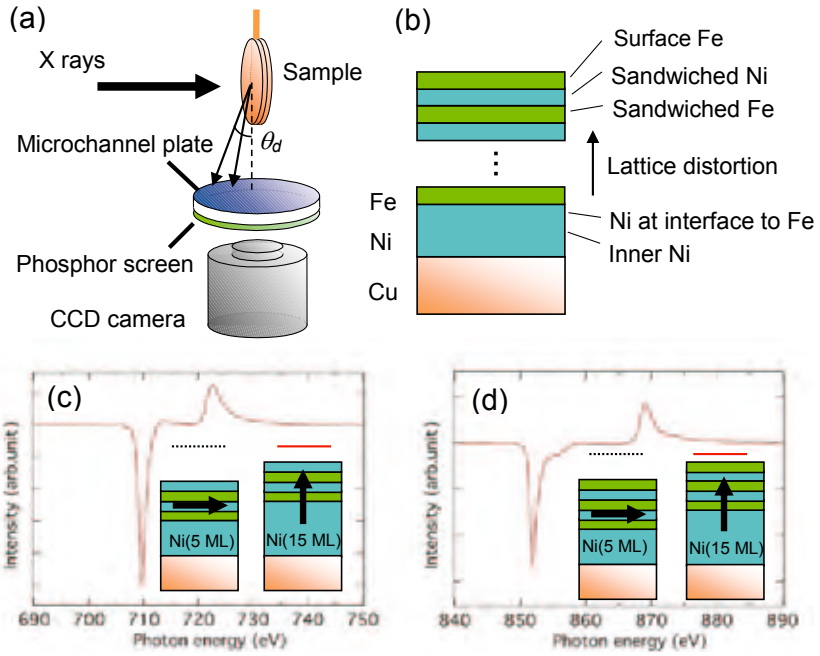

Figure 4-22
(a) Schematic diagram of the depth-resolved XMCD technique, in which the depth resolution is realized by recording the electron-yield XMCD data at different detection angles, which correspond to different probing depths. (b) Factors which determine the magnetic anisotropy of an Fe/Ni multilayer, and XMCD spectra for (c) Fe layers sandwiched by Ni and (d) Ni layers sandwiched by Fe.

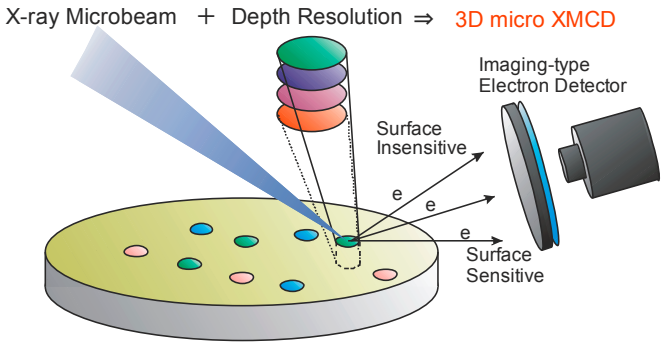

Figure 4-23
Schematic diagram of a three-dimensional micro XMCD technique, in which the X-ray microbeam is combined with the depth-resolved XMCD.

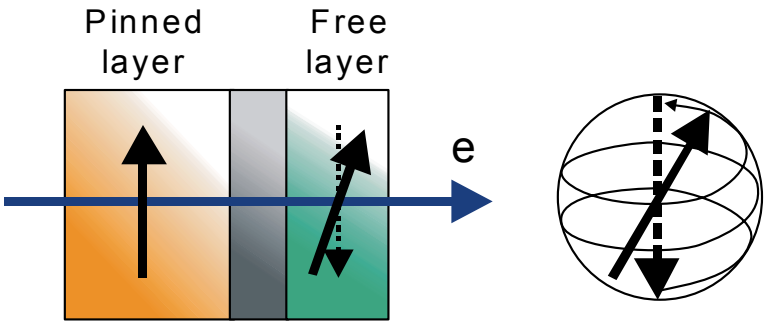

Figure 4-24
Schematic illustration of a magnetization reversal process induced by spin transfer torque.

4.3.5.4 Future prospects with ERL

One of the simplest ways to achieve both the lateral and depth resolutions simultaneously is to combine the X-ray microbeam with depth-resolved XMCD as illustrated in Fig. 4-23. Since an X-ray beam size of several nm can be realized by using ERL and an atomic layer resolution has already been achieved in depth-resolved XMCD, a powerful three-dimensional micro XMCD technique will be developed. Moreover, this technique can be applied to general X-ray absorption spectroscopy including the extended X-ray absorption fine structure (EXAFS), which yields information on the geometric structure around the X-ray absorbing atom. Therefore, the crystalline, electronic, and magnetic structures can be determined three dimensionally at a lateral resolution of several nm and a depth resolution of sub nm.

Another prospect is the observation of spin dynamics. Figure 4-24 shows a magnetization reversal process induced by a current through two magnetic layers, which is used in the data writing process in a magnetic random access memory. Magnetization of the free layer undergoes a spin transfer torque and precession is induced as illustrated in Fig. 4-24. The duration of the precession depends on the damping factor and magnetic anisotropy of the free layer, and is several ns at present. Although it must be drastically reduced to achieve ultrahigh-speed data recording, the interface is likely to affect the magnetization reversal process at such an ultrafast regime. Therefore, observation of the magnetization dynamics with a three-dimensional spatial resolution and a ps time resolution is necessary to clarify the limitations of the spin reversal process and improve the data writing speed.

REFERENCES

[1] "*Magnetic Microscopy of Nanostructures*", edited by H. Hopster and H.P.Oepen, (Springer 2005).
[2] K. Amemiya *et al*., *Appl. Phys. Lett*. **84**, 936 (2004). ; K. Amemiya, *Phys. Chem. Chem. Phys*. **14**, 10477 (2012).
[3] M. Sakamaki and K. Amemiya, *Appl. Phys. Express* **4**, 073002 (2011).

4.3.6 Electron dynamics explored by resonant soft X-ray emission spectroscopy in strongly correlated electron systems

4.3.6.1 Introduction

One of the advantages of using resonant soft X-ray emission spectroscopy (RSXES) is its wide range of energy detection and information about element-specific, charge-neutral excitations which is not accessible by low energy photon (visible-VUV) scattering and/or photoemission spectroscopy. Technical advances in RSXES in the last two decades have increased the figure of merit (detection rate/energy resolution) by hundreds or thousands of times, and specific excitation in the energy range within 100 meV has been detected [1]. Figure 4-25 shows the typical energy range of elementary excitations essential for various physical properties of strongly correlated electron systems. Using a conventional soft X-ray emission spectrometer, the focus of interest has been *d-d*, *f-f* excitations reflecting crystal field splitting or charge transfer excitations describing hybridization between a metal and ligands in transition-metal and rare-earth compounds. Recent topics in ultrahigh resolution RSXES include the observation of charge (electronic), lattice (vibronic), spin or orbital excitations as the dynamic response of materials due to the evolution in energy resolution and introduction of momentum dependence [2–4]. This should make RSXES a highly informative tool for investigating the electronic properties of Mott insulators, topological insulators, heavy fermions, magnetic semiconductors, high-temperature superconductors, new classes of superconductors such as iron pnictides, and so on.

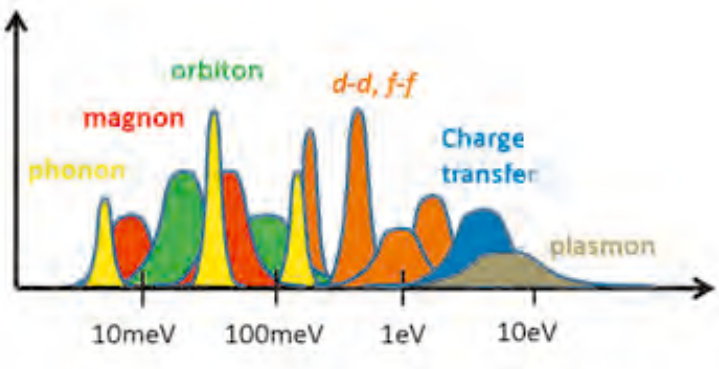

Figure 4-25
Typical energy range of elementary excitations.

4.3.6.2 Scientific goals and challenges

The dynamics of charge, lattice, spin, orbital excitations and their coupling of degrees of freedom describe various physical properties of strongly correlated electron systems. RSXES will reveal not only the energy of each elementary excitation but also their mutual interactions. Ultrahigh resolution RSXES spectra with energy resolution down to 10 meV will separate out excitation originating from the exchange interaction of magnetic materials, superconducting gaps in superconductors or Kondo resonance excitations [5] as individual peaks. Ultrahigh resolution will help solve a more practical problem in RSXES, i.e. violation of the symmetry selection rule due to vibronic coupling. Many peaks whose intensity does not follow expected polarization or excitation-energy dependence have been overlooked. The origin of this violation will be explained by the contribution of low-energy vibrational excitations in ultrahigh resolution RSXES.

Occasionally it is difficult to distinguish the type of excitation or mutual interaction only by the energy and/or momentum distribution of elementary excitations; they can be explored by time-resolved pump-probe (e.g. laser excitation, RSXES detection) experiments. The lifetime of each excitation and the duration of interactions range from sub-fs to ns depending on the type of elementary excitation involved (Fig. 4-26). A soft X-ray photon source with a pulse of less than 100 fs will distinguish the lattice contribution to elementary excitations, i.e. electron-phonon and/or spin-phonon interactions. The most challenging and important experiment in this time domain will be the detection of electron-spin interactions which may be related to spin-mediated superconductivity [6] or may clarify how magnetism is manipulated on an ultrafast time scale [7].

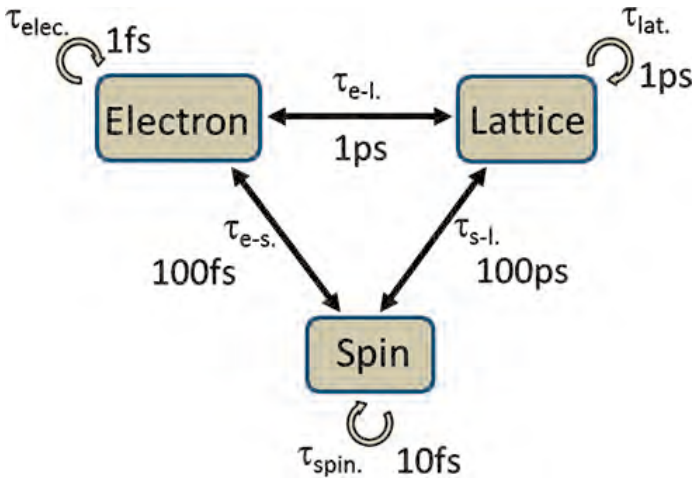

Figure 4-26
Ultrafast dynamics of elementary excitations and their mutual interactions. (ref [7] modified)

4.3.6.3 Current status and limitations

The energy resolution of RSXES is intrinsically limited only by the lifetime of the valence excited state, which is one or two orders of magnitude narrower than the best energy resolution of around 100 meV available at present. Technically the energy resolution could be lowered to 10 meV by using several or dozens of meters-long spectrometers in the near future, but what actually limits the resolution is the signal intensity since there is a well-known trade-off between resolution and detection efficiency. Energy resolution is also limited by the light source; a resolving power $E/\Delta E > 50000$ is required at O *K*-edge, which is not feasible using conventional optics.

Resolution in the time domain is limited both by the light source and detector. Using the 10–100 ps bunch of existing synchrotron radiation sources, we cannot approach most of the electron dynamics shown in Fig. 4-26.

4.3.6.4 Future prospects with ERL

The most notable property of the ERL is the time structure of electron bunches with a width of around 100 fs, which may yield breakthroughs in RSXES experiments. The energy resolution of RSXES is not limited by the energy uncertainty principle, which is only 3 meV for a 100-fs pulse width. The use of low energy photons (visible to VUV) and soft X-rays from the same electron bunch will help solve the timing problems for 100-fs resolution pump-probe experiments [8]. Another important characteristic of the ERL is its high repetition frequency. Since RSXES is one of the most photon-hungry experiments, total flux of the incident beam is much more important than the peak intensity of each photon pulse, and thus RSXES will benefit greatly from using the ERL.

REFERENCES

[1] G. Ghiringhelli, A. Piazzalunga, X. Wang, A. Bendounan, H. Berger, F. Bottegoni, N. Christensen, C. Dallera, M. Grioni, J.-C. Grivel, M. Moretti Sala, L. Patthey, J. Schlappa, T. Schmitt, V. Strocov and L. Braicovich, *Eur. Phys. J. Special Topics* **169**, 199 (2009).
[2] L. Braicovich, J. van den Brink, V. Bisogni, M. Moretti Sala, L.J.P. Ament, N.B. Brookes, G.M. De Luca, M. Salluzzo, T. Schmitt, V.N. Strocov and G. Ghiringhelli, *Phys. Rev. Lett*. **104**, 077002 (2010).
[3] S. Glawion, J. Heidler, M.W. Haverkort, L.C. Duda, T. Schmitt, V.N. Strocov, C. Monney, K. Zhou, A. Ruff, M. Sing and R. Claessen, *Phys. Rev. Lett.* **107**, 107402 (2011).
[4] C. Ulrich, L.J.P. Ament, G. Ghiringhelli, L. Braicovich, M. Moretti Sala, N. Pezzotta, T. Schmitt, G. Khaliullin, J. van den Brink, H. Roth, T. Lorenz and B. Keimer, *Phys. Rev. Lett*. **103,** 107205 (2009).
[5] A. Kotani, *Phys. Rev. B* **83**, 165126 (2011).
[6] G.M. Zhang, Z.Y. Lu and T. Xiang, *Phys. Rev. B* **84**, 052502 (2011).
[7] E. Beaurepaire, J.C. Merle, A. Daunois and J.Y. Bigot, *Phys. Rev. Lett*. **76**, 4250 (1996).
[8] I. Matsuda, private communication.

4.3.7 Dynamics in strongly correlated electron systems

4.3.7.1 Introduction

In strongly correlated electron systems (SCES) such as transition metal oxides, mutual interactions of charge/spin/orbital degrees of freedom of electrons and lattice degree of freedom determine their electronic properties. In order to understand the mechanism of these properties, it is necessary to clarify the roles of the interactions by observing excitations and fluctuation of the degrees of freedom. In other words, investigating the dynamics of the degrees of freedom is indispensable in the study of SCES. In addition, momentum-resolution is important for the study of condensed matter to observe the dispersion relation of the excitations; for example, the magnitude of magnetic interaction can be elucidated from the dispersion relation of magnons, as described in solid state physics textbooks. X-rays are a suitable probe for this purpose.

There are two approaches for studying dynamics using X-rays. One is time-resolved experiments, which will be a powerful technique since short duration (~ 0.1 ps) is a key characteristic of the X-rays from the ERL. The other approach is inelastic scattering, which uses rather faster time scales (ps to fs, or equivalently meV to eV) by working in the energy space. In SCES, the latter is suitable because the energy scale of most interactions is above the order of 1 meV (~ 4 ps), so we restrict ourselves to inelastic X-ray scattering (IXS) in this section. The hierarchy of interactions in SCES and related excitations (gaps) is shown in Fig. 4-27.

In the last decade, IXS has been developed by utilizing X-rays from third-generation synchrotron radiation facilities and is now an established tool for measuring phonon and electronic excitations. However, most IXS experiments are still limited by photon flux, and in particular, it is much harder to observe electronic excitation with IXS because its intensity is weaker by a factor of $1/Z^2$, where Z is atomic number, than that of the phonon. Only several studies on electronic excitations in SCES have been reported so far. Improvement of the incident photon flux will facilitate the progress of IXS, and so the next-generation X-ray source, XFELO, perfectly meets the requirement of IXS. It has been estimated [1] that XFELO can deliver photons of high spectral purity with ~ 1 meV bandwidth ($\Delta E/E = 10^{-7}$ at 10 keV), 10^9 photons per pulse, and 1-MHz pulse repetition rate; in total, a flux of 10^{15} photons/sec/meV will be available. In contrast, the present flux at the IXS beamlines at SPring-8, e.g. BL11XU and BL35XU, emitted from an undulator is approximately 10^9 photons/sec/meV [2, 3], namely, XFELO will increase the flux by 6 orders of magnitude. Two other characteristics of XFELO, transverse coherence and short duration of the pulse, will be useful for space- or time-resolved IXS experiments.

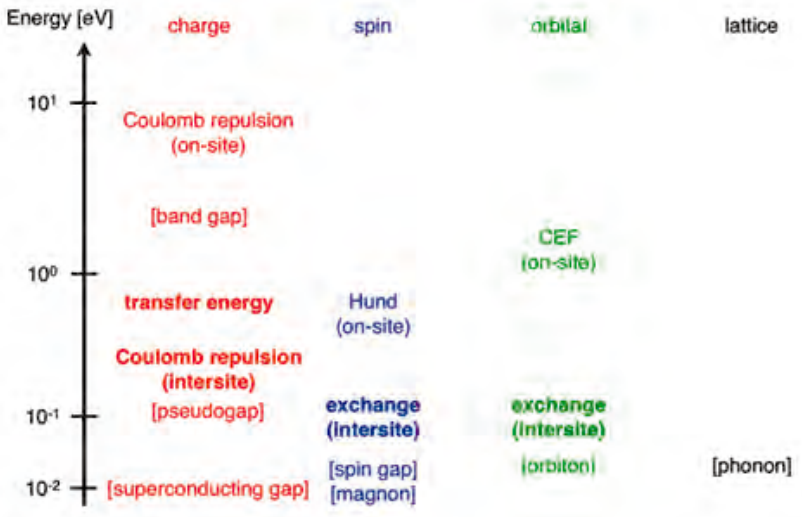

Figure 4-27
Hierarchical interactions of electronic (charge/spin/orbital) and lattice degrees of freedom and related excitations (gaps) in strongly correlated electron systems. Observation of momentum dependence is important for the intersite interactions denoted by bold letters.

4.3.7.2 Scientific goals, challenges, and future prospects with XFELO

Improvement of the incident flux by 10^6 may revolutionize the science of using the IXS technique. First of all, electronic excitations will be practical by overcoming the factor of $1/Z^2$. X-rays are predominantly scattered due to the charge of electrons, and the intensity of IXS is proportional to the dynamic charge correlation function $N(Q,\omega)$ which is a fundamental physical quantity. If observation of charge excitations with meV resolution is possible, IXS would greatly complement inelastic neutron scattering, with which we can measure the dynamic spin correlation function $S(Q,\omega)$, to study the dynamics of electronic degrees of freedom. To date, charge excitations have been mostly investigated by resonant inelastic X-ray scattering (RIXS) but due to the limitation of optical elements the energy resolution of RIXS (~ 100 meV) is insufficient to discuss the charge dynamics coupled to other degrees of freedom.

Copper oxides are the most intensively studied material in SCES. They have attracted great interest not only in view of their high transition temperature of superconductivity but also the anomalous behavior of a strongly correlated metal [4], including pseudogap, kink in the electronic band observed in ARPES, and stripe order which is regarded as a self-organization of doped holes. These phenomena are a consequence of coupling of the charge with the spin and possibly with the lattice. While the dynamics of spin and lattice in the Q-ω space have been investigated with inelastic neutron scattering (and also by IXS for the lattice), the charge sector, which is necessary for a comprehensive understanding of these phenomena, still remains unexplored. Furthermore, in most cuprates, only the single $d_{x^2-y^2}$ orbital (and oxygen 2p orbitals) is relevant for the physical properties, which means that their electronic structure is considered to be a simple and basic model of correlated electrons. Hence, observation of $N(Q,\omega)$ of strongly correlated copper oxides is of great importance and will have a significant impact in the field of SCES.

Charge order is often found in SCES. In some cases, the charge order is adjacent to a superconducting phase and the charge fluctuation may lead to superconductivity. The primary interaction of the charge order in SCES is considered to be the Coulomb interaction between electrons rather than the Peierls instability by the electron-phonon interaction in conventional CDW materials. In the charge ordered state, new excitations are expected, for example, a charge collective mode which is analogous to the magnon in magnetic ordered states. A recent RIXS study suggested such a collective mode [5], but detailed examination of the charge excitation spectra with better energy resolution is required to prove the new excitation mode.

Orbital excitations are also accessible with IXS. Non-dipole transitions become allowed at the high momentum transfer of IXS and *d-d* excitations of transition metals have been reported [6]. Orbital physics is an attractive area in strongly correlated transition metal oxides [7]. In this field, exploration of a collective orbital excitation, the so-called orbiton, is a long-standing issue. While the orbital excitation at zero momentum transfer could be observed with Raman scattering, it is considered that IXS could be used as an experimental technique to measure the dispersion relation of the orbital excitation, which has never been measured to date. Another subject regarding orbital excitation is related to Fe-based high-temperature superconductors, which are attracting much interest in condensed matter physics. In contrast to cuprates, the orbital degree of freedom is active in Fe-based superconductors and the orbital fluctuation may be the glue for forming Cooper pairs [8]. If this is the case, observation of the orbital fluctuation would be an essential experiment for understanding superconductivity.

So far, observing electronic excitations has been discussed as a new possibility of IXS, but IXS could also be used to extend the current phonon measurement using XFELO. Fine focusing (nm size) of X-rays enables us to measure phonon spectra with spatial resolution. Though they do not belong to SCES, we exemplify relaxors as a suitable sample for this technique. In the relaxors, the frequency-dependent dielectric constant shows a broad peak in its temperature dependence and inhomogeneity, that is, polar nanoregions implanted in the paraelectric matrix are essential for the relaxor behavior. Spatially-resolved phonon measurement, which can detect ferroelectric instability, can be useful for understanding the formation of the polar nanoregions. Such inhomogeneity sometimes emerges spontaneously in transition metal oxides as a result of multiple competing phases [9] and spatially-resolved IXS may also be helpful in SCES. In addition, it will be possible to observe phonons at the surface and at the interface.

Finally, we describe a few challenging issues for IXS in the future. One is observing excitation across the superconducting gap, which is a dream for researchers of IXS. Symmetry of the superconducting gap in reciprocal space is crucially important to understand the mechanism of unconventional superconductivity. At present, it is possible with ARPES or STS, but both experimental techniques are surface sensitive. Fortunately, the main unconventional superconductors with high transition temperature, namely copper oxides and iron arsenides, have a layered structure and their surface can be cleaved and used for these experiments. In contrast, IXS is bulk sensitive and applicable to superconductivity in three-dimensional materials. Another challenge is magnetic excitation. In the case of diffraction, the ratio of magnetic scattering to charge scattering was estimated to be 10^{-6} [10]. If the ratio is comparable in inelastic scattering, observation of magnetic excitation with IXS may be possible.

In summary, improvement of incident flux by 6 orders of magnitude will revolutionize the study of dynamics and XFELO will open up many possibilities in IXS. When ERL and XFELO are realized, we will be able to observe qualitatively new excitations of charge, orbital, lattice, and maybe spin degrees of freedom in strongly correlated electron systems.

REFERENCES

[1] K.J. Kim *et al*., *Phys. Rev. Lett*. **100**, 244802 (2008).
[2] A.Q.R. Baron *et al*., *Nucl. Instrum. Methods Phys. Res. A* **627**, 467 (2001).
[3] T. Inami *et al*., *Nucl. Instrum. Methods Phys. Res. A* **1081**, 467 (2001).
[4] P.A. Lee *et al*., *Rev. Mod. Phys.* **78**, 17 (2006).
[5] S. Wakimoto *et al*., *Phys. Rev. Lett*. **102**, 157001 (2009).
[6] B. Larson *et al*., *Phys. Rev. Lett*. **99**, 026401 (2007).
[7] Y. Tokura and N. Nagaosa, *Science* **288**, 462 (2000).
[8] C.C. Lee *et al*., *Phys. Rev. Lett.* **103**, 267001 (2009).
[9] E. Dagotto, *Science* **309**, 257 (2005).
[10] M. Blume, *J. Appl. Phys.* **57**, 3615 (1985).

4.3.8 Multiferroic materials

4.3.8.1 Introduction

Research on magneto-electric (ME) multiferroics has been increasing rapidly because of the interest in a strong coupling between magnetism and electricity in materials [1–3]. In the 1960s, scientists found that electricity and magnetism in some special magnetic materials can be coupled in a different way from Maxwell's equations thanks to Pauli's exclusion principle and relativity with regard to electron spin, that is, the induction of electric polarization by the application of a magnetic field and that of magnetic polarization by the application of an electric field [4–6]. Most of the ME coupled phenomena in matter reported in the 20th century were linear or quadratic effects with very few exceptions. H. Schmid provided the concept of multiferroics in the 1990s to enhance the ME effect [7], but did not achieve great experimental success. The discovery of phase-transition type ME coupling in $TbMnO_3$ in 2003 [8] introduced the concept of spin-driven ferroelectricity [3]. This concept led to the discovery of many ME multiferroics exhibiting a giant and novel type of ME response.

4.3.8.2 Scientific goals and challenges

The primary order parameter in most spin-driven ferroelectrics is a spin correlation function. The application of a magnetic field strong enough for metamagnetic transition can cause some change in ferroelectric polarization. This enables magnetic control of ferroelectric polarization in a rather straightforward way. On the other hand, electric control of magnetization in multiferroics is still challenging. Demands for the modification of magnetization in insulators, including multiferroics, by an external electric field are increasing also from the viewpoint of spintronics applications. A promising route to combining magnetization and electric polarization is domain-wall control in multiferroics [9, 10]. If a ferromagnetic domain wall can be firmly clamped to a ferroelectric domain wall, it would be fairly easy to manipulate the magnetization by an electric field. It has also been pointed out that the dynamics of a ferroelectric domain wall in multiferroics play an essential role in the gigantic magneto-capacitance effect in some multiferroics like $DyMnO_3$ [11]. Understanding the structure and dynamics of domain walls in multiferroic materials is hence a central issue in the research of multiferroics.

In some multiferroics, a THz electric field can excite a spin wave [12, 13]. Such an AC electric-field induced magnetic excitation, which has recently been referred to as electro-magnons, would pave the way for the ultrafast (~ pico-second) control of magnetism by light. Nevertheless, the microscopic origins of electro-magnons are not yet fully understood. An ultimate goal is to observe the time evolution of spin alignment in multiferroics after irradiation.

4.3.8.3 Current status and limitations

Extensive studies since the discovery of giant ME response in $TbMnO_3$ [8] have revealed the microscopic mechanisms of spin-driven ferroelectricity. In particular, neutron diffraction studies of the single-domain ferroelectric state have clearly shown the relation between spin alignment and electric polarization. Scientists are convinced that several types of magnetic structure can induce ferroelectric polarization.

On the other hand, investigations on the spatially inhomogeneous or temporarily evolved states in multiferroics is still ongoing. The domain structures in multiferroics have been investigated by second-harmonic generation (SHG) of light or scanning-probe microscopy in most cases [14–16]. However, the spatial resolution of SHG imaging is limited by the wavelength of light. Scanning-probe microscopy provides only information on the surface, so a bulk-sensitive high-resolution imaging technique needs to be developed for understanding the structure and dynamics of domains in multiferroics.

Electro-magnons in multiferroics are now being extensively studied by means of theoretical calculation, THz spectroscopy, electron spin resonance (ESR), neutron inelastic scattering, and so on. However, the microscopic mechanisms of electro-magnons are still under debate [13]. If one could conduct a transient magnetic structure analysis after femto-second pulsed-laser irradiation, the nature of electro-magnons would become much clearer.

4.3.8.4 Future prospects with ERL

The ERL will provide a coherent, intense, and short-pulsed X-ray beam, which will be invaluable for overcoming the abovementioned challenges. Several imaging techniques utilizing a coherent X-ray beam have been proposed; they are bulk-sensitive and have a spatial resolution much better than that of optical imaging. If we can distinguish different types of domains with X-ray diffraction, imaging techniques will become a most useful tool for multiferroic science. The short-pulsed nature of the X-ray beam from the ERL would enable us to study the time evolution of magnetic X-ray scattering from multiferroics, thus providing key information to reveal the nature of the electro-magnon.

REFERENCES

[1] Special edition of multiferroics; *J. Phys.: Condens. Matter 20*, **43**, (2008).
[2] Y. Tokura and S. Seki, *Adv. Mat*. **22**, 1554 (2010).
[3] T. Arima, *J. Phys. Soc. Jpn*. **80**, 052001 (2011).
[4] I.E. Dzyaloshinskii, *Zh. Exp. Teor. Fiz*. **37**, 881 (1959). [*Sov. Phys. JETP* **10**, 628 (1959)].
[5] D.N. Astrov, *Zh. Exp. Teor. Fiz*. **38**, 984 (1960) [*Sov. Phys. JETP* **11,**708 (1960)].
[6] V.J. Folen, G.T. Rado and E.W. Stalder, *Phys. Rev. Lett.* **6**, 607 (1961).
[7] H. Schmid, *Ferroelectrics* **162**, 317 (1994).
[8] T. Kimura, T. Goto, H. Shintani, K. Ishizaka, T. Arima and Y. Tokura, *Nature* **426**, 55 (2003).
[9] Y. Yamasaki, S. Miyasaka, Y. Kaneko, J.-P. He, T. Arima and Y.Tokura, *Phys. Rev. Lett*. **96**, 207204 (2006).
[10] Y. Tokunaga, N. Furukawa, H. Sakai, Y. Taguchi, T. Arima and Y. Tokura, *Nature Mater*. **8**, 558 (2009).
[11] F. Kagawa, M. Mochizuki, Y. Onose, H. Murakawa, Y. Kaneko, N. Furukawa and Y. Tokura, *Phys. Rev. Lett*. **102**, 057604 (2009).
[12] A. Pimenov, A.A. Mukhin, V.Yu. Ivanov, V.D. Travkin, A.M. Balbashov and A. Loidl, *Nature Phys*. **2**, (2006) 97.
[13] N. Kida, Y. Takahashi, J.S. Lee, R. Shimano, Y. Yamasaki, Y. Kaneko, S. Miyahara, N. Furukawa, T. Arima and Y. Tokura, *J. Opt. Soc. Am. B* **26**, A35 (2009).
[14] M. Fiebig, Th. Lottermoser, D. Fro¨hlich, A.V. Goltsev and R.V. Pisarev, *Nature* **419**, 818 (2002).
[15] D. Meier, M. Maringer, T. Lottermoser, P. Becker, L. Bohatý and M. Fiebig, *Phys. Rev. Lett*. **102**, 107202 (2009).
[16] T. Choi, Y. Horibe, H.T. Yi, Y.J. Choi, W. Wu and S.-W. Cheong, *Nature Mater*. **9**, 253 (2010).

4.3.9 Photoinduced phase transitions

4.3.9.1 Introduction

Photoinduced phase transitions (PIPT) have been attracting attention since their discovery in the 1990s. The number and variety of target materials have grown rapidly to include conjugate polymers, molecular crystals, metal oxides, metal complexes, and so on. This progress has been closely related to progress in laser technology, namely, the ultrafast technique for femtosecond spectroscopy. Meanwhile, theoretical progress has been made by newly developed numerical techniques. Such techniques are similar to those of strongly correlated electron systems, and the above-mentioned systems are often described in this context.

Regarding the phenomena themselves, some of the known PIPTs are described as insulator-to-metal transitions induced by the melting of some orderings such as charge and orbital orders. Since such transitions result in huge changes in both the DC-conductivity and finite-frequency region of optical conductivity, they are prospective candidates for future switching devices. Other phenomena are, for example, charge-density-wave (CDW) to Mott-insulator transitions, which are regarded as one of the order-order transitions, spin-state transitions, between high- and low-spin states, and some conformation changes. It is also important to note that such transitions have been found mainly near the phase boundary of the equilibrium states, whichever type it is. The PIPTs are thus closely related to the multi-stability inherent to materials.

4.3.9.2 Scientific goals and challenges

In our present understanding, there are at least two goals to be kept in mind.

Goal 1: Real-time tracing of molecular and/or atomic movements like making a movie. Since the PIPTs are accompanied by global structural changes, we inevitably need much information, and resultant snapshots will visualize the details and essence of the dynamics vividly. Regarding the time scales, the typical time periods of atomic motions correspond to their phonon or vibration frequencies. Although some of the mode frequencies are high at more than 1000 cm^{-1}, many other modes relevant to structural transitions have low frequencies of less than 100 cm^{-1}. Note that the frequency of 30 cm^{-1}, for example, corresponds approximately to a time period of around 1 ps. Moreover, the global motions, or at least cluster-like motions, will take a much longer time. From a theoretical viewpoint, the problem is first to grasp an image of the adiabatic potential surfaces and possible new orders as illustrated in Fig. 4-28. We will then proceed to the next step, which is the time-dependent treatments like molecular dynamics (MDs) based on the potential surfaces.

Goal 2: The second goal is to understand ultrafast dynamics on a time scale of femtoseconds "immediately" after the photoexcitation. In Fig. 4-28, this stage of the dynamics is depicted by the red region labeled "Ultrafast Phenomena." This stage is mainly governed by electronic motions since its energy scale of 1 eV corresponds to about 1 femtosecond. This type or aspect of the dynamics is attracting more attention nowadays, because its nature as an electronic phase change is directly associated with the strong electron correlation.

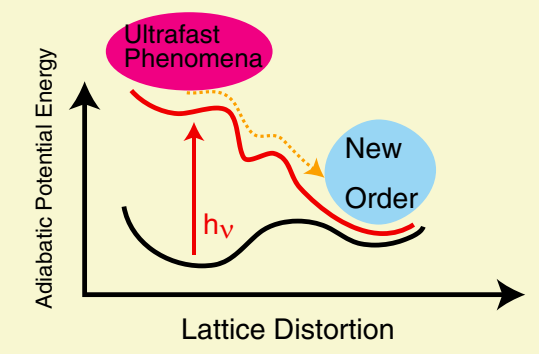

Figure 4-28
Schematic picture of PIPTs. Present and future goals to be investigated are specified as "Ultrafast Phenomena" and "New Order."

Below, we summarize the two aspects or goals. Strictly speaking, these two goals are not completely separated, because Goal 1 also has the aspect of Goal 2 in the sense that atomic motions are affected by preceding electronic motions. However, our categorization is conceptually useful.

Table 4-1 Comparison of the two goals

	Time scale	What is moving?
Goal 1 (Molecular Movie)	Picoseconds	Atom and/or Molecule
Goal 2 (Ultrafast Dynamics)	Femtoseconds	Electrons

4.3.9.3 Current status and limitations

As already mentioned, progress to date is mainly the result of developments in optical laser technology and associated experiments via pump-probe spectroscopy. In such experiments, the time resolution is as short as several femtoseconds, which confirms that the PIPTs in certain materials occur really quite fast and that the phenomena are electronic in nature, i.e., the aspect of Goal 2 [1, 2]. Considering the electronic nature, however, we immediately notice that the present experimental result is still imperfect, because it lacks spatial information that is very important when discussing how the phase change proceeds, i.e., the problem of *domain growth*. This is of course because the wavelength of visible or near-IR light is more than several thousand Angstroms and the momentum is almost zero in the Brillouin zone. We consider this point in more detail in Section 4.3.9.4.

As for Goal 1, intensive efforts have already been made at the NE14A at the Photon Factory, producing many scientific results [3, 4]. However, the remaining problem is the time resolution of about 100 ps. As discussed in the previous section, the dynamics of atomic motions have a time scale of several picoseconds as the shortest possible scale, so the present time resolution is insufficient for future developments in this direction.

4.3.9.4 Future prospects with ERL

For Goal 1, the prospects are good because the expected time resolution of the ERL is less than 100 fs. Not only such substantially improved resolution but also the expected high brilliance will make it feasible to obtain the molecular movie mentioned in the preceding sections.

Regarding the possibilities of Goal 2, the first simple but attractive possibility is inelastic X-ray scattering (IXS). Iwano [5] recently argued that domains formed at the initial stage of a PIPT, as shown in Fig. 4-29. Since this domain formation is of purely electronic nature, it is expected to be related to Goal 2. The time scale of this process is estimated to be $1/t_0$, where t_0 is the nearest-neighbor electron transfer energy, and is typically of the order of 0.1 eV in molecular crystals. We hence expect the time scale of 10 fs. Since this time scale might still be challenging even for the ERL, we change our approach as follows. Namely, the dynamics can be seen as spectroscopy by applying a Fourier transform. Figure 4-30 shows a theoretical demonstration for IXS, which was obtained in the system shown in Fig. 4-29. In this figure, the horizontal arrow indicates the bandwidth of the smallest domain state, while the vertical ones indicate the quantization of domain sizes, namely, the existence of different domain sizes.

Note that the former is even larger than that of the bare electron, which is quite abnormal, since electron correlations usually make the band narrower. An energy resolution of 10 meV is needed to make both features detectable, which is expected to be feasible using the ERL.

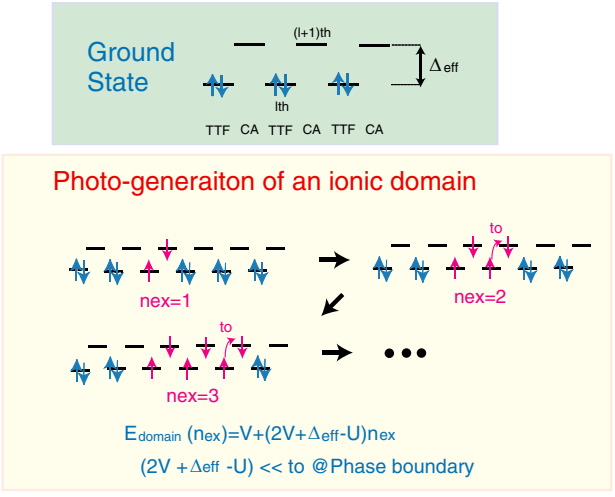

Figure 4-29
Schematic picture of domain formation.

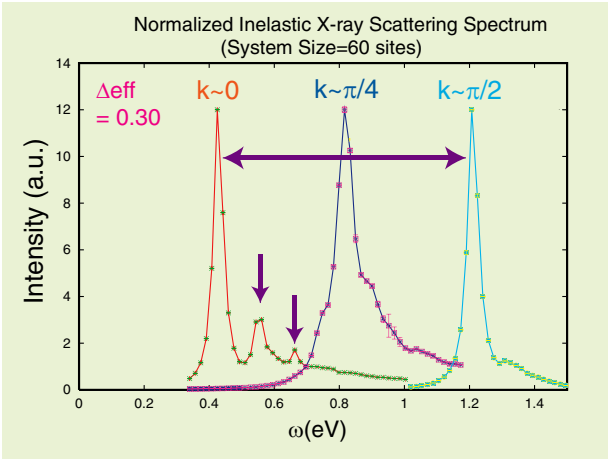

Figure 4-30
Calculated results of IXS.

Finally, we discuss the possibility for using the excellent temporal coherence of the ERL. Without going into detail, a coherent X-ray pulse enables us to prepare an initial coherent electronic wave packet, by which we can trace the evolution of the dynamics via transient spectroscopy [6]. This spectroscopy is thus capable of analyzing quantum dynamics in both ω and k space, yielding important information about mechanisms essential to the systems, if the resolutions allow it. However, as already mentioned, the expected time resolution is limited to 100 fs. Since the electron transfer energy of strongly correlated electron systems is typically 0.1–1.0 eV, the materials need a resolution of at least 10 fs. Further efforts to improve the time resolution are required in order to perform time-resolved experiments in these systems.

REFERENCES

[1] H. Mastuzaki, M. Ymamashita and H. Okamoto, *J. Phys. Soc. Jpn*. **75**, 123701 (2006).
[2] H. Uemura and H. Okamoto, *Phys. Rev. Lett*. **105**, 258302 (2010).
[3] S. Nozawa *et al*., *J. Am. Chem. Soc*. **132**, 61 (2010).
[4] H. Ichikawa *et al*., *Nature Materials* **10**, 101 (2011).
[5] K. Iwano, *Phys. Rev. Lett*. **102**, 106405 (2009).
[6] K. Iwano, *Phys. Rev. B* **84**, 235139 (2011).

4.3.10 Electronic structure of transition metal compounds

4.3.10.1 Introduction

Transition-metal compounds exhibit surprisingly rich electric and magnetic properties due to strongly correlated *d* electrons with spin, charge, and orbital degrees of freedom. In the field of condensed matter physics, much research has focused on understanding exotic electronic states in various transition-metal compounds including HTSC cuprates and CMR manganites [1, 2]. Among them, advanced diffraction and spectroscopy measurements using high brilliance synchrotron radiation have provided decisive experimental evidence for fundamental issues such as the d-wave superconductivity in cuprates [3] and the orbital ordering in manganites [4]. In addition to the bulk systems, new types of two-dimensional electronic systems have been formed at interfaces of transition-metal compounds such as $SrTiO_3$/$LaTiO_3$ [5] and are expected to show new electronic states. Also, many transition-metal compounds have been attracting great interest as key materials for battery electrodes, spintronics devices, and photocatalysts which will play an important role in solving the energy and CO_2 problems of the 21st century. In many cases, the functionality of transition-metal compounds derives from their frustrated electronic states under multi-phase competition which can give rise to drastic responses to external stimuli such as magnetic field and optical excitation. For example, various photo-induced phase transitions have been found in transition-metal compounds such as manganites [6] and diluted magnetic semiconductors [7]. Very recently, the discovery of Fe-based superconductors has had a huge impact in the field of condensed matter physics [8] and their multi-band electronic structure and mechanism of superconductivity are still under debate. Also, topological phases or topological defects have been found in magnetic transition-metal compounds and are an exciting topic in the physics community [9].

4.3.10.2 Scientific goals and challenges

Transition-metal compounds show various anomalous metallic states which are believed to be related to quantum criticality of (hidden) spin and/or charge and/or orbital orders of transition-metal *d* electrons. Understanding the mysterious electronic states and (hidden) orders is a major challenge in the field of condensed matter physics. Such electronic states realized under multi-phase competition or quantum criticality are often accompanied by real-space inhomogeneity of spin and/or charge and/or orbital channels. The detailed texture and dynamics of such inhomogeneous states should be revealed by advanced experimental techniques. Photo-induced phase transitions are another important subject in transition-metal compounds under multi-phase competition. Photo-control of spin, charge, and orbital states at room temperature is an ultimate goal not only for basic science but also for application to optical devices.

4.3.10.3 Current status and limitations

The inhomogeneous electronic states realized in transition-metal compounds including HTSC cuprates are mainly studied by scanning microscopy methods such as STM. In order to study the dynamics of the inhomogeneous electronic distribution, real-time imaging techniques such as X-ray speckle are well suited. However, the space resolution of the current X-ray speckle technique is not sufficient to study the inhomogeneous spin-charge-orbital distribution in transition-metal compounds. The dynam-

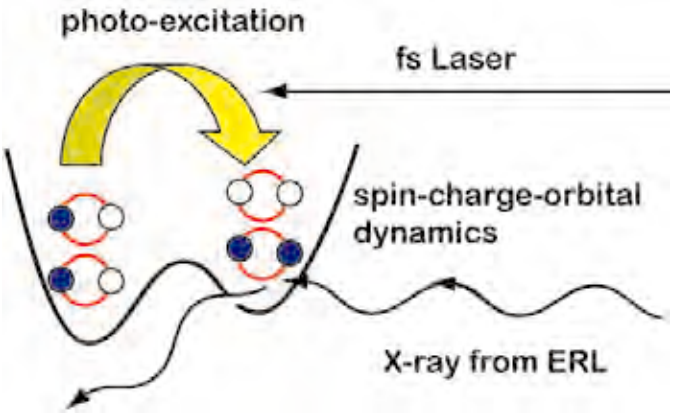

Figure 4-31
A schematic drawing of pump-probe resonant X-ray scattering to study ultrafast photo-induced phase transitions.

ics of photo-induced phase transitions are usually studied by pump-probe ultrafast reflectivity measurements. For example, $Pr_{0.5}Ca_{0.5}CoO_3$ has been found to show an ultrafast insulator-to-metal transition accompanied by spin change [10]. In order to observe the dynamics of spin, charge, and orbital channels, time-resolved core-level X-ray spectroscopy or resonant X-ray diffraction should be developed. The time resolution and photon flux of pulsed X-ray sources are currently around 200 fs and 10^6 photons/s, which are estimated to reach 100 fs and 10^7 photons/s in future to comfortably study ultrafast phase transitions widely observed in bulk and at the interfaces of transition-metal compounds.

4.3.10.4 Future prospects with ERL

The spatially coherent X-rays delivered from the ERL will enable us to perform X-ray speckle measurement with very high spatial and time resolutions. Such innovative X-ray speckle using the ERL can be used to study inhomogeneous electronic states found in various transition-metal compounds including the HTSC cuprates, CMR manganites, and Fe-based superconductors. Detailed information on the texture of spin-charge-orbital states and their dynamics is expected to open up a new paradigm in the study of cuprate and Fe-based superconductors and may lead to the development of new superconductors with higher T_c. This method can also be used to study diluted magnetic semiconductors, battery materials such as Li_xCoO_2, and transition-metal interfaces to study the inhomogeneous distribution and dynamics of spin and charge, which will be very useful to improve spintronics devices and battery materials.

The pulsed X-rays from the ERL can also be used for various time-resolved X-ray spectroscopy and X-ray diffraction measurements with time resolution of better than 100 fs (Fig. 4-31). Resonant X-ray diffraction experiments provide information on the dynamics of spin-charge-orbital order or fluctuations, and core-level X-ray absorption spectroscopy provides information on local electronic configuration such as the low-spin to high-spin transition. The combination of ultrafast resonant X-ray diffraction and X-ray absorption experiments will be very useful to study the mechanism of various photo-induced phase transitions by decomposing the photo-induced change to spin, charge, and orbital channels. This method can also be applied to identify hidden ordered states induced by photon excitation (for example, exciton BEC state, skyrmion lattice state) which are usually very difficult to probe with reflectivity measurements. New X-ray imaging, X-ray diffraction, and X-ray spectroscopy techniques using the ERL are expected to provide new opportunities to explore unknown states of matter in strongly correlated transition-metal compounds.

REFERENCES

[1] M. Imada, A. Fujimori and Y. Tokura, *Rev. Mod. Phys*. **70**, 1039 (1998).
[2] "*Physics of Transition Metal Oxides*", S. Maekawa *et al*., (Springer Verlag, Berlin, 2004).
[3] Z.-X. Shen *et al*., *Phys. Rev. Lett.* **70**, 1553 (1993).
[4] Y. Murakami *et al.*, *Phys. Rev. Lett*. **80**, 1932 (1998).
[5] A. Ohtomo, D.A. Muller, J.L. Grazul and H.Y. Hwang, *Nature* **419**, 378 (2002).
[6] K. Miyano, T. Tanaka, Y. Tomioka and Y. Tokura, *Phys. Rev. Lett*. **78**, 4257 (1997).
[7] S. Koshihara *et al*., *Phys. Rev. Lett*. **78**, 4617 (1997).
[8] Y. Kamihara, T. Watanabe, M. Hirano and H. Hosono, *J. Am. Chem. Soc*. **130**, 3296 (2008).
[9] X. Z. Yu *et al*., *Nature* **465**, 901 (2010).
[10] Y. Okimoto *et al*., *Phys. Rev. Lett*. **103**, 027402 (2009).

4.4 Materials under Extreme Conditions

4.4.1 Overview

Materials under high pressure show novel behavior that is hard to imagine from the behavior at ambient pressure, and so various high-pressure studies are conducted throughout the scientific fields of physics, chemistry, biology, and geoscience. High-pressure techniques are also used in various industrial applications, from the synthesis of functional materials and exploration of new materials to food processing. High-pressure science and technology have progressed dramatically since the birth of modern high-pressure research in the early 20th century, greatly accelerated by the development of synchrotron facilities in the 1980s. This is because X-ray diffraction techniques with brilliant and high-energy synchrotron sources are very effective for studying structural changes in small samples sealed in high-pressure cells. Future prospects of structural studies under high pressure will be discussed in Section 4.4.2, focusing on noncrystalline and polycrystalline materials, by taking advantage of the features of the ERL.

High-pressure experiments are conducted not only at room temperature but also at low temperatures mainly in the field of physics and at high temperatures mainly in the field of earth and planetary science (geoscience). The pressure and temperature conditions of the interiors of the Earth and some planets in the solar system are shown in Fig. 4-32. The targets of high-pressure science cover various phenomena occurring at a very wide range of temperatures, from below 0.1 K in physics to above 10,000 K in earth and planetary science. Moreover, experiments under multiple extreme conditions, i.e., high pressure, high/low temperature, and high magnetic field, have been conducted recently. In addition to diffraction studies, spectroscopic studies with synchrotron sources have become popular. Future prospects of high-pressure physics and high-pressure earth and planetary science with the ERL will be discussed in terms of the structure and properties of materials under extreme conditions in Sections 4.4.3 and 4.4.4, respectively. How to achieve the scientific goal of high-pressure physics, which is to elucidate exotic phenomena at the microscopic level, will be discussed by taking examples such as unconventional superconductivity, quantum criticality, and the metallization of hydrogen (which is also of interest in earth and planetary science but has not yet been attained). The discussion will also include how to achieve the scientific goal of high-pressure earth and planetary science, which is to clarify the internal structures of the Earth and planets (including extrasolar planets) and various dynamic phenomena occurring there such as convection, volcanism, and earthquakes.

As history has shown, more brilliant X-ray sources are the key to conducting studies under more extreme conditions, and therefore the ERL will surely accelerate high-pressure science. In addition to brilliance, spatial coherence will be greatly improved because the ERL is designed to achieve low emit-

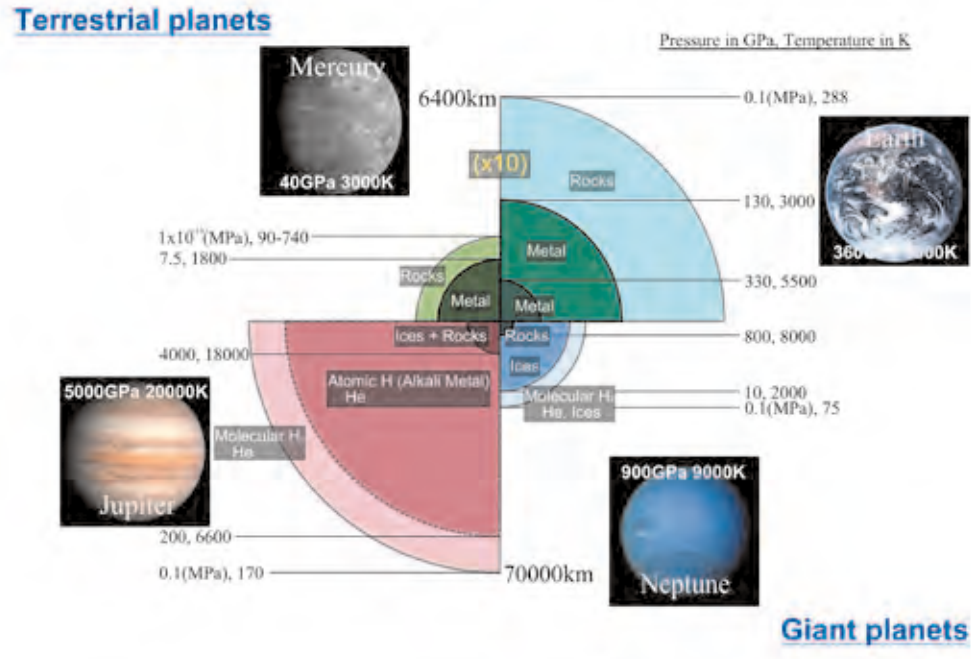

Figure 4-32
Earth and some planets in the solar system.

tance. For example, sophisticated imaging techniques, such as phase imaging, diffraction imaging, and nanobeam-scanning imaging, will be used depending on the spatial scale of samples and the purpose of studies. Improved brilliance will reduce the exposure time for small samples in high-pressure cells. The short pulses of the ERL will also enable the study of phenomena which occur on shorter time scales. Thus, the ERL will open up a new era of high-pressure science.

4.4.2 Structural characterization of materials under high pressure

4.4.2.1 Introduction

When materials are pressurized, their volumes are reduced to lower the free energy. In order to achieve this efficiently, many materials undergo pressure-induced phase transitions. From a different viewpoint, the transitions can be considered to be the result of large effects of pressure on the interatomic potential of materials. Changes in the interatomic potential, i.e., changes in the interatomic bonding, in turn cause changes in physical properties, such as thermoelasticity and electromagneticity. For example, many insulators (or semiconductors) have been found to be metallic under high pressure. The behavior of materials under high pressure is often hard to imagine from that at ambient pressure, and therefore high-pressure experiments are conducted in all the scientific fields of physics, chemistry, biology, and geoscience.

Brilliant X-ray sources are particularly useful in high-pressure science because the samples for high-pressure experiments are very small (and the maximum achievable pressure and sample size are inversely correlated). The second-generation synchrotron facility made it possible to conduct precise structural measurements mainly for crystalline materials under high pressure. Especially, the progress in studies on unquenchable structures (i.e., high-pressure structures which cannot be recovered to ambient pressure) owes much to synchrotron X-ray diffraction. Moreover, following the completion of the third-generation synchrotron facility, noncrystalline materials such as liquids and glasses have been studied intensely.

Previously, it was considered that all materials eventually have a simple close-packed structure under extremely high pressure, but it has been revealed that it is not so simple due to electronic transitions and other factors [1]. As history has shown, more brilliant sources will enable us to conduct studies at higher pressures. Therefore, the high-brilliance X-ray beam of the ERL, a fourth-generation synchrotron facility, will be an invaluable tool for high-pressure science. In addition to the brilliance, the spatial coherence will be much improved because the ERL is designed to achieve low emittance. In this Section, we envision new “classical” high-pressure researches such as structural measurements with a diamond-anvil cell (DAC), which is the most popular high-pressure apparatus, that take advantage of the features of the ERL.

4.4.2.2 Scientific goals and challenges

Samples in DAC are typically polycrystalline (or powdered). Even if the starting material is a single crystal, it usually becomes polycrystalline after phase transitions. Conventionally, structural measurements on bulk polycrystalline samples have been conducted by powder X-ray diffraction and other techniques. Characterization of the individual constituent crystals of polycrystalline materials, i.e., individually measuring the crystal structure, chemical composition, textures (ultimately, dislocations and impurities in them), and so on, is one of the biggest goals of high-pressure experiments.

Compared to crystalline materials, there have been fewer studies on noncrystalline materials due to experimental difficulties; it is extremely difficult to measure their three-dimensional structures and equations of state, which are the most fundamental and important pieces of information in high-pressure science. Intermediate-range order is especially important for understanding the structure of noncrystalline materials, because it is known to exist in many noncrystalline materials such as melts and glasses of silicates and polymers and thought to be related to interstitial voids in these materials. As the pressure effect on voids is very large, the high-pressure behavior of voids, such as changes in chemistry of voids, compaction and deformation of voids, and accompanying phase transitions, are of great interest in various fields of both science and engineering (of course, voids play an important role also in crystalline materials).

Phase separation and chemical reaction in liquids are also interesting topics. At high pressures, materials tend to become reactive and are therefore unlikely to be in a state of phase separation. It is interesting to explore the pressure dependence of the tendency of phase separation or that of the spatial scale of chemical ordering near the critical point in systems such as silicate-water, metal-oxide, and block copolymers.

4.4.2.3 Current status and limitations

DAC is a powerful tool for high-pressure studies, and experiments at pressures over 400 GPa, which is higher than that at the center of the Earth (360 GPa), have been reported [2]. A wide variety of optical techniques can be used, because anvils made of single-crystal diamond serve as windows transparent to visible light (and also for infrared and ultraviolet light). In measurements with X-rays, on the other hand, high energies of 15–20 keV or more are desirable to reduce the absorption by a pair of anvils, having a total thickness of about 4 mm.

The typical grain size of polycrystalline samples in DAC is about 100 nm. If high-pressure phases are quenchable to ambient pressure, individual crystals can be characterized by using a transmission electron microscope (TEM) [3]. However, TEM observations of samples in DAC are inherently impossible (because the penetration depth of the electron beam is very small). Therefore, a powder X-ray diffraction method is used to determine the structure of high-pressure phases which are not quenchable to ambient pressure [4]. However, it is often very difficult to determine even the unit-cell parameters of the unknown phase, especially when it has a low-symmetry structure.

Synchrotron X-ray measurements of liquids and glasses with DAC require a higher technical level. Their structures and equations of state at pressures of 50–100 GPa have begun to be reported only recently [5, 6], but many of the experimental data are still of low quality. Moreover, direct measurements of three-dimensional structures are currently not possible (only one-dimensional pair-distribution functions can be obtained).

4.4.2.4 Future prospects with ERL

The undulator beamlines of the ERL are suitable for DAC experiments. As discussed above, high-energy X-ray beams are indispensable for DAC experiments and therefore the relatively little degradation of higher order harmonics compared to the first order harmonics is a very important aspect of the undulators in the ERL. Table 4-2 lists some examples of target materials and phenomena with their typical spatial scales. A variety of studies will become possible by using one or a combination of the following three methods depending on the spatial scales and purposes; absorption/phase imaging (better than 100 nm, the present maximum resolution), diffraction microscopy (coherent X-ray diffraction; 2–3 nm, ibid.), and scanning microscopy (nanobeam imaging; 20–30 nm, ibid.). For example, after checking the texture (grains) of polycrystalline materials by phase imaging, one can measure the single-crystal X-ray diffraction and/or chemical composition of individual crystals by using nanobeams (scanning is also conducted as necessary). This will make it possible to characterize each constituent crystal of polycrystalline materials individually and solve unknown structures even with a low symmetry. Also, equations of state for liquids and glasses can be determined by using three-dimensional tomography to measure the

Table 4-2 Spatial scale of interest (some examples for DAC experiments)

Material and/or Phenomenon	Scale (nm)
Intermediate-range order in SiO_2 glass	0.5
Intermediate-range order in polystyrene	1
Interstitial voids of zeolites	0.5-2
Pores of mesoporous materials	2-50
Micro phase separation in block copolymer melts	1-100
Critical phenomenon of miscible-immiscible transition in binary liquids	> 0.5
Grain size of polycrystalline samples in DAC	$10\text{-}10^3$
Bulk sample size for 500 GPa experiments in DAC	$< 10^4$
Bulk sample size of noncrystalline materials in DAC	$10^4\text{-}10^5$

pressure dependence of the size of bulk samples. When diffraction microscopy achieves the resolution of the diffraction limit (about 0.3 nm) in future, direct three-dimensional observations of the intermediate-range order of liquids and glasses may become possible. (Even if the diffraction-limited resolution is not achieved, important information may be obtained by assuming the periodicity or short- and/or intermediate-range order of the sample or giving available information of the sample.)

The spatial resolutions of the above three methods at present are not sufficient for our purposes: technologies for the necessary equipment such as lenses, mirrors, and detectors need to be developed. To be successful, researchers in high-pressure science should actively participate in the development. We think that it is time to seriously work with these methods, which are new for most researchers in high-pressure science, despite the limited spatial resolutions of the methods. We must prepare thoroughly for the forthcoming construction and operation of the ERL.

REFERENCES

[1] "*Phase diagrams of the elements*", D.A. Young, (University of California Press 1991).
[2] Y. Akahama and H. Kawamura, *J. Phys.: Conf. Ser*. **215**, 012195 (2010).
[3] N. Funamori et al., *J. Geophys. Res*. **103**, 20,813 (1998).
[4] N. Funamori et al., *Science* **275**, 513 (1997).
[5] T. Sato and N. Funamori, *Phys. Rev. Lett.* **101**, 255502 (2008).
[6] T. Sato and N. Funamori, *Phys. Rev. B* **82**, 184102 (2010).

4.4.3 High-pressure physics

4.4.3.1 Introduction

High-pressure techniques are a powerful tool for examining the physical properties of materials. Since the atomic distances in materials decrease with applied pressure, it is possible to control various electronic interactions without introducing any disorder. Recently, exotic phenomena in materials, for example, unconventional superconductivity and quantum criticality under high pressure at low temperature, have been observed by using macroscopic experimental techniques. These exotic phenomena can be clarified by investigating microscopic phenomena which are closely related to them. X-ray scattering using synchrotron radiation is a powerful and selective probe for investigating these microscopic phenomena under high pressure at low temperature. The structural properties, such as the lattice and atomic position parameters in the unit cell, obtained by X-ray diffraction are important and fundamental in high-pressure physics. Moreover, the electronic and dynamical properties of materials obtained through resonant/non-resonant elastic and inelastic X-ray scattering are necessary for a clear and deep understanding of those exotic phenomena under high pressure at low temperature.

Both the diamond-anvil cell (DAC) and multi-anvil press are employed for X-ray diffraction experiments under high pressure at room temperature. Although the sample volume is limited in experiments using DAC, this limitation has been overcome for X-ray diffraction experiments at pressures up to about 50 GPa and temperatures down to about 10 K except for light elements in the third-generation synchrotron facilities. Above 100 GPa, however, the pressure distribution becomes prominent. An intense X-ray beam having a tiny focal spot from synchrotron radiation can overcome these difficulties. Although the X-ray scattering cross sections in resonant elastic and inelastic processes are very small, high-brilliance nano-size X-ray beams will make it possible to develop high-pressure and low-temperature sample environments for these state-of-the-art experiments using synchrotron radiation.

4.4.3.2 Scientific goals and challenges

High-pressure physics addresses many different important scientific goals and challenges. Among them, one important subject is the relation between high-temperature and unconventional superconductivity and the structural, electronic, and magnetic degrees of freedom. Just 100 years have passed since the discovery of superconductivity, and many kinds of materials have been proved to exhibit superconductivity as shown in Fig. 4-33. T_c of BCS-type conventional superconductors was raised to 38 K for MgB_2 in 2001. In 1986, copper oxide high-T_c superconductors were discovered, in which the highest T_c of 164 K was realized under high pressure [1]. In 2008, another category of superconductor was developed: the so-called iron-based superconductors. Takahashi and co-workers were the first to achieve T_c above 40 K in this system using high-pressure techniques [2]. Thus, high-pressure techniques have played an

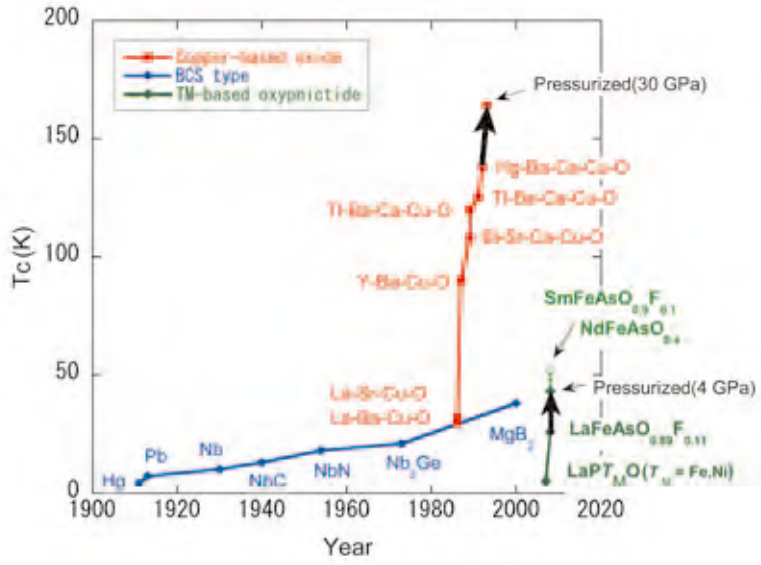

Figure 4-33
T_c vs. year for several superconductors. T_c's measured under high pressure are also plotted. Enhancement of T_c is indicated by arrows.

important role in developing high-T_c materials. One of the scientific goals of high-pressure physics is to find new superconducting materials having higher T_c, for which it is important to understand the mechanism of high-T_c superconductivity, such as copper oxide and iron-based systems. Although substitution experiments have been performed extensively, such experiments induce disorder in the atomic network in the materials as a side effect. In high-pressure experiments, T_c may vary for a single material, in contrast to substitution measurements. Structural data under high pressure at low temperature are essential for analyzing the electronic state.

Several light elements (Li, Ca, Sc, etc.) show pressure-induced superconductivity above 20 K [3]. A light element such as hydrogen is predicted theoretically to show high-T_c superconductivity. However, metallic hydrogen has not been obtained due to experimental difficulties. Recently, hydrogen dominant materials, such as silane, have shown pressure-induced superconductivity [4]. One challenge is to obtain the metallic state of hydrogen in the form of the hydrogen dominant materials. Metal hydrates are also an attractive material for hydrogen storage.

Another important subject is the evolution and development of long-range orders in magnetic and charge degrees of freedom near the quantum critical points in correlated electron systems [5]. When the phase transitions occur at finite temperatures, macroscopic orders in materials are destroyed by thermal fluctuations. Meanwhile, the quantum criticality, which is, in the strict sense, accessed at zero temperature by a non-thermal control parameter, such as pressure and magnetic field, influences the behavior of electronic properties in a system. The quantum phase transition occurs as a result of competing ground state phases because long-range order in the system is destroyed solely by quantum fluctuations. Recently, it has been revealed that the competition among ground state phases is closely related to exotic and unsolved physical phenomena at low temperatures.

For example, the breakdown of Fermi liquid behavior in metal is observed near the magnetic quantum critical point, where Fermi liquid theory is the standard theory of metals [6]. The mechanism of this breakdown has been actively discussed. Consequently, one of our scientific goals in this subject is to understand the unconventional behavior near the magnetic quantum critical point. For these scientific goals, low-temperature (below 1 K) sample environments with finely tunable pressure must be developed for state-of-the-art experiments using synchrotron radiation to study the dynamical and electronic properties of materials near the magnetic quantum critical point. These advanced sample environments are likely to produce exciting scientific results.

4.4.3.3 Current status and limitations

Data have been accumulated on the electronic, magnetic, and optical properties of superconducting materials under high pressure. Crystal structure data have also been obtained by various experiments. Powder diffraction techniques using synchrotron radiation have produced qualified structural results so far. However, because of the pressure distribution and smallness of sample amount, it is difficult to refine the crystal structure precisely for high-T_c materials. Although pressure effects on lattice parameters, atomic coordinates, bond distance, bond angle, etc. for high-T_c materials have been reported by several groups, these results are not enough to evaluate the theoretical calculation of electronic structure.

Concerning the beam intensity, the diffracted intensity from the light element is very weak even using synchrotron radiation; neutron diffraction measurements are often more suitable for light elements. However, since neutron diffraction measurements need large specimens, high-quality experiments under high pressure, especially above 10 GPa, are difficult.

In high-pressure X-ray diffraction experiments using synchrotron radiation, temperatures down to 30 K can be accessed on BL-18C at PF. High-pressure and low-temperature X-ray diffraction measurements down to about 10 K are ongoing at the third-generation synchrotron facilities. The extreme conditions of the combination of low temperature (3 K), high pressure (20 GPa), and high magnetic field (70 kOe) are currently being developed for nuclear resonant scattering experiments on AR-NE1 at PF-AR. We have measured the ^{57}Fe nuclear resonant time spectra for some iron-based superconductors at these multi-extreme conditions, with data accumulated for up to 12 hours. Similar sample environments have been set up for nuclear resonant scattering and X-ray magnetic circular dichroism experiments at the third-generation synchrotron facilities.

When investigating the evolution and development of long-range orders near the quantum critical points, the high-pressure sample environment is used in combination with temperatures below 1 K. As the thermal boundary resistance between sample and substrate increases with decreasing temperature, it becomes difficult below 1 K to remove the heat deposited in the sample by the incident X-ray photons. Techniques have to be developed to overcome this problem.

4.4.3.4 Future prospects with ERL

The combination of the ERL and DAC is a powerful tool to obtain high-quality diffraction data for materials under high pressure (see Section 4.4.2 for details). This is especially true for low-temperature experiments: because the sample is not only compressed in DAC but also located in a cryostat, it is impossible to put the collimator for the incident X-ray beam very close to the sample to minimize the influence of the pressure distribution across the sample.

The high-brilliance nano-size X-ray beam from the ERL will also be the best incident beam to create those advanced sample environments for resonant elastic and inelastic X-ray scattering experiments. Furthermore, the ultrashort X-ray pulse (<100 fs) allows us to study the dynamical properties of materials with a faster time resolution and access to almost all Mössbauer isotopes such as Ni and rare-earth elements, which have a resonant nuclear excited state with a shorter lifetime. Nuclear resonant scattering experiments are one of the few experiments using synchrotron radiation which has high potential for the combination of high pressure (~20 GPa) with very low temperature (~80 mK) since the highly monochromatized X-ray beam is used as an incident beam. The X-ray beam from the ERL will enable us to investigate exotic phenomena, such as unconventional superconductivity and quantum criticality, in materials under high pressure and at low temperature.

REFERENCES

[1] L. Gao et al., *Phys. Rev. B* **50**, 4260 (1994).
[2] H. Takahashi et al., *Nature* **453**, 376 (2008).
[3] K. Shimizu et al., *Nature* **419**, 597 (2002).
[4] M.I. Eremets et al., *Science* **319**, 1506 (2008).
[5] H.v. Löhneysen et al., *Rev. Mod. Phys*. **79**, 1015 (2007).
[6] G.R. Stewart, *Rev. Mod. Phys*. **73**, 797 (2001).

4.4.4 High-pressure earth and planetary science

4.4.4.1. Introduction

The largest planet in our solar system, Jupiter, has huge ranges of pressure and temperature, up to 5 TPa and 20,000 K, and yet the conditions within some extrasolar planets such as Super-Earth recently reported by astronomers could exceed even those of Jupiter. Achieving these extreme conditions and solving the dynamics of planetary bodies are the dreams of earth and planetary scientists. High-pressure studies on earth and planetary materials have revealed many phase transformations, stability field of each phase, elastic properties, and so on, which are essential to understanding the internal structure and evolution of planetary bodies. Recent progress of high-pressure techniques has made it possible to generate the conditions at the center of the Earth, 360 GPa and 6000 K [1], by static compression and even higher conditions to 2 TPa and 40,000 K by shock compression [2].

Dynamic processes, such as convection, volcanism, and seismicity in the interior (or on the surface) of the Earth and planets (Fig. 4-34), are controlled by elementary processes on relatively short time scales. However, such processes as material transport, deformation and fracturing of rocks, and separation of crystals and magmas, are not yet well understood. The ERL is expected to stimulate research not only on the structure and properties of constituent materials of the Earth and planetary interiors but also on various dynamic phenomena, such as plastic deformation, fracturing, and melting of rocks.

4.4.4.2 Scientific goals and challenges

Our scientific goals are to clarify various key phenomena and processes occurring in the Earth and planets. It is important to understand the structure and properties of materials of the Earth and planetary interiors in more detail. Moreover, in situ observation of fast elementary processes relevant to the dynamic processes occurring in the Earth and planets are challenging targets.

Among the constituents of the Earth (and Earth-like planets), iron is the heaviest element among the major components and strongly affects both gravitational and electromagnetic phenomena of the Earth. Iron-bearing materials show complicated behavior due to changes in electronic states. It is important to describe the pressure and temperature dependence of the electronic configuration and spin state of major iron-bearing minerals and alloys with simultaneous observation of crystal structure up to, and even beyond, the conditions at the center of the Earth.

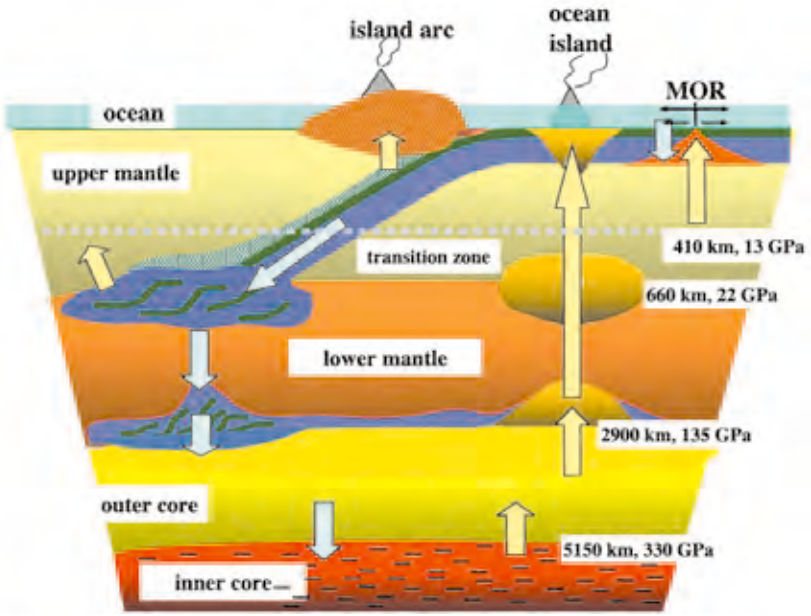

Figure 4-34
Internal structure and dynamic processes of the present Earth.

The occurrence of the magma ocean and subsequent stratification and formation of the core and crust were the most important processes in the early stage of the Earth's evolution (Fig. 4-35), while the generation, separation, transportation and eruption of magma are the most important processes in the present Earth. Fracturing of the crust and mantle materials and impact phenomena on the Earth and planets are also very important. Especially, the source mechanism and origin of deep earthquakes, which may be related to some phase transformations and dehydration reactions, are key unsolved issues in seismology. Planetary collision is one of the most important processes in the early stage of planetary formation, and it is essential to clarify the impact processes in order to understand the early evolution of the Earth, moon, and planets.

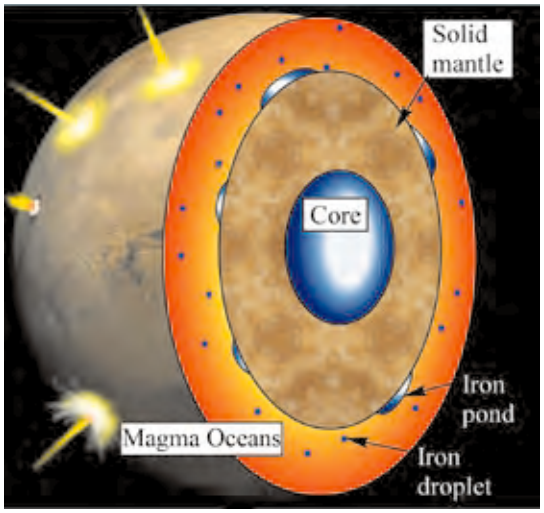

Figure 4-35
Formation and evolution of the early Earth.

4.4.4.3 Current status and limitations

We have so far achieved a static pressure of 400 GPa at room temperature and also simultaneous generation of high temperature equivalent to the conditions of the Earth's core using a diamond-anvil cell (DAC), but the sample volume is extremely limited under these conditions. In order to extend the pressure and temperature ranges of experiments, it may be necessary to introduce heating techniques with a short duration, i.e., application of a temperature pulse to avoid damaging the diamond anvils. Dynamic compression, such as laser-shock compression, is a useful tool to study the interior of giant planets. However, it is still difficult to obtain information on the structure and properties of materials under such extreme conditions by in situ X-ray diffraction and spectroscopy.

Recent X-ray spectroscopic measurements at the third-generation synchrotron facilities made it possible to clarify the sound velocity [3], magnetic properties, and spin states [4] of core and mantle materials of the Earth and planets. The complicated behavior of iron-bearing materials has recently been noted from spectroscopic measurements. For example, valence change at phase separation and high-spin to low-spin transition have been reported by using synchrotron Mössbauer [5] and electron energy loss spectroscopies and X-ray emission spectroscopy [6], respectively. However, these basic properties cannot always be investigated well. X-ray intensities by inelastic processes are very weak for tiny samples in DAC experiments. Furthermore, diamond becomes less transparent at X-ray energies below 18 keV. For example, absorption spectra for near K-edge of iron (around 7 keV) in mantle minerals have barely been obtained for bulk samples through diamonds under high pressure. These spectroscopic measurements may be possible at pressures at least up to 100 GPa with currently available synchrotron sources (including PF-AR). However, the samples are often inhomogeneous because laser heating promotes phase transformations and chemical differentiation only in a limited area of the samples. Although attempts have been made to collimate the X-ray beam to obtain better spectra, the significant decrease of X-ray flux results in degradation of the signal to noise ratio.

4.4.4.4 Future prospects with ERL

The high-brillant nature of the ERL source is suitable for tiny samples in DAC experiments. In addition to diffraction studies, spectroscopic studies (which require a longer exposure time) will become possible to yield time-resolved information on phase transformations, electromagnetic properties, and so on. The brilliant nanobeam from the ERL will enable us to perform more quantitative (or even mapping) studies of heterogeneous samples in a shorter exposure time. Moreover, the ERL will be useful for clarifying the internal structure of giant planets, such as Jupiter and Super-Earth, by using in situ X-ray diffraction and spectroscopic methods combined with laser-shock compression.

Micro-imaging or tomography for samples in DAC can utilize the characteristics of the ERL: high coherency and nanobeam for high-resolution images. This method will provide important information for partially molten samples to understand fluid migration in polycrystalline materials and core-formation of the early Earth. This method will also be used to clarify the fracturing process of rocks and the source mechanism of earthquakes. If time-resolved X-ray imaging or tomography in a few nanoseconds to microseconds can be realized by using the highly brilliant and coherent source of the ERL, then it may be possible to observe the dynamic processes of impact phenomena and shock metamorphism on planetary surfaces. This would contribute greatly to our understanding of planetary evolution and open up new research fields in Earth and planetary sciences.

REFERENCES

[1] S. Tateno *et al*., *Science* **330**, 359 (2010).
[2] H. Nagao *et al*., *Phys. Plasma* **13**, 052705 (2006).
[3] M. Murakami *et al*., *Nature* **485**, 90 (2012).
[4] J.F. Lin *et al*., *Nature* **436**, 377 (2005).
[5] J.M. Jackson *et al*., *Am. Mineral*. **90**, 199 (2005).
[6] J. Badro *et al*., *Science* **300**, 789 (2003).

4.5.Environmental Science

4.5.1 Environmental behaviors of various elements by micro-XRF-XAFS-XRD analysis

4.5.1.1 Introduction

It is often said that the 21st century is the century of the environment. In order to address various environmental problems, environmental science and technology has been selected as one of four main fields with high priority in the Basic Program for Science and Technology decided by the Japanese Government. Environmental science and technology deals with science and technology related problems in natural systems and those of human origin.

In many subfields of environmental science and technology, chemical analyses such as determination of chemical compositions and speciation of elements in environmental samples and materials are essential to understand chemical processes in the environment and to establish remediation methods. Such studies can include (i) characterization of various elements in aerosols related to their source analysis and their effects on climate change and environmental impacts [1, 2], (ii) speciation of toxic elements such as arsenic and lead in soils and sediments related to their dissolution into soil water, ground water, and seawater [3–5], and (iii) chemical processes of enrichment of rare metal elements into ore minerals related to securing resources [6].

X-ray spectroscopies, especially X-ray fluorescence spectroscopy (XRF), X-ray absorption fine structure (XAFS) spectroscopy and X-ray diffraction (XRD) with synchrotron radiation (SR), have been frequently used in environmental studies [7] to solve various problems. In the leading journals in this field, such as Environmental Science & Technology (American Chemical Society; for general environmental science and technology) and Geochimica et Cosmochimica Acta (Geochemical Society; for basic chemical processes in the environment), the proportion of manuscripts using X-ray spectroscopies started increasing in the late 1990s and leveled off after 2000 at 4% and 11% of all manuscripts in the two journals, respectively. Thus, environmental studies, especially on clarifying chemical processes in natural systems, are a large field where X-ray spectroscopies can play an important role.

4.5.1.2 Scientific goals and challenges

Various chemical reactions occur in the aqueous phase in the environment and in living organisms. The dynamics of such reactions in gas or water proceed at nano-, pico-, and even femto-second order. The reactions are often catalyzed at a particular site such as a solid-liquid interface. Then, the chemical processes in natural systems will be understood by speciation analyses of various elements at nanometer scale with femtosecond time resolution. X-ray spectroscopy is one of the best methods with sufficient spatial and time resolutions. Resolutions of nm scale and fs order are required to observe these reactions and processes. Two main applications of X-ray spectroscopy are suggested: (i) characterization of aerosols related to their effects on global warming and human health and (ii) chemical reactions at bacterial cell surfaces.

First, characterization of aerosols is important in view of their effects on climate change and human health, their roles as carriers of contaminants, and their contribution to marine phytoplankton as nutrients. Aerosols have two main sources, anthropogenic and natural, which have different particle sizes (Fig. 4-36). Among them, finer particles below 100 nm, namely ultrafine particulate matter (UFP), are of anthropogenic origin and are important fractions because of their serious effects on human health [8]. For example, UFP can be breathed into and remain in pulmonary tissue, increasing the risk of pulmonary disease and ultimately, lung damage. On the other hand, organic aerosols are the main component of fine particles (FP) smaller than 1 micron. Among them, soluble organic aerosols such as dicarboxylic acid can absorb water due to their high hygroscopicity, thus promoting cloud formation in the atmosphere. However, the small sizes of FP and UFP have inhibited the elucidation of chemical species of various elements in the particles. Thus, it is important to characterize these aerosols by nanometer-scale X-ray probe, which allows us to study the following environmental processes: (i) the rate of oxidation of carbon species in aerosols can be determined related to the hygroscopic nature of organic aerosols and evaluation of the role of organic aerosols in the formation of clouds and their cooling effect by reflecting sunlight [9] and (ii) speciation of toxic elements such as zinc and lead in UFP can be conducted related to the prediction of their chemical behavior, such as whether soluble or insoluble, in subsequent environmental processes after deposition and in the human body after inhalation [2].

A second important scientific application of X-ray spectroscopy is chemical processes at bacterial cell surfaces (Fig. 4-37). Bacteria are ubiquitous in the environment and it has been gradually realized that bacteria control various chemical reactions in the environment. Iron-oxidizing bacteria, for example, accelerates the oxidation of ferrous ion to ferric ion [10–12]. Meanwhile, bacteriogenic iron (III) oxides (BIOS), products of bacterial activity, control the migration of various elements including toxic elements such as arsenic and lead by their adsorption on the surface of BIOS (Fig. 4-37). The contribution of bacterial activity to the formation of Fe oxides must be clarified, as this will clarify its effect on the migration of toxic elements. Iron-oxidizing bacteria have membrane protein (cytochromes) in the cell membrane for the oxidation of ferrous ion, enabling the iron-oxidizing bacteria to gain energy without uptake of organic carbon. Such bacteria are classified as chemoautotrophic and can synthesize organic carbon by the energy of the chemical reaction. However, the chemical processes at bacterial cell surfaces are not well understood. Thus, the X-ray nanobeam is important to observe the chemical reactions at the surface, while time-resolved analysis is also important to understand the kinetics and reaction mechanisms of ferrous ion and other metal ions at bacterial cell surfaces.

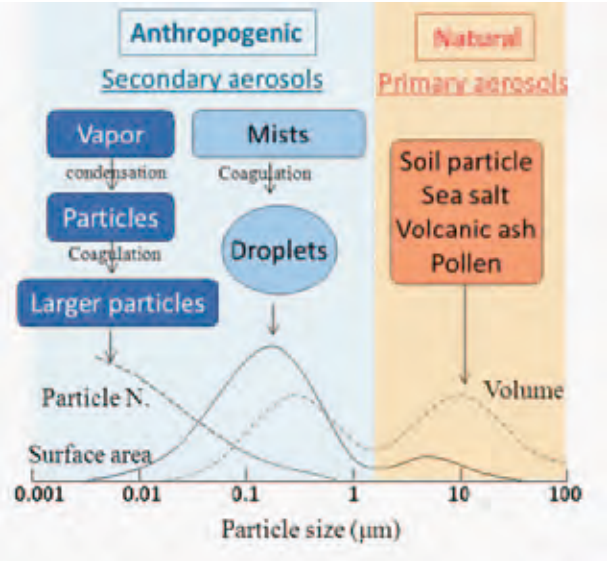

Figure 4-36
Size distribution of aerosols and their origins.

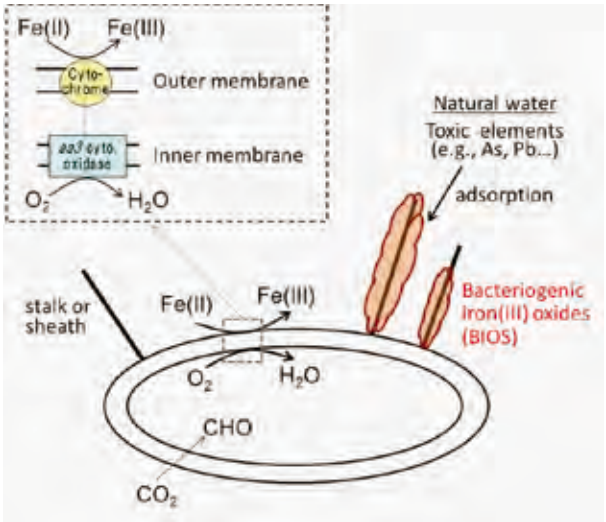

Figure 4-37
Iron oxidation at cell walls of iron-oxidizing bacteria and its effect on the adsorption of toxic elements by bacteriogenic iron oxides (BIOS).

4.5.1.3 Current status and limitations

X-ray microbeam analyses including XRF, XAFS and XRD have been used widely in various fields of environmental studies as noted in the previous section. However, a spatial resolution of around nanometer scale and time resolution of femtosecond order with sufficient sensitivity have not yet been attained by synchrotron based X-ray radiation.

Aerosols have been studied by scanning transmission X-ray microscopy (STXM) [13] to clarify the chemical species in particles of less than 1 μm. The method has been mainly applied to near-edge X-ray absorption fine structure (NEXAFS) spectroscopy of carbon K-edge in transmission mode but not often applied to trace elements, which need higher sensitivity. The method must be developed to perform these measurements on trace elements with an intense X-ray beam in fluorescence detection mode.

Chemical reactions at bacterial cell surfaces have been studied by STXM [10] but mainly using transmission mode. The kinetics of the oxidation of ferrous ion at the surface must be studied for a full understanding of the reactions. The reaction results in the formation of biogenic iron oxide (BIOS), where various toxic elements can be adsorbed (Fig. 4-37). However, it is not clear whether the biogenic component is important in the adsorption reaction. For this purpose, time-resolved XAFS study at the cell surface using an X-ray nanobeam is required.

4.5.1.4 Future prospects with ERL

XAFS with a spatial resolution of around nanometer scale and time resolution of femtosecond order with sufficient sensitivity will be attained by the ERL. It will be a powerful next-generation SR facility with very high coherent flux with extremely short pulse and a high repetition rate. New XAFS techniques with the X-ray beam of the ERL will improve our understanding of various environmental processes and reactions. The coherent beam provided by the ERL will be a unique tool to analyze the amorphous phase formed in aerosols at bacteria cell surfaces and in other environmental materials. Particle-by-particle aerosol measurements will be performed not only for major elements but also for trace elements, and the mechanism and origin of formation will be revealed. It is crucial to conduct XAFS and XRD/SAXS measurements for exactly the same particle at the same time in order to characterize the true features of the particle. An X-ray nanometer-sized beam can be targeted at bacterial cell surfaces to observe the specific reactions. The kinetics and mechanisms will be revealed by time-resolved XAFS measurements characterized by the high repetition rate of the ERL, which is suitable for capturing a movie of the reaction in order to analyze it in real time. Thus, wide-ranging research will be possible at the ERL, from macro to micro scale (see Fig. 4-38): aerosols travel hundreds of kilometers over days and years, while bacteria are microscopic reaction sites.

One concern is the effect of radiation (damage) on soft samples caused by using the intense X-ray beam. Techniques for experiments at low temperature, quick energy scanning XAFS measurement, etc. must be developed to avoid such radiation damage, then the advantages offered by the ERL will rapidly spread to a very wide range of environmental sciences. X-ray spectroscopic methods utilizing the features of the ERL will enable us to probe deeper into various fields of environmental science and nature.

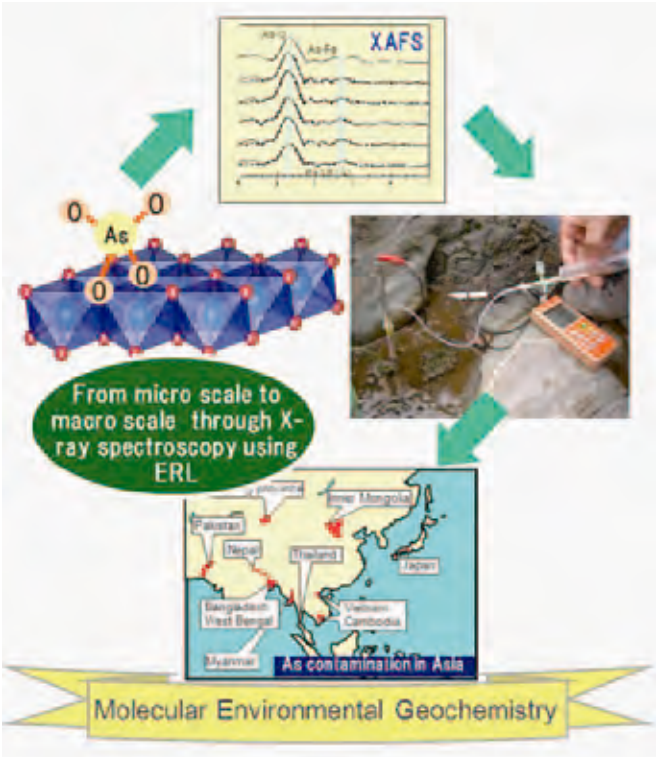

Figure 4-38
X-ray spectroscopies using ERL deal with a very wide range of science, and from the atomic to global scale.

REFERENCES

[1] Y. Takahashi, T. Miyoshi, M. Higashi, H. Kamioka and Y. Kanai, *Environ. Sci. Technol*. **43**, 6535 (2009).
[2] T. Furukawa and Y. Takahashi, *Atom. Chem. Phys*. **11**, 4289 (2011).
[3] Y. Takahashi, R. Minamikawa, K.H. Hattori, K. Kurishima, N. Kihou and K. Yuita, *Environ. Sci. Technol*. **38**, 1038 (2004).
[4] S. Mitsunobu, Y. Takahashi, Y. Terada and M. Sakata, *Environ. Sci. Technol*. **44**, 3712 (2010).
[5] Y. Takahashi, A. Manceau, N. Geoffroy, M.A. Marcus and A. Usui, *Geochim. Cosmochim. Acta* **71**, 984 (2007).
[6] Y. Takahashi, M. Yamamoto, Y. Yamamoto and K. Tanaka, *Geochim. Cosmochim. Acta* **74**, 5443 (2010).
[7] A. Manceau, M.A. Marcus and N. Tamura, *Rev. Miner. Geochem*. **49**, 341 (2002).
[8] P. Biswas and C.-Y Wu, *J. Air Waste Manage. Assoc*. **55**, 708 (2005).
[9] M. Kanakidou, J.H. Seinfeld, S.N. Pandis, I. Barnes, F.J. Dentener, M.C. Facchini, R.Van Dingenen, B.Ervens, A. Nenes, C.J. Nielsen, E. Swietlicki, J.P. Putaud, Y. Balkanski, S. Fuzzi, J. Horth, G.K. Moortgat, R. Winterhalter, C.E. Myhre, K. Tsigaridis, E. Vignati, E.G. Stephanou and J. Wilson, *Atmos. Chem. Phys*. **5**, 1053 (2005).
[10] D. Fortin and S. Langley, *Earth Sci. Rev*. **72**, 1 (2005).
[11] S.C. Chan, G.D. Stasio, A.A. Welch, M. Girasole, B.H. Frazer, M.V. Nesterova, S. Facra and J.F. Banfield, *Science* **303**, 1656 (2004).
[12] S. Kikuchi, H. Makita, S. Mitsunobu, Y. Terada, N. Yamaguchi, K. Takai and Y. Takahashi, *Chem. Lett*. **40**, 680 (2011).
[13] S. F. Maria, L.M. Russell, M.K. Gilles and S.C.B. Myneni, *Science* **306**, 1921 (2004).

4.5.2 Understanding the formation process of dioxins by XAFS

4.5.2.1 Introduction

The world is facing destruction of the environment, including problems such as global warming, deforestation, rising sea level, and environmental pollution. Pollution of the environment involves many issues. For example, persistent organic pollutants contaminate the environment, both locally and globally. In particular, the dioxins, polychlorinated dibenzo-p-dioxins (PCDDs) and polychlorinated dibenzofurans (PCDFs), are notorious as persistent organic pollutants. Dioxins are formed during solid waste incineration, and their subsequent emission into the air is a serious social concern. As dioxins are produced by incomplete combustion, improving the combustion conditions may reduce their emission levels. Advanced flue gas treatment systems have been developed and installed to minimize the emissions of dioxins into the air.

Although macro-engineering methods have significantly reduced dioxin emissions by improving combustion conditions and flue gas treatment, the problem has not been completely solved. Unburned carbon still remains in flue gas, and dioxins are also formed during the cooling process of the gas. Indeed, the mechanism of formation of dioxins is not yet fully understood.

X-ray absorption fine structure (XAFS) experiments have been carried out to study the mechanism of dioxin formation in solid waste incinerators. Although the major roles of some metals have been clarified, the entire reaction mechanism is not understood. Further progress in the investigations and a new way to reduce the formation of dioxins are required.

4.5.2.2 Scientific goals and challenges

This study aims to clarify the mechanism of dioxin formation, especially during the process of cooling flue gas after combustion, and to develop a new technology to inhibit the formation. Current flue gas clean-up processes involve the conversion of dioxins from the gaseous phase to the solid phase in fly ash, and thus dioxins in fly ash must be treated appropriately. Various sites in the samples should be successively observed in order to understand the various reactions in different sites. The sites are nanometers in size, and should be individually studied to reveal particular roles. Environmental samples such as fly ash, dust and soil are complex, variable and inhomogeneous. When a reaction in a bulk sample is observed on a macroscopic scale, it reflects the sum of various reactions in different local reactions. The typical size of local reactions is in the range of nanometers, and so a nanometer-sized X-ray beam is required in order to irradiate interesting sites in the samples and to clarify the differences among reaction sites. It is important to observe all the reactions that occur in incinerators in order to understand the mechanism of dioxin formation and to reduce them. Note that these reactions are not only major reactions but also minor, fast and intermediate reactions. These intermediate reactions during dioxin formation, which have not been observed yet, may play an important role in the whole reaction. Simultaneous fast characterizations of several elements are required to understand the role of each element, because there are many elements involved in the reaction.

New methods with capabilities of simultaneous ultra-fast XAFS measurements should be developed to study specific sites in samples by nanometer-scale irradiation for several elements in turn. These revolutionary methods will surely lead to progress in environmental science and technology, and will be indispensable for studying not only environmental reactions and dioxin formation but also other chemical reactions.

4.5.2.3 Current status and limitations

The mechanism of dioxin formation has been studied by measuring XAFS for model fly ash and actual fly ash. Carbon, chlorine, hydrogen and oxygen are the basic elements of dioxin formation, and metal compounds also play important roles in promoting dioxin formation. Many researchers have reported that copper chloride is an important catalyst for generating relatively large amounts of dioxins in heat experiments using model fly ash [1]. The detailed roles of copper, however, have not been revealed yet in the dioxin formation of actual fly ash; actual fly ash has a more complex composition than model fly ash, and consists of numerous elements including a trace amount of copper in unknown chemical states.

XAFS measurements have been carried out to investigate the chemical forms of copper in actual fly ash [2]. The species of copper in fly ash samples were successfully identified. Copper was present as cupric and cuprous compounds, but not as pure cupric chloride. These chemical states of copper identified in actual fly ash sampled from solid waste incinerators are indicative of the chemical states of copper after dioxin formation. The final state of copper has been observed, which is important information for deducing the reactions in incinerators, but is not enough to estimate the dynamic changes and true reactions of copper during dioxin formation.

The changes of copper in actual and model fly ash samples were directly observed during dioxin formation using in situ XAFS [3]. As shown in Fig. 4-39, cupric compounds in actual fly ash were reduced to cuprous compounds or elemental copper at a low temperature (~200°C). The changes in the Cu X-ray absorption near-edge structure (XANES) spectrum were similar between the actual fly ash and the model fly ash containing $CuCl_2 \cdot 2H_2O$. Furthermore, these changes are in agreement with dioxin formation. Oxychlorination has been found to be the key mechanistic step in the formation of dioxins in fly ash from municipal solid waste incinerators. Thus, the reactions in municipal solid waste incinerators have been successfully observed, but many unexplored areas remain. The actual dynamic changes and reactions are not yet known because the time resolution available at present is not enough; the reactions might be successive reactions and also temperature dependent, and so a good time resolution is needed to observe them.

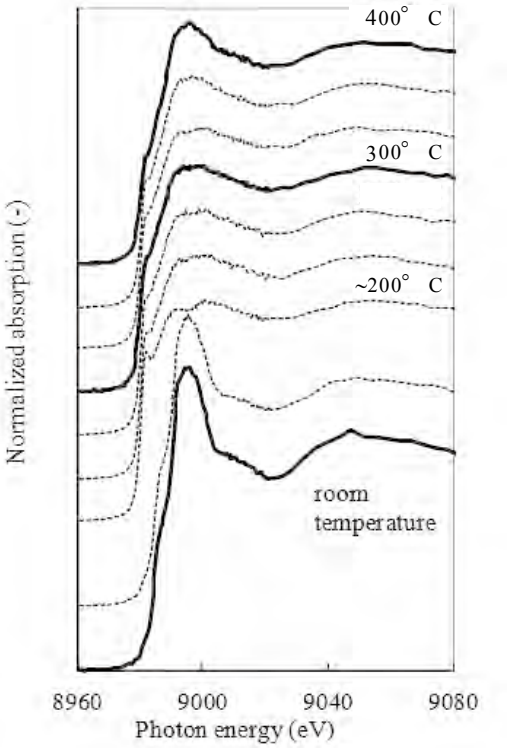

Figure 4-39
Cu K edge XANES spectra in actual fly ash on heating. Bold lines: spectra at constant temperatures, Dotted lines: intermediate spectra.

Cuprous compounds were identified in fly ash samples at temperatures of around 300°C, based on the spectra shown in Fig. 4-39. These spectra, however, do not coincide with the linear combination of the spectra of pure reagents of CuCl, Cu_2O and others. Fly ash contains unknown compounds which are not listed in the references used here. Alternatively, the very fast redox reactions in fly ash might have distorted the spectra at 300°C. A new technique of simultaneous ultra-fast measurements is required to study the formation mechanism.

Although our experiments targeted copper in fly ash, the chemical states of carbon and chlorine are also assumed to change. The dioxin formation mechanism could be better clarified by also examining the behaviors of these elements. Chlorine K-edge XANES spectra have confirmed a change in copper and the binding of chlorine with carbon [4, 5]. In the near future, detailed examination of carbon interactions will further clarify the dioxin formation mechanism. In addition to copper, carbon and chlorine, actual fly ash also contains iron, zinc,

lead and other elements that may undergo reactions during dioxin formation [6, 7]. The influence of these metals on dioxin formation should be further investigated. A more detailed understanding of the dioxin formation mechanism will facilitate the development of technology to inhibit the process.

Copper has been observed to play a major role in the dioxin formation mechanism. However, the whole mechanism including minor and intermediate reactions should be clarified to reduce dioxin emissions further. Techniques for simultaneous ultra-fast XAFS measurements should be developed to study the dynamics of the reactions. The X-ray beams currently in use are not small enough to clarify the dioxin formation mechanism further, because the formation reactions would occur at specific sites on a nanometer scale.

4.5.2.4 Future prospects using ERL

The X-ray beams of the ERL of nanometer size will enable the observation of specific sites of interest in samples. Environmental samples are exceedingly complex, variable and inhomogeneous compared with industrially-made materials. The local distribution of elements, local atmospheric conditions and other environmental factors cause huge variations among environmental samples such as fly ash. The nanometer-sized beam of the ERL will be a powerful tool to clarify the specific features of each reaction site and to compare the differences among them. With more detailed information, it will be possible to understand and to reproduce the actual composition and ingredients of samples; it has been too difficult to do so by using only the data sets of bulk samples so far. The nanometer-sized beam may reveal unknown chemical states in samples, and will help to understand the real mechanisms of reactions in the environment and human-made systems. Techniques for simultaneous ultra-fast XAFS measurements by utilizing the high repetition rate of the ERL should be developed to study the dynamics of reactions in real time for elements of interest one after another. Ultra-fast measurements will provide information on intermediate reactions during dioxin formation and clarify the formation mechanism. When the reaction mechanism in municipal solid waste incinerators is revealed, new ways to reduce dioxins and other harmful compounds will emerge, and it will be possible to make human life more convenient and environmentally friendly.

New revolutionary methods will be developed at the ERL facility. These will be crucial to study not only dioxin formation but also other chemical reaction mechanisms, and will greatly advance the field of environmental science and technology, thus helping to save the world.

REFERENCES

[1] R. Addink and K. Olie, *Environ. Sci. Technol*. **29**, 1425 (1995).
[2] M. Takaoka et al., *Chemosphere*, **59**, 1497 (2005).
[3] M. Takaoka *et al*, *Environ. Sci. Technol*. **39**, 5878 (2005).
[4] T. Fujimori and M. Takaoka, *Environ. Sci. Technol*. **43**, 2241 (2009).
[5] T. Fujimori et al., *Bunsekikagaku* **58**, 221 (2009).
[6] T. Fujimori et al., *Environ. Sci. Technol*. **43**, 8053 (2009).
[7] T. Fujimori, et al., *Environ. Sci. Technol*. **44**, 1974 (2010).

4.6 Life Sciences

4.6.1 Membrane proteins

4.6.1.1 Introduction

Membrane proteins continue to be among the most challenging targets in structural biology. All cells and organelles are contained within a hydrophobic lipid bilayer, in which integral membrane proteins are embedded. These proteins are involved in a wide variety of biological processes including photosynthesis, respiration, signal transduction, molecular transport and catalysis. Membrane protein structures are also of crucial importance for medicine. Historically, the discovery of new drugs has been led by chemistry and pharmacology. The advent of genomic sciences has opened up the possibility of identification of genetic determinants of different drug responses across a population and the possibility of drug therapy based on the patient's genetic profile. Structural data can inform library design, library screening, selection of targets, optimization of lead compounds, and engineering of selectivity to improve the overall efficiency of drug discovery.

Membrane proteins represent between 20 and 30% of the proteomes of most organisms and more than 40% of drug targets and yet very few structures of these molecules have been solved. The first membrane protein structure was published in 1985, and since then the number has increased slowly but steadily. There are currently over 70,000 entries in the Protein Data Bank (PDB), but less than 1% of these entries are membrane proteins. Of the 891 membrane protein structures in the 'Membrane proteins of known 3D structure' database (http://blanco.biomol.uci.edu/Membrane_Proteins_xtal.html), 304 belong to unique proteins (Fig. 4-40). Mammalian membrane proteins are particularly underrepresented, with less than 30 examples.

4.6.1.2 Scientific goals and challenges

Membrane proteins are difficult to study for a number of reasons. Their surface is hydrophobic and they can only be extracted from the cell membrane with detergents. They are also often flexible and unstable. This leads to challenges at all levels, including expression, solubilization, purification, crystallization, data collection and structure determination.

The most important scientific goal is to bring membrane protein crystallography up to the current level of soluble protein crystallography. This would allow us to directly address the structures of proteins that are relevant for biology and medicine. To achieve this, it is essential to establish a pipeline for membrane protein crystallography from protein production to structure determination, but many problems remain to be overcome and new technical developments are required.

4.6.1.3 Current status and limitations

An analysis of the Protein Data Bank depositions suggests that the number of membrane protein structures is increasing at a rate that is comparable to that for soluble proteins observed about 25 years ago (Fig. 4-40). Solving membrane proteins is still a difficult but not impossible task. With new technical developments, we estimate that membrane protein crystallography will be improved to the current state of soluble protein crystallography within 5 to 10 years. Recently, several structural genomics consortia on membrane proteins have been established, which are addressing the expression, production and crystallization of membrane proteins. However, there has been little emphasis on data collection.

4.6.1.4 Future prospects with ERL

The planned ERL will be an excellent means of addressing the data collection problems in membrane protein crystallography.

It has been shown that microbeams are very useful for X-ray data collection from membrane protein crystals, particularly from microcrystals obtained in the lipidic cubic phase. The method has been shown to be suitable for obtaining the crystals of G-protein coupled receptors, which are major drug targets. However, studies have also shown the limitation of the technique. Because microcrystals are susceptible to radiation damage, it is often necessary to collect data using many crystals to complete a dataset. These microcrystals in the lipidic cubic phase are almost invisible once mounted in a loop, so it is necessary to screen the whole loop surface using raster scanning. Even with a fast detector, this is an extremely time-consuming process: in the case of histamine H_1 receptor, it took 7 months to complete a dataset using more than 1,000 crystals.

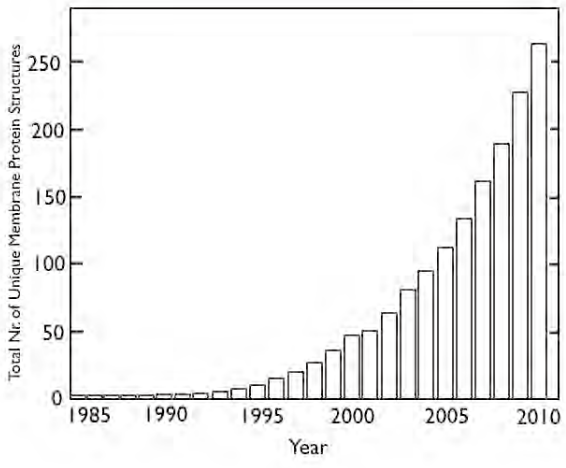

Figure 4-40
Cumulative number of unique membrane protein structures.

More recently, Chapman and his colleagues published a method to determine protein structure using femtosecond pulses from a hard-X-ray free-electron laser, the Linac Coherent Light Source (LCLS). For the experiments, they used nanocrystals of photosystem I, one of the largest membrane protein complexes. More than 3 million diffraction patterns were collected in the study, and a three-dimensional dataset was assembled. In the study, they showed that the problem of radiation damage in crystallography could be conquered using X-ray pulses briefer than the timescale of most damage processes. The study thus provides a new approach to determining the structure of macromolecules that do not yield crystals of sufficient size for studies using conventional radiation sources.

The methods using micro- or nano-crystals and an intense X-ray microbeam should also be applicable to membrane protein crystallography at the ERL and XFEL-O. For the ERL, where non-perturbed measurements will be performed, an experimental set-up similar to the current microfocus beamline at the synchrotron radiation facility could be used. Faster data collection using sub-micron crystals will be possible, particularly in combination with a fast readout detector. Shorter exposure time is also advantageous to avoid radiation damage by collecting data before the diffusion of generated radicals. The ERL has some advantages over the XFEL for membrane protein crystallography. For the XFEL, beam time is very limited because only one beamline at a time is available. In contrast, the ERL will provide multiple beamlines for users such as storage ring facilities. Once the XFEL-O becomes available, it will be possible to perform one-shot measurements, which will allow data collection from nanocrystals and further minimize the radiation damage problem.

For the experiments at the LCSC, a liquid jet system was used for crystal injection. Although this system is much more efficient than the conventional loop mounting system, it requires a large amount of unfrozen crystals. Membrane protein crystals are very temperature sensitive and not suitable for transportation. Setting up a protein crystallization facility nearby will create a seamless link to X-ray beamlines to allow high-throughput crystal screening and high-quality data collection. The ERL offers a unique opportunity to establish this cutting-edge facility, which is a key step in the full exploitation of the ERL for membrane protein crystallography. The facility will serve as a center of expertise for both Japanese and overseas scientists who are facing difficult crystallographic problems in membrane protein crystallography.

4.6.2 Epigenetics

4.6.2.1 Introduction

The proliferation and differentiation of eukaryotic cells are one of the central topics in biology. Several types of cells, which have distinct functions and characteristics, are generated in the course of development, although these cells have the same genetic information in DNA molecules. How can cells differentiate to various cells with distinct functions and characteristics? How do the differentiated cells maintain their specific functions over cell generations? Molecular biology has answered these questions with the concept of epigenetic information.

Typical forms of epigenetic information are methylation of DNA and post-translational modifications (PTMs) of histones. Since the epigenetic information can control the expression patterns of genetic information in the cell, the difference of epigenetic information causes the difference of cell types. In addition, epigenetic information is inherited from parental to daughter cells. As a result, an expression pattern of genetic information in a parental cell is copied to daughter cells. The concept of epigenetic information is therefore critical to understanding the mechanisms of proliferation and differentiation of the cell, and many researchers consider that epigenetics is one of the most important fields of study in biology in the 21st century. Of various types of epigenetic information, DNA methylation has been well studied. Not only its biological effect but also its inheritance mechanisms have been investigated based on the crystal structures of relevant proteins (or complexes). On the other hand, the molecular mechanisms of histone epigenetic information are not well understood.

Histones are abundant basic proteins in the cell nucleus and form nucleosomes with DNA [1]. PTMs of histone proteins (histone epigenetic information) are considered to regulate various nuclear events such as gene expression, DNA repair, and DNA replication (Fig. 4-41) [2]. However, the molecular mechanisms of histone epigenetic information processing—generation, utilization, editing, maintenance, and transfer of histone epigenetic information—remain elusive. Of the various unsolved problems in

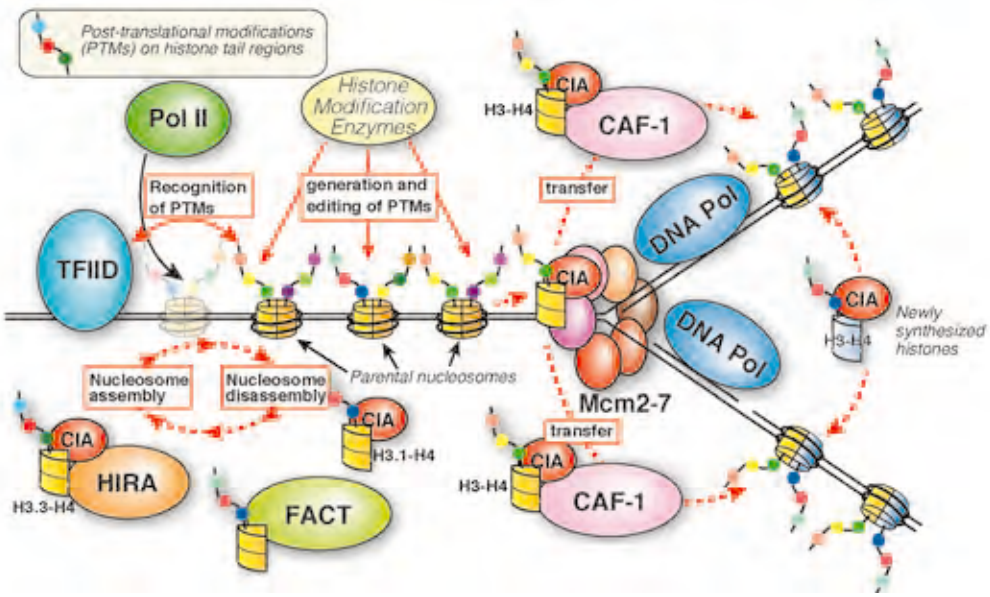

Figure 4-41
Histone epigenetic information processing in the cell. Several large protein complexes such as TFIID (app. 1MDa), HIRA (app. 0.5MDa), CAF-1 (app. 0.5MDa), Mcm2-7(app. 0.9MDa), FACT (app. 0.2 MDa) are involved in histone epigenetic information processing such as its generation, editing, maintenance, and transfer. In the epigenetic information processing, these complexes are considered to interact to each other in a transient manner. In order to analyze the molecular event in the nucleus, the combination of crystal structures of these complexes and high-resolution *in situ* images are required.

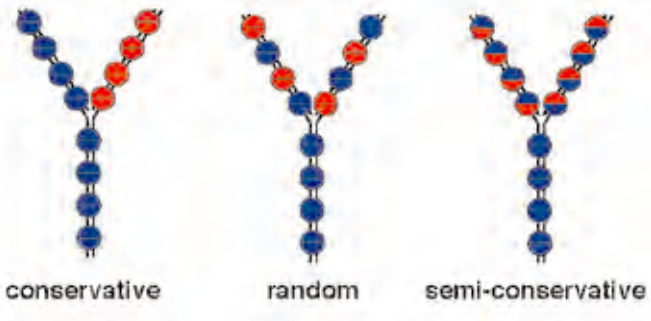

Figure 4-42
Three major modes of nucleosome replication. Blue and red semicircles represent parental and newly synthesized histones, respectively. Recent biochemical, crystallographic, and MS analyses reveled that random and semi-conservative replications of nucleosomes occur in the nucleus.

the field of epigenetics, the molecular mechanism of the histone transfer from parental to daughter cells is the most important one. In the course of cell division, not only DNA but also nucleosomes are replicated (Fig. 4-42). Replicated nucleosomes on daughter cells are composed of parental and/or newly synthesized histones. Since parental histones convey parental epigenetic information, the replication mode of nucleosomes—random, conserved, and semi-conserved—has an impact on the fate of daughter cells. Biochemical, crystallographic, and mass spectroscopic analyses suggested that both random and semi-conservative replications occur in the nucleus [3–5]. However, we cannot exclude the possibility that the conservative replication of nucleosomes occurs as a minor event, because biochemical experiments do not yield definitive evidence confirming or denying the existence of minor events in the cell. Furthermore, the molecular mechanisms of nucleosome replication and its regulatory machinery are totally unknown because of the complexity of the molecular process. In order to solve these problems in the field of epigenetics, a novel method to overcome the limitations of present biochemical experiments is required. In-cell direct observation of large molecular complexes with their localization and interactions is one of the most promising methods to overcome the limitation.

4.6.2.2 Scientific goals and challenges

The scientific goal of our study on histone epigenetics is *in situ* visualization of the series of molecular events relevant to epigenetic information processing. This could be achieved by the combination of structural information of protein complexes at atomic resolution and *in situ* high-resolution images of particular events (Fig. 4-43). The combination method would reveal not only the localization but also the molecular interactions of various protein complexes in the cell and would overcome the limitations of biochemical and biological methods. To achieve this scientific goal, there are two major challenges.

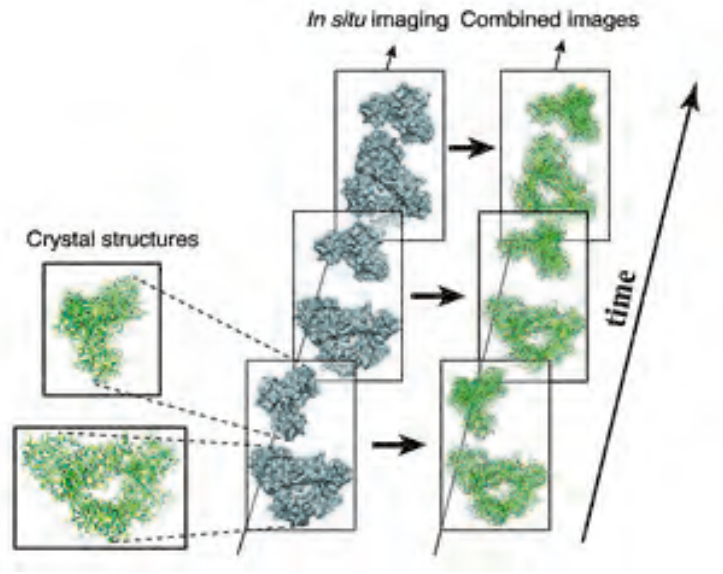

Figure 4-43
Combined study between crystallography and in situ imaging using ERL. The combined method is the most promising approach to overcome the limitation of the present biochemical and biological methods. It would be possible to obtain a series of molecular images in the nucleus through utilizing ERL X-ray.

1) The first challenge is determination of the crystal structures of large protein complexes. The protein complexes involved in the processing of histone epigenetic information (TFIID, HIRA complex, CAF-1 complex, Mcm2-7, FACT, etc.) are quite large (Fig. 4-41), and only small amounts of these complexes can be prepared. The small amount of purified sample causes difficulties for crystallization and crystallographic analysis (μm-order small crystals, poor crystal quality, fewer crystal samples, weak diffraction, large unit cell, etc.). A method and facilities for this type of difficult structural analysis need to be developed.

2) The second challenge is the development of an *in situ* imaging technique using a coherent X-ray beam. Epigenetic information processing is a dynamic molecular event involving the assembly and disassembly of several molecules and/or molecular complexes. In many cases, typical biochemical data from equilibrium systems are not suitable to explain the dynamic process *in vivo*. Molecular processes regarding epigenetic information should be directly observed *in vivo* (Fig. 4-43). Since no physicochemical methods that can observe the time development of *in vivo* macromolecular behavior at high resolution are available, a new method is needed.

4.6.2.3 Current status and limitations

1) Although some crystal structures of histone chaperones involved in histone transfer have been determined, no overall crystal structures of large protein complexes serving histone epigenetic information processing (Fig. 4-41) have been obtained due to difficulties of crystal structure analysis of large protein complexes. A present typical method for tertiary structure analysis of large protein complexes combines cryo-electron microscopy (EM) and X-ray crystallography. However, this combined method is insufficient to reveal the details of molecular mechanisms at atomic resolution. Atomic resolution structures are required to analyze the structural changes of these complexes occurring in histone epigenetic information processing. Therefore, methods to determine high-resolution crystal structures of the large protein complexes are essential.

2) In the last decade, several techniques for in situ imaging have been developed. Techniques with fluorescence microscopy have made great progress, furthering our understanding of macromolecular dynamics in the cell [6]. However, the resolution of these methods is insufficient to analyze individual molecular events at the molecular level. Although electron tomography is a powerful method to observe macromolecular structures at high resolution *in vivo* [7], it cannot observe the development of the system over time because observations are conducted under cryo conditions. Single molecular imaging techniques with microscopy or high-speed AFM have become a powerful tool in the field of biophysics, and have succeeded in direct observation of movements of protein machinery such as motor proteins and F1-ATPase [8]. However, most of these methods cannot be used for *in vivo* systems.

4.6.2.4 Future prospects with the ERL

1) The high flux and finely focused X-ray beam from the ERL will revolutionize the crystallographic analysis of large protein complexes. It will become possible to determine the crystal structures of large protein complexes with μm-order crystals in a routine manner by combining the ERL with an advanced two-dimensional detector and other new technologies. Crystal structure analysis of large protein complexes such as TFIID, CAF-1, HIRA, Mcm2-7 would therefore be possible. In addition, crystal structure analysis of these complexes in different structural states would also become routine. Although sample preparation of large complexes would be the biggest problem, the development of new expression systems over the next decade will greatly improve the situation. Small angle scattering and other analytical methods in solution will be important for assisting the crystallization of large protein complexes.

2) Advanced imaging techniques using the coherent X-ray beam from the ERL and XFEL-O would yield more fruitful results. When the *in situ* imaging techniques can produce individual images of large protein complexes involved in epigenetic information processing, higher-order structural information such as interactions and localizations of these complexes in the cell could be obtained through combination with crystal structure information of these protein complexes (Fig. 4-43). In particular, a high-resolution localization map of protein complexes, which has never been obtained, will help to understand the functions of each protein complex.

The development of *in situ* real-time imaging using pulse X-rays from the ERL is also important. Time-resolved observation of the histone delivery process on the replication fork would uncover all nucleosome replication modes in the nucleus. In addition, information about the molecular machinery required for each replication mode could be obtained from the *in vivo* images. This information will contribute to analyzing the molecular mechanisms of histone delivery on the replication fork.

The results of these studies will not only contribute to the understanding of epigenetic information processing but also could be applied to various fields of medical science including tissue engineering, because epigenetics is the basis of cell differentiation and proliferation. Furthermore, these methods with the ERL will open up a new era of biological science, since new techniques will yield spatial information on individual protein complexes in the cell in a time-dependent manner, which cannot be obtained by biochemical and biological methods.

REFERENCES

[1] R.D. Kornberg, *Science* **184**, 868 (1974).
[2] B.D. Strahl and C.D. Allis, *Nature* **403**, 41 (2000).
[3] V. Jackson, *Biochemistry* **26**, 2315 (1987).
[4] R. Natsume *et al*., *Nature* **466**, 338 (2007).
[5] M. Xu *et al*., *Science* **328**, 94 (2010).
[6] J. Zhang *et al*., *Nat. Rev. Mol. Cell. Biol*. **3**, 906 (2002).
[7] C.V. Robinson, A. Sali and W. Baumeister, *Nature* **450**, 973 (2007).
[8] K.Jr. Kinosita *et al*., *Cell* **93**, 21 (1998).

Chapter 5 Accelerator

5.1 Overview

The energy recovery linac (ERL) is expected to bring innovation to materials science [1]. In the ERL, electron beams having extremely-low emittances are produced using an innovative photocathode DC gun. The beams are then accelerated with a superconducting linac to the beam energy of several GeV, and used to produce synchrotron radiation (SR). The spent beams are then decelerated through the same superconducting linac, and dumped. The continuous use of fresh beams allows us to achieve ultimately-low beam emittances in six-dimensional phase-space with high average currents.

The ERL can provide high-brightness electron beams having normalized emittances of 0.1-1 mm·mrad at beam currents of 10-100 mA. The ERL can also produce ultra-short electron bunches having rms lengths of about 100 femto-seconds for ultra-fast science. Furthermore, the ERL accelerator can produce high-quality electron bunches at high repetition rates, which is required to drive the proposed X-ray free-electron-laser oscillator (XFEL-O) [2–4]. The XFEL-O can provide an unprecedented fully-coherent X-ray laser having extremely-high brightness of 10^{26} photons/s/mm^2/mrad^2/0.1%bw (or higher). The produced X-ray will consist of X-ray pulses at a high repetition rate of 1 MHz (or higher), and will have full temporal and full spatial coherence, with pulse widths of about 1 ps (rms). Thus, the XFEL-O will provide a “true” X-ray laser, and will open up a new paradigm in materials science research.

Incorporating the above-mentioned features, we propose for the future project of the KEK Photon Factory to construct a 3-GeV ERL that can be upgraded to the XFEL-O. A conceptual layout of the 3-GeV ERL is shown in Fig. 5-1. In the first stage of the project, we construct a 3-GeV ERL which comprises an injector linac, a superconducting main linac, and a return loop. In the return loop, we will install 20-30 insertion devices which are used to emit synchrotron radiation. Using state-of-the-art undulator technology, we cover a broad spectrum range of synchrotron radiation from vacuum ultra-violet (VUV) to hard X-rays.

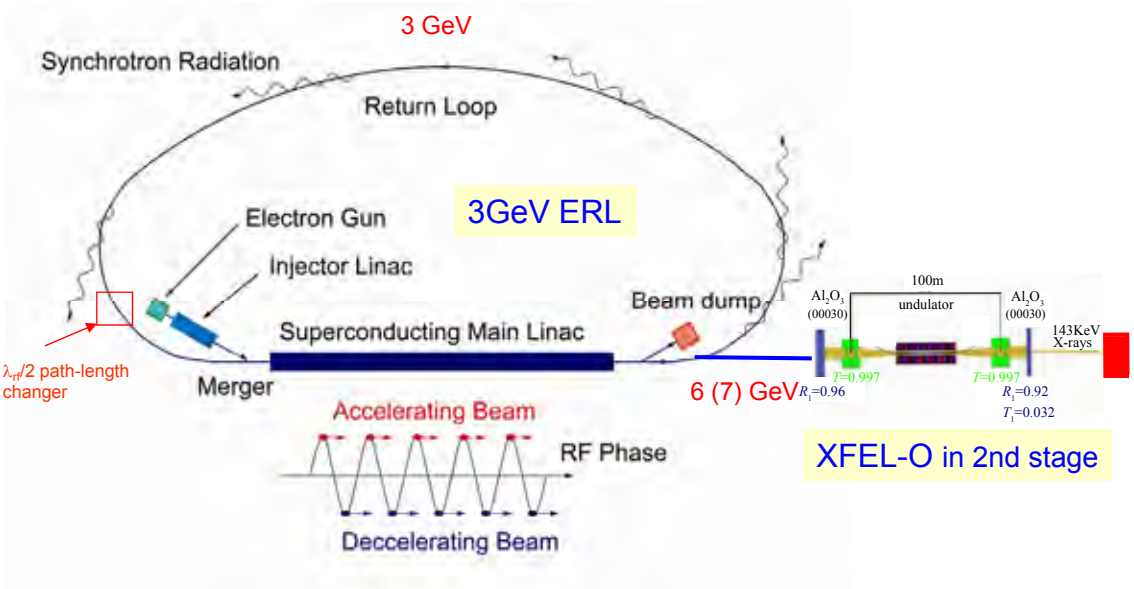

Figure 5-1
Conceptual layout of 3-GeV ERL plan that is integrated with an X-ray free electron-laser oscillator (XFEL-O).

In the second stage of the project, we will build an XFEL-O system which comprises a long undulator and an X-ray resonator. To deliver high-energy beams for the XFEL-O system, we change the path length in the return loop by a half RF wavelength of 115.3 mm. In this configuration, the beams are first accelerated to 3 GeV through the main linac, and they pass through the return loop. The beams are then accelerated again (without energy recovery) through the main linac up to 6 GeV (or 7 GeV with a slight upgrade in the main linac). Then, the beams are used to drive the XFEL-O, and are dumped without energy recovery.

Target parameters of the 3-GeV ERL are given in Table 5-1. Since the ERL is a very flexible light source, we have shown some typical operational modes in this table. For the major users requiring highly brilliant SR, we provide high-coherence or high-flux modes of operation. Among these modes, the high-flux mode imposes more challenges for the lifetime of the photocathodes. The “ultimate” mode requires both very-low emittance and high currents; this imposes much greater challenges in the accelerator physics and engineering, and thus it is a long-term goal. In the ultra-short-pulse mode, we compress the electron bunches down to a hundred femto-seconds or lower. In this mode, the beam emittances are largely influenced by the coherent synchrotron radiation in the return loop. Then, bunch charges under this mode will be chosen by compromising the SR intensity and the beam emittance.

Table 5-1 Target parameters of the 3-GeV ERL which is integrated with the X-ray free-electron-laser oscillator (XFEL-O).

	Operation modes				
	High-coherence mode	High-flux mode	Ultimate mode	Ultra short-pulse mode	XFEL-O
Beam energy (E)	3 GeV				6-7 GeV
Average beam current (I_0)	10 mA	100 mA	100 mA	Typically, 77 μA (flexible)	20 μA
Charge/bunch (q_b)	7.7 pC	77 pC	77 pC	Typically, 77 pC (flexible)	20 pC
Repetition rate of bunches (f_{rep})	1.3 GHz	1.3 GHz	1.3 GHz	Typically, 1 MHz (flexible)	1 MHz
Normalized beam emittances (ε_{nx}, ε_{ny})	0.1 mm·mrad	1 mm·mrad	0.1 mm·mrad	To be investigated (typically, 1-10 mm·mrad)	0.2 mm·mrad
Beam emittances at full beam energy (ε_x, ε_y)	17 pm·rad	170 pm·rad	17 pm·rad	To be investigated (typically, 0.2-2 nm·rad)	15 pm·rad
Energy spread of beams; in rms (σ_E/E)	2×10^{-4}	2×10^{-4}	2×10^{-4}	To be investigated	5×10^{-5}
Bunch length; in rms (σ_t)	2 ps	2 ps	2 ps	100 fs	1 ps

In the ERL, the beam emittances are primarily determined by the injector. First, the development of the high-brightness electron guns is critical. In addition, there are some effects that can dilute the beam emittances in the injector and in the merger section:

- self-defocusing force due to space charges that can enlarge the projected beam emittance,
- transverse-emittance dilution due to both longitudinal space-charge effect and coherent synchrotron radiation (CSR) in a dispersive section of the merger, and
- time-dependent focusing force in the injector cavities.

The emittance dilution due to these effects can be minimized by optimizing the injector design; an optimized design is briefly described in section 5.2.1.

In the main linac and in the return loop, there are some other issues that should be investigated:

- beam-breakup instability due to higher-order modes in the cavities,
- beam-breakup instability due to resistive-wall impedance of the vacuum chamber,
- emittance dilution due to CSR in dispersive sections of the return loop,
- focusing forces due to trapped ions; the possibility of electron-ion instability,
- time-dependent self kicks due to transverse wakefields in superconducting cavities and in vacuum components,
- protection against radiation hazard due to beam losses or to accelerated dark currents from the superconducting cavities.

To realize the X-FELO, there are other issues that should be resolved:

- developing Bragg mirrors having very-low losses for the X-ray resonator,
- extremely high-precision control and stabilization for the X-ray resonator,
- more stringent requirement for the beam quality,
- controlling radiation hazard at the beam dump for high-energy beams.

Some of these issues are discussed in the following sections.

In order to establish critical technologies for the ERL project, we have conducted extensive R&D since 2006, including the development of photocathode DC guns at Japan Atomic Energy Agency (JAEA) and at KEK, developing two kinds of superconducting cavities that are required for the injector and the main linac, high-precision low-level RF-control system, and so on. To demonstrate reliable operation of these R&D products, as well as to investigate the accelerator-physics issues of the ERL, a test accelerator named the "Compact ERL (cERL)" [5-7] is under construction at KEK. Using the cERL, many accelerator issues will be clarified. The cERL is scheduled to be commissioned at the end of Japanese fiscal year 2012.

REFERENCES

[1] See, for example, D.H. Bilderback, J.D. Brock, D.S. Dale, K.D. Finkelstein, M.A. Pfeifer and Sol M. Gruner, *New J. Phys.* **12,** 035011 (2010).
[2] K.-J. Kim, Y. Shvyd'ko and S. Reiche, *Phys. Rev. Lett.* **100**, 244802 (2008).
[3] R.R. Lindberg and K.-J. Kim, *Proc. 23rd* PAC09 1198 (2009).
[4] K.-J. Kim and Y.V. Shvyd'ko, *Phys. Rev. ST Accel. Beams* **12**, 030703 (2009).
[5] "Design Study of the Compact ERL" edited by R. Hajima, N. Nakamura, S. Sakanaka and Y. Kobayashi, *KEK Report* **2007-7**/ *JAEA-Research* **2008-032** (2008).
[6] S. Sakanaka *et al.*, *Proc. IPAC'10* 2338 (2010).
[7] S. Sakanaka, H. Kawata, Y. Kobayashi, N. Nakamura and R. Hajima, *Proc. XXV* LINAC10 398 (2010).

5.2 Beam Dynamics Issues

When starting to develop ERL-based light sources, there are many beam dynamics issues to be solved in order to achieve excellent performance. This section outlines the issues concerning the beam dynamics of the 3-GeV ERL light source including the XFEL-O.

5.2.1 Injector design and optimization

Injector design and optimization are very important for transporting high-current low-emittance beams to the main linac without serious degradation of beam quality. Injection design issues are emittance compensation, merger optics and envelope matching to the main linac. Multi-objective optimization with a genetic algorithm is a very powerful tool [1] and gives a better result than manual optimization though the optimization result should be compared to the beam dynamics.

Figure 5-2 shows the layout of the compact ERL (cERL) injector. The cERL injector consists of a 500-kV photocathode DC gun (DCG01), two solenoid magnets (SLA01 and SLA02), a buncher cavity (BCA01), three superconducting RF cavities (SCA01, SCA02 and SCA03), five quadrupole magnets (QMA01 – QMA05) and a merger section. The merger consists of three rectangular magnets with the bending angles of -16, 16 and -16 degrees, and two quadrupole magnets. In the multi-objective optimization with the genetic algorithm and the simulation code GPT, 19 injector parameters were optimized for the bunch charge of 80 pC (more than 100 mA at 1.3 GHz repetition) to minimize the transverse emittances at 1 m from the exit of the merger. Figures 5-2 and 5-3 show the optimization result. The optimized horizontal and vertical normalized emittances are smaller than 0.6 mm mrad with the bunch length of 0.6 mm (2 ps) and the electron kinetic energy of about 8 MeV [2]. In the injector of the 3-GeV ERL, the emittance should be reduced further to improve the light source performance. Higher injector energy and higher gun voltage are possible approaches, in addition to improving the injector design.

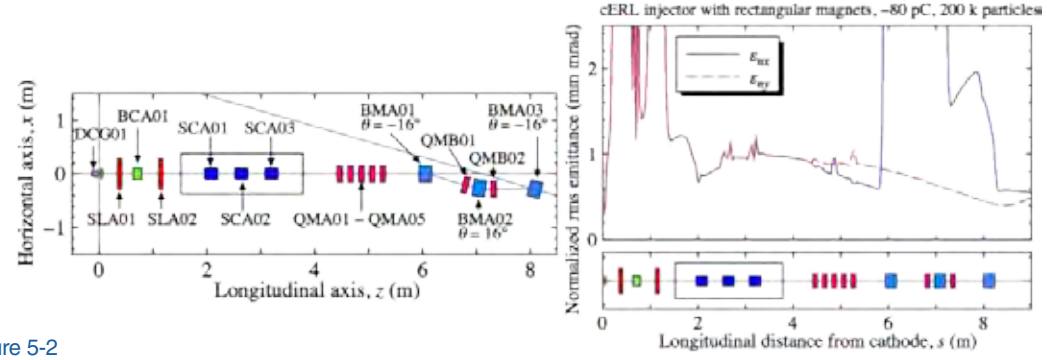

Figure 5-2
Layout of cERL injector(left) and the horizontal and vertical normalized emittances(right) optimized for the bunch charge of 80 pC by multi-objective optimization.

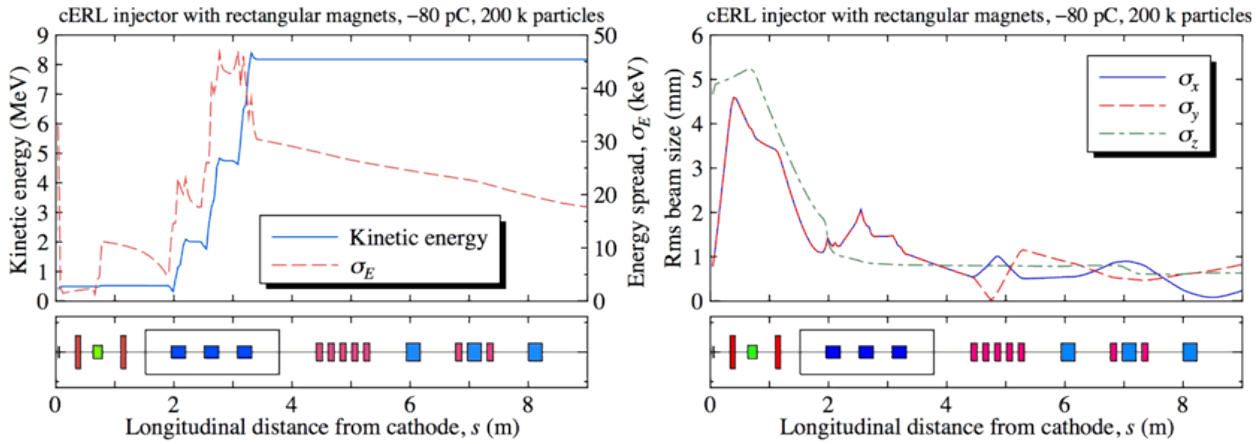

Figure 5-3
Beam kinetic energy and energy spread(left) and horizontal and vertical beam sizes and bunch length(right) optimized for the bunch charge of 80 pC by multi-objective optimization.

5.2.2 Lattice and optics of return loop and main linac

There are many considerations for the lattice and optics design of the return loop and main linac of the 3-GeV ERL light source. It is very important to preserve emittance for such a low-emittance light source. The lattice and optics should be designed to suppress emittance growth due to coherent and incoherent synchrotron radiation (CSR and ISR) effects. The optics of the main linac and the return loop should be optimized in order to obtain a high BBU threshold current. A large energy acceptance is needed to avoid serious beam loss because large energy deviation can be induced by Touschek and residual-gas scatterings and other sources of beam halo and then amplified by deceleration. Path length control is a common issue to ERLs for energy recovery and is also used for switching from energy recovery operation to XFEL-O operation in our case. Furthermore, a bunch compression scheme is needed for generating an ultra-short bunch.

The return loop of the 3-GeV ERL will have about 30 TBA cells with long straight sections for insertion devices and the main linac will consist of more than 200 9-cell cavities for acceleration and deceleration. Figures 5-4 and 5-5 show the optical functions of TBA cells with 6-m and 30-m straight sections designed for the 3-GeV ERL [3]. The bending radius is 19.1 m, which is sufficiently long to suppress emittance growth and increase of energy spread due to the ISR effects. Each of these cells is achromatic and isochronous and has a horizontal betatron phase advance of π per two cells so that CSR kicks can be considerably cancelled. Bunch compression will be achieved by using off-crest acceleration in the main linac and non-zero R_{56} in the return loop. The optics of the main linac are being designed so that the betatron function is well suppressed for achieving a high BBU threshold current [4]. Figure 5-6 shows the tentative result of the optical functions for the main linac and the return loop of the 3-GeV ERL. In this optics, the emittance growth and energy spread increase due to the ISR and CSR effects are negligibly small for both Ultimate and XFEL-O modes.

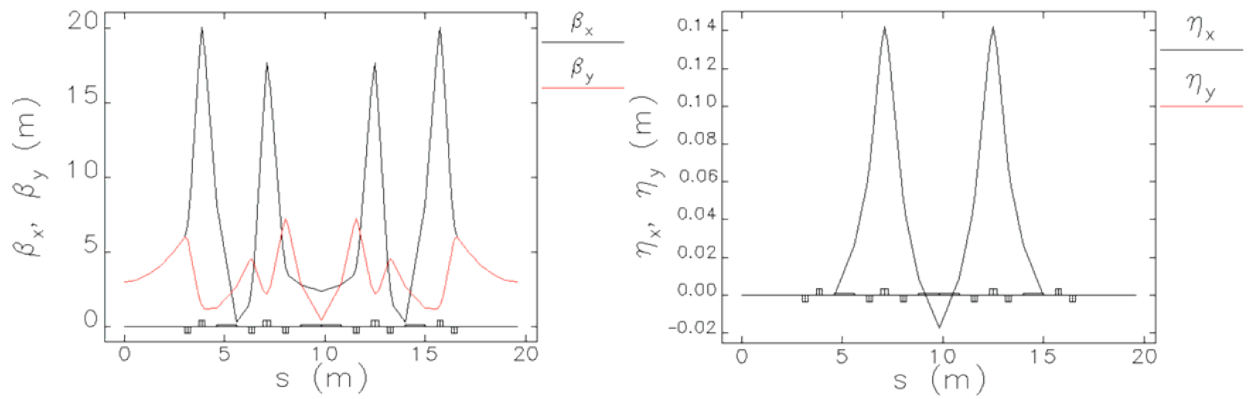

Figure 5-4
Betatron(left) and dispersion(right) functions of the short TBA cell with a 6-m straight section for the 3-GeV ERL light source.

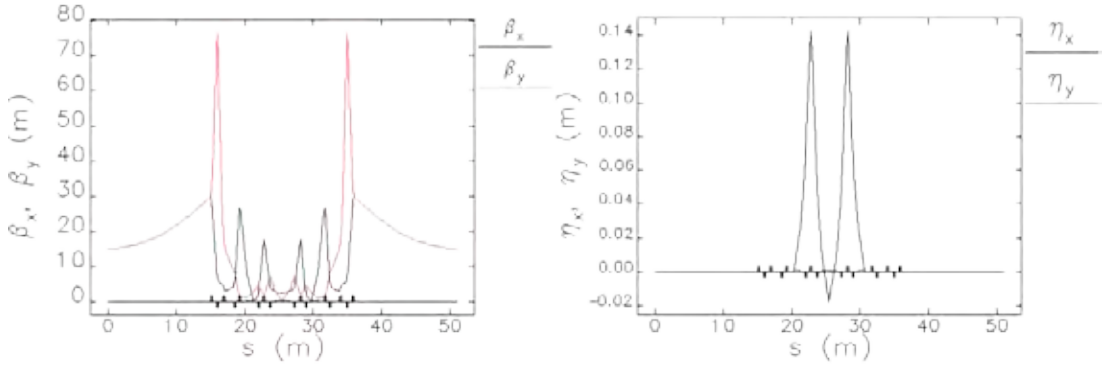

Figure 5-5
Betatron(left) and dispersion(right) functions of the long TBA cell with a 30-m straight section for the 3-GeV ERL light source.

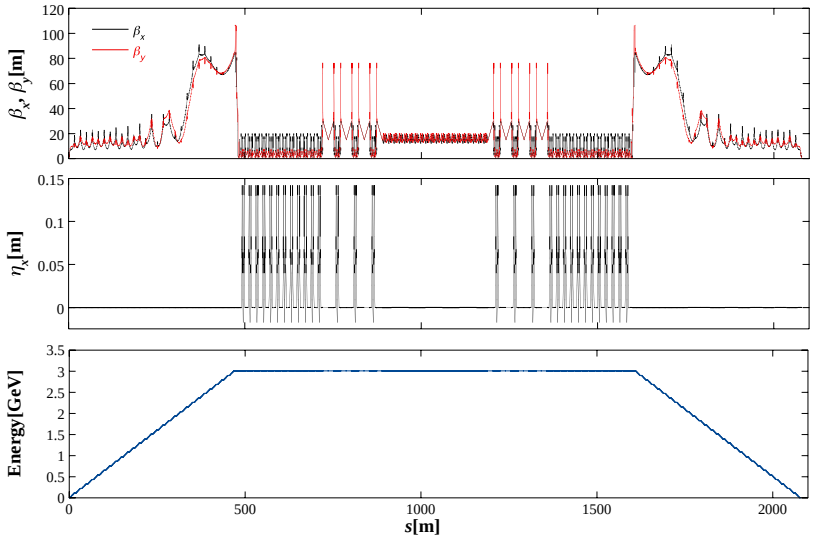

Figure 5-6
Betatron function (upper), dispersion function (middle) and beam energy (bottom) of the main linac and the return loop for the 3-GeV ERL.

5.2.3 HOM BBU and heating

Transverse beam breakup (BBU) due to cavity HOMs usually limits the beam current in ERLs. In previous experiments at the JLAB ERL, BBU simulations agreed with the measurements of the BBU threshold current [5], so we can predict the BBU threshold current without a large error. The threshold current can be increased by optics optimization, polarized cavities and HOM frequency randomization.

The current design (Model 2) of the superconducting cavity, which has enlarged beam pipes and on-axis HOM dampers, can increase the transverse BBU threshold current up to 600 mA without any HOM randomization and about 2 A with HOM frequency randomization of 2 MHz for a 5-GeV ERL [6]. Therefore, it is expected that the target threshold current of 100 mA or more will be easily achieved for the 3-GeV ERL light source.

It should be noted that heating due to longitudinal HOMs also limits the beam current depending on the bunch length in the main linac. Therefore, the bunch length may be adjusted in the injector not to be considerably smaller than 2 ps in the high current operation, though a shorter bunch length reduces the momentum spread and hence increases the brightness of the undulator radiation as described in Section 5.2.7.

5.2.4 Resistive-wall wake

It was suggested that the resistive-wall (RW) wake of beam pipes can cause transverse multi-bunch BBU because of its long-range feature [7]. In order to study the RW-BBU more precisely, exact impedances and wakes of beam pipes with finite thickness were calculated [8]. Multi-bunch BBU simulations showed that the transverse beam position displacement due to the exact RW wake is saturated within a

short time because the cumulated RW wake reaches the ceiling. As a result, it is expected that RW-BBU will be manageable, though further study might be needed for beam pipes surrounded by thick material such as magnets and undulators.

Heating due to longitudinal RW wake can be serious because of the short-bunch and high-current ERL beams. Such heating was already observed at the JLAB wiggler chamber [9]. Parasitic loss P_{RW} in a resistive round pipe with radius *b* and length L is expressed with the loss factor k_{loss} as:

$$P_{RW} = k_{loss} Q_b^2 f_b L = k_{loss} I^2 L / f_b \tag{5-1}$$

$$k_{loss} \approx \frac{Z_0}{8\pi^2 bc}\sqrt{\frac{2\rho_e}{\mu}}\Gamma\left(\frac{3}{4}\right)\sigma_t^{-1.5} \tag{5-2}$$

where Q_b, f_b, and I are the bunch charge and the repetition frequency of bunches and the average beam current. The loss factor of the resistive-wall thick pipe is expressed as Eq. (5-2) with the vacuum impedance Z_0, the electrical resistivity of the pipe ρ_e the magnetic permeability of vacuum μ_0, the speed of light c, the gamma function Γ, and the bunch length σ_t for a bunch with a Gaussian distribution. Since ERL light sources have much shorter bunches than storage-ring based light sources, they have much higher loss factors. The parasitic loss per unit length in each stainless steel (SS) pipe with diameter of 16 or 6 mm is calculated as 21.0 and 54.7 W from Eq. (1) for a typical ERL-based light source (σ_t = 1 ps, I = 100 mA, f_b = 1.3 GHz), while the parasitic loss is 13.3 and 35.3 W for the same pipes in SPring-8 (σ_t = 13 ps, I = 100 mA, f_b = 0.045 GHz). ERL-based light sources can have higher parasitic loss than storage-ring based light sources.

In order to cover a wide energy range of photons in the 3-GeV ERL light source, an undulator tends to have a smaller gap and hence the longitudinal RW wake at the undulator becomes stronger. Impedance calculations suggest that copper sheet or plating can be effective in suppressing RW heating of the undulator or its chamber [8]. In addition, a powerful cooling system should be added depending on the undulator gap.

5.2.5 Ion trapping

Ion trapping can be a serious problem because trapped ions induce fast ion instability. Two approaches are proposed for eliminating trapped ions. One is to install ion clearing electrodes which can repel the trapped ions by high voltage. For the Cornell ERL, such an electrode will be installed every 10 m for suppressing ion trapping [10]. The other approach is to insert a small gap in the bunch train [11], as shown in Fig. 5-7 This method is widely employed in existing storage rings including the PF ring. A short bunch gap (~50 ns) and ultra-high vacuum are possible solutions for ion trapping in the 3-GeV ERL light source, though we must manage variations of beam loading in the gun and cavities. Ion effects have never been observed or intensively studied at existing ERLs. The compact ERL at KEK could be used for an experimental study on ion trapping for the 3-GeV ERL.

5.2.6 Beam loss

Beam loss can be a huge operational problem for ERLs. There are many potential sources: Touschek scattering, intrabeam scattering (IBS), residual gas scattering, space charge and CSR effects, stray light from a laser, bunch tail at the photocathode, RF field and field emission of cavities and so on. Several

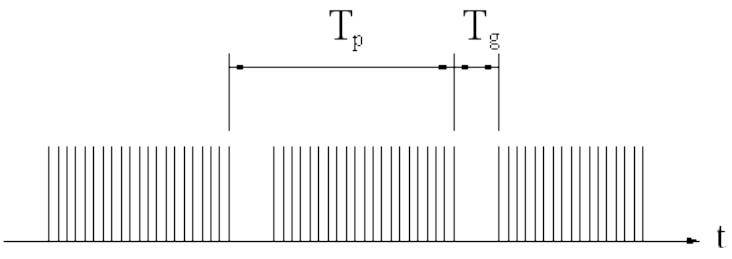

Figure 5-7
Gap in the bunch train for suppressing ion trapping. T_p: period of bunch gap, T_g: duration of bunch gap.

existing simulation codes include space charge and/or CSR effects, and calculations of Touschek scattering and IBS are already implemented in some codes. The effects of field emission from RF cavities are also being studied [12, 13]. For the 3-GeV ERL, beam halo formation as well as beam collimation and machine protection schemes should be further studied based on beam dynamics.

5.2.7 Error tolerances

Error tolerances should be evaluated for determining the specifications of ERL elements such as maximum ripples and drifts of magnet power supplies and stability of the RF system.

In ERL-based light sources, higher stability of the RF system is required, because the beam has a shorter bunch length and smaller momentum (energy) spread compared with that of the existing ring-based light sources. Denoting the momentum variation due to the RF amplitude and phase variations of the main linac as $\Delta p/p$, the relative spectral width of the undulator light, $\Delta\varepsilon_{ph}/\varepsilon_{ph}$, is expressed by

$$\frac{\Delta\varepsilon_{ph}}{\varepsilon_{ph}} \approx \sqrt{\left(\frac{1}{kN_u}\right)^2 + \left(\frac{4\sigma}{p}\right)^2 + \left(\frac{4\Delta p}{p}\right)^2} \tag{5-3}$$

where N_u, k and σ_p are the number of the period in the undulator, harmonic number of the undulator light and momentum spread of the electron beam. On the other hand, since the bunch compression is achieved by non-zero R_{56} in the return loop and off-crest acceleration in the main linac, the momentum variation also causes variations of bunch arrival time ΔT and hence lengthens the effective bunch length $\sigma_{t,\,eff}$ in the bunch compression mode as follows.

$$\sigma_{t,eff} = \sqrt{\sigma_t^2 + (\Delta T)^2} \quad \left(\Delta T = \frac{R_{56}}{c}\frac{\Delta p}{p}\right) . \tag{5-4}$$

The conditions under which the momentum variation does not degrade the spectral and temporal performances of the undulator light are given for the normal and bunch compression modes respectively as follows:

$$\frac{\Delta p}{p} << \frac{\sigma_p}{p} \tag{5-5}$$

$$\frac{\Delta p}{p} << \frac{c\sigma_t}{R_{56}} . \tag{5-6}$$

Assuming that $\sigma_p/p = 10^{-4}$ in the normal mode and $R_{56} = 0.15$ m and $\sigma_{t,eff} = 50$ fs in the bunch compression mode, both conditions (5) and (6) become $\Delta p/p << 10^{-4}$. If the RF phase is assumed to be 15 degrees in the bunch compression mode, the stability required for the RF amplitude V_0 and phase φ_0 of the main linac are given by:

$$\frac{\Delta V_0}{V_0} \approx \frac{\Delta p}{p} << 10^{-4}, \quad \Delta\phi_0 \approx \frac{\Delta p}{p}\frac{1}{\tan\phi_0} << 0.021^\circ. \tag{5-7}$$

If the RF system of the main linac consists of 200 equivalent RF units and the RF amplitude and phase variations in the RF units have no correlation with one another, the conditions are relaxed by a

$$\frac{\Delta V_0}{V_0} << 1.4\times10^{-3}, \ \Delta\phi_0 << 0.30^\circ . \tag{5-8}$$

factor of the square root of 200 as follows:

At present, it is unclear whether the requirements of the RF system are closer to (7) or (8), because the correlation of the RF amplitude and phase variations is unknown. The characteristics of the RF amplitude and phase variations will be investigated in the cERL to determine the final specifications of the RF unit.

The positional and magnetic tolerances of magnets and positional tolerance of the RF cavities will also be evaluated for the 3-GeV ERL optics. The lattice and optics should be optimized for achieving

large error tolerances, which would relax the requirements for ERL elements, enable the light source to be operated easily and enhance the orbit stability.

REFERENCES

[1] I. Bazarov and C. Sinclair, *Phys. Rev. ST - Accel. and Beams* **8**, 034202 (2005).
[2] T. Miyajima *et al.*, *Proc. PAC09* 521 (2009).
[3] Y. Kobayashi, private communication.
[4] M. Shimada *et al.*, WG2010, *Proc. of ERL11* (2011).
[5] D. Douglas *et al.*, *Phys. Rev. ST – Accel. and Beams* **9**, 064403 (2006).
[6] R. Hajima and R. Nagai, *Proc. ERL07* 133 (2007).
[7] J. Wang and J. Wu, *Phys. Rev. ST – Accel. and Beams* **7**, 034402 (2004).
[8] N. Nakamura, *Proc. ERL09* 85 (2009).
[9] S. Benson *et al.*, *Proc. LINAC06* 115 (2006).
[10] G. Hoffstaetter and M. Liepe, *Nucl. Instr. and Methods A* **557**, 205 (2006).
[11] S. Sakanaka, *Proc. ERL07* 41 (2007).
[12] C. Mayes, *PLT009, ERL11* (2011).
[13] E. Cenni, *Proc. ERL11* (2011).

5.3 Electron Gun

5.3.1 Introduction

The brightness and intensity of a light source depend on the electron-beam emittance, which depends on the beam quality (which is, in turn, related to the size and the spread of the beam) and the beam intensity. Therefore, the electron gun used for producing small-emittance electron beams with a high average current is the most important component of an ERL since the flux and brightness of such light sources depend on the emittance and current of the electron beam. Two photocathode DC electron guns are under development at JAEA and KEK site to meet the requirements (Fig. 5-8, 5-9).

A DC electron gun using a negative electron affinity (NEA) GaAs photoemission cathode can generate a high-current electron beam that has a low initial emittance. The gun development programs aim to achieve an average current of more than 10 mA and a normalized emittance of less than 1 mm·mrad. To suppress the increase in emittance induced by the space charge effect, the gun voltage must be 500 kV or higher. In the electron gun, an acceleration voltage should also be applied within a short gap in order to generate a high-brightness electron beam. In addition, the gun chamber requires an extreme-high vacuum to preserve the NEA surface and hence guarantee a high quantum efficiency of more than several percent, at wavelengths up to 800 nm. Therefore, all of the vacuum components in the gun system should have a low outgassing rate, and the pumps should function under the extreme-high vacuum.

5.3.2 Goals and challenges

The most important issues for designing a GaAs-based high-brightness photoemission DC gun are cathode lifetime and operating voltage.

5.3.2.1 Cathode lifetime

The cathode lifetime in the gun chamber depends on several factors: 1) the adsorption of atoms or molecules of residual gas in the gun chamber, 2) the ion back-bombardment of positive ions produced by the collision between residual gas molecules and electron beams, and 3) the dark current between the cathode and anode or chamber wall which produces additional outgas, ions, and X-rays and increases the damage due to processes 1) and 2). In the ultra-high vacuum (UHV) condition of ~1×10^{-9} Pa, the cathode lifetime in high-current operation is limited by ion back-bombardment which is induced by corrosion between residual gas molecules and electron beams. In order to achieve a long cathode lifetime of more than 100 hours for 10 mA continuous operation, an extreme-high vacuum of ~1×10^{-10} Pa near the cathode is indispensable.

5.3.2.2 Operating voltage

A high operating voltage is important for suppressing emittance growth by the space charge effect. However, the field emission from the cathode electrode and its support structures damages the NEA sur-

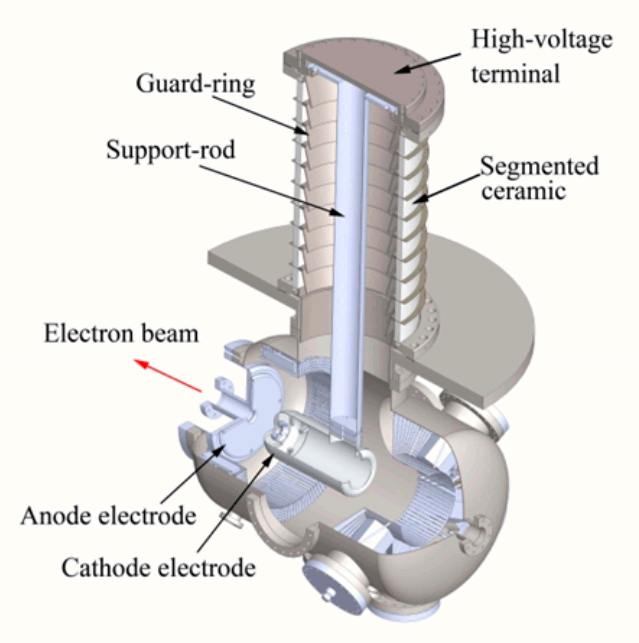

Figure 5-8
Schematic view of the JAEA 500 kV DC gun.

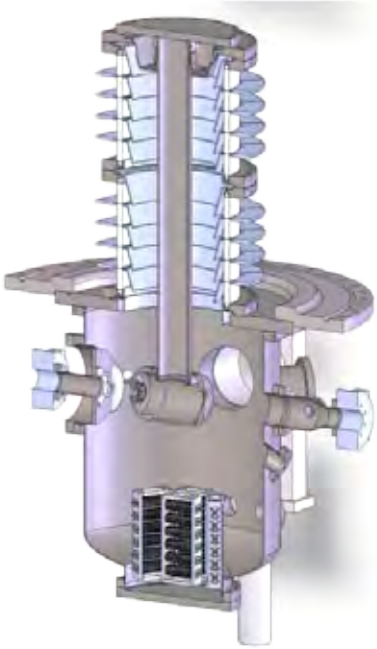

Figure 5-9
Schematic view of the KEK 2nd 500 kV DC gun.

face and causes serious breakdown of the insulators. A high operating voltage of more than 500 kV and low dark current of less than 10 nA are important milestones for stable gun operation.

5.3.3 Current status

A typical experimental cathode lifetime was reported in [1]. Currently, a charge lifetime of around 1000 Coulomb has been obtained with an ultimate pressure of about 1×10^{-9} Pa (equivalent for hydrogen) in recent apparatus. At KEK, an ultra-low total outgassing rate DC-gun system and vacuum pump with a fast pumping speed at extreme-high vacuum are under development [2].

The field emission current from electrodes is predicted by the Fowler-Nordheim equation and field enhancement factor of β. However, the field enhancement factor depends on the electrode gap [3], since the limitation for field strength for large-gap DC high-voltage breakdown in UHV is about ~10 MV/m for conventional electrodes with a gap of several tens of millimeters. The actual DC high-voltage electron sources of Cornell University, TJNAF, Daresbury and JAEA were designed on the basis of this limitation. A maximum applied voltage of over 500 kV was achieved at JAEA by eliminating the electrons that are generated by field emission and that strike the insulator directly using a segmented insulator and guard-ring electrodes [4].

Initial emittance and temporal response for a GaAs cathode were obtained by a 200-kV DC gun system and beam diagnosis system developed jointly by Nagoya and KEK [5]. Currently, the rms normalized emittance of 0.1226±0.0081 mm mrad and 0.101±0.018 mm mrad was obtained from bulk GaAs when excited with 544 nm and 785 nm light for a 1.2 mm diameter uniform laser spot size. These results were almost consistent with those of other experiments [6]. The temporal response of 80.6 ps, which is defined as 90% included of total charge, was obtained by exciting with 785 nm, ~3 ps pulse-width laser light [7].

REFERENCES

[1] J. Grames *et al.*, *Proc. Spin Symposium* (2006).
[2] M. Yamamoto *et al., Proc. IPAC2011* (2011).
[3] F. Furuta *et al., Nucl. Instr. and Meth. A* **538**, 33 (2005).
[4] R. Nagai *et al., Rev. Sci. Instrum.* **81**, 033304 (2010).
[5] T. Miyajima *et al., Proc. IPAC2010* (2010).
[6] I. V. Bazarov *et. al., J. Appl. Phys.* **103**, 054901 (2008).
[7] S. Matsuba *et al., Proc. 8th Annual Meeting of Particle Accelerator Society of Japan* (2011) in press.

5.4 Superconducting Cavity for Injector Linac

5.4.1 Introduction

An injector linac for the proposed 3-GeV ERL light source is required to accelerate CW electron beams of 100 mA from the beam energy of 500 keV to 10 MeV. This requirement is the same as that in an injector linac for the compact ERL (cERL), which is under construction [1–3]. Therefore, demonstration of stable operation in the cERL injector is an important milestone for the 3-GeV ERL injector. In these applications, the critical hardware components are not superconducting cavities but high-power input couplers and higher-order-modes (HOM) dampers. An injector cryomodule, which consists of three 2-cell cavity systems as shown in Fig. 5-10, was chosen for the 3-GeV ERL injector linac as well as the cERL injector linac. Each cavity is driven by two input couplers [4] to reduce the required power handling capacity and also to compensate for coupler kick. A water cooling channel is inserted inside the inner conductor of the input coupler. An HOM coupler scheme [5] was chosen for HOM damping, and five HOM couplers are attached on both beam tubes of each cavity. A slide-jack tuner system [6] with a piezo actuator, which was developed for STF 9-cell cavities, is used for controlling the resonant frequency of a cavity. The 2-cell cavities are dressed with a He vessel made of titanium, and magnetic shields are put inside the He vessel.

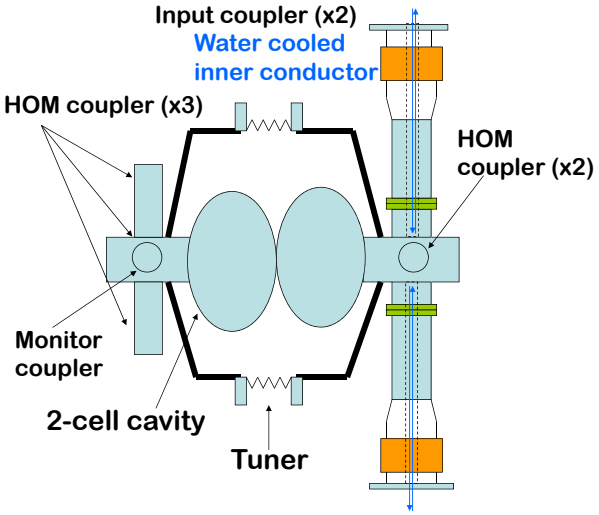

Figure 5-10
Conceptual design of 2-cell SC cavity system for injector Linac.

5.4.2 Goals and challenges

The main parameters of the injector linac for the 3-GeV ERL light source are summarized in Table 5-2. Critical components for beam acceleration of 100 mA in CW operation are high-power input couplers and HOM couplers with a pick-up probe. Reduction of the static heat load from these components and the dynamic heat load due to RF losses is another important issue. Schematic drawings of the 2-cell cavity, input coupler and HOM coupler designed for the cERL injector linac are shown in Fig. 5-11.

The key R&D themes for the injector linac are as follows:

- Stable beam acceleration of CW 100 mA electron beams with low emittance.
- High-power input couplers with a power handling capacity of CW 170 kW.
- HOM couplers and RF feedthroughs suitable for CW 100 mA operation.

Table 5-2 Main parameters of injector Linac for 3 GeV ERL light source.

Frequency	1.3 GHz	Effective cavity length	0.23 m
Total accelerating voltage	10 MV	Ave. accelerating gradient	15 MV/m
Average current	100 mA	Input RF power /coupler	170 kW
Number of cavities	3	R / Q	204
Number of cells /cavity	2	Geometrical factor	288
Number of input couplers /cavity	2	Esp / Eacc	2.25
Number of HOM couplers /cavity	5	Hsp /Eacc	42.2 Oe/MV/m

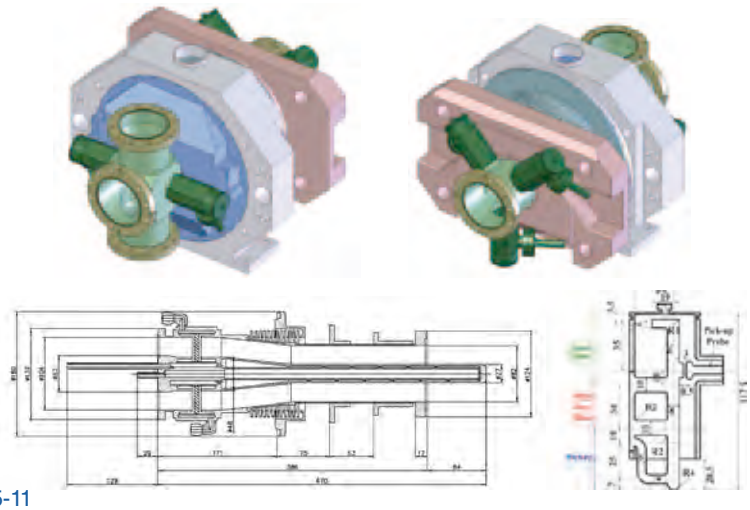

Figure 5-11
Design of 2-cell cavity (top), input coupler (left in bottom) and HOM coupler (right in bottom).

5.4.3 Current status

2-cell cavity

The completed three 2-cell cavities to be installed in the injector cryomodule for the cERL are shown in Fig. 5-12. They have a TESLA-like cell shape and a larger beam pipe aperture of 88 mm. The first vertical test of the 2-cell cavity #3 was carried out recently. The set-up of the vertical test and the results are shown in Fig. 5-13. As a result of improved cooling at feedthroughs of HOM pick-up probes, an accelerating gradient of 25 MV/m under CW operation in the vertical tests (not dipping in liquid He) was successfully maintained without heating at the Nb-antenna tip of the HOM pick-up probe. Vertical tests of the other two 2-cell cavities will be successively carried out in the autumn of 2011.

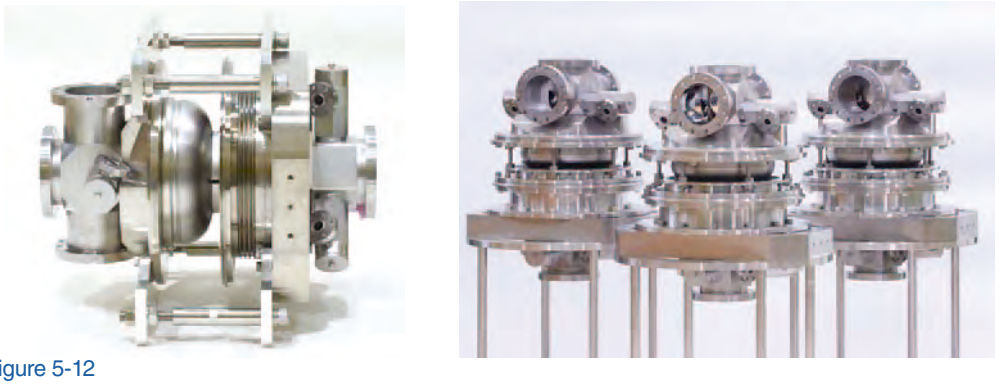

Figure 5-12
Completed 2-cell #3 cavity (left) and three 2-cell cavities (#3, #4 and #5) for cERL injector cryomodule (right).

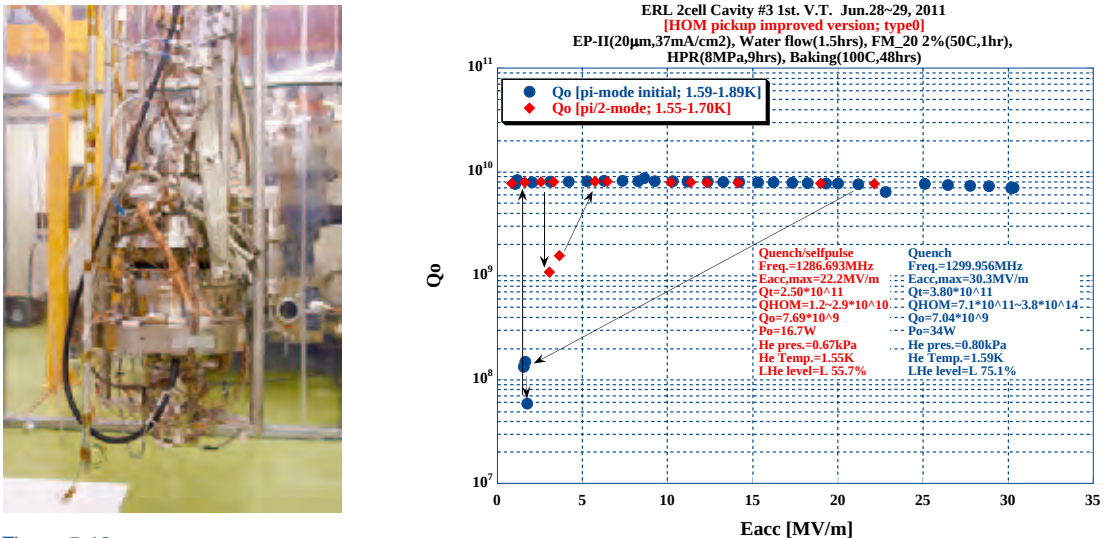

Figure 5-13
Set-up of vertical test of 2-cell cavity (left), and Qo – Eacc plots in the first test of the 2-cell #3 cavity (right).

Input coupler

The completed six input couplers to be installed in the injector cryomodule for the cERL are shown in Fig. 5-14 (left), and they are under preparation for conditioning at a high-power test stand. High-power tests of a pair of the prototype input couplers, as shown in Fig. 5-14 (right), were performed by using a newly developed 300 kW CW klystron. The input couplers were successfully processed up to 100 kW in a pulsed operation with a duty of 10% and 50 kW in CW operation for 30 minutes. The conditioning was limited by excessive heating at the bellows of an inner conductor at a coaxial line located between a coaxial RF window and a doorknob-type transition. Sufficient cooling of the inner conductor needs to be improved to achieve the required input RF power of 170 kW in CW operation.

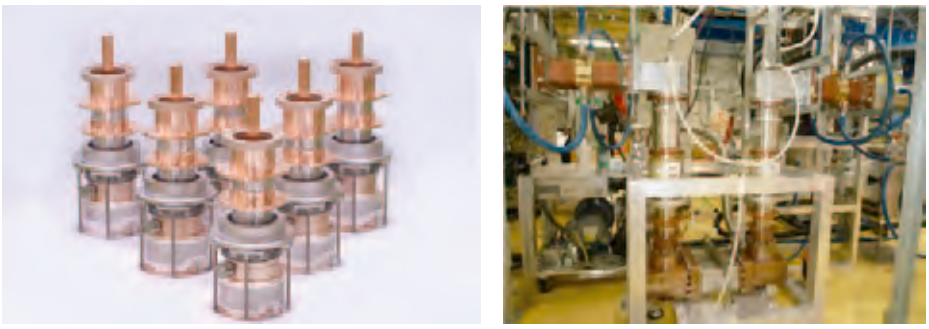

Figure 5-14
Six input couplers for cERL injector cryomodule (left) and high power test stand for RF conditioning of two prototype input couplers (right).

RF feedthrough for HOM pick-up antenna

The limitation on cavity performance in the 2-cell cavities is not thermal quenching at defects on the RF surface in the cells, but the drop in Qo due to heating-up at the Nb-antenna tip of the HOM pick-up probe. New feedthroughs with more efficient cooling were developed, as shown in Fig. 5-15. An Nb-antenna was joined with a center conductor made of Kovar by a screw in the original RF feedthrough (Type 0). In the new Type-I feedthroughs, the Nb-antenna is joined by brazing and the material of the center conductor was changed to Mo to increase the thermal conduction. Furthermore, the material of the outer conductor was changed from Kovar to copper to improve the cooling efficiency by liquid He (Type II). These new RF feedthroughs will also be tested in the vertical tests of the 2-cell cavities.

Figure 5-15
Development of new RF feedthroughs; Type-0 (left), Type-I (center) and Type-II (right).

Injector cryomodule

The designed cERL injector cryomodule is shown in Fig. 5-16. The estimated cryogenic loads in 100 mA and 10 MeV operation are 26 W at 2 K and 55 W at 4.5 K as the sum of the static and dynamic heat loads. It is critical to take the dynamic heat load of the input couplers (4 W at 2 K, 16 W at 4.5 K) and HOM power extraction cables (7 W at 2 K, 4 W at 4.5 K). They are anchored to the 4.5 K He-reservoir panels put on both sides of the cavities, which act as thermal shields as well. Assembly of the cERL injector cryomodule will be started in April 2012, then the first cool-down test of the cryomodule is scheduled for July 2012.

REFERENCES

[1] K. Watanabe, *et al.*, *Proc. SRF'2009* 359 (2009).
[2] S. Noguchi, *et al.*, *Proc. IPAC'10* 2944 (2010).
[3] K. Watanabe, *et al.*, *Proc. LINAC'10* 401 (2010).
[4] E. Kako, *et al.*, *Proc. SRF'2009* 485 (2009).
[5] K. Watanabe, *et al.*, *Proc SRF'2007* 530 (2007).
[6] S. Noguchi, *Proc. SRF'07* WE303 (2007).

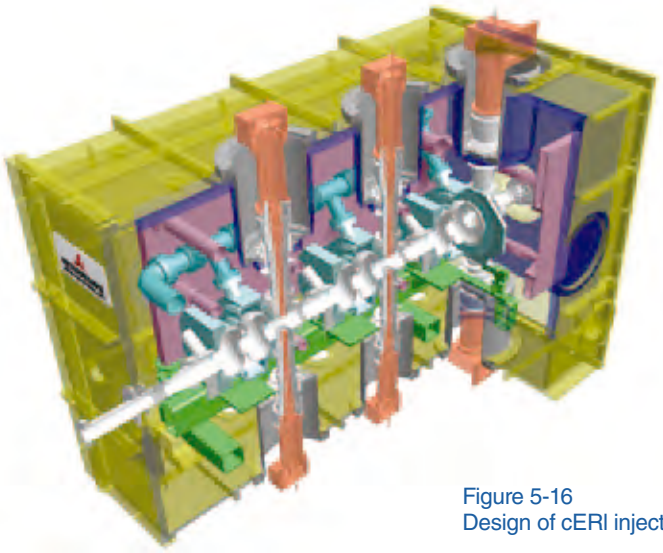

Figure 5-16
Design of cERI injector cryomodule.

5.5 Superconductiong Cavity for Main Linac

5.5.1 Introduction

Application study of superconducting (SC) cavities in a particle accelerator started in the 1960s, aiming to achieve a high gradient continuous wave (CW) linac with excellent power efficiency. In the five decades since then, the use of an SC-RF has steadily expanded in both low β and high β structures. In ERLs, the principle of ERL acceleration using SC cavities was proposed in 1965 for a high-energy particle collider, however, actual application was limited to a small scale due to insufficient understanding of SC linac technology. Thanks to technology development over the last 20 years for the international SC linear collider, the gradient of multi-cell SC cavities has increased to ~35 MV/m, and a large-scale ERL has become a promising next-generation light source.

An ERL of 3 GeV class, in which short electron bunches of 77 pC are accelerated by 1.3 GHz SC cavities, is under discussion at KEK as a future light source. A medium-class gradient of 15 MV/m is reasonable for the main linac to reduce the total cryogenic load and to suppress the RF trips caused by discharging in the cavity. On the other hand, a high-intensity beam of 200 mA including both accelerating and decelerating beams excites the strong higher order modes (HOM) over a wide frequency range in the cavities. Therefore, the HOM impedance of the main linac cavity must be sufficiently damped to avoid beam break-up and emittance growth. Consequently, the cavity shape of the main linac is optimized to satisfy both the limits of gradient and HOM damping.

5.5.2 Goals and challenges

To achieve the final energy of the ERL, the main linac consists of several tens of SC cavity modules in which four or eight 9-cell SC cavities are installed and provide the gradient of 15 MV/m in CW. The challenge of the main linac is to achieve stable CW operation at 15 MV/m without trips under the beam of 200 mA, where various obstacles are expected, such as mechanical vibration, degradation due to field emission electrons, residual gas condensation, quenches, and so on. Each cavity is equipped with a power coupler, HOM absorbers and a frequency tuner. Besides the completed technology of these components, the procedure for mass-producing the SC modules has to be established.

5.5.2.1 Optimization of the cavity shape

The 9-cell cavity has been developed for the international SC linear collider, the so-called TESLA cavity, to achieve the high accelerating gradient [1]. In the case of the ERL, the cavity shape must also satisfy the need for sufficiently low HOM impedance against the heavy beam loading of 200 mA. Our proposal, called ERL Model 2, is shown in Fig. 5-17 [2]. The 9-cell cavity with a wide aperture is equipped with beam pipes with a large diameter at both ends, so the HOMs propagate out from the cavity and are damped by the ferrite absorbers located on the beam pipes. Further, as a new trial, eccentric fluted beam

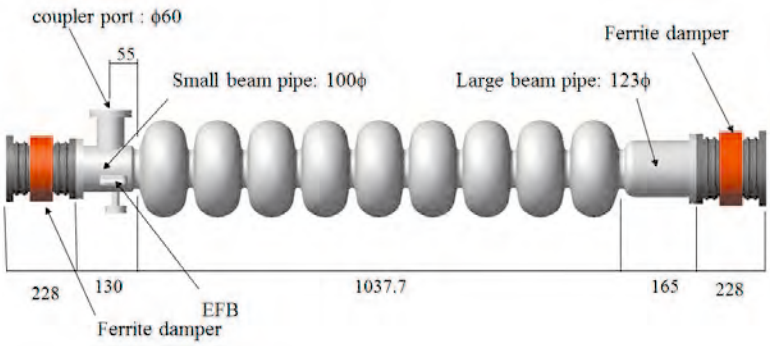

Figure 5-17
ERL main linac cavity, Model-2.

Table 5-3 RF parameters and typical dipole modes of the ERL Model-2 cavity.

Frequency	1300 MHz	Dipole mode	$(R_T/Q)\times Q_{ext}$ (Ωcm^{-2})
R/Q	897 Ω	1835 MHZ	8.90×10^{3}
Rs/Q	289 Ω	1856 MHz	1.24×10^{4}
Cell coupling	3.8%	2428 MHz	1.15×10^{4}
Esp/Eacc	3.0	3002 MHz	9.75×10^{3}
Hsp/Eacc	42.5 Oe/(MV/m)	4001 MHz	3.66×10^{4}

pipe (EFB) is added on the beam pipe to allow the quadrupole HOMs to propagate toward the ferrite. The cell shape was carefully chosen so that the frequencies of longitudinal HOMs do not match the higher harmonic of 1.3 GHz. If this cavity shape is chosen, 200 or more of the 9-cell cavities will be required to achieve the linac energy of 3 GeV. The first step of our challenge is to demonstrate the performance of this cavity design. The RF parameters are summarized in Table 5-3 with the typical HOM modes [3].

5.5.2.2 Power coupler technology

The main linac is supplied the RF power by the decelerated beam. Therefore, the input power of only 200 W is enough to compensate the cavity wall loss and the HOM power. However, the deviation of the accelerating gradient caused by the frequency-detuning due to mechanical vibration may require additional power of 10 kW, which requires optimization of the design of not only the RF characteristic but also the thermal property. Optimization of the coupling strength is another key issue for stable operation.

5.5.2.3 HOM damper

Each cavity has HOM dampers on both sides which absorb the HOM power of 150 W at the maximum beam current. To avoid the heat flow toward the 2 K cavity, the HOM dampers are thermally isolated from the cavity by the bellows with a comb-type RF shielding structure, and are cooled by liquid nitrogen. The material of the absorber for use at 80 K must also be found.

5.5.3 Current status

In preparation for the performance test of the prototype module and for accumulating operation experience, a compact ERL (cERL) of 35 MeV is now under construction. The beam current of 10 mA upon beam commissioning will be upgraded to 100 mA, establishing the fundamental technology. For this purpose, a prototype module including a pair of 9-cell cavities is being fabricated.

Prior to the prototype module, a couple of experimental cavities of the Model 2 shape were built to confirm the characteristics of the cavity shape and also to establish the cavity fabrication process. The results of these tests were acceptable and the gradient of 25 MV/m was achieved as shown in Fig. 5-18 [4]. Performance tests of another couple of cavities are now in progress, and these will be installed on the prototype module. The pair of 9-cell cavities is shown in Fig. 5-19.

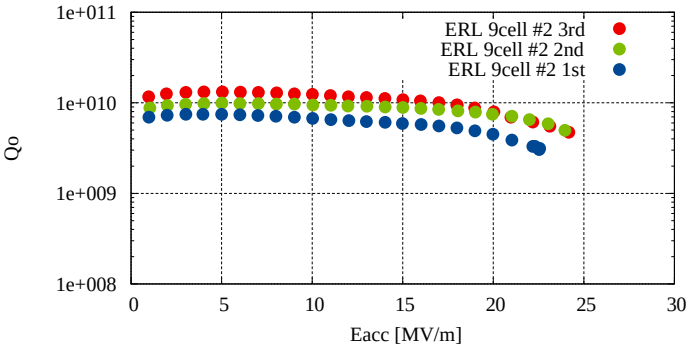

Figure 5-18
Q-E curve of an ERL 9-cell cavity measured in a vertical cryostat.

Figure 5-19
A pair of 9-cell cavities for the prototype module.

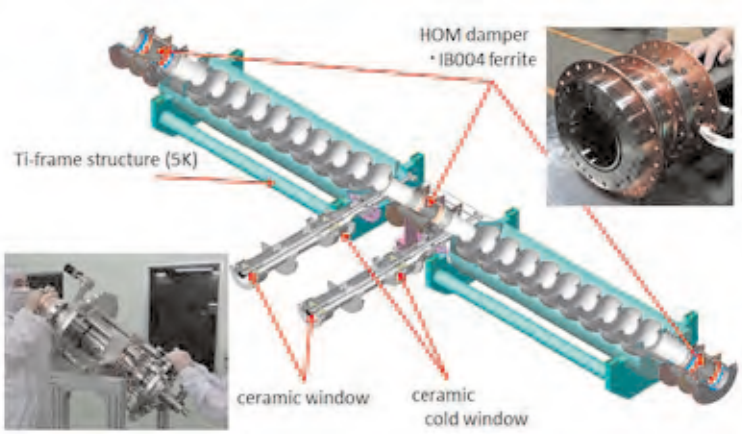

Figure 5-20
Assembly of the prototype module.

Design and prototyping of the input coupler have been completed. RF power to 25 kW was supplied successfully to the test coupler at 80 K [5]. The structure test of a HOM model has finished [6], dampers with IB004 ferrite are being fabricated, and a prototype of the cryo-module is being designed. A couple of 9-cell cavities are connected through the HOM dampers and held in the titanium frame structure of 5 K as shown in Fig. 5-20.

5.5.4 Summary

Basic studies on the main components have finished and performance tests of the experimental models are under way. A prototype module including a couple of cavities for the cERL project is now being designed.

REFERENCES

[1] *TESLA Technical Design Report*, DESSY-2001-000, ECFA-2001-209, TESLA-2001-000, FEL-2001-000, (2001).
[2] K. Umemori *et al., Proc. APAC'07* 570 (2007).
[3] *Design Study of Compact ERL*, KEK Report 2007-7, JAEA-Research 2008-032, (2008).
[4] E. Cenni *et al., Proc. SRF2011* THPO034 (2011).
[5] H. Sakai *et al., Proc. SRF2011* TUPO005 (2011).
[6] M. Sawamura *et al., Proc. SRF2009* THPPO050 (2009).

5.6 RF Sources

5.6.1 HPRF and LLRF

RF sources are classified into high-power RF (HPRF) and low-level RF (LLRF). The former type includes vacuum tubes (such as klystrons and inductive output tubes (IOT)), power supplies (PS), and waveguide distribution systems. The latter type is used to stabilize the cavity gradient, and includes digital feedback systems, RF monitors, and machine protection systems (MPS). An RF system is shown schematically in Fig. 5-21.

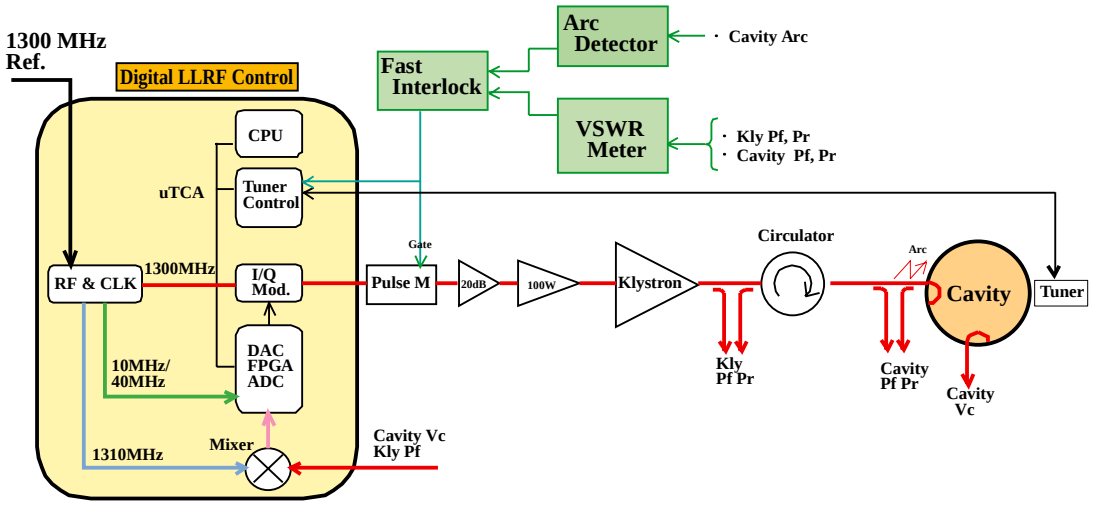

Figure 5-21
Schematic of RF system.

The RF output from the master oscillator (MO) is modulated by an IQ modulator. The modulated signal is then amplified by a klystron and/or an IOT and drives a cavity. The cavity pick-up signal is down-converted by an RF mixer, and the intermediate frequency signal is provided as an input to an ADC on a digital feedback board. The digital signal is then divided into in-phase (I-component) and quadrature-phase (Q-component) signals, and feedback is carried out inside an FPGA (PI-control). The output from the DACs drives the IQ modulator.

5.6.2 RF configuration at the ERL and their specifications

5.6.2.1 HPRF

Two types of high-power RF devices are required for the ERL, namely, a 300-kW device for the ERL injector and a 30-kW device for the ERL main linac. A high-power klystron (300 kW) has been installed for the cERL [1], as shown in the photograph in Fig. 5-22. The PS for the 300-kW klystron is shown in Fig. 5-23. Note that the klystron can be operated at 300 kW, while the other devices can be operated at 30 kW. One of the candidates for 30 kW use is the IOT (Fig. 5-24). The IOT is preferred in view of its

Figure 5-22
Photograph of the 300-kW klystron.

Figure 5-23
Photograph of the 300-kW klystron PS.

Figure 5-24
Photograph of the 30-kW IOT.

running cost because it exhibits high efficiency at different values of output power. Other devices such as klystrons and high-power semiconductors are considered to be suitable alternatives to the IOT in cases where the IOT is not available, as well as for future research and development.

5.6.2.2 LLRF

The stability requirements for the cavity gradient at the ERL are that the amplitude should have an rms of 0.01% and a phase of 0.01º. In order to satisfy these requirements, we adopted a digital feedback system. The main component of the digital feedback system is an FPGA board having four 16-bit ADCs and four 16-bit DACs. Flexible feedback configuration and correction are available owing to digital processing. We have developed a digital LLRF for the J-PARC linac (normal conducting, 324 MHz, 600 μs) [2] and for the STF (superconducting, 1300 MHz, 1.5 ms) [3]. Stabilities obtained at these facilities are ±0.2% and ±0.2Cº at the J-PARC linac (with beam) [2] and 0.007% rms and 0.0018º rms at the STF (without beam) [3]. On the basis of the LLRF system at these facilities, we have developed a prototype FPGA board based on the uTCA for the cERL [4]. Figure 5-25 shows a photograph of the FPGA board. The gradient stability depends not only on the digital system (such as the FPGA board) but also on various perturbations. The perturbations of the cavity gradients are as follows:

1) Phase drift due to the temperature change in the MO cable during one day
2) Phase drift due to the change in the cavity pick-up cable
3) Cavity detuning change due to microphonics (slow vibration of the cavity by pressure change in He)
4) Change in the applied high voltage of the PS
5) Change in the beam loading

Because perturbations 1 and 2 cannot be compensated for by the feedback loop, such drifts should be compensated for in other ways such as by using an energy stabilizer. We can improve the temperature stability of the cable, and we can also, to some extent, compensate for perturbations 3 to 5 by feedback, because these perturbations occur in the upstream of the cavity pick-up, as shown in Fig. 5-26. Afast MPS is composed of an arc detector and an RF power interlock system. The arc detector (Fig. 5-27) is equipped with a photomultiplier developed at the STF, owing to which it exhibits high sensitivity and fast response. The MPS is slightly modified for CW operation at the cERL. A similar configuration of RF monitors and the MPS with the cERL will be adopted at the ERL.

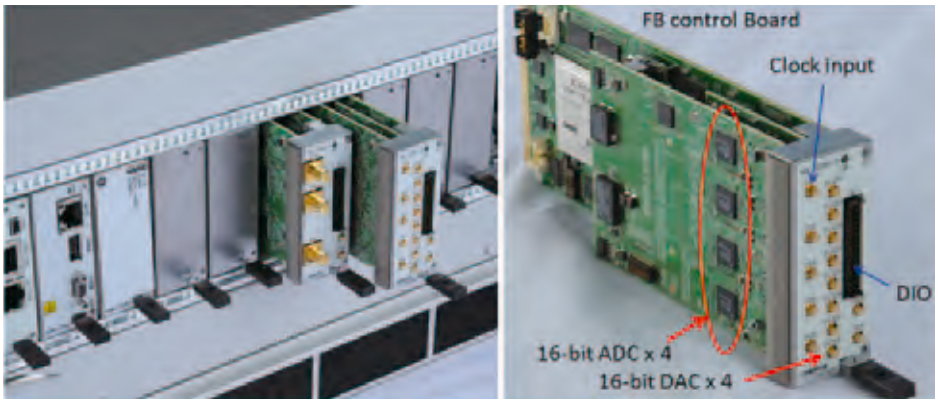

Figure 5-25
Photograph of the FPGA board for cERL.

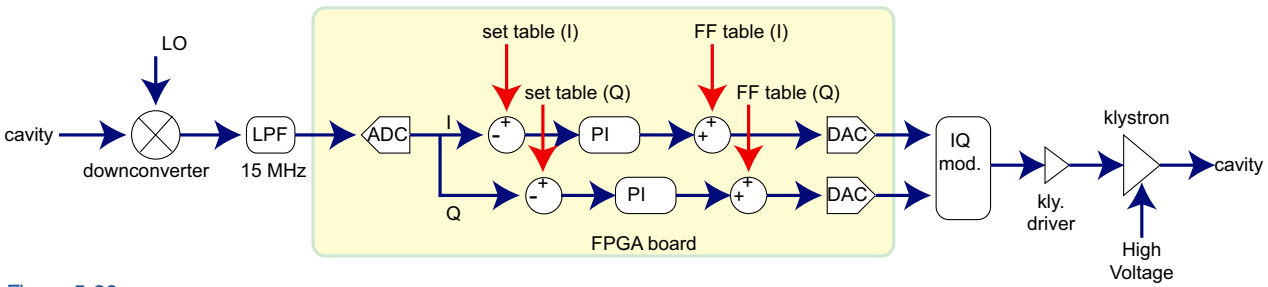

Figure 5-26
Schematic of the feedback loop.

Figure 5-27
Photograph of the arc detector.

5.6.3 Current status and future plan for the RF sources

The main HPRF components for the cERL have been installed, and a similar configuration will be adopted for the ERL. In order to satisfy the requirement of the cavity gradient, the stability of the high voltage in the PS needs to be improved at the ERL. This improvement should be examined through the cERL operation. A high-power circulator has been developed for installation at a waveguide distribution system. This circulator operated well on the cERL test stand.With regard to the LLRF components, further research and development will be necessary to satisfy the stability requirements. The short-term stability (during 1 ms) of the current system should be improved by approximately 1.5 times in phase. A further study on the LLRF components during the cERL operation will help improve the system.However, it is necessary not only to improve the digital feedback system but also to suppress the perturbations noted in 5.6.2.2 in order to satisfy the requirements.

REFERENCES

[1] S.Fukuda *et al*., *Proc. IPAC'10* 3981 (2010).
[2] Z.Fang *et al*., *Proc. IPAC'10* 1434 (2010).
[3] S.Michizono *et al*., *Proc. PAC'09* 2204 (2009).
[4] T. Miura *et al*., *Proc. IPAC'10* 1440 (2010).

5.7 Cryogenics

5.7.1 Introduction

The 3-GeV ERL employs superconducting RF cavities for the injector and the main linacs. The operation temperature of the cavities is 2 K, which is achieved by immersing the cavities in the superfluid helium bath at 2 K. The cryogenic system for the 3-GeV ERL should be designed and constructed to produce 2 K superfluid helium continuously and to supply it to the superconducting RF cavity cryomodules.

The cryogenic system consists of four major subsystems as shown in Fig. 5-28: 1) a helium liquefier/refrigerator, 2) 2 K helium refrigerator cold boxes and a helium gas pumping system (not shown in the figure), 3) cryomodules, which accommodate superconducting RF cavities in them, and 4) high-performance transfer lines, which connect the helium liquefier/refrigerator and the 2 K refrigerator cold boxes for the superconducting RF cavity cryomodules. The cross section of the multi-channel transfer line is shown in Fig. 5-29. The transfer lines are designed to minimize the heat load from the room-temperature environment, and are constructed with materials whose thermal conductivity is low. These high-performance transfer lines reduce the static heat load to the cryogenic system.

Superfluid helium, which is often expressed as He II, is the second liquid phase of helium as shown in Fig. 5-30; normal liquid helium is expressed as He I. Superfluid helium exists at temperatures below 2.17 K at saturation pressure. A simple way to produce superfluid helium is to evacuate normal liquid helium by a vacuum pump (i.e. forced boiling). The thermodynamic state of liquid helium varies along the saturation line and enters the He II domain (the blue curve in Fig. 5-30).

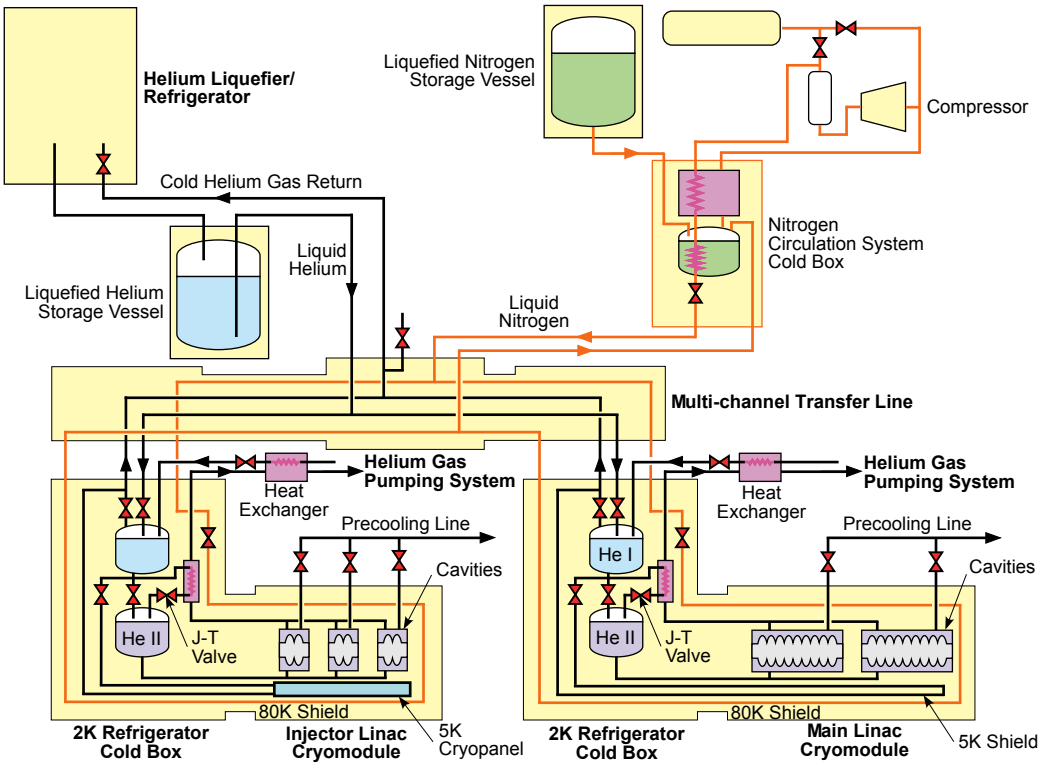

Figure 5-28
Schematic diagram of 2K cryogenic system for ERL.

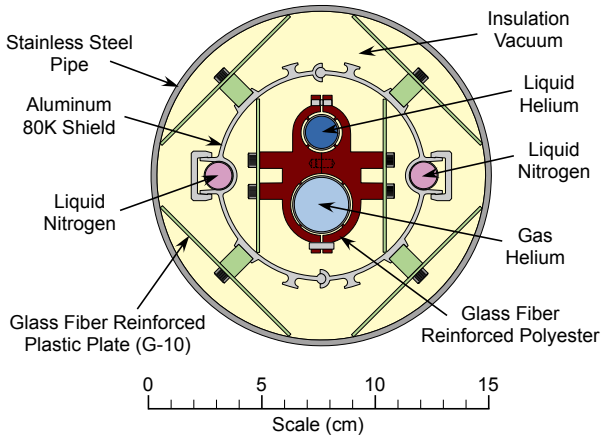

Figure 5-29
Cross section of high-performance multi-channel transfer line (multi-layer insulation not shown).

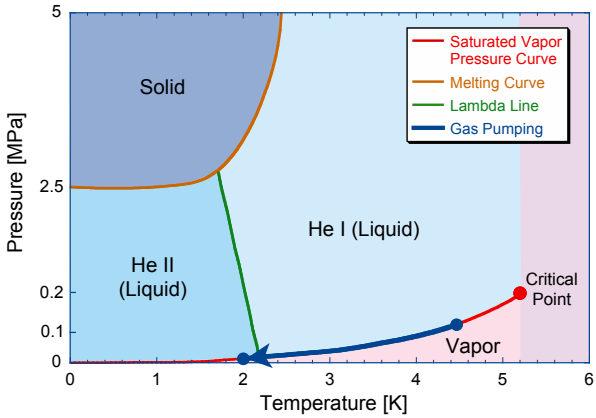

Figure 5-30
Phase diagram of helium.

Normal liquid helium is produced by a helium liquefier/refrigerator and the produced liquid helium is once stored in a liquefied helium storage vessel. Then liquid helium is distributed into He I pots of the 2 K refrigerator cold boxes for the superconducting RF cavity cryomodules through the high-performance transfer lines. Some fraction of liquid helium is sent to liquid-helium-temperature thermal shields, such as the 5 K cryopanel in the injector linac cryomodule and 5 K thermal shields in the main linac cryomodules. During the precooling step of the cavities, liquid helium in the He I pots is transferred directly into the cryomodules through the He II pots of the 2 K refrigerator cold boxes. After filling up the helium vessels surrounding the cavities in the cryomodules with normal liquid helium, the helium gas pumping system is gradually activated and helium pressure in the helium vessels decreases to the He II domain pressure. The exhausted cold helium gas from the cryomodules is used to cool down normal liquid helium from the He I pots through heat exchangers, and the cooled normal liquid helium is converted continuously to superfluid helium through Joule-Thomson (J-T) valves, as shown in Fig. 5-28.

Heat loads to the cryogenic system can be divided into two sources: one is the static heat load from all of the low-temperature devices including the cryogenic system itself, and the other is the dynamic heat load, which comes mainly from the superconducting RF cavities. The cryogenic system for the ERL

should be designed to remove all the heat loads from these two sources. The dynamic heat load from a superconducting RF cavity, P_{cav}, can be estimated theoretically as follows:

$$P_{cav}=\frac{V_a^2}{\left(\frac{R}{Q}\right)\cdot Q_0} \tag{5-9}$$

Equation (5-9) shows that the dynamic heat load is proportional to the square of the acceleration voltage of the superconducting RF cavity, V_a, and inversely proportional to the unloaded quality factor, Q_0, of the cavity and to R/Q, which is a unique factor of the cavity. The higher the acceleration voltage and the lower the quality factor, the larger the cooling power required.

5.7.2 Current status

A similar cryogenic system, which has a cooling power of 30 W at 2 K, has already been constructed and operated with a helium liquefier/refrigerator which has a cooling power of 600 W at 4.4 K (this is the saturation temperature of liquid helium under the operation pressure of the cryogenic system) or a liquefaction rate of 250 L/hour. Since superfluid helium at 2 K is produced by pumping down liquid helium at 4.4 K, the exhausted helium gas from the pumping system is contaminated with oil from the pumping system. The pressure of the helium gas pumping system is about 3.2 kPa at 2 K, and so there is some possibility that air may be sucked into the pumping line, because the pressure in the pumping line is lower than atmospheric pressure. This means that exhausted helium gas from the pumping system cannot be transferred directly to the suction of the helium compressor. Hence, it is crucial to purify the exhausted helium gas from the pumping system before returning it to the helium liquefaction cycle. The purification rate of the cryogenic system is not sufficiently large to purify all the exhausted helium gas from the pumping system while the helium liquefier/refrigerator is operating continuously; this is one of the major technical issues for long-term operation of the cryogenic system.

In the existing cryogenic system, the helium gas pumping system consists of several oil rotary vacuum pumps and mechanical booster pumps because of the very low saturation pressure of superfluid helium. As the heat load from the superconducting RF cavities to the cryogenic system increases, so do the mass flow rate of helium gas and required pumping capacity. This increases the number of vacuum pumps and the inefficiency of the cryogenic system.

5.7.3 Goals and challenges

The 3-GeV ERL requires 200 superconducting RF cavities for the main linac, if all of the cavities can generate an acceleration voltage of 15 MV. A report on the cryogenic system for the ERL project [1] shows that if one cryomodule for the main linac accommodates four superconducting RF cavities, the total heat load from the one main linac cryomodule to the cryogenic system is estimated at 500 W at 4.5 K. This means that the cryogenic system for the 3-GeV ERL should absorb about 25 kW heat load at 4.5 K. The heat load from the cryogenic system itself, such as transfer lines and 2 K refrigerator cold boxes, is estimated at about 2 kW, and that from one cryomodule for the injector linac, which accommodates three RF cavities, is estimated at only 250 W, if the total acceleration voltage of the three cavities is 10 MV. Including a margin for the cooling power for stable operation of the cryogenic system (about 50%), the required cooling power of the cryogenic system for the 3-GeV ERL is estimated at 41 kW in total.

This specification is almost twice as large as that of one of the eight cryogenic units in the LHC cryogenic system at CERN [2, 3]. To increase the total efficiency of the cryogenic system for the 3-GeV ERL, comprehensive consideration is needed to design the cryogenic system properly. One option is to introduce cold compressors instead of the helium gas pumping system at room temperature. These cold compressors compress low-pressure helium gas at low temperature, and occupy much less space in the cryogenic system compared with the helium gas pumping system. The introduction of cold compressors would make a large contribution toward increasing the efficiency of the cryogenic system. The second option in the case of long-term operation of the ERL is to use a nitrogen circulation system to reduce the consumption of liquid nitrogen. A schematic diagram of the nitrogen circulation system is illustrated in Fig. 5-28. This system reuses the enthalpy (in other words, “coldness”) of the cold nitrogen gas just after evaporation in the 80 K thermal shields and the remaining liquid nitrogen which does not evaporate in the shields.

In addition to these major options, there is still some room for improving the total efficiency of the cryogenic system. The design and materials of the heat exchangers in the 2 K refrigerator cold boxes should be considered to improve their heat exchange rate. The valves located at low temperature should also be researched to improve their reliability even at low temperature. If we employ additional heat exchangers in the helium gas pumping line, as shown in Fig. 5-28, the enthalpy of cold helium gas evaporated from 2 K superfluid helium can still be used to liquefy some amount helium gas and then to increase the cooling power of the cryogenic system, even after the cold helium gas cools normal liquid helium before entering the Joule-Thomson valves.

The cryogenic system for the 3-GeV ERL should be designed and constructed carefully with consideration of these options for improving the cryogenic system and reducing the cost of construction.

REFERENCES

[1] H. Nakai, private report on the cryogenic system for the 3.5GeV-ERL (2011).
[2] S. Claudet, *Proc. 2005 Particle Accel. Conf.*, Knoxville, 9 (2005), for example.
[3] N. Saji *et al.*, *TEION KOGAKU* **40**, 372 (2005).

5.8 Magnets for 3-GeV ERL

Since the beam energy of the 3-GeV ERL is almost the same as that of the Photon Factory storage ring, magnets having similar parameters are required. The parameters of typical magnets for the PF ring and 3-GeV ERL are shown in Table 5-4. The magnetic gap and bore diameter are assumed to be 60 mm which is the same as that of the compact ERL.

Table 5-4 Typical parameters of the magnets.

(a) Typical bending magnet

		PF	ERL
Number		28	120
Bending angle	degree	12.9	3.0
Curvature radius	m	8.7	20.0
Core length	m	1.94	1.05
Half Gapm	m	35	30
Magnetic field	T	1.15	0.50
Total Current	A Turns	32161.8	11936.6
Coil turn number	turns/pole	24	25
Maximum current	A	1340.1	477.5

(b) Typical quadrupole magnettt

		PF	ERL
K value	m^{-1}	0.9	2
Core length	m	0.4	0.8
Bore radius	mm	35	30
Maximum field gradient	T/m^2	22.5	25.0
Total current	A Turns	10966.8	8952.5
Coil turn number	turns/pole	23	20
Maximum current	A	476.8	447.6

(c) Typical sextupole magnet

		PF	ERL
K value	m^{-2}	12.6	40
Core length	m	0.2	0.3
Bore radius	mm	45	30
Maximum field gradient	T/m^2	315.00	666.67
Total current	A turns	7614.07	4774.65
Coil turn number	turns/pole	17	20
Maximum current	A	447.89	238.73

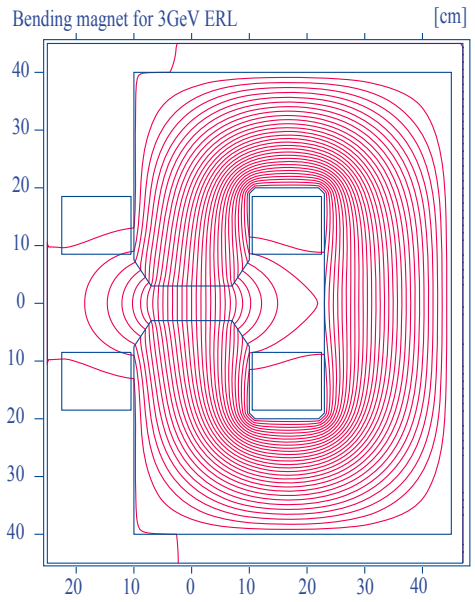

Figure 5-31
Model bending magnet and magnetic lines of force.

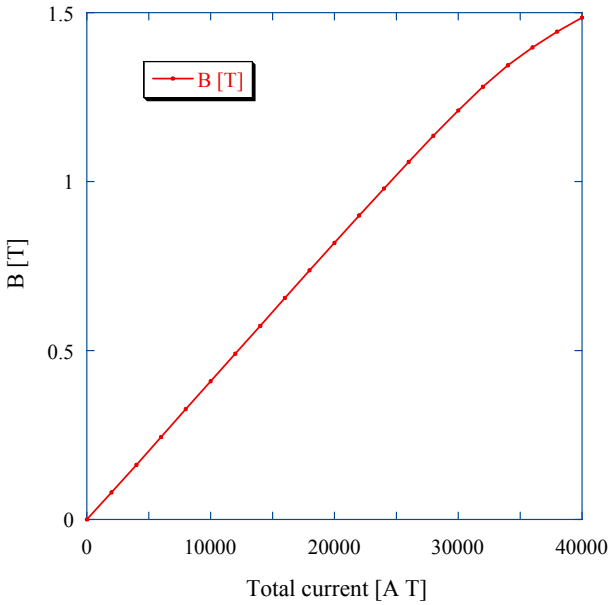

Figure 5-32
Excitation curve for model bending magnet.

For the bending magnet of 3-GeV ERL, the maximum magnetic field is about 0.5 T, which is about half the strength of that of the PF ring. The saturation effect of the magnetic field is very small and the magnet can have a wide good field region. The model bending magnet and the magnetic lines of force are shown in Fig. 5-31 and the excitation curve in Fig. 5-32.

The optical functions of the higher energy (3GeV) beam at the end of the main linac section may increase to a very large value in order to optimize the optics for smaller energy (10MeV) beams. In order to join the optical functions of the linac section smoothly to the recirculation path, strong quadrupoles are essential. Stronger quadrupoles are also required for the recirculation path where the bunch length is kept short by the isochronous optics or is compressed to a shorter one by changing the momentum dependent trajectory length (R_{56}). The quadrupole magnets have more than twice the integrated magnetic field gradient compared with those of the PF ring. In order to avoid strong saturation, we keep the magnetic field gradient smaller than about 25 T/m. Because of the saturation effect, magnets having twice the core length are required for the 3-GeV ERL to achieve twice the focusing strength compared with in the PF ring quadrupole. The model quadrupole magnet and the magnetic lines of force are shown in Fig. 5-33 and the excitation curve in Fig. 5-34.

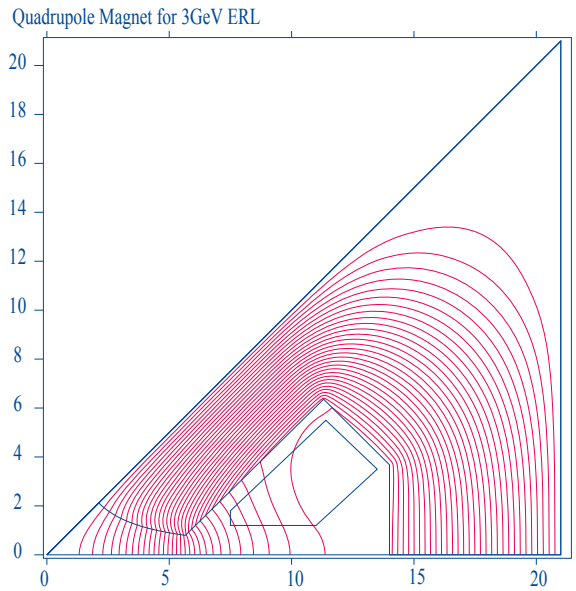

Figure 5-33
Model quadrupole magnet and magnetic lines of force.

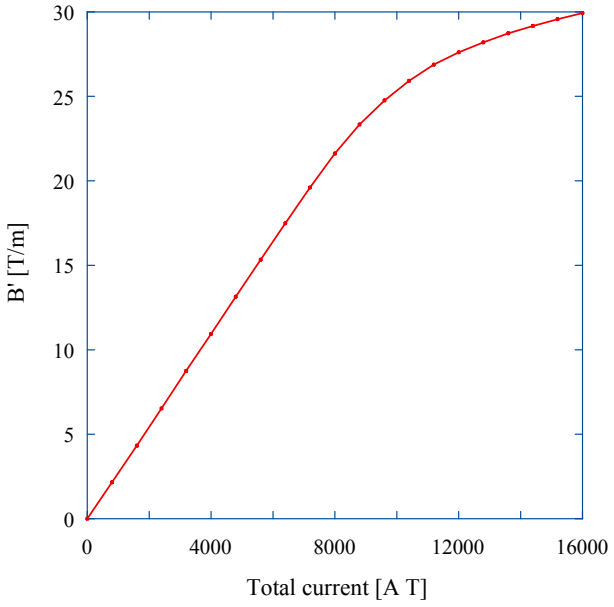

Figure 5-34
Excitation curve for model quadrupole magnet.

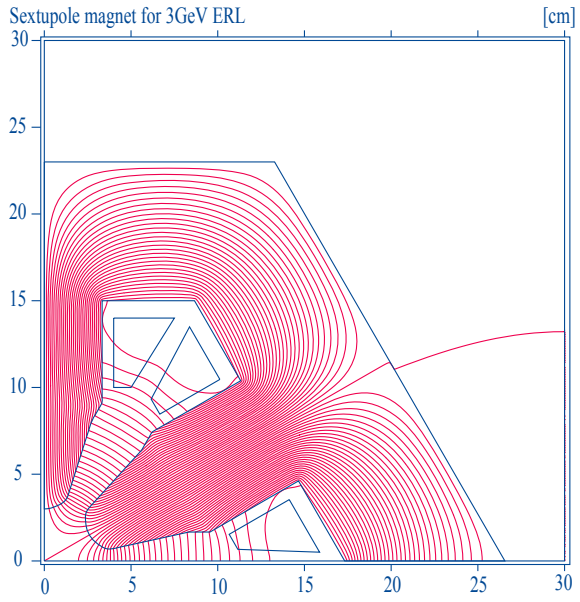

Figure 5-35
Model sextupole magnet and magnetic lines of force.

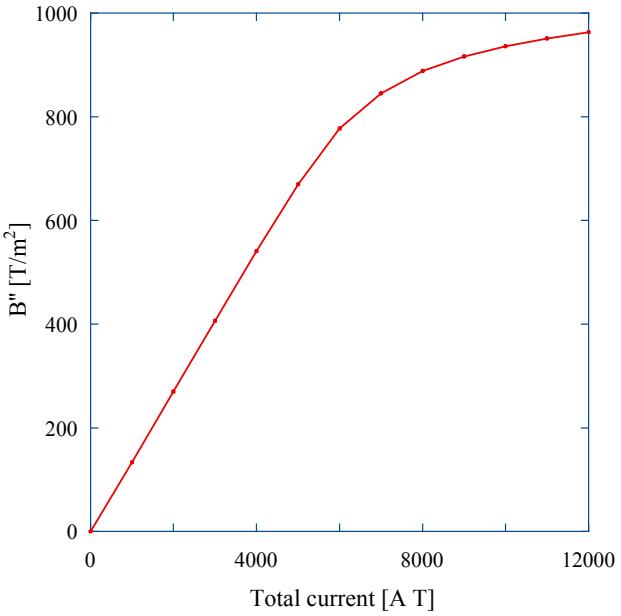

Figure 5-36
Excitation curve for model sextupole magnet.

While the PF ring has sextupole magnets for chromaticity correction to maintain a large dynamic momentum aperture, the ERL needs sextupoles to maintain the bunch length or the bunch compression at the recirculation path. Compared with the chromatic sextupoles of the storage ring, stronger second order field gradients are required to correct higher order momentum and amplitude dependent trajectory length differences (T_{566}, T_{166}, T_{366}) at the recirculation path. In order to avoid strong saturation, we keep the second-order magnetic field gradient smaller than about 800 T/m^2. The model sextupole magnet and the magnetic lines of force are shown in Fig. 5-35 and the excitation curve in Fig. 5-36.

5.9. Vacuum

5.9.1 Introduction

The beam current of the 3-GeV ERL is planned to be 100 mA. The heat load of synchrotron radiation (SR) loss is comparable with the storage ring of the latest third-generation light source, and so absorption of the heat load is a principal issue of the vacuum design. The bunch length is as short as 2 ps for the high-flux mode and a very short bunch length of 0.1 ps is estimated for the ultra-short-pulse mode. The handling of CSR power must be considered when designing the SR absorbers, and suppression of the higher-order mode loss in various vacuum components is also an important issue. The RF contacts in the bellows and gate valves will require sufficient shielding.

Ultra-high vacuum is necessary to suppress the ion-trapping instability and to minimize the beam loss due to residual gas scattering. Another important role of the ERL vacuum system is to protect the superconducting cavities and the electron gun from any contamination.

5.9.2 Goals and challenges

The radiation loss per turn for a single electron is calculated as,

$$U_0\,[\mathrm{keV}] = P_{SR} \times \Delta T = 88.5 \times \frac{E^4\,[\mathrm{GeV}]}{\rho\,[\mathrm{m}]} \qquad (5\text{-}10)$$

where P_{SR} is the incoherent SR power of a single electron, ΔT is the passage time in the B magnets, and P is the bending radius. For E = 3GeV and , $P = 19.1\mathrm{m}$, U_0 equals 375 keV. The total SR loss for a beam current of 100 mA amounts to 37.5 kW. The return loop of the 3-GeV ERL will have 90 B magnets, with an average SR loss at each B magnet of 417 W. The SR power increases by the generation of CSR

when the bunch length becomes sufficiently short. The SR power of a -electron bunch including CSR is given by[1]:

$$P_{all} = N_b P_{SR} + N_b(N_b - 1)P_{SR}T(\frac{3\sigma_z\gamma^3}{2\rho\beta}) \quad (5\text{-}11)$$

where σ_Z is the bunch length, and

$$T(a) = \frac{9}{32\sqrt{\pi}a^3}\exp(\frac{1}{8a^2})K_{5/6}(\frac{1}{8a^2}) - \frac{9}{16a^2} \quad (5\text{-}12)$$

The first term N_bP_{SR} is the contribution from the incoherent SR. The total SR power will be enhanced by the factor $f = (1+N_b\text{-}1)T(a))$. For a bunch length of σ = 2ps (σ_Z =0.6mm) and 0.1 ps (0.03 mm), the enhancement factor f equals 1.21 and 12.6, respectively. The average CSR power at each B magnet amounts to 87.6 W for σ = 2ps . The shortest bunch length of 0.1 ps will be achieved in the ultra-short-bunch mode and the beam current will be limited to less than 0.1 mA. As the beam current is low in this mode, the average CSR power at each bending magnet is estimated to be less than 1 W.

Though the incoherent SR power is concentrated within a narrow angle of $1/\gamma$ ~ 0.17 mrad, the CSR power disperses to an angle of ($3\sigma_z/2\pi\rho$) ~25 mrad for σ = 2ps. The shielding of CSR by parallel plates is effective when the gap is smaller than $h = 2(3\sigma_z^4\rho^2)^{1/6}$ ~46 mm. The magnetic gap of the B magnet is planned to be 60 mm, so the height of the beam duct is comparable in dimension with the shielding height. Perfect shielding cannot be expected at this dimension, so the adsorption of CSR power will be an important point to be considered. The radiation angle of the CSR is so wide that the heat load is inevitably distributed to all the inner walls of the beam duct, so the material of the beam duct should have good heat conductivity; OFHC copper is thought to be a suitable candidate. We are also studying a copper alloy which has high heat tolerance. When the non-evaporable getter (NEG) coating is applied in the distributed pumping system, high heat tolerance is favorable for the efficient activation of the NEG coating.

5.9.3 Current status

Construction of the compact ERL is presently under way. The beam energy of the compact ERL is limited to 30–60 MeV at the first stage, so the incoherent SR power is negligible and no SR absorber is prepared for the compact ERL. But when the beam current of 10 mA or more is successfully achieved with a short bunch length of 1 ps, the impedance issue related to the HOM loss can be inspected using the real beam. We will install many RF shielded bellows and gate valves equipped with RF contacts. We have designed a new low-impedance flange (Fig. 5-37) which has no gaps at the joint of the beam duct. These vacuum components developed at the compact ERL can be used for the 3-GeV ERL.

Figure 5-37
Development of low-impedance flange for the compact ERL. The circular beam duct is combined with no gap. Either a copper O-ring or metal O-ring can be used as the gasket.

5.10 Beam Diagnostics

5.10.1. Introduction

State-of-the-art diagnostics and instrumentation are required for the smooth commissioning and operation of the 3-GeV ERL. Standard beam diagnostics tools such as beam size, position and beam charge measurement are essential during the stages of commissioning and stable energy recovery. In order to deliver high-quality photon beams for users, an even more important topic is to diagnose the detailed distribution of electron beams in six dimensions, because the distribution of electrons in the bunch does not reach equilibrium like that of the storage ring.

5.10.2. Goals and challenges

Transverse profile

Measurement of the horizontal and vertical beam distribution is fundamental to determine the transverse phase space of the bunch. At low beam current, beam size can be measured with screen monitors with YAG crystals or metal foils to produce optical transition radiation (OTR). However, these techniques are not suitable under continuous, high-current CW operation. When the bunch length becomes short, coherent OTR will overlap the normal OTR image, and the precise beam size cannot be measured [1]. For measuring the small beam size in the high energy part of the ERL, synchrotron radiation with the interferometric method [2] can be used.

Longitudinal profile

The longitudinal beam profile at the circulation part can be measured with a streak camera with the resolution of sub-ps range. For shorter bunch length measurement, several kinds of electro-optic method have been proposed and demonstrated in many laboratories [3, 4].

Beam position

The typical beam size at the circulating part of the ERL ranges from several mm to 10 mm. It is suggested that the resolution required for beam position monitoring is at least 1/10 of the beam size with the bandwidth of the SR users' measurement time. In a recent storage ring experiment, the frequency range varied widely from 1 mHz to the MHz region. The orbit must also be stabilized with the same order of magnitude.

One of the specific issues for the ERL is to have the accelerated and decelerated beams in the same vacuum chamber at the SRF cavity section of the linac. Therefore, the beam rep-rate is doubled to 2.6 GHz. Only the average beam position can be measured with the conventional detection circuit, so we are planning to utilize fast gate switching to select two beams in the time domain, which was originally developed for the Super KEKB [5]. Further development is required because the present switching speed of 3 ns is not fast enough for the ERL.

Beam Loss

Beam loss detection is a crucial system to protect the accelerator components from damage due to unwanted electron beam motion. Experience at the Jefferson Laboratory [6] is beneficial for designing the loss monitor and interlock system.

5.10.3. Current status

In the high-coherence or high-flux mode operation of the ERL, a standard beam diagnostics system such as RF beam position monitoring (BPMs), SR monitoring, beam current monitoring, or instability monitoring can be achieved using similar techniques developed in recent third-generation light sources because the average current above the range of several mA is not difficult to handle with modern analog and digital circuitry. At the same time, the detection circuit is required to be used under the pulsed beam, because the average beam current must be decreased to minimize the beam loss when the OTR or YAG screen monitor is inserted into the beam orbit. The heterodyne down-converter type of circuit was tested and showed sufficient single-shot resolution with the macro-pulse width of 1 ms. On the other hand, commercial off-the-shelf solutions are available, such as Libera Brightness from I-tech Corporation. It will be possible to evaluate many kinds of detection circuits at the compact ERL.

To achieve a very good time response of the BPM, we have developed a glass-type feedthrough with smaller relative permittivity than normal alumina-ceramic types [7].

For the machine protection system, PMT will be used for fast interlock, and a high-sensitivity PIN-diode type loss monitor will be used to detect small beam losses. Furthermore, beam loss monitoring based on optical fiber is now being tested at KEK-Linac and PF; it can cover a wide area along the beam pipe, and is cost effective.

It is also important to measure and manage beam halo in the ERL. A wide dynamic range greater than 10^6 is required for the proposed 3-GeV ERL machine; one promising solution is the coronagraph developed by KEK [2].

A deflecting cavity to measure longitudinal distribution has been developed and tested in the injector development area at PF-AR [8]. Further experience will be gained and development conducted at the compact ERL facility.

REFERENCES

[1] H. Loos, *et.al., Proc. FEL08* 485 (2008).
[2] T. Mitsuhashi, *Proc. DIPAC05* 7 (2005).
[3] B. Steffen, *et.al., PRST AB* **12**, 032802 (2009).
[4] A. Cavalieri *et al., Phys. Rev. Lett.* **94**,144801 (2005).
[5] M. Tobiyama, to be published in *Proc. ERL11*.
[6] K. Jordan, to be publishd in *Proc. ERL11.*
[7] K. Furukawa, *et.al., Proc. ERL07* 50 (2007).
[8] Y. Honda, S. Matsuba, *et.al.* to be published in *Proc. ERL11.*

5.11 Insertion Devices

5.11.1 Introduction

The electron beam of the 3-GeV energy recovery linac (ERL) has very low emittance of $\varepsilon_{x,y}$ = 17 pm-rad and average current of 100 mA with high repetition rate of 1.3 GHz. By using an undulator for the light source of the 3-GeV ERL, the interference property is effectively used to produce a photon beam with high brilliance. The synchrotron radiation (SR) light from the undulator using this electron beam has a transverse coherence of the diffraction limit in the photon energy region from VUV and the soft X-ray region. The undulator also provides a more brilliant light in the X-ray region. We use the undulator as the main insertion device for the SR source throughout the photon energy region. The insertion devices are designed with many straight sections in the 3-GeV ERL: more than 20 straight 5-m sections, and four 20-m straight sections. For future development of the light source, one 200-m long straight section is reserved. In this report, we describe the prospects for the insertion devices for the VUV-SX region and for the X-ray region, respectively.

5.11.2 Goals and challenges

5.11.2.1 Insertion device for the VUV-SX region

The 3-GeV ERL is the optimum light source in the VUV-SX photon energy region for experiments with diffraction limited SR. As a VUV-SX light source, the required photon energy region is very wide, from less than 100 eV to 2 keV. In addition, there are strong requests to use the SR with various polarization states. To satisfy these experimental demands, the undulator should have multifunctional capabilities.

Another issue when designing the undulator in the VUV-SX region is the total radiation power and density, which cause the serious problem of heat load on the optical elements in the beam line. To cover the wide range of photon energy in the VUV-SX region by a single undulator with long length, the maximum magnetic field of the undulator should be strong, which increases the radiation power. Especially in the case of the usual planar undulator, it is important to investigate the heat load because the radiation power concentrates on the beam axis. Countermeasures for radiation power are a key issue when designing the undulator in the VUV-SX region. It will be effective to adopt an elliptical undulator and a multi-undulator.

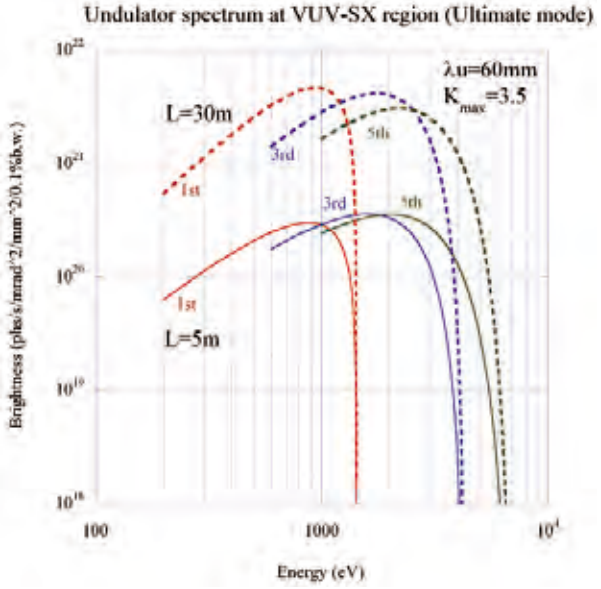

Figure 5-38
The undulator spectrum for the VUV-SX source.

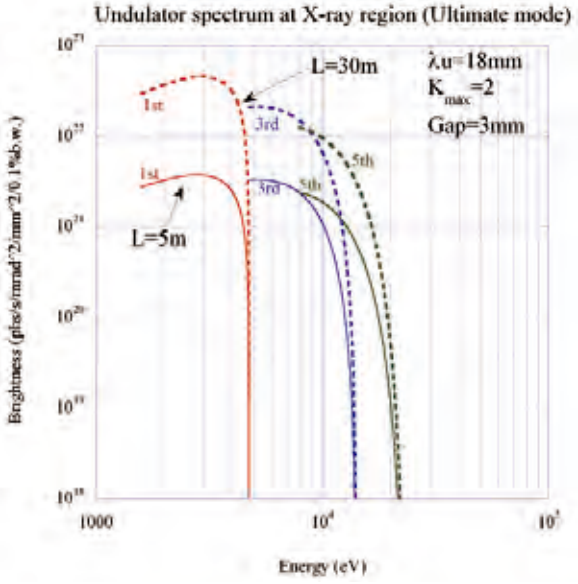

Figure 5-39
The SGU spectrum for the X-ray source.

5.11.2.2 Insertion device for the X-ray region

As the light source for the X-ray region, a short gap undulator (SGU) with period length of less than 20 mm is essential at the 3-GeV ERL. The undulator radiation with photon energy of around 10 keV is covered by using the higher harmonics of the SGU. In the Photon Factory storage ring (PF ring), three 0.5-m long SGUs with a minimum gap of 4 mm are already working well as the X-ray light source for user experiments. To utilize the longer straight section of the 3-GeV ERL, the first step of the light source project is to develop an SGU with a length of 5 m. To develop an SGU with a shorter period length, the next step is to investigate increasing the maximum magnetic field of the SGU and shortening the minimum gap. However, a shorter gap of the SGU may cause a strong resistive wall effect because the electron bunch length of the ERL is very short: σ = 2 ps. As the resistive wall effect causes instability of the electron beam and heating of SGU magnets, the design of the SGU in the ERL requires a detailed analysis of the resistive wall effect.

5.11.2.3 Calculated spectrum of undulator radiation in the 3-GeV ERL

Figures 5-38 and 5-39 show samples of the calculated spectrum using the undulators described above at the 3-GeV ERL. Figure 5-38 shows the undulator spectrum for the VUV-SX source. The period length of the undulators is 60 mm and the maximum K value is 3.5. Figure 5-39 shows the SGU spectrum for the X-ray source with period length of 18 mm. In this calculation, the minimum gap is assumed to be 3 mm and the maximum K value is 2. For a 30-m SGU, the brightness of the SR would exceed 10^{22}.

5.11.3 Current status

In the PF ring, various undulators have been developed for the VUV-SX light source, i.e., ID#02 is a planar undulator, ID#19 is a multi-undulator, ID#28 is a circular polarizing undulator, and ID#16-1 & 2 are the polarization switching source. Especially, ID#16-1 & 2 have many operation modes of various polarization states. The available polarization modes are circular polarization (B_x/B_y = 1), elliptical polarization (B_x/B_y = 1/2), and linear polarization along the horizontal and vertical directions. An undulator with multifunctional capabilities like ID#16-1 & 2 is an important light source of the VUV-SX region in the 3-GeV ERL.

As the undulator for the X-ray light source, three SGUs have been developed in the PF ring [1, 2] (Table 5-5). These SGUs in the PF ring (PF-SGUs) were constructed after the straight sections of the PF ring had been upgraded. Figure 5-40 shows photographs of the SGU#03 and the inside of the magnetic array. We have summarized the magnetic specifications for the PF-SGUs. The SGU is expected to be a suitable X-ray light source of the 3-GeV ERL.

Table 5-5 Parameters of three SGUs.

Magnetic specification for SGUs.							
SGU	**Material**	B_r	iH_c	λ_u	$\mathbf{Gap_{min}}$	B_{max}	K_{max}
#17	NEOMAX35EH	12kG	25kOe	16mm	4.0mm	9196G	1.374
#03	NEOMAX35AH	12kG	30kOe	18mm	4.0mm	10014G	1.684
#01	NEOMAX35VH	12kG	28kOe	12mm	4.0mm	6966G	0.781

(a)

Figure 5-40 (a)
The SGU#03 in the PF ring.

(b)

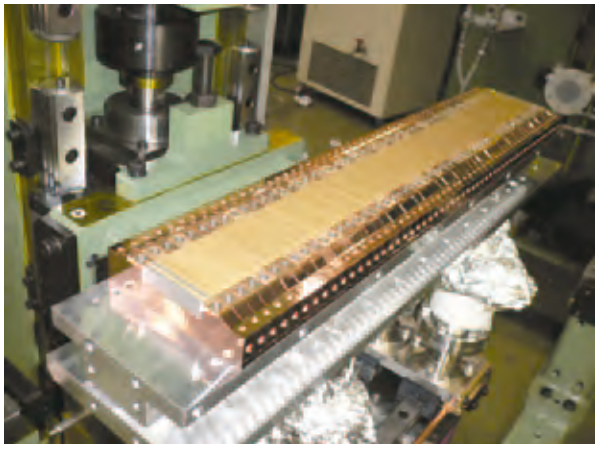

Figure 5-40(b)
The magnetic array of the SGU#03.

All the PF-SGUs have a magnetic array with a length of 0.5 m long and minimum gap of 4 mm, and the maximum K values are limited to less than 2. As a result, the photon energy region of each odd harmonic has no overlap section. The tuning area of photon energy is limited in the case of the PF-SGU. When the SGU is used as the X-ray light source of the 3-GeV ERL, the maximum K value should be more than 2 to avoid inconvenience for the user experiments. Further R&D is necessary to increase the maximum K value of the SGU. Figure 5-41 shows the correlation between K value, period length and gap distance. The parameters of the magnetic block are the same values as those of PF-SGUs in this magnetic simulation. The first target of the SGU for the ERL is to develop a 5-m SGU with K value of 2.

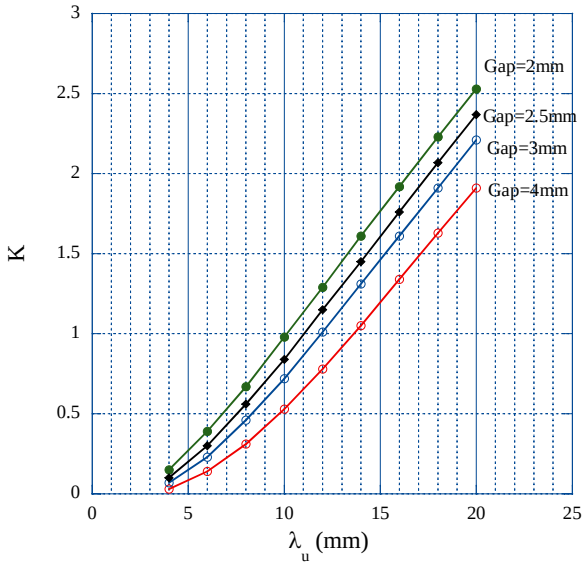

Figure 5-41
The K values of the SGU with various period lengths and gaps.

REFERENCES

[1] S.Yamamoto *et al.*, *AIP Conf. Proc*. **879**, 87 (2007).
[2] S.Yamamoto *et al., AIP Conf. Proc*. **1234**, 599 (2010).

5.12 XFEL Oscillator

5.12.1 Introduction

ERL produces an electron beam of small emittance and short bunch duration at high repetition rate, which yields X-ray radiation of high brightness and ultra-short pulse duration. Furthermore, the ERL light source can accommodate an FEL oscillator operated in the hard X-ray region (XFEL-O) to produce X-ray pulses of excellent temporal coherence, which cannot be obtained in FELs operated in the SASE mode [1–3]. The XFEL-O delivers unprecedented X-ray pulses, hard X-ray pulses with both spatial and temporal coherence, which will open the way for cutting-edge X-ray science. Therefore, we are planning to build an XFEL-O as a part of the KEK ERL.

Figure 5-42 shows a schematic view of the XFEL-O. The XFEL-O consists of a long undulator, mirrors and additional X-ray focusing elements (not shown here). The mirrors are perfect crystals which have a high reflectivity in the X-ray energy region of interest. For example, a diamond (4, 4, 4) surface can be used for an XFEL-O operated at an X-ray energy of 12.0 keV.

Figure 5-43 shows a possible layout of an XFEL-O installed at the ERL light source. The electron beam from the injector is accelerated twice in the main linac and transported to the XFEL-O undulator. The electron beam energy is assumed to be 6 GeV. In this configuration, we can accelerate an electron beam with a small current of 10 μA without energy recovery, which is enough to operate the XFEL-O. Table 5-6 lists an example set of parameters for the 6-GeV XFEL-O.

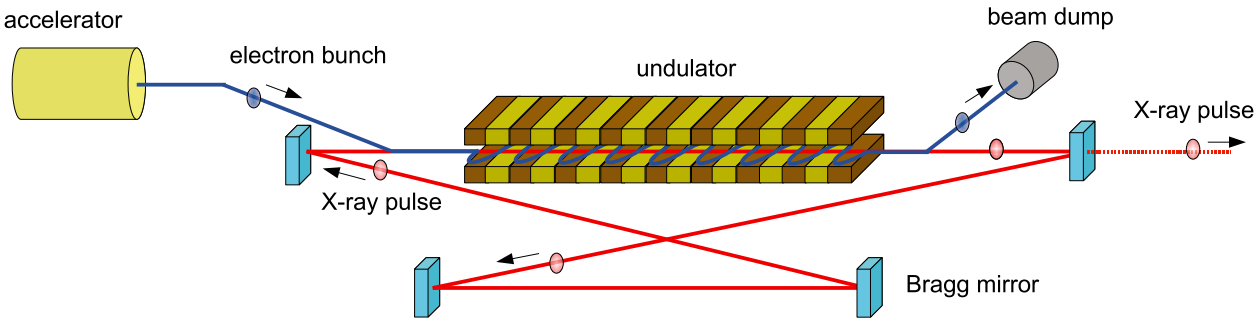

Figure 5-42
A schematic view of XFEL Oscillator.

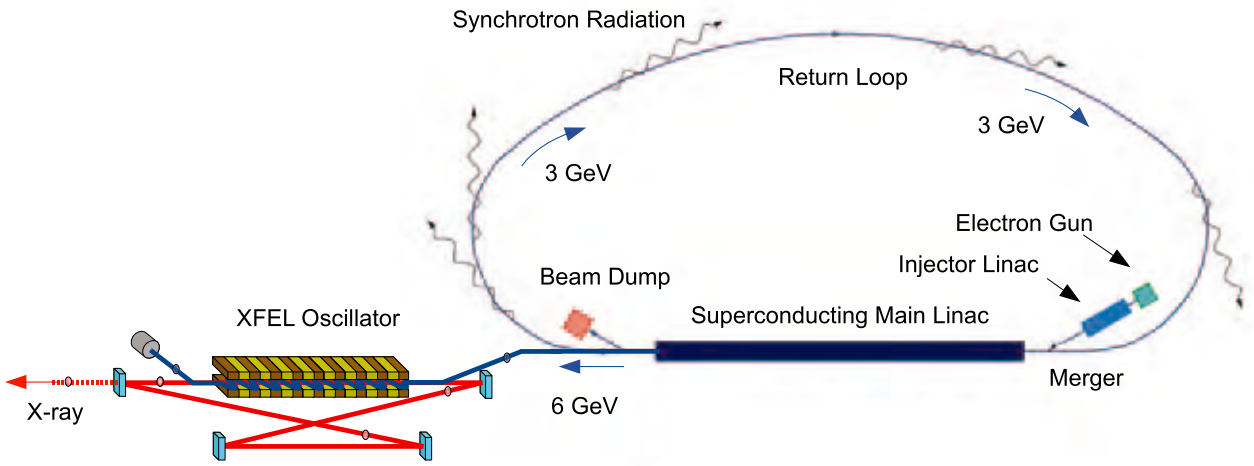

Figure 5-43
A layout of the XFEL Oscillator at KEK ERL.

Table 5-6 An example set of parameters for the 6-GeV XFEL-O.

Electron energy	Bunch charge	Bunch length	Energy spread	Normalized emittance	Repetition rate
6 GeV	20 pC	1 ps (rms)	0.005% (rms)	0.2 mm-mrad	1 MHz
Undulator parameter	Undulator pitch	The number of undulator period	Betatron function in the undulator	Cavity round-trip loss	X-ray energy
K=0.92	1.94 cm	3000	17 m	< 15%	12 keV

5.12.2 Goals and challenges

In order to realize the XFEL-O, the following research issues must be resolved:

1. Generation and transportation of small-emittance electron beam
2. Fabrication of high-quality crystals for the Bragg mirrors
3. Alignment and feedback control of the X-ray oscillator
4. Optimization of the design of the accelerator, undulator and oscillator

5.12.3 Current status

To generate small-emittance electron beams, two approaches have been proposed: a photocathode DC gun and a photocathode RF gun. In JAEA and KEK, photocathode DC guns are being developed for future ERL light sources. The guns are equipped with a GaAs photocathode to produce 10–100 mA electron beams with normalized emittance of 0.1–1 mm-mrad [4]. The guns can be used for the XFEL-O as well. Transportation of an electron beam while preserving the small emittance is another concern. The electron beam in an ERL recirculation loop suffers from emittance growth due to coherent and incoherent synchrotron radiation, wakes from beam pipes, aberration and errors in beam optics, etc. The generation and transportation of small-emittance electron beams should be demonstrated at the Compact ERL.

Bragg mirrors for the XFEL-O are under development at Argonne National Laboratory (ANL), where reflectivity of more than 99% from the (8, 0, 0) atomic planes of a diamond crystal at 13.9 keV X-ray energy has already been demonstrated [5]. Robustness against radiation damage during operation of the XFEL-O and extraction of X-rays through a thin crystal remain to be demonstrated.

For operation of the XFEL-O, the Bragg mirrors must be aligned with accuracy of 10 nrad at 1 kHz bandwidth. The group at ANL has confirmed that monochromator stabilization via null feedback achieves stability of 15 nrad at bandwidth of 1 Hz [6]. This feedback technique is promising for the XFEL-O.

FEL oscillators have been studied in many laboratories [7, 8]. The FEL gain including inhomogeneous effects such as emittance and energy spread of the electron beam, as well as errors in the undulator magnet field, can be estimated both analytically and numerically. Lasing dynamics including exponential growth, saturation and establishment of temporal coherence can be calculated by FEL simulation codes. We have made a preliminary estimation of FEL performance using a one-dimensional FEL simulation code as shown in Fig. 5-44. Further studies are necessary to survey the parameter space for the design optimization and possible FEL gain reduction due to three-dimensional effects.

An FEL oscillator can be operated in harmonics of the fundamental wavelength. Lasing at the third, fifth and seventh harmonics has been demonstrated at JAEA-FEL and AIST NIJI-IV [9, 10]. If we apply third-harmonic lasing to the XFEL-O, an electron beam of 3 GeV can be used for X-ray lasing at 12 keV. The feasibility of this approach should be further studied as an alternative to XFEL-O at the KEK ERL.

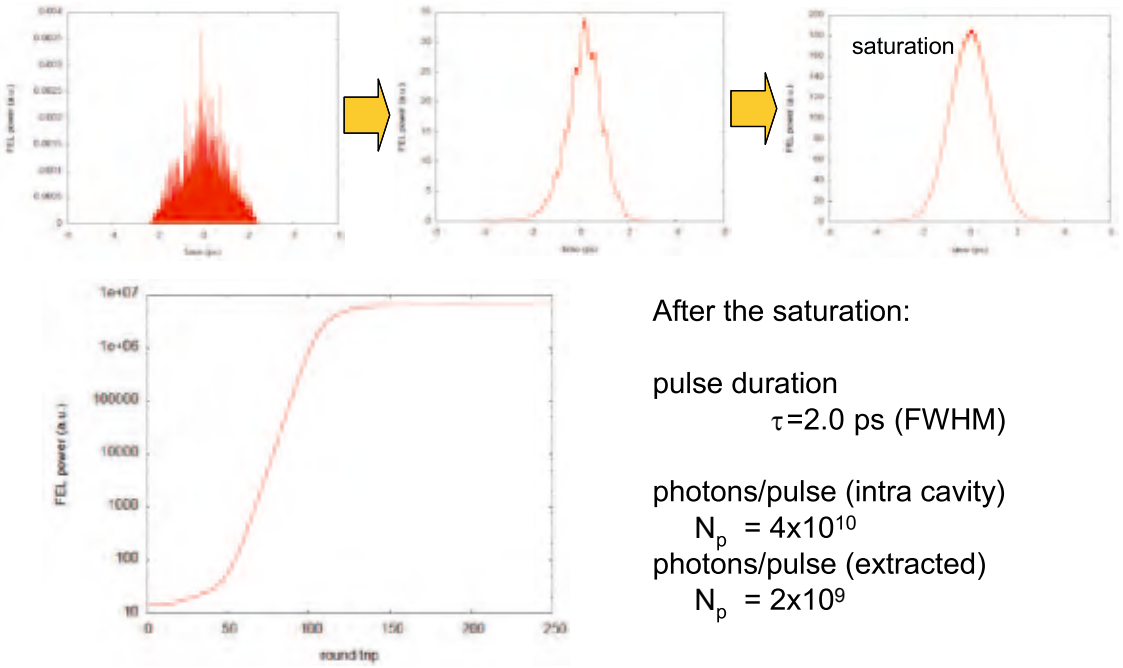

After the saturation:

pulse duration

τ=2.0 ps (FWHM)

photons/pulse (intra cavity)

N_p = 4x10^{10}

photons/pulse (extracted)

N_p = 2x10^{9}

Figure 5-44
Result of 1-D FEL simulation for an XFEL-O [11].

REFERENCES

[1] R. Colella and A. Luccio, *Opt. Commun.* **50**, 41 (1984).
[2] Kwang-Je Kim, Yuri Shvyd'ko and Sven Reiche, *Phys. Rev. Lett*. **100**, 244802 (2008).
[3] Kwang-Je Kim and Yuri V. Shvyd'ko, *Phys. Rev. ST Accel. Beams* **12**, 030703 (2009).
[4] N. Nishimori *et al., J. Phys.: Conf. Ser*. **298**, 012005 (2011).
[5] Yuri Shvyd'ko, Stanislav Stoupin, Vladimir Blank and Sergey Terentyev, *Nature Photonics* **5**, 539 (2011).
[6] Kwang-Je Kim, ERL-2011 Workshop.
[7] N. Nishimori *et al., Phys. Rev. Lett*. **86**, 5707 (2001).
[8] T. Yamazaki *et al., Nucl. Instr. Meth. A* **331**, 27 (1993).
[9] R. Hajima *et al., Nucl. Instr. Meth. A* **475**, 43 (2001).
[10] N. Sei *et al., J. Phys. Soc. Jpn*. **79**, 093501 (2010)., *Opt. Express* **20**, 308 (2012).
[11] R. Hajima *et al., Nucl. Instr. Meth. A* **637**, S37 (2011).

Chapter 6 Beamlines

6.1 Introduction

The undulators installed in the transport loop of the ERL are expected to deliver brilliant, highly-coherent and short-pulsed X-rays as shown in Table 6-1. Thanks to these advantages, the ERL will open up new frontiers in both material and life sciences. However, these advantages will impose severe conditions on the beamline optical elements such as beryllium windows, monochromators and mirrors. In order to meet these severe requirements, it is necessary to develop X-ray optical elements with much higher quality, performance and durability. The calculations for the ERL were made for the third harmonics emitted by the undulator with target parameters (Table 1-1).

Table 6-1 The comparisons between ERL in the ultimate made and SPring-8. The energy spread of the electron beam was assumed to be zero for both of the ERL and SPring-8.

		ERL undulator @ 3 GeV Ultimate-mode E = 8 keV (3rd harmonics)		SPring-8 undulator @ 8 GeV E = 8 keV (1st harmonics)	
Beam current		100 mA		100 mA	
Bunch length (psec)		2		20	
Undulator length		30 m	5 m	25 m	5 m
Source size (μm)	horizontal	35.6	31.5	892	892
	vertical			22.8	10.6
Source div. (μrad)	horizontal	4.86	9.7	37.4	38.4
	vertical			4.3	10
Beam size @ 50m (μm)	horizontal	279	519	2761	2813
	vertical			236	509
Brilliance (ph/s/0.1%/mm^2/mr^2)		1.09×10^{23}	5.7×10^{21}	2.2×10^{21}	5.0×10^{20}
Flux (ph/s/0.1%)		4.22×10^{15}	7.0×10^{14}	9.0×10^{15}	2.4×10^{15}
Coherent flux (ph/s/0.1%)		6.5×10^{14}	3.4×10^{13}	1.3×10^{13}	3.0×10^{12}
% beam coherence		16	4.9	0.14	0.13
Total Power		9.4 kW	1.57 kW	31.2 kW	15.7 kW
Power/Area @ 20 m		261W/mm^2	43 W/mm^2	4687 W/mm^2	1894 W/mm^2

6.2 R&D Items for Optical Elements

6.2.1 Monochromator crystals

The undulators of the ERL will emit sharply collimated X-rays in both the vertical and horizontal directions. As shown in Table 6-2, however, typical values of the total power and power density at the ERL are less than those at SPring-8. Therefore, standard monochromators used at the third-generation SR facilities will also be available at the ERL. One of the candidates is, for example, the cryogenically-cooled rotated-inclined double-crystal monochromator installed at BL19LXU of SPring-8 [1].

Table 6-2 The comparisons of the thermal properties between the silicon crystal and the diamond crystal. Here, α is the thermal expansion coefficient and k the thermal conductivity. The parameter, $|\alpha/k|$, signifies the figure of merits (the smaller the better).

	Silicon		Diamond	
Parameter	300 K	100 K	300 K	100 K
$\alpha(K^{-1}) \times 10^{-6}$	2.6	-0.4	1	0.05
k (W cm^{-1} K^{-1})	1.5	8.8	9 - 20[a]	30 - 100[a]
$\lvert\alpha/k\rvert$ (W) x 10^6	1.7	0.045	0.11 - 0.05	0.002 - 0.0005

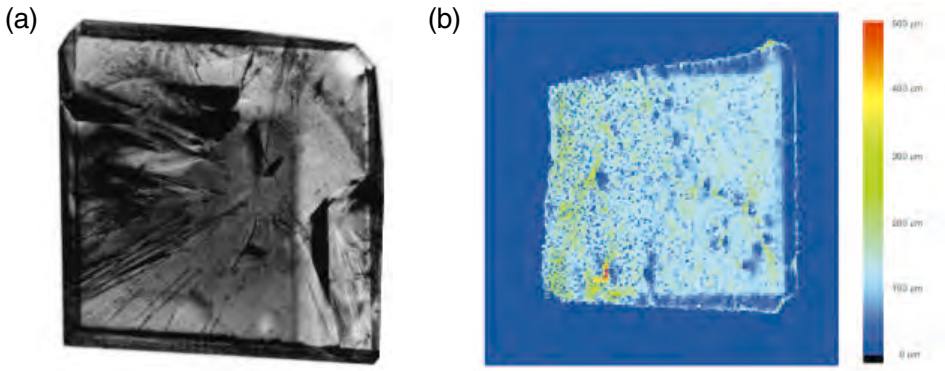

Figure 6-1
X-ray plane-wave topographic images of diamond crystals grown by (a) the HPHT method and (b) the plasma CVD method.

Diamond crystals have excellent thermal properties as shown in Table 6-2. For example, $|\alpha/k|$, where α is the thermal expansion coefficient and k is the thermal conductivity, of a diamond crystal is about two orders of magnitude smaller than that of a silicon crystal at 100 K. At the long-undulator beamlines, cryogenically-cooled diamond crystals will be required in order to handle the heat load. To date, high-quality synthetic diamond crystals of type IIa grown by high-pressure/high-temperature synthesis (HPHT) [2] have been mainly used at the SR facilities. However, the HPHT method cannot easily grow a single crystal larger than 10 mm. One possible way to overcome this problem is to use microwave plasma chemical vapor deposition (CVD). Figure 6-1 shows X-ray plane-wave topographic images of diamond crystals grown by (a) the HPHT method [3] and (b) the plasma CVD method [4]. It is worth noting that there are several small regions where the crystallinity is almost perfect in Fig. 6-1 (b). This indicates good prospects for large, high-quality diamond crystals which are indispensable optical elements for the ERL and XFEL-O [5].

6.2.2 Gratings

One of the most important optics in the soft X-ray region is a diffraction grating, which produces wavelength dispersion and thus is used in a monochromator. The energy resolution of monochromatic X-rays strongly depends on the design and quality of the diffraction grating, as well as those of the monochromator. Although the mirror used for focusing and collimation of X-rays is also an essential optics, the R&D elements.

The required energy resolution in the soft X-ray region is continuously increasing. Although the spectral resolution in X-ray absorption is limited by the core-hole life-time broadening, which is typically ~100 meV, such a limitation does not apply to, for instance, the inelastic scattering or valence photoemission process. In fact, ~10 meV resolution is desirable to observe spin-wave excitation in X-ray inelastic scattering. In some cases, even a resolution of several meV is still effective in the photoemission. The energy resolution of the grating monochromator basically depends on the dispersion and focusing at the exit slit

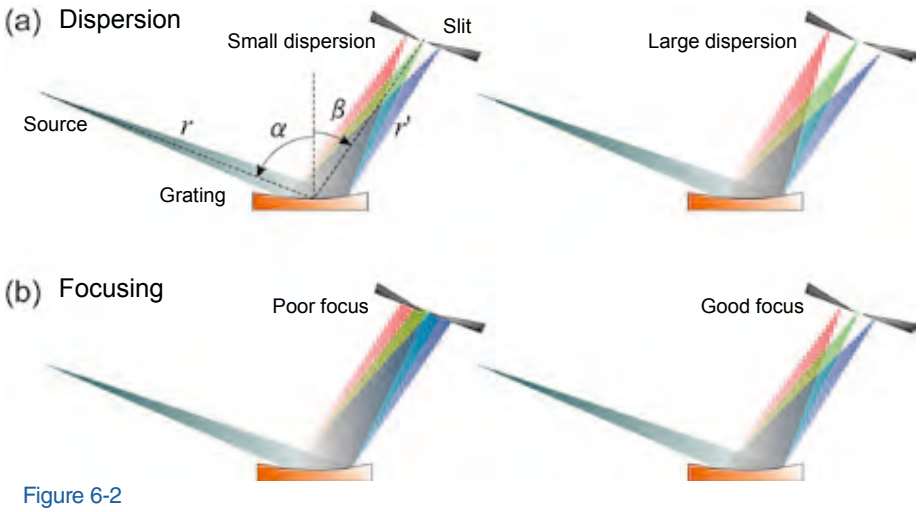

Figure 6-2
Schematic illustration for effects of (a) dispersion and (b) focusing on the energy resolution.

position as illustrated in Fig. 6-2; larger wavelength dispersion and smaller focus lead to higher energy resolution. The wavelength dispersion and focusing can be controlled, in principle, by the monochromator parameters such as the demagnification factor, the groove density of the grating, and the curvature of the grating and mirrors. In addition, the quality of the diffraction grating itself is essential, especially in the ultra-high resolution regime such as several meV at 1 keV. For instance, a slope error of < 0.1 arcsec is required to achieve a 100 meV resolution at 1 keV in a typical monochromator. It should also be emphasized that the illumination area on the grating should be large enough in order to achieve a high energy resolution, because the number of illuminated grooves should be larger than N to achieve an energy resolution, $N=E/\Delta E$. Therefore, a high groove density and/or large illumination area are necessary, though the divergence of X-rays from the ERL is relatively small.

The slope error of a grating is determined by that of the substrate, which is typically made of silicon, and is ~0.1 arcsec for a commercially available substrate at a reasonable cost. On the other hand, the groove density of the grating can be well controlled and varied-line-spacing gratings with precise groove density parameters are readily available [6]. Today, thanks to the development of optical design and alignment techniques, the slope error is one of the most critical limitations for the energy resolution. However, the maximum groove density is limited to ~4800 l/mm due to difficulties in the process of fabricating the grooves. In the case of high groove density, a sharp groove shape is difficult to attain, resulting in a reduction in reflectivity and increase of stray light. This might be a serious problem when trying to achieve an ultra-high energy resolution, because the wavelength dispersion is proportional to the groove density. It is essential R&D item to increase the groove density in order to archieve a high energy resolution.

In the case of high-brightness sources such as the ERL, thermal distortion is one of the most serious problems concerning the optics, causing a reduction of energy resolution, a shift in energy, and deterioration of the beam size. It is essential to develop a more effective cooling system, or an optical design to reduce the effects of thermal distortion. For instance, the use of a virtual source, such as the entrance slit of a monochromator, is effective to stabilize the position and size of a practical source.

To achieve an ultra-high energy resolution such as several meV at 1 keV, a smaller slope error, a higher groove density and a smaller thermal distortion are necessary, as well as a higher mechanical stability. Fortunately, a slope error of << 0.01 arcsec is available by ultrafine control of the mirror surface, which can be applied to the fabrication of diffraction gratings. Moreover, mechanical instability can be effectively reduced by designing an appropriate vibration isolator.

6.2.3 Zone plates

A zone plate is one of the most convenient optics for focusing X-rays. Although the principle of focusing is the same both in the hard and soft X-ray regions, practical targets of R&D are a little different, mainly due to the difference in the wavelength and absorbance.

The beam size of X-rays focused by a zone plate depends on the source size, demagnification factor, diffraction limit determined by the illuminated area, and energy resolution. Since the zone width decreases from the center to the periphery of the zone plate as shown in Fig. 6-3, a narrower outermost zone width is required to fabricate a larger zone plate to achieve a larger illumination area and thus smaller beam size. In fact, the zone-width limited resolution is known to be ~1.22ΔR, where ΔR denotes the out-

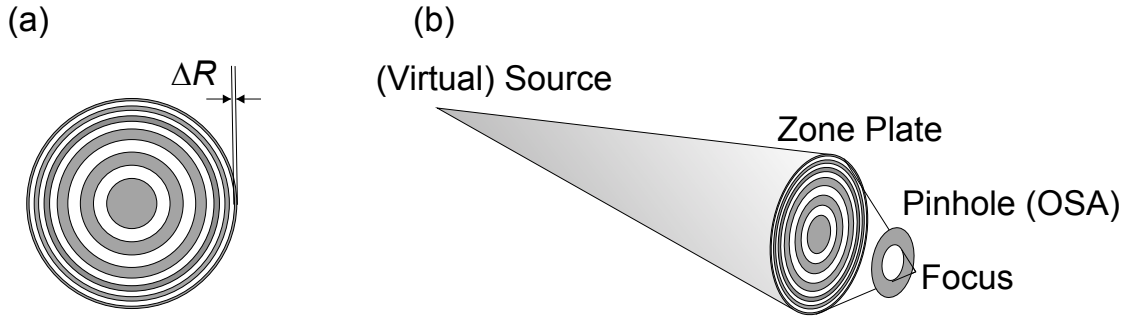

Figure 6-3
Schematic illustration of a zone plate (a) and a focusing optics using the zone plate (b). A pinhole is placed as an order sorting aperture (OSA).

ermost zone width. As electronics device structures are becoming smaller, a beam size of < 10 nm, corresponding to $\Delta R < 8$ nm, is strongly required.

The quality of zone plates is improving with the development of electron beam lithography techniques, and an outermost zone width of ~25 nm is now commercially available. Even $\Delta R \sim 15$ nm has been reported [7], though it was not for commercial use. Since the absorbance of soft X-rays is relatively large, a thick zone plate is not necessary, which is advantageous in the fabrication process of a zone plate for the soft X-ray region. In addition, since the focal length is inversely proportional to the wavelength, a short focal length, corresponding to a high demagnification factor, can be rather easily obtained in the soft X-ray region. However, the diffraction efficiency of a zone plate is typically several %, which should be improved by optimizing the parameters of the zone structures.

The heat load problem is more critical for a zone plate, because it is hard to cool down and the high thermal power from the ERL may cause fatal damage to the zone structures. To reduce the thermal damage of the zone plate, a SiC membrane is being developed in place of SiN, because SiC is more robust against thermal damage.

6.2.4 Mirrors

The total-reflection mirror is one of the most important optical elements for the ERL. In order to preserve the spatial coherence, atomically smoothed surfaces and extremely high accuracy of nanometer order are necessary. To meet these requirements, for example, the numerically controlled EEM (Elastic Emission Machining) system [8] and X-ray metrologic method sensitive to atomic-level roughness [9, 10] have been successfully developed. These technologies will be useful for the ERL.

Wave-front correction techniques are also important for preserving the spatial coherence. In this method, the distorted wave-front of X-rays is analyzed and then corrected by wave-optical techniques. To date, several methods of wave-front analysis have been developed for estimating the surface roughness of total-reflection mirrors [9, 10] and for X-ray phase-contrast imaging [11]. On the other hand, several efforts have been made on wave-front modification based on adaptive engineering [12]. The combination of wave-front analysis and modification will open up new possibilities for coherence control. To pursue this direction, both basic and advanced research of X-ray wave-optics are required. Especially, it is necessary to develop a complete set of wave-optical simulation codes for the design and estimation of each optical element and overall beamline.

6.2.5 Other optical elements such as beryllium windows

ERL provides almost diffraction-limited X-rays in both the vertical and horizontal directions. As shown in Table 6-1, the coherent fraction of the ERL is 4.9-10% at E = 8 keV, while it is about 0.1% at SPring-8. Therefore, the beamline optical elements must preserve the spatial coherence, otherwise speckle noise will be produced and the quality of sample images will suffer serious deterioration. For example, in order to suppress the speckle noise, the beryllium windows must be highly pure and their surfaces must be polished [13]. Figure 6-4 shows an X-ray image of a beryllium window observed at the BL-15C of the Photon Factory (PF) [14]. It can be clearly seen that the impurities and the uneven surface of the beryllium window produce noisy background which is a serious hindrance to X-ray imaging experiments. Therefore, the quality of the beryllium windows for the ERL must be much higher than the existing ones.

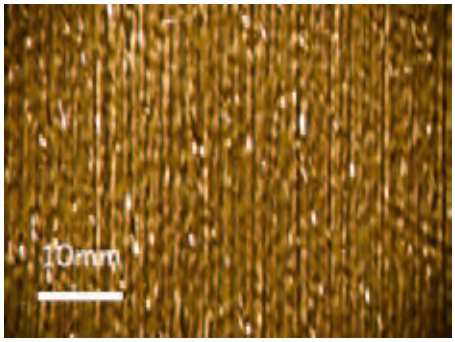

Figure 6-4
The X-ray topographic image of the beryllium window observed at the BL-15C of the Photon Factory.

6.3 R&D Items for Instrumentation

Adjustment mechanism/vibration/cooling

Beamline components such as the mirror system, as well as optical elements, play essential roles for utilizing the high-quality X-ray beam from the ERL without deterioration of quality. More precise alignment of the optics is necessary to achieve a higher energy or spatial resolution. Moreover, some optical elements, especially those placed upstream of a beamline, should be effectively cooled in order to avoid thermal distortion or damage. The cooling must be performed while precisely controlling the position and angle of the optics without mechanical vibration. The curvature of the mirrors and gratings is also important. Although the precision of fabricating mirrors is being improved, online adjustment of the curvature is sometimes necessary. However, this makes the mechanism more complicated, because the position, angle, and curvature of optical elements must be controlled while maintaining effective cooling and avoiding mechanical vibration.

The required precision of optical alignment strongly depends on the beamline design and required performance. For instance, assume that X-rays are focused by an elliptical mirror down to 10 nm at a glancing angle of 1 deg, a divergence of 5 mrad, and a focal length of 50 mm. In this case, a ~2 μm shift in the focal length results in a ~5 nm broadening of the spot size. Since a misalignment of the mirror angle of $\sim 4\times10^{-5}$ degrees corresponds to a ~2 μm shift in the focal length, the mirror angle must be adjusted with a precision of $\sim10^{-5}$ degrees in order to achieve a spot size of 10 nm. Or, if a mirror bending system is available, the curvature must be controlled with a precision of $\sim10^{-5}$. Of course, the position of the sample along the beam should also be precisely adjusted with a precision of < 1 μm.

A similar argument applies to mechanical vibration. In the case of high demagnification optics, a shift of the source point does not seriously affect the spot position. In fact, a 10% shift of the source point with respect to the source size results in a 10% shift of the spot at the focal point with respect to the spot size. That is, simultaneous vibration of the focusing optics and the sample does not cause a serious problem. For instance, if a 100 μm source is focused to 10 nm by the focusing optics, a vibration of even 10 μm results in only a 1 nm shift of the focused beam. On the other hand, a relative shift between the focusing optics and the sample directly affects the relative spot position; only a 10 nm shift of the optics results in a 10 nm shift at the sample. Moreover, a vibrational change in the angle of the focusing mirror affects the spot size quite seriously. In the case of the same optics described in the previous paragraph, a $\sim5\times10^{-6}$ degree shift of the mirror angle corresponds to a ~10 nm shift of the spot. Thus, vibration must be kept within $\sim10^{-6}$ degrees to achieve a spot size of 10 nm.

Cooling of the mirror is another challenge, especially for a high-brightness source like the ERL. In fact, a total power of > 1 kW is predicted for a planar-type undulator in the soft X-ray region. Although the power distribution can be controlled by adopting other undulators such as figure-of-8 and elliptical undulators, the power at the first mirror may exceed 100 W. We must remove such power while precisely maintaining the mirror position, angle, and curvature as mentioned above. Cooling of the mirror is typically achieved by indirect side cooling with water flow. At present, the heat load at the first mirror must not exceed ~50 W to keep the beam angle stable within ~1 μrad in the sagittal direction. One of the limitations is the amount of water flow, because a large flow induces mechanical vibration. Although a monochromator crystal in the hard X-ray region can be cooled by direct cooling, vibration might be a serious problem in the ERL.

Owing to developments in the mirror adjusting system, the minimum step for the adjustment is becoming smaller and the reproducibility is getting better. In fact, a < 0.1 μm translation and $< 10^{-4}$ degree rotation can be achieved even in the case of ultra-high vacuum, by using a goniometer-like system. More precise position control of ~nm order is available by using a piezo actuator. However, angle adjustment of 10^{-5} degrees might be somewhat difficult without using a sine-bar system. Mirror bending systems are already used, especially in the hard X-ray region, but precise control of the mirror surface such as elliptical shape is difficult to achieve due to the complicated surface shape. Although a simple bending mechanism combined with a conical mirror has been shown to be effective [15], the process for fabricating a conical mirror is not fully established. However, a method of precisely controlling the wavefront using an additional mirror with many actuators has recently been developed, and a < 10 nm spot size was reported [16, 17].

From the above discussion, fine adjustment of the position and angle itself seems possible, with sufficient precision to achieve high energy and spatial resolution using the ERL. However, the stability might be a serious problem, such as thermal drift of the position and mechanical vibration. For the drift, some feedback system will be needed to keep the energy and beam position stable. For instance, if an electron energy analyzer is placed in front of a focusing mirror placed downstream of a monochromator, the actual photon energy can be checked, at least relatively, and such data can be used for the real-time feedback system. On the other hand, mechanical vibration is difficult to remove due to the use of many pumps and the water cooling system. Although the vibration problem can be solved by coupling the focusing optics with the sample in the case of the focusing system, the effects on the energy resolution remain a serious problem to be solved.

The mirror bending system is another important target of R&D for the ERL. A multi-actuator system would be necessary for ultra-fine control of the focusing mirror. This should be realized in the ultra-high vacuum condition in the case of the soft X-ray region. Moreover, even the curvature of the diffraction grating should be controlled according to the energy scan, in order to achieve an ultra-high energy resolution over a wide energy range. In fact, an “active grating” has been developed [18], in which a third-order polynomial surface can be controlled. It may be beneficial to apply this control system to both the mirror and grating, in combination with an effective cooling system.

In this section, we looked at several R&D issues for beamline components. There are many other important issues. The ERL will open up new optical possibilities; for example, novel optical elements based on X-ray multiple diffraction will enter practical use at the ERL. In order to solve such a wide range of R&D issues, it will be important to build a global framework of cooperation.

REFERENCES

[1] T. Mochizuki *et al.*, *Nucl. Instrum. & Meyhods Phys. Res. A* **467-468**, 647 (2001).
[2] H. Sumiya *et al.*, *New Diamond Frontier Carbon Technology* **10**, 233 (2000).
[3] K. Hirano, private communications.
[4] H. Sugiyama, K. Hirano, K. Ito and N. Fujimori, to be submitted.
[5] K. J. Kim *et al.*, *Phys. Rev. Lett.* **100**, 244802 (2008).
[6] K. Amemiya *et al.*, *J. Synchrotron Rad.* **3** 282 (1996).
[7] W. Chao *et a*l., *Nature* **435**, 1210 (2005).
[8] K. Yamauchi *et al.*, *Jpn. J. Appl. Phys.* **42**, 7129 (2003).
[9] A. Souvorov *et al.*, *J. Synchrotron Rad.* **9**, 223 (2002).
[10] K. Yamauchi *et al.*, *Appl. Opt.* **44**, 6927 (2005).
[11] P. Cloetens *et al.*, *Appl. Phys. Lett.* **75** 2912 (1999).
[12] J. Susini, D. Labergerie and L. Zhang, *Rev. Sci. Instrum*. **66**, 2229 (1995).
[13] A. Snigirev *et al*., *Nucl. Instrum & Methods Phys. Res. A* **370**, 634 (1996).
[14] K. Hirano, private communications.
[15] M. Nomura and A. Koyama, *J. Synchrotron Rad.* **6**, 182 (1999).
[16] H. Mimura *et al*., *Rev. Sci. Instr.* **81**, 123704 (2011).
[17] H. Mimura *et al.*, *Nature Physics* **6**, 122 (2010).
[18] S.–J. Chen, *Nu cl. Instr. Meth. A* **467**, 298 (2001).

Chapter 7 Detector Developments

When future plans for light sources are proposed to users of synchrotron radiation, detectors are also important to obtain better experimental results with new experimental methods and in new research fields. Here, focusing on time-resolved X-ray diffraction and on X-ray imaging, two detector development projects are briefly introduced. These projects will contribute to the ERL project.

Fast Pixelated X-ray detector system

In order to investigate changes in the structure of materials using fast pulsed X-rays, the fast response of the detector itself is important for continuous observation and speed in time-resolved measurements. If the detector has a pulse-resolving time of shorter than the pulse interval of the incident beam, observation at each time the X-ray pulses arrive is possible in the time-resolved experiments. The shortest pulse interval of the ERL will be 0.77 ns in the multi-bunch mode [1]. A pixel array detector with such a fast response would yield new information on the lattice dynamics of crystals after stimulation by a laser or by a pulsed impact, if the detector records the changes in intensity or position of X-ray diffraction spots. The silicon avalanche photodiode (Si-APD) is a candidate for the X-ray sensor with a sub-nanosecond order response. We are now developing a linear-array detector using Si-APD under one of the KEK-DTP projects, named “FPIX” [2]. The Si-APD detector has 64 pixels of a linear array, where the pixel size is 100 μm by 200 μm with a 50-μm gap between pixels and a depleted thickness is 10 μm. As a frontend circuit of the linear array, an ultra-fast ASIC was designed by 0.8-μm BiCMOS process for processing nanosecond-width pulses from each pixel of the Si-APD. The frontend ASIC had four channels in 4×4 mm^2 and each channel consists of a preamplifier, a comparator, a current monitor, a feedback amplifier for baseline restoration, toggle flip flops, and PECL drivers. Two of 125-MHz PECL outputs are available in the fast ASIC circuit. A prototype of the 64-channel linear array system was tested by synchrotron X-ray beam. A 10-ns time resolution and a high count-rate at each channel were confirmed by recording X-ray pulse trains of a focused 8-keV beam with 30-ns gaps in time course [3]. Figure 7-1 shows an illustration of an area detector formed by a stack of linear array detectors of Si-APD. The fast pixelated detector system may play an important role in time-resolved X-ray diffraction experiments carried out in a future beamline of the ERL.

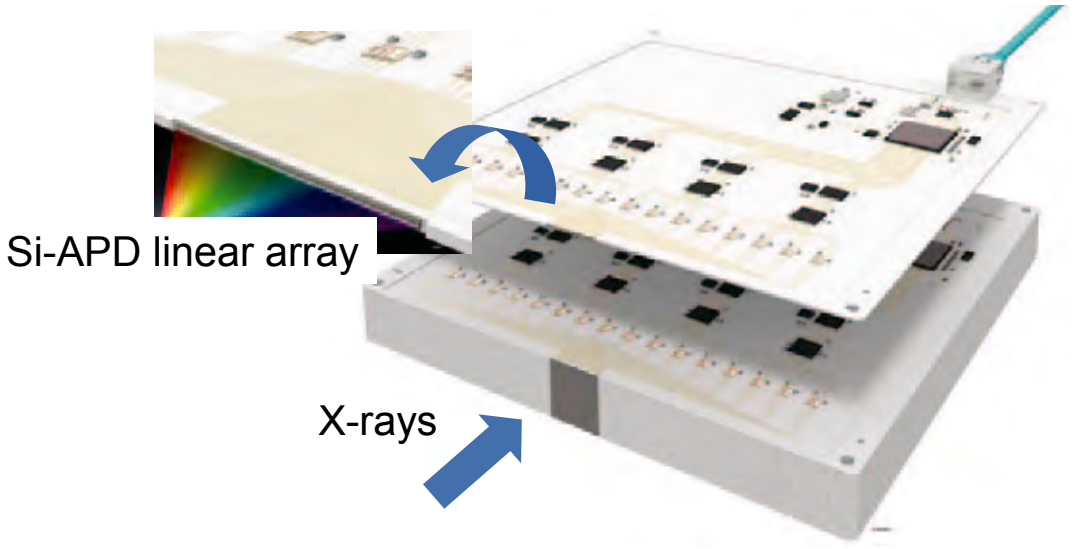

Figure 7-1
Illustration of an area detector by a stack of the Si-APD linear-array detector.

SOI Pixel X-ray sensor for ERL experiments

A new area detector which has a spatial resolution of 10-μm order, an area of more than several 10 mm^2, and a fast readout speed is needed for X-ray imaging. The SOI (Silicon-On-Insulator) detector is a candidate for such advanced monolithic pixel detectors. SOI technology has been developed recently in industry for fast and low-power solid state devices [4]. This is another example of R&D on detectors, which is proceeding through collaboration between material science and high-energy physics in KEK. For the application of SOI to radiation sensors, the bottom layer of the wafer is used as a sensing part, as shown in Fig. 7-2.

The most serious obstacle to practical application, the "back-gate effect" (the detector bias voltage applied at the bottom could cause failure in the electronics above), was recently solved by the concept of "buried P well" (BPW) implantation. This makes it possible to have a thick enough layer of silicon in the SOI chip to detect X-rays up to several tens of keV with high efficiency. The most recent prototype has a sensing layer with a thickness of up to 500 μm.

There are two directions of current R&D: one is to achieve fine imaging with pixels smaller than 10 μm. In high-precision structure analysis of X-ray diffraction and X-ray diffraction microscopy, high-resolution reconstruction can be obtained from finely pixilated images with a high signal-to-noise ratio. Figure 7-3 demonstrates the performance of such a prototype (430k pixel chip of 17 μm size) developed in 2010, where very high quality imaging up to 20 lines/mm is shown comparing with other conventional X-ray imaging devices. Another direction of R&D is to attain a time-resolved/fast framing imaging device. In coherent x-ray diffractive imaging, a fast frame rate of such as each 100 ns will be very useful to col-

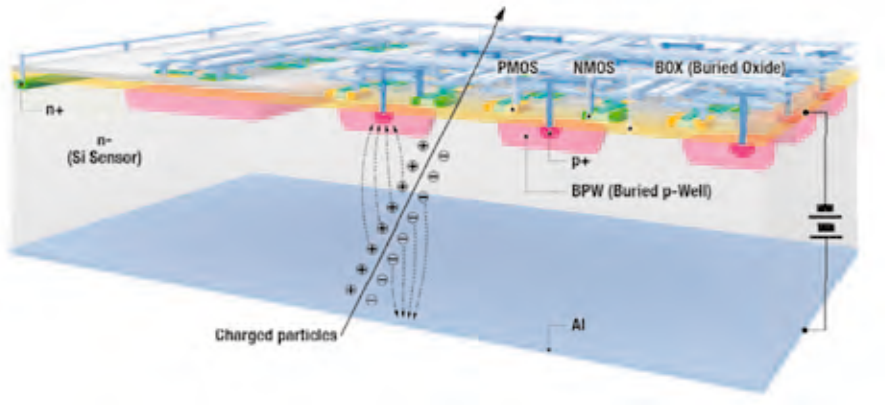

Figure 7-2
Cross-sectional view of the SOI pixel detector.

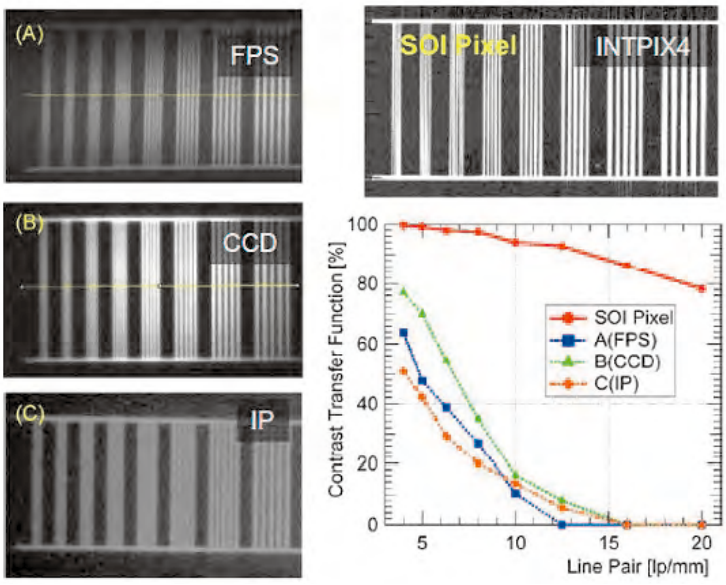

Figure 7-3
X-ray images taken by the SOI sensor and other detectors. Contrast transfer functions of those detectors are also shown.

lect diffraction patterns corresponding to a shorter exposure time. Since the electronics layer of the SOI wafer can be designed and fabricated to the industrial standard of 0.2-μm CMOS technology, it is not difficult to achieve rather high functionalities such as comparators, high-level logics, registers/counters or even digital converters (ADC or TDC) inside each pixel. These features enable the sensor chip to perform high-speed data processing with data sparsification, imaging with large (arbitrary in principle) dynamic range or with precise timing information. Devices with these innovative features provided by SOI pixels could replace existing imaging systems such as the most popular CCD.

REFERENCES

[1] S. Adachi, http://pfwww.kek.jp/ERLoffice/perl/1perl_adachi_090218.pdf.
[2] KEK Detector Technology Project: http://rd.kek.jp/index_e.html.
[3] S. Kishimoto *et al.*, J. of Phys.: Conf. Series (2012), to be published.
[4] Y. Arai *et al.*, Nucl. Instr. and Meth. *A* **636**, S31 (2011).

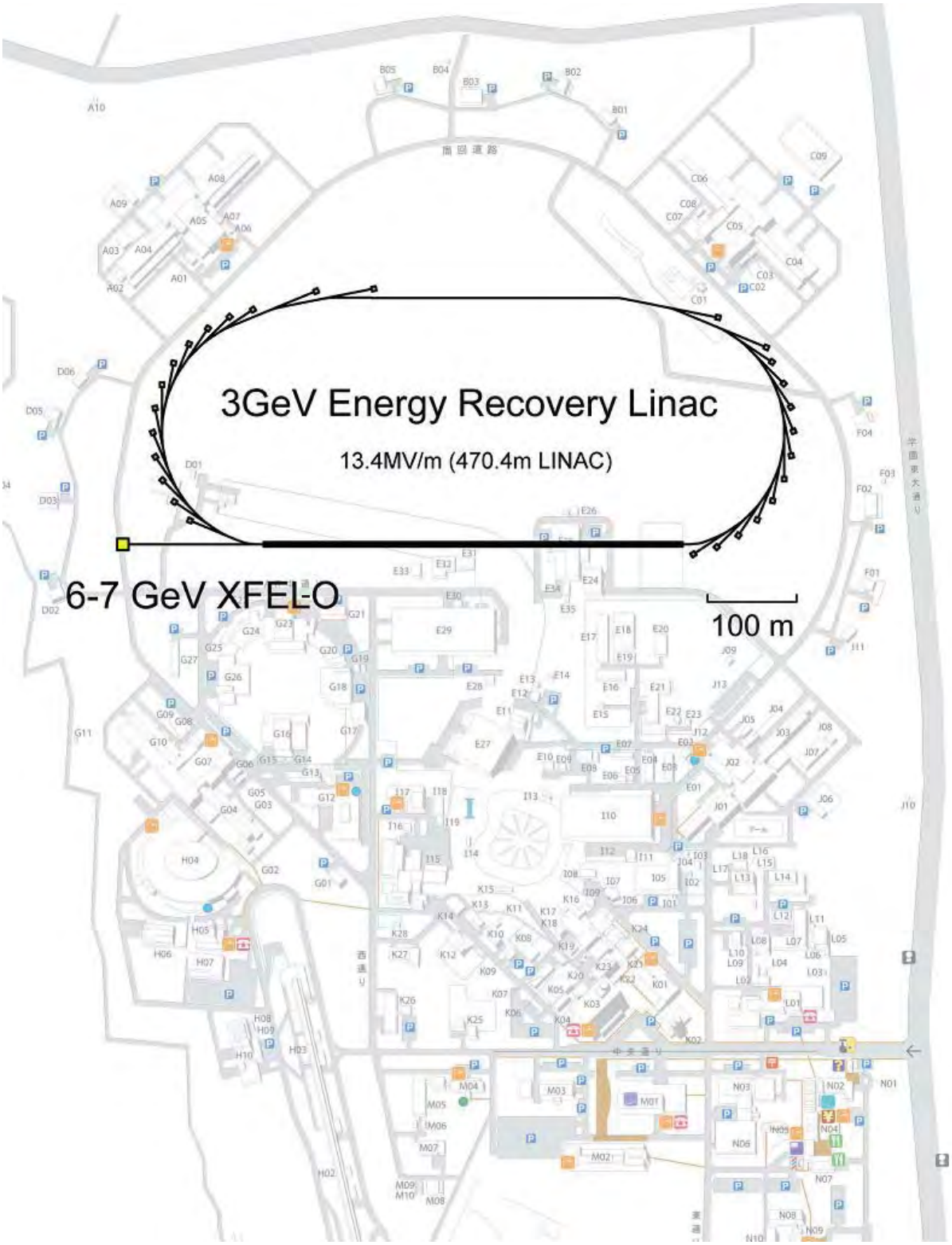

Layout of the 3GeV ERL and 6~7 GeV XFEL-O in KEK.